Deposit & Copying of Dissertation Declaration

UNIVERSITY OF CAMBRIDGE

Board of Graduate Studies

Please note that you will also need to bind a copy of this Declaration into your final, hardbound copy of thesis - this has to be the very first page of the hardbound thesis.

1 Surname (Family Name)	Forenames(s)	Title
Campbell	Callum James	Mr

2 Title of Dissertation as approved by the Degree Committee
Time to quit? Non-genetic heterogeneity in cell fate propensity after DNA damage

In accordance with the University Regulations in *Statutes and Ordinances* for the PhD, MSc and MLitt Degrees, I agree to deposit one print copy of my dissertation entitled above and one print copy of the summary with the Secretary of the Board of Graduate Studies who shall deposit the dissertation and summary in the University Library under the following terms and conditions:

1. Dissertation Author Declaration

I am the author of this dissertation and hereby give the University the right to make my dissertation available in print form as described in 2. below.

My dissertation is my original work and a product of my own research endeavours and includes nothing which is the outcome of work done in collaboration with others except as declared in the Preface and specified in the text. I hereby assert my moral right to be identified as the author of the dissertation.

The deposit and dissemination of my dissertation by the University does not constitute a breach of any other agreement, publishing or otherwise, including any confidentiality or publication restriction provisions in sponsorship or collaboration agreements governing my research or work at the University or elsewhere.

2. Access to Dissertation

I understand that one print copy of my dissertation will be deposited in the University Library for archival and preservation purposes, and that, unless upon my application restricted access to my dissertation for a specified period of time has been granted by the Board of Graduate Studies prior to this deposit, the dissertation will be made available by the University Library for consultation by readers in accordance with University Library Regulations and copies of my dissertation may be provided to readers in accordance with applicable legislation.

3 Signature	Date

Corresponding Regulation

Before being admitted to a degree, a student shall deposit with the Secretary of the Board one copy of his or her hardbound dissertation and one copy of the summary (bearing student's name and thesis title), both the dissertation and the summary in a form approved by the Board. The Secretary shall deposit the copy of the dissertation together with the copy of the summary in the University Library where, subject to restricted access to the dissertation for a specified period of time having been granted by the Board of Graduate Studies, they shall be made available for consultation by readers in accordance with University Library Regulations and copies of the dissertation provided to readers in accordance with applicable legislation.

Time to quit? Non-genetic heterogeneity in cell fate propensity after DNA damage

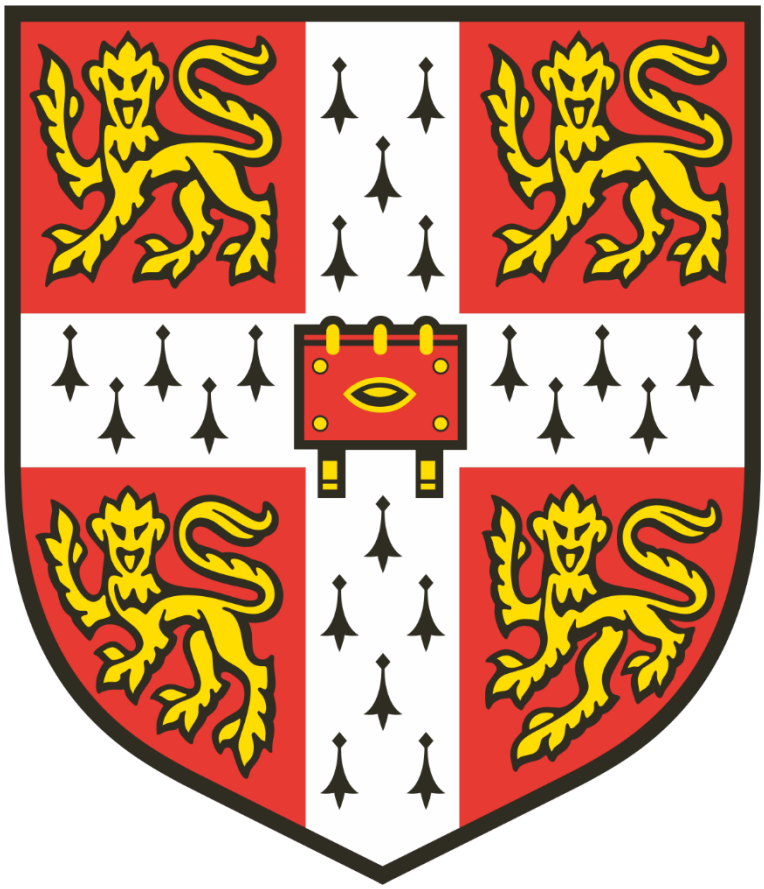

Callum James Campbell

Fitzwilliam College

MRC Cancer Unit

University of Cambridge

2018

This dissertation is submitted for the degree of Doctor of Philosophy

Abstract

Time to quit? Non-genetic heterogeneity in cell fate propensity after DNA damage

Callum James Campbell

Cellular checkpoints are typically considered to both facilitate the ordered execution of the cell cycle and to act as a barrier to oncogene driven cell cycles and the transmission of unresolved genetic lesions from one phase to the next. Furthermore, these mechanisms are also believed to underpin the responses of cells, both in normal and cancerous tissues, to those therapies that either directly or indirectly generate DNA damage.

In recent studies however, it has become clear these checkpoints permit the passage of significant genomic aberrations into subsequent cell cycle phases and even descendant cells, and that heterogeneous responses are apparent amongst genetically identical cells. The consequences of this checkpoint 'negligence' remain relatively uncharacterised despite the importance of checkpoints in current models for how genomic instability is avoided in the face of ubiquitous DNA damage. Unresolved DNA damage is presumably inherited by subsequent cell cycle phases and descendant cells yet characterisation of the consequences of this has been relatively limited to date.

I therefore utilised microscopy-based lineage tracing of cells expressing genetically encoded fluorescent sensors, particularly the Fluorescent Ubiquitination-based Cell Cycle Indicator (FUCCI) probes (Sakaue-Sawano et al., 2008), with semi-automated image analysis to characterise the response of single cells and their descendants to DNA lesions across multiple cell cycle generations. This approach, complemented by generational tracing by flow cytometry, permitted me to characterise the timing of cell fate determination in treated and descendant cells, the non-genetic heterogeneity in checkpoint responses and overall lineage behaviour, correlations between cells (similarly to Sandler et al., 2015) and cell cycle timing dependencies in the response to DNA damaging agents.

With these single cell analytical approaches I show that the consequences of DNA damage on descendant cell fate is dramatic, suggesting checkpoint mechanisms may have consequences and even cooperate across phases and generations. U2OS cell lineages traced for three generations following the induction of DNA damage in the form of strand breaks showed greatly induced cell death in the daughters and granddaughters of DNA damaged cells, termed delayed death. Furthermore, lineage behaviour was characterised as highly heterogeneous in when and whether cell death occurred. Complementary flow cytometric approaches validated the findings in U2OS cells and suggested HeLa cells may show similar behaviour. These findings indicate that checkpoint models need to incorporate multigenerational behaviour in order to better describe the response of cells to DNA damage. Understanding the processes governing cell fate determination in descendant cells will impact upon

our understanding of the development of genomic instability during carcinogenesis and how DNA-damaging chemotherapeutics drive cells to 'quit' the cell cycle.

Declaration

This dissertation is the result of my own work and includes nothing which is the outcome of work done in collaboration except as declared in the Preface and specified in the text.

It is not substantially the same as any that I have submitted, or, is being concurrently submitted for a degree or diploma or other qualification at the University of Cambridge or any other University or similar institution except as declared in the Preface and specified in the text.

I further state that no substantial part of my dissertation has already been submitted, or, is being concurrently submitted for any such degree, diploma or other qualification at the University of Cambridge or any other University or similar institution except as declared in the Preface and specified in the text

It does not exceed the prescribed word limit for the Degree Committee for Clinical Medicine and Clinical Veterinary Medicine.

Callum James Campbell

May 2018

Acknowledgements

I would like to thank Dr Alessandro Esposito first of all, without whom this project would have not existed and whose day-to-day supervision and support deserves recognition. It has been an enjoyable time working with him as part of his team of underlings, the other members of which (past and present) also deserve thanks for their contributions to my experience in the lab; I have learnt a very great deal from them. Maximilian Fries earns a special mention for having shared the PhD experience with me.

Thanks go to Professor Ashok Venkitaraman for making room for me in his group. His guidance and comments as supervisor have been much appreciated, except perhaps when he announces “so what?” or calls me ‘fatface’!

The CRUK Cambridge Centre have been generous supporters and I would like to thank them for the resources they chose to invest in me and my research (and the dinners!), I hope they feel it was money well spent!

This process has taken a long time, but the roots go back much further and there are too many people to mention who helped me along the way. I will however single out my family, and the people like Carol Harris, who encouraged me with my interests in science when I was very small.

Callum

For Granny (Gwendrah Eleanor Smith), who just missed seeing me reach the end.

Table of Contents

List of Figures

List of Tables

List of Frequently Used Abbreviations

aa	Amino acid(s)
ATM	Ataxia Telangiectasia Mutated protein
ATR	Ataxia Telangiectasia and Rad3 related protein
CDK	Cyclin Dependent Kinase
DDR	DNA Damage Response
DNA	Deoxyribonucleic Acid
DNA-PK	DNA dependent protein kinase
FUCCI	Fluorescent Ubiquitination-based Cell Cycle Indicator
G1	Gap 1 (phase)
G2	Gap 2 (phase)
hCdt1	Human Cdt1 protein
hGem	Human Geminin protein
HPNE	Human Pancreatic Nestin-Expressing
HR	Homologous Recombination
hTERT	Human Telomerase Reverse Transcriptase
M	Mitosis
mAG	Monomeric Azami Green
NES	Nuclear Export Signal
NHEJ	Non-Homologous End Joining
NLS	Nuclear Localisation Signal
PIKK	Phosphatidylinositol 3-kinase-related kinase
Plk1	Polo-like Kinase 1
Rb	Retinoblastoma protein
S	Synthesis (phase)
SAC	Spindle Assembly Checkpoint
SASP	Senescence-Associated Secretory Phenotype

Introduction

1.1 Cell fate determination, to die or thrive?

Mammalian organisms are composed of large numbers of cells each developed into a specific state that normally carries out a physiological role for the development and maintenance of the soma or reproductive germline cells. The differences between cells can be vast, some actively proliferate, e.g. blood cell progenitors, producing a great many descendants, some, such as hepatocytes, may cycle only when necessary to repair injury and others, once terminally differentiated, should never divide again; cells making up the outer layers of the skin are disposable and short lived while neurones can last a lifetime; a motor neuron may stretch the entire length of a limb while red blood cells are a few microns in diameter (Milo et al. 2009). Despite this diversity, almost all cell types possess the same genome, the few exceptions including immune cells that have undergone recombination to generate sequences encoding novel antibodies, germ cells that have undertaken meiosis and red blood cells which lack nuclei. This diversity is generated during the processes of development as cells integrate information and make decisions over which programmes of behaviour encoded in DNA to activate and which to suppress in order to determine their ultimate cell fate. This cell fate determination continues throughout life as cells maintain organismal homeostasis in response to tissue turnover, damage, injury and infectious agents. When cells make inappropriate cell fate decisions, whether during development or during homeostasis, diseased states such as cancer, the abnormal growth of cells in the body, may result.

Of particular relevance to cancer are the fate decisions cells make over life, proliferation and death. In tissues and organs these decisions must be balanced to maintain function over time; excessive cell death will lead to organ degeneration and excessive proliferation will lead to tissue metaplasia, the risk of tumour formation and thus potentially organismal death. Furthermore, these decisions are important in ensuring correct tissue function in response to cellular damage, cells must evaluate whether they can continue to function normally or if they must sacrifice themselves to facilitate their own replacement.

This work focuses on the cell cycle arrest, proliferation, survival and death decisions made in the circumstance of responding to damage to DNA, a form of cellular damage that has particular significance as it may produce mutations that alter the encoded information governing cellular processes. Certain mutations are capable of deregulating cellular pathways in such a way to promote the development of cancer, with the creation of oncogenes or the loss of tumour suppressors being two well studied classes of several characteristically cancer-promoting changes (Hanahan & Weinberg 2011). Thus, DNA damage in one cell may lead to negative consequences for the whole organism if this cell continues to survive and proliferate without repairing and, ideally, reversing the DNA damage.

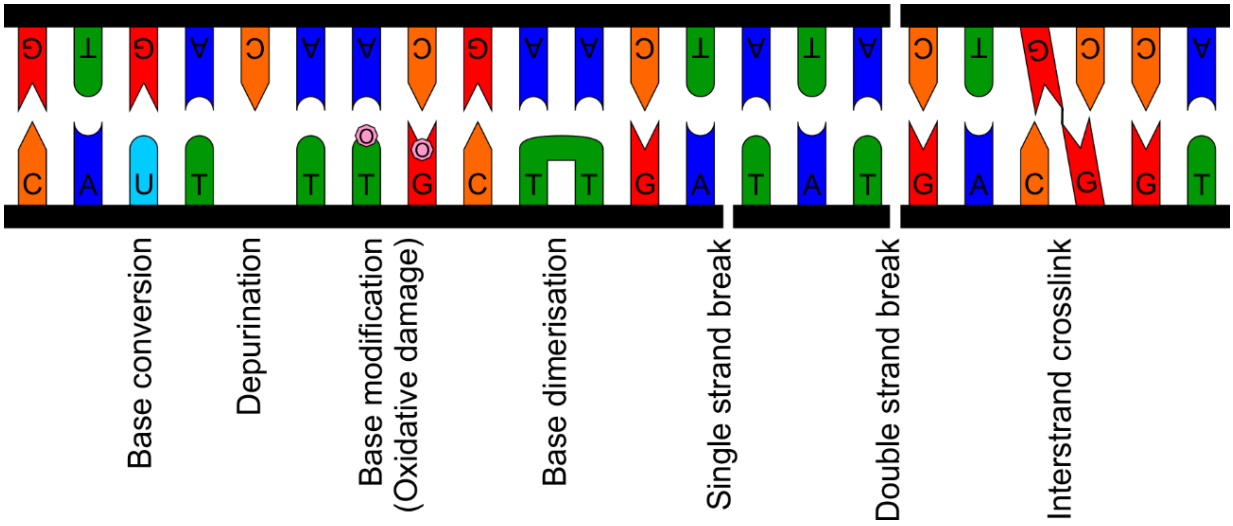

Figure 1: DNA lesions come in a myriad of different forms

DNA damage is ubiquitous (Ciccia & Elledge 2010) and with an estimated 37 trillion cells in the human body (Bianconi et al. 2013), many of which presumably possess some potential capability to give rise to cancer, the chances of one of these many cells experiencing DNA damage induced mutations that result in the formation of a tumour might be expected to be very high. Indeed, many humans do develop cancer, but typically after many decades of life (CRUK 2016) and thus the turnover of trillions of cells, suggesting that the vast majority of DNA damage received by cells does not lead to the development of cancer. Our current understanding of the decisions taken by cells following DNA damage has explained one of the major mechanisms for restraining carcinogenesis, namely the existence of DNA damage monitoring 'checkpoints'. However, as these checkpoints have in recent years been demonstrated to possess some apparent failings (Deckbar et al. 2011), there remain open questions over how DNA damage is dealt with by the damaged cells and indeed, by their descendants.

1.2 DNA damage – corrupting the molecule of Inheritance

Despite being a long-term information storage molecule, DNA is susceptible to numerous types of alterations that may result in information corruption or loss. These chemical modifications, often termed 'DNA damage' and 'lesions', come in many forms (Figure 1), for example conversion of bases, loss of bases, base modification, base dimerisation, single and double strand deoxyribose-phosphate backbone breaks, and DNA crosslinks (Griffiths et al. 2000).

1.2.1 Endogenous sources of damage

There are many different specific endogenous sources of DNA damage which fall into several broad categories. Firstly, the cell's own metabolic activity, in a perhaps surprisingly self-sabotaging role, is one source of damage through the generation of reactive oxygen species (ROS) capable of reacting with DNA to produce oxidised bases and strand breaks (Ames 1989; Fraga et al. 1990). Secondly, spontaneous chemical reactions result in base deamination, where cytosine converts to uracil, a base

not found in DNA and capable of pairing with adenine, and depurination, the breaking of the bond between the deoxyribose moiety and the base resulting in an abasic site (Lindahl 1993). Thirdly, the activities of transposable elements such as the human L1 retrotransposon introduce DNA breaks during the process of transposition, in this particular example via an encoded L1 endonuclease (Feng et al. 1996). Finally, errors arising in the processes of replication can also lead to the generation of DNA lesions (Branzei & Foiani 2005), while induction of DNA breaks have been implicated in the regulation of transcription (Ju et al. 2006; Haffner et al. 2010).

1.2.2 Exogenous sources of damage

Internal sources of damage are far from the only significant source of damage (Ciccia & Elledge 2010). There are numerous known environmental sources including: Ionising particle (e.g. alpha/beta/proton/neutron) and electromagnetic (X- and gamma rays) radiation, ultraviolet light, chemicals which react directly with DNA and chemicals which interfere with the proper processing of DNA by the cell, for example topoisomerase I and II inhibitors which abolish religation of DNA after a deliberate enzymatic cleavage.

Estimations of the number and type of lesions introduced from endogenous and exogenous processes are included in Table 1.

1.2.3 The consequences of DNA damage

The specific consequences of DNA damage vary depending upon the particular lesion, for example an abasic site in a codon can no longer encode an amino acid for a protein, a base transition may change the amino acid encoded and a double strand break structurally breaks the chain of information which would prevent transcription from generating a full length RNA, but conceptually there are two major negative considerations. Firstly, the ability of the cell to survive or carry out its function in tissue may be impaired, this could arise if genes essential for survival or function experience a deleterious mutation. Thus the organism experiences an actual or functional loss of a cell in a tissue. An individual cell might be dispensable but if it happens too frequently then tissue function will be impaired. Secondly, mutations arising from DNA damage may drive or predispose the cell to inappropriate proliferation giving rise to cancer, disruption of tissues, organ dysfunction and ultimately organismal death. Many of the most well studied genes in relation to cancer feature mutations that are highly selectively advantageous and so occur in multiple tumour types, arising independently in individual patients (Vogelstein et al. 2013). Even a single mutation can change cell behaviour, for example the mutation of the codon for Glycine to one that encodes Aspartic acid in the KRasG12D mutation. This results in a mutant KRas impaired in GTPase activity and which thus drives aberrant pro-growth signalling activity (Stolze et al. 2015).

Endogenous DNA damage	Lesion type:	Lesions generated (per cell per day):
Depurination	Abasic site	10,000 [a]
Cytosine deamination	Base transition	100-500 [a]
Oxidation	Oxidised guanine	400-1500 [b]
Exogenous DNA damage	**Lesion type:**	**Lesions generated (per cell):**
Peak sunlight	Pyrimidine dimers and photoproducts	100,000 per day [c]
Cigarette smoke	Aromatic DNA adducts	45-1029 [d]
Chest X-ray	Double-strand breaks	0.0008 [e,f,g,h]
Body CT scan	Double-strand breaks	0.28 [e,h]
Airline travel	Double-strand breaks	0.0002 per hour [e,h]
Chernobyl	Double-strand breaks	12 [e,h]
Hiroshima and Nagasaki atomic bombs	Double-strand breaks	0.2-160 [h,i]

Table 1: Estimation of numbers of DNA lesions generated daily endogenously and from specific exogenous sources

Adapted from (Ciccia & Elledge 2010)

[a](Lindahl & Barnes 2000)

[b](Klungland et al. 1999)

[c](Hoeijmakers 2009)

[d](Phillips et al. 1988)

[e] http://www.merckmanuals.com/home/injuries-and-poisoning/radiation-injury/radiation-injury (originally published link: http://www.merck.com/mmhe/sec24/ch292/ch292a.html)

[f] https://www.fda.gov/Radiation-EmittingProducts/RadiationSafety/RadiationDoseReduction/ucm199994.htm#ft6

[g](Hall & Giaccia 2006)

[h](Elkind & Redpath 1977)

[i] http://www.icrp.org/docs/Low-dose_TG_rept_for_web.pdf

DNA damage may itself also lead to further DNA damage and loss of genome integrity. Unrepaired or misrepaired DNA breaks present the possibility of producing chromosomes or chromosome fragments missing centromeres (acentric) that are not correctly, if at all, attached to the mitotic spindle during mitosis. These are likely to lead to the failure to segregate genomic DNA evenly to the daughter cells causing extensive losses or gains of DNA sequences. If these then fail to be incorporated into the nucleus of the daughter cell they are known to form 'micronuclei' (Carrano & Heddle 1973), separate smaller nucleus-like structures, which have been shown to generate further DNA damage in two ways. Firstly, via aberrant inefficient replication no longer synchronous with the rest of the genome and secondly, as a consequence of the DNA in micronuclei undergoing DNA replication during mitotic chromosome compaction resulting in chromosome 'pulverisation' (Crasta et al. 2012). This pulverisation entails further breaking of the DNA strands into multiple fragments, rejoining of these may explain the phenomenon of 'chromothripsis' (Stephens et al. 2011), the observation of extensive rearrangements within a chromosome in some cancer cells. Clearly such extensive structural changes

to the DNA represent a significant loss of genome integrity and, as with simpler mutations, pose the risk of facilitating cancerous transformation by deregulating typical cell functions.

Fortunately however, cells are equipped with many processes facilitating repair of the DNA and, where necessary, a permanent exit from the cell cycle via senescence or programmed cell death in order to protect the organism from the proliferation of aberrant cells. Such mechanisms explain, at least in part, the apparent contradiction of ubiquitous DNA damage with the ability of multicellular organisms like humans to survive for decades and turn over trillions of cells before experiencing life threatening loss of function of tissues or the development of cancer. Many of these processes are ordered and regulated by the existence of cell cycle checkpoints.

1.3 Cell cycle checkpoints and the maintenance of genetic integrity

1.3.1 The Cell Cycle

The eukaryotic cell cycle whereby a cell reproduces to form two daughter cells is characterised by a series of four sequential phases (G1, S, G2 and mitosis) facilitating the timely separation of DNA synthesis from DNA segregation (Figure 2) (The cell cycle is reviewed extensively in Poon 2016). The first phase, G1 (or gap phase 1), involves growth of the cell and preparation for beginning the synthesis of DNA. G1 contains the Restriction Point where an irreversible commitment to continuing the cell cycle may be made if certain cell-type dependent conditions relating to external, e.g. growth factor signalling, and internal stimuli are met, allowing the cell to continue to S phase. S phase, named for 'Synthesis', is when the cell copies its entire nuclear genome via semi-conservative replication to allow for the subsequent division into two cells. G2 (or gap phase 2), another growth phase, allows further time for the cell to prepare for Mitosis, the final phase where the cell divides into (typically) two daughter cells, segregating the DNA into both daughter cells along with the contents of the cell, including organelles and macromolecules. There exists also a G0 phase where a cell may withdraw from the cell cycle either temporarily, commonly referred to as quiescence, re-entering the cell cycle subsequently when certain environmental conditions are met, or for the duration of its lifespan in the case of terminally differentiated cells.

At its simplest, progression through the cell cycle is driven by the regulation of target proteins by phosphorylation by Cyclin Dependent Kinases (CDK) complexed with regulatory Cyclins (Obaya & Sedivy 2002). Which complexes are active changes throughout the cell cycle as different Cyclins are expressed, resulting in changing patterns of protein regulation and thus the resultant changes in the proteome drive the cell cycle forward. (Figure 3)

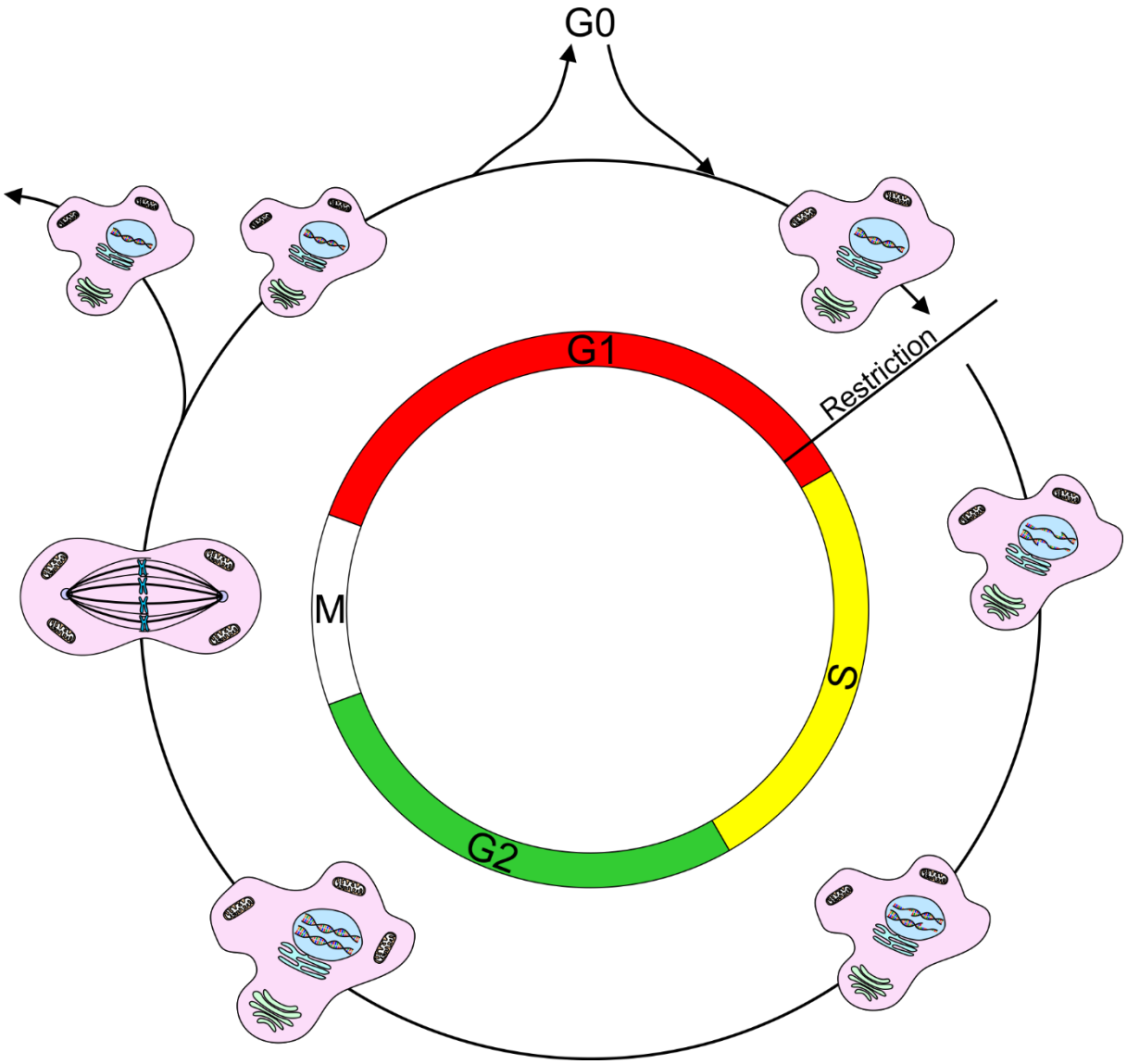

Figure 2 The eukaryotic cell cycle

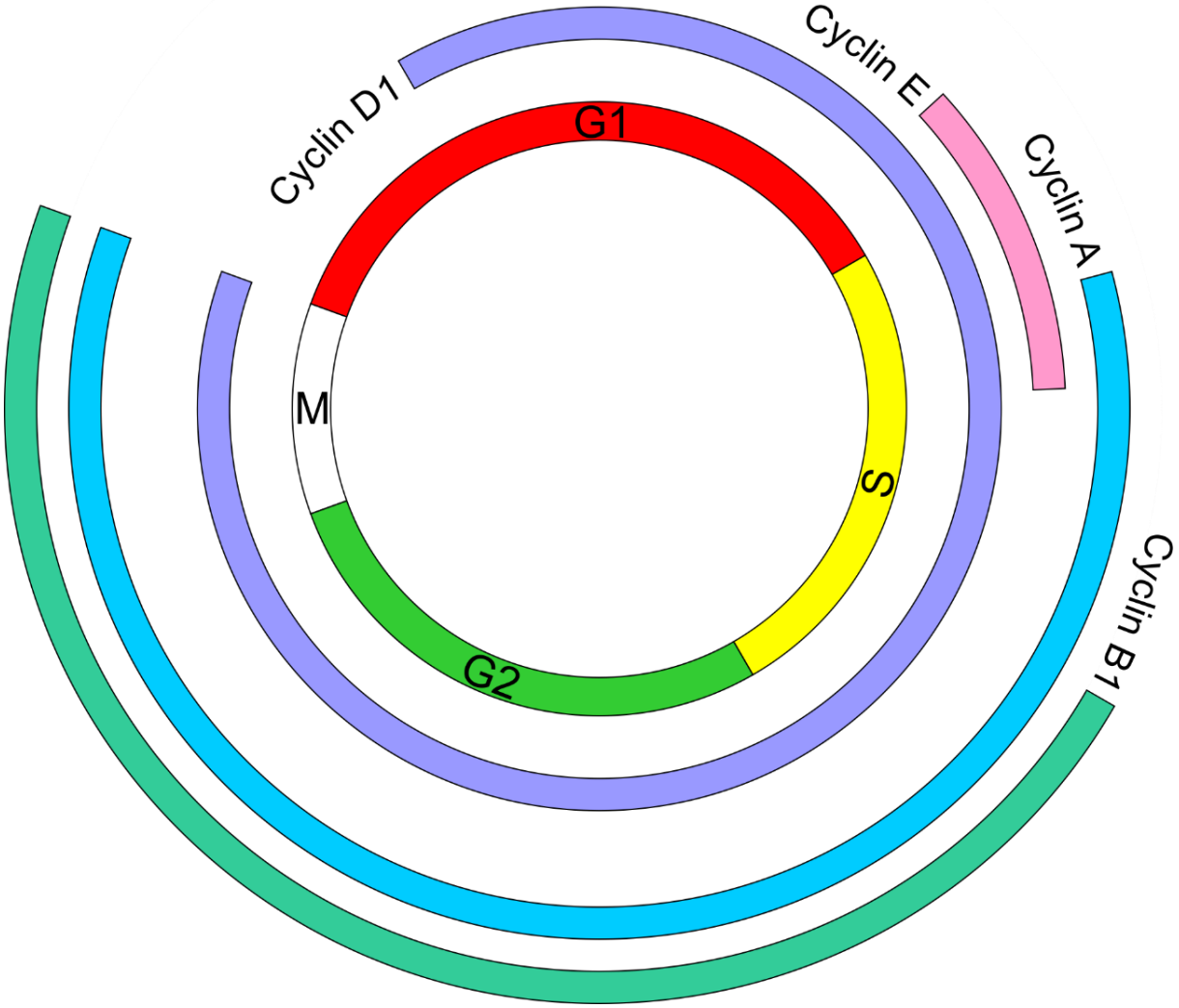

Figure 3 The distribution of cyclins throughout the cell cycle
Particular cyclins are only expressed at certain points in the cell cycle. Adapted from 'Regulation of cyclin-Cdk activity in mammalian cells' (Obaya & Sedivy 2002)

Further controlling cell cycle progression are many layers of regulatory complexity that govern entry into and commitment to the cell cycle, progression through the individual phases, the activity of the processes taking place in each phase and exit from the cell cycle in the form of either terminal differentiation, quiescence or senescence (Reviewed extensively in Poon 2016; Ruijtenberg & van den Heuvel 2016; Chandler & Peters 2013; Johnson & Skotheim 2013). Many of these regulatory processes address the problem of maintaining genetic integrity and cell function in the face of the myriad forms of DNA damage that can result from endogenous and exogenous sources. Depending on the position in the cell cycle, DNA damage presents different challenges as the cellular machinery operates different processes, for example, mRNA transcripts may be truncated or incorrect if the DNA template is damaged, DNA replication during S phase may stall leaving regions of the genome unreplicated, replication may fix damage as permanent base mutations in the copied strand if a damaged template is misread, and broken DNA strands may prevent correct segregation of chromosomes to descendant cells during mitosis.

Certain cellular processes are capable of detecting DNA damage, initiating repair, slowing or halting progression through the cell cycle and determining the ultimate cell fate. Together these mechanisms are known as the DNA Damage Response (DDR) and allow for damage to be repaired where possible and for permanent exit from the cell cycle in the form of cell death or senescence where DNA damage cannot be resolved adequately (Reviewed extensively in Ciccia & Elledge 2010).

1.3.2 Detection of DNA damage and the response

The many types of DNA damage possible must all be sensed in order for any repair to be effected; while our understanding of these processes remains far from complete the components of this sensing system oriented around activation of the phosphatidylinositol 3-kinase-like protein kinase (PIKKs) family proteins ATM, ATR and DNA-PK are fairly well characterised. The binding of initial sensing proteins to the site of damage is followed by the recruitment of other mediators, signalling through transducers and ultimately the regulation of effectors that lead to DNA repair and cell fate determination, so forming the complete DDR (Figure 4). Some of the detail known about the DDR is discussed here.

The DDR-related PIKK family proteins are recruited to the site of damage and activated early in the DDR by the sensing proteins/complexes that directly recognise DNA lesions. The Mre11-Rad50-Nbs1 (MRN) complex detects double-strand breaks where it recruits and activates ATM (Lee 2005). The Ku70/Ku80 heterodimer ring complex loads onto the ends of double strand breaks then recruits and activates DNA-PK (Uematsu et al. 2007; Mahaney et al. 2009). For ATR, single stranded DNA, as might be exposed by a replication fork that has stalled in response to a DNA lesion, is recognised and coated by the RPA protein which recruits ATR via its ATRIP regulatory subunit (Zou & Elledge 2003). RPA also

recruits the 9-1-1 complex and TopBP1 to the coated DNA which then stimulate ATR activity (Kumagai et al. 2006; Delacroix et al. 2007; Lee et al. 2007).

The poly(ADP-ribose) polymerase (PARP) family proteins PARP1 and PARP2 also play an important role in sensing DNA damage, achieving this through interacting with both double and single strand broken DNA via zinc finger motifs where they then generate poly(ADP-ribose) (PAR) chains on histone proteins (Caldecott 2008). These PAR chains are disassembled soon after by the PAR hydrolysing enzyme PARG (Davidovic et al. 2001) but while present provide a recruitment platform for chromatin modifying complexes (Polo et al. 2010; Chou et al. 2010), permitting reorganisation of chromatin structure to facilitate DNA repair, and many DDR factors, some of which are the effectors of DNA repair themselves, e.g. XRRC1 and Lig3, or are mediators like ATM (Gagné et al. 2008).

Once recruited to a site of DNA damage and activated, the PIKK proteins ATM, ATR and DNA-PK can then phosphorylate their substrates at characteristic S/TQ amino acid sites (Kim et al. 1999). ATM and ATR have hundreds of substrates influencing a great many processes (Matsuoka et al. 2007) while DNA-PK is mostly concerned with regulating substrates that favour a mechanism of DNA repair called Non-Homologous End Joining (NHEJ) (Mahaney et al. 2009). One of these substrates is the variant histone H2AX which upon phosphorylation allows amplification of the DDR (Rogakou et al. 1998). This phosphorylation site provides a docking site for MDC1, which can then recruit further ATM, which in turn phosphorylates more H2AX (Stucki & Jackson 2006), so propagating phosphorylated H2AX across up to a megabase from the site of damage (Rogakou et al. 1999). As well as providing further ATM activity, the phosphorylation of H2AX and of MDC1 provides a platform for recruitment of other DNA damage response components, for example the assembly of 53BP1 and BRCA1 at the site of damage via the actions of the Rnf8 ubiquitin ligase (Wang & Elledge 2007; Huen et al. 2007; Kolas et al. 2007; Mailand et al. 2007). This process results in a large focus of a great many DDR factors around the DNA lesion. Other DDR PIKK substrates include further kinases, such as Chk1 for ATR and Chk2 for ATM, which can themselves phosphorylate various substrates, as well as a range of effectors of other behaviour, such as regulators of p53 signalling, DNA repair, cell cycle progression and DNA replication (Matsuoka et al. 2007).

Ultimately a vast number of proteins are altered during the DDR which allows for the activation of all the processes necessary to attempt DNA repair. While many of these processes may be common across the cell cycle some differ and observation of these differences has resulted in the definition of multiple checkpoints that can be activated by the DDR, including the G1/S, intra-S and G2/M (Shaltiel et al. 2015). These along with the Spindle Assembly Checkpoint (SAC) present the major surveillance mechanisms that allow for the maintenance of genome integrity throughout the cell cycle.

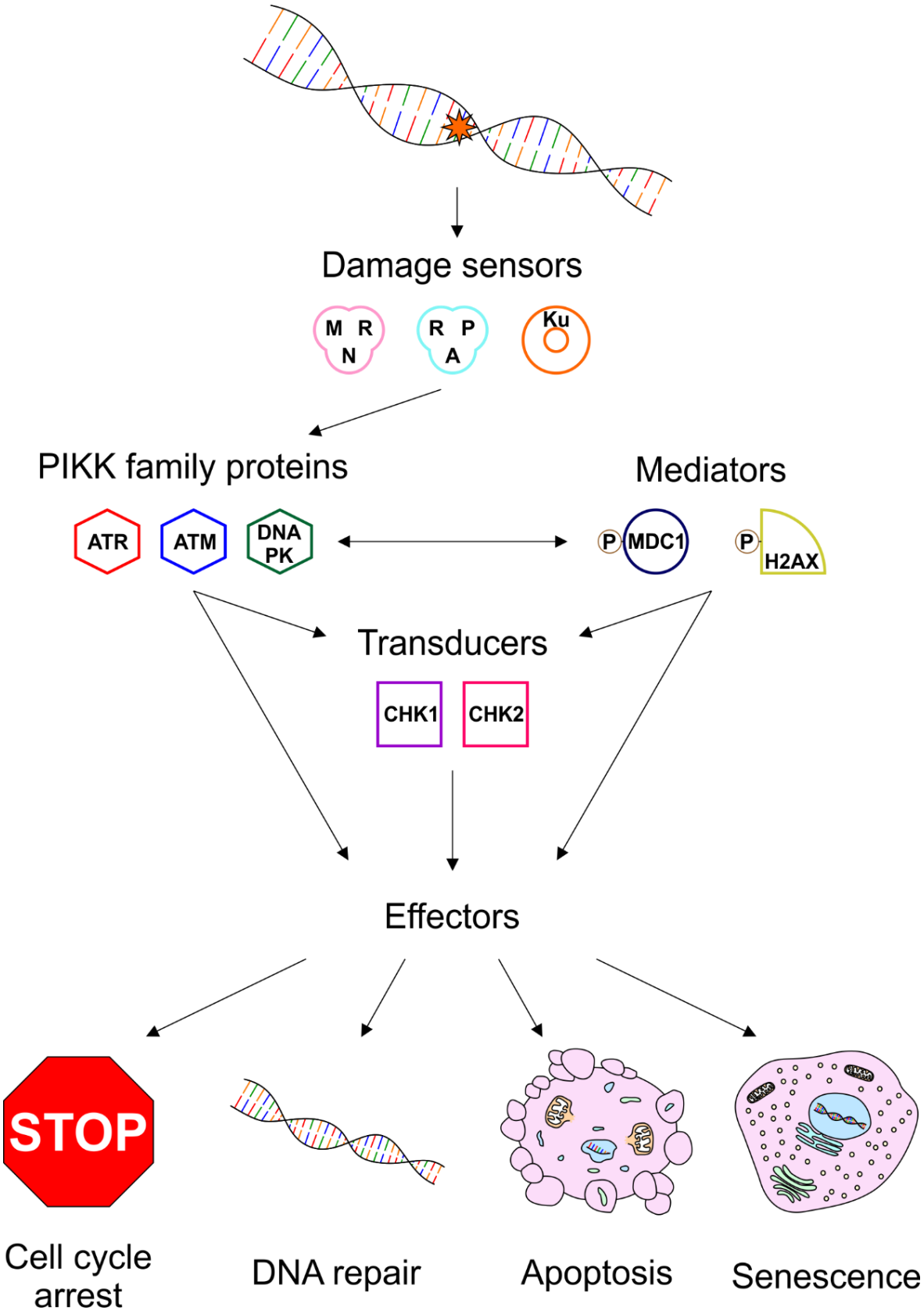

Figure 4: The DNA Damage Response
DNA lesions are directly sensed by proteins resulting in the recruitment of PIKK family proteins. These then act via mediators, transducers and directly with the effectors to bring about cell cycle arrests and DNA repair. Cells may subsequently resume progression through their cell cycle or permanently exit the cell cycle via a death mechanism such as apoptosis or by entering a state of senescence.
Adapted in part from 'The DNA damage checkpoint: putting checkpoints in perspective' (Zhou & Elledge 2000)

1.3.3 G1/S checkpoint

DNA damage experienced before Restriction during the G1 phase poses particular challenges in that it occurs before cells have made an irreversible commitment to entering the cell cycle. Additionally, even if the commitment to cycling has been made the damage now presents a problem for the following S phase where DNA replication must take place. Damaged DNA templates may disrupt replication or result in the production of mutant copied strands that will then be inherited as fixed mutations. The G1/S checkpoint allows for these problems to be avoided via the induction of a cell cycle arrest that gives time for DNA damage recognition, repair and cell fate determination where necessary. Mechanistically there are two major pathways achieving this, quick posttranslational modifications and a slower p53 mediated transcription based process. In the former ATM and ATR kinase activity results in the phosphorylation of the phosphatase Cdc25a, inhibiting it from dephosphorylating inhibitory phosphorylations on Cdk2 (Mailand 2000). Furthermore, cyclin D1 is rapidly degraded inhibiting the formation of active CyclinD-Cdk4/6 complexes (Diehl et al. 1997; Agami 2000). In the latter process phosphorylations stabilise p53 and inhibit its negative regulator Mdm2, thus allowing its transcriptional activity to activate expression of multiple target genes (Vogelstein et al. 2000). These genes are involved in many relevant processes for DNA damage repair but one target in particular, p21, is a CDK inhibitor that prevents cell cycle progression by binding CyclinE-Cdk2 and CyclinD-Cdk4/6 (Wade Harper et al. 1993; Harper et al. 1995; Sherr & Roberts 1995; Dotto 2000).

1.3.4 G2/M checkpoint

During G2 DNA damage occurs in a different context to G1, forthcoming DNA replication is no longer an issue but the irreversible separation into two cells in mitosis is. While in G2 each chromosome has a copy that can be used for error-free DNA damage repair via homologous recombination, but after mitosis this is no longer possible and more error-prone methods become necessary potentially permanently fixing mutations. Furthermore, unrepaired DNA damage during mitosis presents further problems such as the formation of micronuclei as discussed above. Therefore, similarly to G1, the G2/M checkpoints induce a cell cycle arrest following DNA damage.

As in G1, progression from G2 to mitosis is controlled by cyclin-CDK activities, in this case CyclinB1-Cdk1, and the response to DNA damage by this checkpoint involves post-translational modifications to proteins and transcriptional changes (Deckbar et al. 2011). CyclinB1-Cdk1 is kept in an inactive state by phosphorylation by Wee1 and Myt1, while opposing dephosphorylation by Cdc25 phosphatases serves to activate the complex allowing progression into mitosis (Parker & Piwnica-Worms 1992; Liu et al. 1997; Booher et al. 1997; O'Connell et al. 1997). DNA damage signalling through the ATM and ATR kinases leads to the phosphorylation of Cdc25C, which results in Cdc25C being bound by the 14-3-3 protein, anchoring it in the cytoplasm where it can no longer dephosphorylate CyclinB1-Cdk1. Thus

the inactive state of CyclinB1-Cdk1 is favoured and cell cycle progress arrested (Furnari 1997; Peng 1997; Sanchez 1997; Chaturvedi et al. 1999; Kumagai & Dunphy 1999; Lopez-Girona et al. 1999). Then, much as in G1, p53 activation by the DNA damage recognition pathways leads to the upregulation of genes, for example p21, that maintain the arrest over longer time periods (Bunz 1998; Taylor & Stark 2001; Bruno et al. 2006).

1.3.5 G1/S and G2/M Checkpoint recovery

The processes by which resumption of the cell cycle from an arrest occurs are not fully known but it is believed necessary that the activation of DNA damage signalling components be reversed by some means to allow the relevant Cyclin-Cdk complexes to resume their activity (Calonge & O'Connell 2008; Wang et al. 2015). Two observed mechanisms are reversal of DDR kinase induced phosphorylations by phosphatases and degradation of signalling components.

The PP2A phosphatase has been observed to dephosphorylate ATM, γH2AX and Chk1 while Wip1 phosphatase dephosphorylates Chk1, Chk2, p53, γH2AX and p38 (Bulavin et al. 2004; Chowdhury et al. 2005; Shreeram et al. 2006; Macůrek et al. 2010; Yan et al. 2010). Ubiquitin-mediated protein degradation has been shown to be involved in degradation of Wee1, see above, and Claspin, a protein which assists ATR activation of Chk1 (Mailand et al. 2006). (Van Vugt et al. 2004; Mailand et al. 2006)

In addition to its role in mitotic progression Plk1 is also known to be involved in triggering the degradation of Wee1 and Claspin (Van Vugt et al. 2004; Mailand et al. 2006) and promoting recovery from the G2/M checkpoint arrest by antagonising the pro-arrest pathways. Plk1 phosphorylation of Cyclin B1 conceals its cytoplasmic retention signal favouring nuclear localisation (Toyoshima-Morimoto et al. 2001) and phosphorylation of Cdc25 triggers nuclear translocation where it removes inhibitory phosphorylations on Cdk1 (Toyoshima-Morimoto et al. 2002). These changes thus favour the formation of an active Cyclin-CDK complex that drives the cell into mitosis.

1.3.6 S phase checkpoints

S phase marks the period the cell is undertaking duplication of its DNA content in preparation for mitosis and the division into two daughter cells. During this period the entire genome must be accurately replicated and any DNA damage encountered by replication forks, the assembled machinery of protein complexes that facilitate DNA replication, risks mutations being permanently fixed in the genome. Three different forms of cell cycle checkpoints active in S phase have been identified, the replication checkpoint, the intra-S-phase checkpoint and the S-M checkpoint, of which the first two are responsive to DNA damage (reviewed extensively in (Bartek et al. 2004). In contrast to the relatively robust G1 and G2 cell cycle arrests following DNA damage detection cell cycle progression in S phase is considered to slow transiently upon the induction of DNA damage and will inevitably continue onto G2 even if the damage remains unresolved.

The replication checkpoint manages active replication forks which encounter stresses, such as damaged DNA or aberrant DNA structures, capable of stalling replication fork progression. DNA helicases ahead of the now stalled replication fork continue to unwind DNA, so exposing single stranded DNA which when coated with RPA activates ATR signalling. Activation of this checkpoint inhibits DNA replication beginning from unfired origins of replication by targeting the cyclin-CDK and CDC7-DBF4 kinases responsible for origin firing (Dimitrova & Gilbert 2000; Jares et al. 2000). This allows time for the DNA repair machinery to repair the damage and for the stalled fork to restart progression following resolution of the damage.

The intra-S-phase checkpoint is activated by double-strand breaks and unlike the replication checkpoints acts independently from active replication forks. This checkpoint appears to have little effect upon the extension of active replication forks but is capable of inhibiting firing of unfired replication origins by inhibiting the recruitment of replication initiation proteins (Painter & Young 1980; Merrick et al. 2004; Costanzo et al. 2000; Falck et al. 2002). As in the G1/S and G2/M checkpoints, ATM and ATR play a central role, with ATM recognising double strand breaks and ATR recognising those breaks that have undergone processing to reveal stretches of single stranded DNA. ATM and ATR signal through their downstream effectors to inhibit cell cycle progression through Cdc25a inhibition (Bartek & Lukas 2003).

1.3.7 Spindle Assembly Checkpoint

The spindle assembly checkpoint differs from the DNA damage responsive checkpoints in how it maintains genomic integrity. This checkpoint contributes to ensuring the reliable segregation of chromosomes to daughter cells, crucial to ensuring that the correct complement of DNA is inherited at each division, preventing daughter cells from having extra or fewer copies of DNA and thus having altered genomes. Following S phase a cell has two copies of each chromosome paired together as sister chromatids. Condensation of the DNA into highly compacted chromatin during mitosis generates sister chromatids physically linked by a multimeric protein ring structure known as cohesin. During metaphase these sister chromatids align at the centre of the cell along the metaphase plate due to regions of the chromatids called centromeres interacting via structures called kinetochores with the mitotic spindle, a microtubule based structure that forms a bipolar structure. Each chromatid in the chromatid pairs binds to a spindle fibre emanating from one of the two poles of the cell. Upon the transition to anaphase the remaining cohesin binding chromatids together is broken, the sister chromatids separate and segregate to the opposite poles of the cell due to the forces generated through the action of motor proteins. Cytokinesis of the cell thereby permanently separates the chromatids as they form chromosomes in the resultant daughter cells.

However, if this process occurs before all chromatid pairs have attached to the mitotic spindle, those left unattached will fail to appropriately separate and segregate, potentially leading to one daughter cell having more copies of some chromosomes than the other. The solution to this problem exists in the form of the mitotic checkpoint complex (MCC), a complex formed of BubR1, Bub3, Mad2 and Cdc20. Assembly of this complex is catalysed by unattached kinetochores ensuring it will remain active until all kinetochores have achieved a bipolar attachment to the mitotic spindle. This MCC is capable of inhibiting the activation of the anaphase promoting complex (APC/C), an ubiquitin ligase responsible for driving degradation of proteins required for completion of mitosis, including securin, the inhibitor of separase, the enzyme responsible for cleaving the cohesin ring. Thus the MCC prevents cleavage of cohesin and so delays the transition to anaphase until all kinetochores are attached (these and other aspects of the SAC are reviewed extensively in Lara-Gonzalez et al. 2012).

1.3.8 Significance for cancer and disease

Intuitively the idea of a period of extra time for DNA repair in the form of a cell cycle arrest before resuming the cell cycle makes sense as a mechanism to restrain mutation of the genome and so avoid the resultant risks of cancer and loss of functional cells. Repairing DNA damage before transitioning from G1 to S avoids fixing mutations by replicating damaged DNA, while repairing DNA damage before mitosis prevents missegregation of damaged strands during mitosis and daughter cells inheriting damaged DNA without having sister chromatids as a template to correct from. The most striking evidence supporting their importance comes from patients carrying germline mutations in various components of checkpoint signalling, indeed some of these components were discovered due to the severe disease that results. One such example is Ataxia Telangiectasia, the syndrome that gives its name to ATM (Ataxia Telangiectasia mutated protein) which is characterised by neurodegenerative symptoms from a young age and an increased predisposition to developing cancer (Painter & Young 1980; Hecht & Hecht 1990; Savitsky et al. 1995). Another example is Li-Fraumeni syndrome, a condition again resulting in a much greater incidence of cancer, but associated with mutations in p53, an important mediator of the checkpoint response (Li & Fraumeni Jr 1969; Kamihara et al. 2014). Clearly the checkpoints are of great importance in restraining the development of cancer and other diseases as losses of even individual components can produce dramatic phenotypes. Furthermore, the importance of checkpoint mechanisms in day-to-day cellular processes is further revealed when one considers that ATR, one of the DNA damage recognition kinases, is an essential gene and that knockout results in embryonic lethality (Takai et al. 2000; De Klein et al. 2000; Liu et al. 2000; Brown & Baltimore 2000).

1.3.9 Checkpoint negligence

Our understanding of the ability of checkpoints to detect and respond to damage has evolved over time. At one point it was thought that both the G1 and the Spindle Assembly Checkpoint (SAC) were likely to be stringent enough to reliably catch a single aberration. For the G1/S checkpoint this is based on studies involving injecting DNA constructs equivalent to a double strand break, such as linearised plasmids, and from estimations of the kinetics of arrest in response to varying doses (Huang et al. 1996; Steven P Linke et al. 1997). Destruction of a single remaining unattached kinetochore was shown to result in the cell entering anaphase, suggesting the SAC was capable of responding to a single unattached kinetochore (Rieder et al. 1995).

However, further studies for both the G1 checkpoint and SAC have revealed that the checkpoints are not so stringent as perhaps thought. Instead they are known under certain circumstances to either not trigger a checkpoint response or once one has been triggered to resume cell cycle progression without fully resolving the damage. For the purposes of this work, this process will be described as 'checkpoint negligence', as used in (Löbrich & Jeggo 2007). One study of the response of the G1/S checkpoint to DNA damage induced when a cell is in late G1 phase proposes the block on S phase entry takes several hours to initiate fully and so late G1 phase fibroblast cells can enter S phase without arresting following irradiation. This period of time has been estimated to extend to as much as 4-6 hours after irradiation even with high doses of DNA damage (Gadbois & Lehnert 1997; S P Linke et al. 1997; Deckbar et al. 2010). Similarly, another study indicates that 65% of late G1 primary Mouse Embryonic Fibroblasts (MEFS) receiving 5 Gy irradiation can enter S phase and that there may exist a point in the G1 phase where cells can no longer respond to the signals that would otherwise initiate a cell cycle arrest (Cann & Hicks 2006).

In terms of actual DNA damage, Artemis -/- fibroblasts (cells defective in repairing a subset of double strand breaks) entering S phase early after irradiation were observed to do so with elevated 53BP1 foci, while wild type fibroblast cells entering S phase early after irradiation in G1 were observed to have elevated γH2AX foci. Furthermore, the formation of chromosome breaks in the subsequent G2 and mitosis of fibroblast cells irradiated in G1 (Deckbar et al. 2010). These results would suggest that even if the G1/S checkpoint can be responsive to single breaks, the ability to initiate and maintain an effective cell cycle arrest until the damage is resolved is lost before the end of the phase.

Similarly, for the SAC experimental manipulation of chromosome attachment to the spindle suggests that cells can still enter anaphase even in the presence of a failed alignment. In one example over 30% of HeLa cells entered anaphase following laser detachment of one chromosome from the metaphase spindle and it has been proposed there may be a time window of approximately 5 minutes before the

onset of anaphase in which the APC/C is no longer responsive to unattached chromosomes (Dick & Gerlich 2013).

The fidelity and behaviour of the G2/M checkpoint has been characterised by a number of observations as being relatively negligent regarding the residual number of double strand breaks left when the transition to mitosis takes place. In yeast cells a G2 arrest with an irreparable double strand break can eventually undergo a process sometimes termed 'checkpoint adaptation' whereby the cell cycle undergoes recovery from the arrest and so continues despite the presence of apparently unresolved DNA damage (Syljuåsen 2007), interestingly a similar phenomenon appears to occur in mammalian cells. Artemis deficient human fibroblast cells are defective in the repair of a subset of double strand breaks, and so they have a number of breaks that persist longer than in wild type cells. Nonetheless these cells were observed to enter mitosis following a G2 arrest when a predicted 9-12 double strand breaks would be present. Assessing chromosomal aberrations in the cells entering mitosis in both Artemis deficient and wild type fibroblast cells revealed that for both cell types chromosome breaks were present at a rate significantly greater than in undamaged cells. The observation that DNA damaged Artemis cells take longer than wild type cells to enter mitosis but do so with similar number of γH2AX foci suggested that a threshold of double strand breaks may exist which determines when cells can enter mitosis. Assessing premature chromosome condensation breaks in cells that entered mitosis provided further evidence suggesting the existence of such a threshold, premature chromosome condensation breaks have been associated with 3-6 double strand breaks thereby giving an estimate of approximately 10-20 breaks. Furthermore, counting of γH2AX foci in various cell types at the entry into mitosis also suggests around 20 breaks per cell. These varying estimates give slightly different but comparable thresholds. (These findings are detailed in Deckbar et al. 2007)

Similarly demonstrating checkpoint negligence, but suggesting a different mode of regulation, a recent study from our laboratory proposed another model to explain the behaviour of the G2 checkpoint regarding unrepaired DNA damage (Liang et al. 2014). Utilizing a FRET reporter for Plk1 activity, U2OS (a human osteosarcoma cell line) cells were seen to accumulate Plk1 activity as they progress towards mitosis, eventually reaching a threshold of activity that results in entry into mitosis. Examining the cells damaged during their G2 phase which went on to enter mitosis revealed that Plk1 activity continued to increase following DNA damage, but at a slower rate than in undamaged cells. In this model therefore it is not the amount of DNA damage that is most important, rather it is Plk1 activity relative to a threshold sufficient for mitotic entry. Supporting this were the observations that cells with higher Plk1 activity at the time of damage tended to enter mitosis earlier than those with lower Plk1 activity and that these cells had higher levels of residual DNA damage, suggesting that in this case the checkpoint was not operating with a defined DNA damage threshold. Instead cells were moving towards mitosis at a slower rate due to the DNA damage but if Plk1 levels were already high at the

time of damage these cells were already more predisposed to mitotic entry. As these observations were based upon those cells that eventually entered mitosis within the experimental timeframe there remain open questions over whether longer G2 arrests might be regulated more directly by the level of DNA damage remaining and/or whether Plk1 activity can decline or remain static rather than always increasing.

These examples demonstrate that checkpoints are clearly capable of varying degrees of negligence, albeit manifesting in different and only partly understood ways, despite the established importance of checkpoints in maintaining genome stability. In the case of a single celled organism such as yeast this is understandable, faced with damage still unresolved after many hours the cell may as well attempt to continue proliferation rather than arrest indefinitely. In the case of multicellular organisms however, the risk of re-entering the cell cycle with unresolved damage is that the damage will ultimately be resolved in a deleterious manner that compromises the cell. This may be as serious as a cell newly set upon the path to unrestrained proliferation. That multicellular organisms apparently tolerate this rather than reliably activating senescence or cell death programmes of behaviour is a curiosity. How we reconcile the observed checkpoint negligence with the apparently low risk of any individual DNA damaged cell acquiring sufficient mutations to lead to cancer is an open question.

1.3.10 The response of subsequent checkpoints

If checkpoints have been established as negligent then this raises the question of what happens to the damage in subsequent phases of the cell cycle and how the cell cycle checkpoint mechanisms respond to it. Perhaps DNA damage tolerated by negligent checkpoints has little consequence as DNA repair mechanisms can fix it in later cell cycle phases. However, if subsequent checkpoints are similarly negligent then DNA damage could potentially persist indefinitely which would be expected to eventually lead to one or more of the consequences outlined previously in 1.2.3. Another possibility is that either DNA damage passing through checkpoints is marked in some way or that DNA damage in previous phases changes the cell context by some mechanism, for example changes in the proteome. This could create an effective ‘memory’ of having previously experienced DNA damage such that checkpoint responses are altered in how they respond to the inherited DNA damage. Such mechanisms could conceivably compensate for previous negligent behaviour.

There are not yet definitive answers to whether any of these speculations are accurate, but there have been several observations of checkpoint responses in both subsequent cell cycle phases and in descendant cells indicating that transmission of DNA damage between cell cycle phases is likely to be a significant biological phenomenon.

In one study NHF3 and RPE-h cells irradiated in G1 which progressed into the first S phase were observed to arrest at the subsequent G1 checkpoint of descendant cells. Interestingly, this was also

observed in p53 null cells that were insensitive to arrest at the initial G1 (Steven P Linke et al. 1997). Similarly, in wild type and Artemis -/- fibroblast cells irradiated during G2 that pass through the G2/M checkpoint and mitosis it was found there were fewer subsequent G2-M phase cells (in the next cell cycle) than unirradiated controls, interpreted as daughter cells having potentially undergone prolonged G1-S arrest (Deckbar et al. 2010).

In another study it was observed that human RPE cells treated transiently with nocodazole, a microtubule depolymerising agent, were capable of completion of mitosis but their daughter cells experience a p38 and p53 dependent G1 arrest if prometaphase took over 1.5 hours. Interestingly, if the activity of p38 in the G1 arrested daughter cells is abolished by a small molecule inhibitor (SB 203580), the G1 arrest is abrogated, cells continue the cell cycle and divide. The resultant cells themselves then, in the absence of the inhibitor, arrest again in G1. These cells are the granddaughters of those cells that were initially treated with nocodazole, suggesting a persistence of the signal to arrest through the generations even when the intervening generation had experienced a cell cycle and mitosis of apparently normal duration (Uetake & Sluder 2010).

Similarly, endogenous replication stress can also cause consequences in daughter cells; for instance, 53BP1 foci containing daughter cells, a marker of unresolved replication errors from the mother cell, were found to enter a transient quiescent state, as determined by a Cdk2 activity sensor, for a duration correlated to the extent of the damage. (Arora et al. 2017)

Therefore, it is becoming apparent that while checkpoints demonstrate a degree of negligence in response to DNA errors, there may be responses by subsequent checkpoints to unresolved damage. Cross-checkpoint cooperation could conceivably compensate for the negligence of earlier checkpoints allowing for DNA damage to be reassessed, further repair to be undertaken or cell cycle exit via senescence or apoptosis to be triggered.

1.3.11 Differential checkpoint activation

Different lesions signal through different components of the checkpoint signalling apparatus but it has also become apparent that the genomic context of a lesion is also important in determining the signalling and resultant cell fate. Telomeres are the end regions of linear chromosomes and therefore represent a break in the DNA strand and inappropriately carrying out DNA repair processes on such ends can trigger massive changes in chromosomal organisation (Artandi et al. 2000). These ends are therefore typically protected by the formation of a T-loop whereby the end of the DNA inserts into a region upstream and by the binding of a protein complex called shelterin which inhibits the DNA repair machinery attempting to process the ends of the chromosomes (Griffith et al. 1999; De Lange 2010). Deprotection of these telomere ends by partial loss of TRF2, a component of shelterin, was shown to result in recognition of the chromosome ends by ATM and the presence of its activating

phosphorylation on residue S1981 indicating ATM activity. However, no activating Chk2 T68 phosphorylation was observed and no G2/M arrest could be inferred from changes in the cell cycle profile of populations of cells experiencing telomere deprotection. Instead cells were observed to pass through to G1 and subsequently arrest there via a p53-mediated G1 arrest and thereafter permit senescence to develop (Cesare et al. 2013). The rationale for this may be that as telomere erosion occurs during replication any resultant deprotected telomeres will be present during G2. If these were to trigger the typical DDR the cell would arrest and attempt to repair what is not actually a genomic break, possibly resulting in fusion of separate chromosomes. The resultant mutant cells could then enter mitosis, risk further mutation via breaking of fused chromosomes, and then risk continued proliferation. Instead, by avoiding the typical DDR in G2 a stable senescence response can be undertaken in the resultant diploid G1 daughter cells withdrawing them permanently from the cell cycle. In this instance, and perhaps in other as yet undiscovered cases by other mechanisms, genomic context influences checkpoint behaviour and ultimately cell fate determination.

1.3.12 Permanent exit from the cell cycle

Activation of the checkpoint arrest allows time for DNA repair by arresting progression of the cell cycle, but in certain circumstances, for example severe levels of DNA damage, it may no longer be capable of accurate repair. In this case there are three options, continue with the cell cycle regardless, activate a programmed cell death mechanism such as apoptosis, or enter a state of senescence (Norbury & Zhivotovsky 2004; d'Adda di Fagagna 2008). The negligence of checkpoints described above clearly indicates the first option is possible, albeit problematic considering the consequences of un/mis-repaired DNA damage. The latter two however provide mechanisms to permanently restrain aberrant cells from proliferating and thus risking cancer development. Additionally, these mechanisms are known to be triggered by other stimuli, for example the activation of oncogenes, also helping restrain the proliferation of aberrant cells.

1.3.13 Programmed cell death - Apoptosis

Prolonged cell cycle arrest allows for numerous pathways promoting cell death to be upregulated. One of the most well studied forms of programmed cell death is apoptosis, a non-inflammatory process resulting in orderly destruction of the cell which can be activated by both an intrinsic and extrinsic pathway (Figure 5) (Reviewed extensively in Nowsheen & Yang 2012). The intrinsic pathway refers to activation of apoptosis by pro-apoptotic Bcl-2 family proteins triggering mitochondrial permeabilisation. This leads to the release of cytochrome c, which activates APAF-1 leading to the formation of the apoptosome which activates caspase 9 by cleavage, caspase 9 then activates downstream effector caspases such as caspase 3 and 7 which themselves lead on to activation of various components that drive the apoptotic process, for example activation of DNAses to destroy the

nuclear genome. The extrinsic pathway in contrast is activated by signalling through external cell receptors called Death receptors. One such receptor is FAS, which is bound by the Fas ligand leading to activation of caspase 8 which in turn activates caspases 3 and 7 much like the intrinsic pathway. These pathways are not mutually exclusive as the extrinsic can trigger the intrinsic pathway via cleavage of BID to tBID, a pro-apoptotic BH3 family protein. A number of signalling pathways are known to activate apoptosis following DNA damage, some of which are described here.

One of the most important signalling nodes is the 'guardian of the genome' p53. p53 is post-translationally modified and expressed at high levels following DNA damage due to the influence of upstream DDR components. Depending on its abundance, dynamics and modification status, p53 influences numerous processes including cell cycle arrest, DNA repair, senescence and indeed apoptosis by several means (Vogelstein et al. 2000). p53-dependent transactivation of pro-apoptotic Bcl-2 family proteins BID, BAD, PUMA and NOXA promotes permeabilisation of the mitochondrial membrane triggering apoptosis via the intrinsic pathway (Oda 2000; Nakano et al. 2001; Sax et al. 2002; Jiang et al. 2006). Additionally, p53 also upregulates FAS, a cell surface receptor for the Fas ligand capable of activating the extrinsic pathway to apoptosis, thus predisposing the cell to apoptosis when Fas ligand is also present (Owen-Schaub et al. 1995). p53 is also capable of activating apoptosis through other means than its role as a transcription factor, p53 directly activates apoptosis through interactions at the mitochondrial membrane via the pro-apoptotic proteins BAK and BAX (Marchenko et al. 2000; Chipuk 2004; Leu et al. 2004).

Several p53-independent mechanisms also exist, explaining apoptotic cell death following DNA damage in cells lacking wild type p53 function. Chk2, once activated by ATM, phosphorylates E2F-1 shifting its specificity for transcriptional upregulation to selected targets, including p73, a homolog of p53 also capable of promoting apoptosis (Nahle et al. 2002; Stevens et al. 2003; Pediconi et al. 2003). Rad9, a component of the Rad9-Hus1-Rad1 (9-1-1) complex involved in DNA damage recognition has been shown to interact with anti-apoptotic Bcl-2 and Bcl-XL and is reported to induce apoptosis when overexpressed, suggesting it may be able to antagonise anti-apoptotic members of the Bcl-2 family (Komatsu et al. 2000). Nur77, a nuclear receptor, is induced by DNA damage and has been implicated in the activation of the intrinsic pathway of apoptosis possibly by translocation to the cytosol (Li et al. 2000; Wilson et al. 2003). Procaspase 2, the inactive form of caspase 2 resident in the nucleus, is activated following DNA damage where it then activates the intrinsic pathway of apoptosis by processing Bid into its pro-apoptotic derivative tBid (Guo et al. 2002).

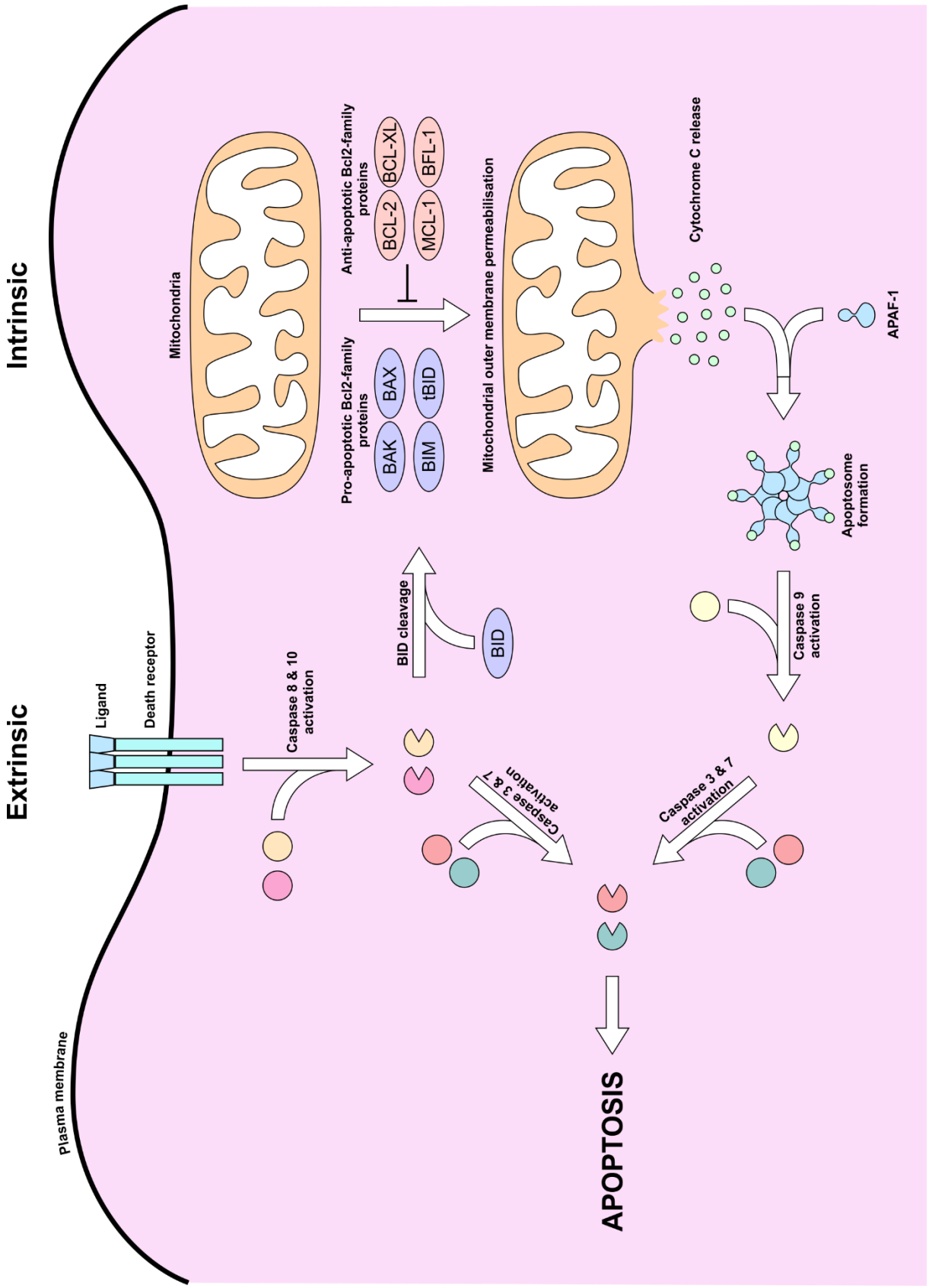

Figure 5 The intrinsic and extrinsic activation pathways in apoptosis
Adapted in part from (Lawton 2016)

An important consideration is that cells differ in their likelihood to engage cell death mechanisms following DNA damage (Liu et al. 2014). The characteristic symptoms of radiation sickness and DNA-damaging chemotherapeutics used to treat cancer comes from the death of many of the cells that actively divide to maintain tissues such as in hair follicles and the intestinal lining (Yu 2006; Blanpain et al. 2011). In contrast, there is evidence that terminally differentiated cells can be less sensitive (Latella et al. 2004; Schneider et al. 2012). This behaviour suggests that cell fate decisions at the DNA damage checkpoint are weighted choices between survival and death: some cells are more at risk of causing cancer than others and so these may preferentially die while less at risk cells are instead more tolerant of DNA damage and survive to prevent unnecessary challenges to the maintenance of tissue homeostasis.

1.3.14 Senescence

Senescence in contrast to apoptosis leaves the cell alive but in a distinctive state of permanent cell cycle arrest mediated by p16 and p21 which potently inhibit Cyclin-Cdk4/6 and Cyclin-Cdk2, so preventing all the steps necessary to commit to cycling at restriction and enter S phase. Senescent cells adopt a different morphology becoming much larger and flatter, exhibit persistent DNA damage foci known as Senescence-Associated Heterochromatin Foci (SAHF), and exhibit a characteristic Senescence-Associated Secretory Phenotype (SASP) featuring the upregulated production and secretion of interleukins, chemokines, growth factors and other inflammatory factors (extensively reviewed in Campisi & d'Adda di Fagagna 2007). Senescence can be triggered by several stimuli including DNA damage, replication stress following erosion of telomeres, and the activation of oncogenes, it has also been implicated in normal development (Muñoz-Espín et al. 2013), acting to shape development of organs and tissues in a similar way to apoptosis, and in wound repair, where senescent cell ablation leads to greater fibrosis and scarring (Krizhanovsky et al. 2008; Jun & Lau 2010; Demaria et al. 2014). It is known to be possible to enter the state of senescence from both G1 and G2 following DNA damage and in the latter case this can involve a 'skipping' of mitosis resulting in the formation of tetraploid senescent cells (Johmura et al. 2014).

In the context of DNA damage senescence therefore is an alternative way of achieving the same end as cell death in the sense of removing the risk of mutated cells proliferating. However, it is becoming clear that other attributes of senescence are also of great relevance to cancer. In contrast to cells undertaking apoptosis, generation of the SASP by senescent cells results in inflammatory paracrine signalling, which has been characterised as being capable of both promoting and preventing the development of tumours. A number of observed effects on cell proliferation, invasion, migration, metastasis and immune infiltration show pro-tumourigenic effects (reviewed extensively in Coppe et al. 2010) while evidence that the SASP can hinder tumour development comes in the form of observations that the SASP may reinforce and maintain the senescent state (Kortlever et al. 2006;

Acosta et al. 2008; Kuilman et al. 2008; Wajapeyee et al. 2008), induce senescence in neighbouring (and thus possibly cancerous) cells through a senescence 'bystander' effect (Acosta et al. 2013), and attract immune cells to clear cancerous cells (Xue et al. 2007; Kang et al. 2011).

1.3.15 Apoptosis vs senescence

Whether a cell undertakes apoptosis or senescence following DNA damage involves decision making processes within the cell that are not completely understood, although, there are some clues to how this decision is made. Different cell types are known to have different sensitivities to senescing; it has been reported that human fibroblasts senesce upon 50 Gy of radiation, while T lymphocytes senesce following only 2 Gy (Childs et al. 2014). Intensity of damage appears to play a role too as MCF7 breast cancer cell lines senesce when treated with relatively low doses of doxorubicin but apoptose following high doses (Song et al. 2005). Human fibroblasts show the same trend of senescence vs apoptosis depending on intensity of dose when treated with UVB irradiation (Debacq-Chainiaux 2005). The type of damage also plays a role as WI38 fibroblasts receiving busulfan treatment, which produces bulky DNA adducts, senesce and do not apoptose at all tested dose intensities (Probin et al. 2006).

Mechanistically, control between temporary cell cycle arrest, apoptosis and senescence is in part regulated through p53 signalling (Kirschner et al. 2015). p53, as discussed above, is a transcription factor known to control the expression of many sets of genes involved in various processes. Regulation of which sets of genes are upregulated is extremely complex but is known to depend on which post-translational modifications are present on p53 molecules, the levels of p53, and the kinetics and dynamics of p53 activation. Examples of these include:

- Loss of acetylation on K117 shifts cell fates to apoptosis as PUMA and NOXA are no longer upregulated, while additionally loss of acetylation on K161 and K162 results in loss of cell cycle arrest and senescence (Li et al. 2012).
- Upon treatment with H_2O_2 human diploid fibroblasts that go on to apoptose have around twice the levels of p53 as those that senesce (Chen et al. 2000).
- Transient pulsatile activation of p53 results in cell cycle arrest and eventual recovery while sustained p53 stabilisation results in senescence. (Purvis et al. 2012)

The p53 target p21 plays a significant role in influencing the senescence vs apoptosis decision. p21 is involved in facilitating cell cycle arrests in the initial response to DNA damage but also functions to generate the permanent state of cell cycle arrest manifested in senescence. Studies have suggested there may be an inverse relationship between p21 and apoptosis whereby high p21 suppresses apoptosis and low p21 is permissive for apoptosis (Gartel & Tyner 2002). Knockdown of the p21 inhibitor DNMT3a in colorectal carcinoma cells treated with high doses of doxorubicin was able to

switch the cells from apoptotic cell fates to senescence instead (Zhang et al. 2011), similarly caspase 3 inhibition switched neuroblastoma cells from apoptosing to senescing (Rebbaa et al. 2003).

The level of mediators of apoptosis in the cell are also known to have a role in influencing which of the terminal cell fates is adopted. Overexpression of anti-apoptotic Bcl-2 can switch irradiated fibroblasts from favouring apoptosis to favouring senescence (Yang et al. 1997), while knockdown of anti-apoptotic Bcl-XL can switch the typical fate of irinotecan-treated colon cancer cells from senescence to apoptosis (Hayward et al. 2003).

Clearly the many ways in which p53 activity can be modulated and how susceptibility to apoptosis depends in part upon the abundance of mediators indicates that whether apoptosis or senescence is favoured by a cell type depends on the proteome.

What exactly the evolutionary rationale might be for some cells favouring apoptosis over senescence and vice versa following DNA damage is unclear but it may be related to whether the relatively cell-autonomous mechanism of apoptosis is sufficient to prevent tumour development or whether the communication with adjacent cells and the engagement of the immune system that the SASP allows is beneficial within the tissue that the cell normally resides (Childs et al. 2014).

1.4 The analysis of cell cycle dynamics and cell fate

In the past decade several studies have advanced the tools and experimental approaches to facilitate greater analysis of cell cycle dynamics and understanding of the significance of these for cell fates. Several examples of these and how they have advanced understanding of the cell cycle are discussed below.

1.4.1 Cell cycle phase determination with the FUCCI system

Progression through the cell cycle can be visualised with a well-established set of fluorescent reporters known as the Fluorescent Ubiquitination-based Cell Cycle Indicator (FUCCI). These genetically encoded reporter proteins are formed from the fusion of fluorescent proteins (proteins that generate a fluorophore capable of emitting light following excitation with light of a higher frequency) with the sequences responsible for ubiquitination mediated degradation of the endogenous hCdt1 and hGeminin proteins within the cell. During the cell cycle the APC^{Cdh1} and SCF^{Skp2} E3 ligase complexes tag proteins for degradation with ubiquitin. The activities of these two ligases alternate throughout the cell cycle with APC^{Cdh1} activity present during mitosis and G1, while SCF^{Skp2} is active during S and G2. Certain proteins are targeted by these ligases for degradation which allows for cell cycle regulation of protein abundance. Cdt1 and Geminin are two such proteins, Cdt1 is targeted for destruction in S and G2 while Geminin is degraded in S and G2. Regions of the proteins identified as responsible for the cell cycle dependent ubiquitination were found to confer the same regulation over abundance when fused

to fluorescent proteins. Importantly, these minimal degradation sequences were also found to not alter the cell cycle so allowing for the generation of sensors that would not directly perturb the cell cycle. The original publication used monomeric Kusabira Orange 2 (mKO2) tagged hCdt1 (mKO2-hCdt(aa30-120)) and monomeric Azami Green (mAG) tagged hGeminin (mAG-hGeminin(aa1-110)), while subsequently an mCherry tagged hCdt1 was also developed (Table 2).

Name:	Biological Origin	Excitation (nm)	Emission (nm)	Reference:
mAG	*Galaxeidae*	492	505	(Karasawa et al. 2003)
mKO2	*Fungia concinna*	551	565	(Sakaue-Sawano et al. 2008)
mCherry	*Discosoma*	587	610	(Shaner et al. 2004)

Table 2: Fluorophores used in combination with hGem/hCdt1 based probes

This produced sensors that allow the identification of which cell cycle phase a cell is in, G1 cells are fluorescently red (mKO2 or mCherry), S and G2 phase cells are green (mAG), mitotic cells show little to no fluorescence and cells transitioning from G1 to S phase exhibit both red and green fluorescence (Sakaue-Sawano et al. 2008) (Figure 6A and B). Furthermore, monitoring the fluorescence in time-lapse microscopy allows determination of the duration of G1 and the combined S&G2 phases of the cell cycle (Figure 6C). This ability has been utilised in a great many studies where cell cycle dynamics are of interest and in the context of DNA damage allows identification of cell cycle arrests following DNA damage. This has been demonstrated in studies assessing the response of HeLa cells to UV and X-ray irradiation which found the FUCCI system to be capable of identifying the known HeLa deficiency in G1 arrest, observed that UV irradiation resulted in differential survival depending on the phase of the cell cycle in which they were treated, and observed that cells arresting for longer following X-ray radiation appeared to have daughter cells that also demonstrated longer cell cycles suggesting some inherited DNA damage response (K Kaminaga et al., 2015; Kiichi Kaminaga, Kanari, Narita, & Noguchi, 2014; Miwa et al., 2015; Narita et al., 2015). Another example has been the use of the FUCCI system to investigate cell cycle checkpoints in three-dimensional spheroid cultures of Capan-2 cells treated with etoposide. This allowed the cell cycle dynamics within a three-dimensional structure to be assessed, revealing a proliferation gradient whereby cells in the outermost layer proliferate the most while those in the centre proliferate by much less, indeed likely entering a state of quiescence. Etoposide treatment indicated that etoposide treatment was able to induce phospho-H2AX throughout the spheroid and a G2/M checkpoint arrest was evident by the increase in abundance of S/G2 FUCCI probe positive cells relative to the G1 FUCCI probe positive cells (Laurent et al. 2013).

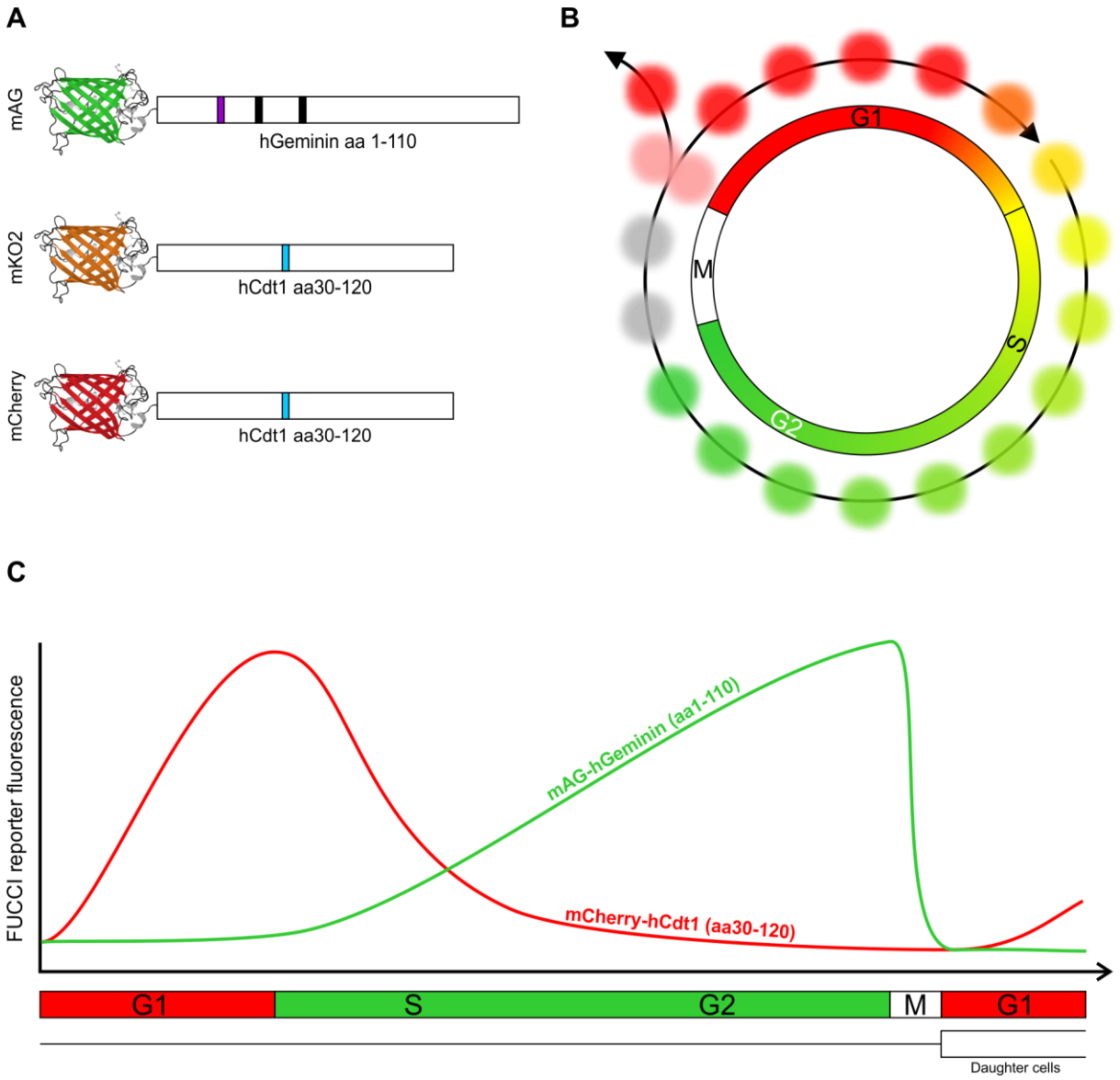

Figure 6: The FUCCI system
***A**) The FUCCI probes are formed from the fusion of a fluorescent protein with the sequences responsible for cell cycle dependent degradation. hCdt1(aa30-120) and hGeminin (aa1-110) confer G1 and S&G2 specificity of the fluorescent probes respectively. Fluorescent protein diagrams kindly provided by Dr Alessandro Esposito.*
***B**) As cells progress through the cell cycle their nuclei will fluoresce different combinations of colours. Red/orange in G1, yellow as the two probes overlap during the transition into S phase and green during the remainder of S phase and G2. During mitosis all FUCCI fluorescence is lost.*
***C**) Example traces of nuclear fluorescence measured throughout a cell's lifetime and the start of a daughter cell's. At birth fluorescence is low but cells accumulate red fluorescence quickly. As the cells transitions into S phase the G1 probe begins to be degraded causing the red fluorescence to peak and decline while the SG2M probe now accumulates. At mitosis fluorescence drops dramatically.*

1.4.2 Microscopy-based lineage tracing

Time-lapse microscopy also permits lineage tracing whereby familial relationships between cells can be identified, and thereby correlations be made. Two examples of studies employing these methods are discussed below in order to exemplify how their work inspired and informed the approaches taken in this work.

One recent study taking this approach with L1210 human lymphoblast cells expressing the two FUCCI probes allowed the cell cycle dynamics of three generations of cells (Figure 7) to be analysed and compared (Sandler et al. 2015). From this data total cell cycle (T^{tot}), G1 (T^{G1}) and combined S, G2 and M (T^{G2}) lengths could be obtained on a single cell basis and compared to their relatives. All three measures of length were found to correlate highly and statistically significantly between sister cells (correlation coefficients $\rho = 0.71 \pm 0.007$ $P < 0.002$) while mother-daughter correlations were close to zero and not statistically significant. Initially these results suggested an inherited factor at birth that siblings inherit together that determines at least partially the length of the cell cycle and the subsequent cell cycle phases. As mothers and daughters do not correlate this factor might be reset at each division leading to the lack of correlation observed. However, somewhat surprisingly, cousin cells were found to correlate significantly as well ($\rho = 0.58 \pm 0.07$ $P < 0.002$) casting doubt on this initial interpretation. If the inherited factor were reset at each division then this cannot explain the correlation of cousins, which are related via mother-daughter relationships. This type of data could then be analysed with the Grassberger-Procaccia algorithm to indicate that deterministic processes were likely to underlie the cell cycle lengths observed, allowing the authors to develop a model of cell cycle behaviour that could better explain their observations than a previously published model (R. & R. 1986). This 'kicked cell cycle' model proposed a cellular oscillator that determines the duration of the cell cycle depending on what phase it is in. Siblings inherit the same phase of the oscillator and thus their cell cycle lengths correlate well together. Mothers and daughters by contrast inherit phases of the oscillator which may be similar or very dissimilar and so do not correlate well. This could also explain the cousin correlations, sisters born with the same phase of the oscillator have cell cycle durations of similar length, thus when they themselves divide, forming a series of cousins, these cousins are also likely to inherit similar phases of the oscillator and thus have cell cycles that will correlate together. This demonstrates that assessment of cell cycle dynamics with the FUCCI system combined with lineage information was capable of providing insights into cell behaviour via mathematical modelling.

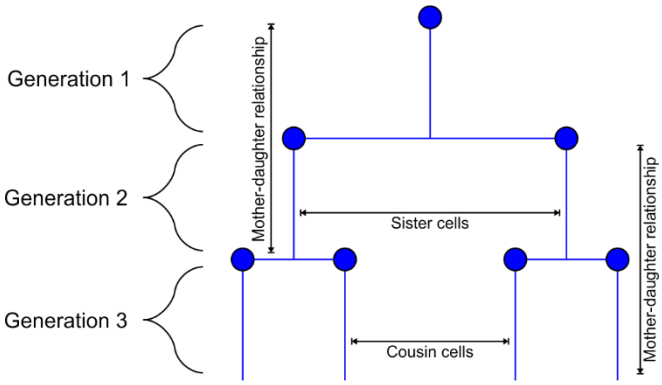

Figure 7: Three generations of a lineage and the familial relationships examined

As this study concerned only unperturbed cells, taking similar approaches to cells that have experienced DNA damage and their descendants might yield further insights. Indeed, one recent publication, briefly mentioned above (Arora et al. 2017), has identified endogenous replication stress in the mother cell's S phase as a cause of a period of entry into a quiescent G0 phase in the daughter

cells. Tracking of unperturbed dividing MCF10A cells showed that a subset of around 20-30% of the resultant daughter cells entered a state of low Cdk2 activity, as reported by a fluorescent sensor, distinct from senescence and appearing to be quiescence due to the extension of time spent in G1. Analysing these cells for the presence of DNA lesions and for the status of the cell cycle regulators and DDR components Rb, p21 and 53BP1 revealed that much of the adoption of quiescence in daughter cells could be linked to spontaneous or experimentally induced damage occurring in S phase, as marked by 53BP1 foci, leading to hypophosphorylation of Rb and elevated levels of p21. Importantly however, it was also clear that 53BP1 foci status was not the sole determinant of hypophosphorylated Rb in daughter cells, as 43-66% of cells, depending on cell lines, with hypophophorylated Rb did not have detectable 53BP1 foci. Thus a model results wherein the population's evident non-genetic heterogeneity in the adoption of the quiescent phenotype and associated altered signalling can be explained in part, but not exclusively, by a deterministic component, namely the inherited replication stress damage marked by 53BP1 (Arora et al. 2017).

The significance of this study was in the identification of an inherited deterministic component contributing to the heterogeneity of cell cycle lengths observed in populations and that this inherited component appears to be either the DNA damage itself from a previous cell cycle phase in the case of 53BP1 foci or the possibility of inheriting a particular signalling context to determine cell behaviour in the case of upregulated p21 and hypophosphorylated Rb. This exemplifies the importance of previous cell cycle phases in determining subsequent behaviour and that the consequences of DNA damage, in this case unreplicated regions, can persist and cause consequences in subsequent cell cycles. Critically it was longitudinal time-lapse studies of single cells that made these observations apparent.

These studies suggest an opportunity in combining the FUCCI based cell cycle dynamics lineage tracing with DNA damage that is likely to prove fruitful in revealing facets of checkpoint behaviour that operate across multiple cell cycle phases and indeed across lineages.

1.5 Understanding the significance of checkpoint responses in subsequent cell cycle phases

In summary, cell cycle checkpoint mechanisms and the DDR occupy a central role in our conceptual models of how cells maintain genomic integrity in the face of DNA damage. Despite this, as we have learnt more about them, especially in recent years, it has becoming increasingly apparent that checkpoints have been repeatedly observed to allow the passage of genomic lesions to subsequent cell cycle phases and even descendant cells. Despite emerging findings concerning how DNA damage incurred in a cell can affect the behaviour of descendant cells, as discussed in 1.3.10, the consequences of DNA damages for later generations remain poorly characterised.

Therefore, the goal of this project is to investigate the determination of cell proliferation vs cell cycle exit across multiple generations following DNA damage. This area of research is of critical importance in developing better models of the role of cell cycle checkpoints in protecting genomic integrity. If a single double strand break is as dangerous to genomic integrity or as lethal to the cell as often cited in the scientific literature why has the G2 checkpoint been reported to allow an order of magnitude more breaks into mitosis, a critical time for the cell and genomic integrity, and thus into the daughter cells that result? Furthermore, given the widespread use of DNA damage to drive cell death or senescence in cancer therapy, characterisation of whether these cell fates are adopted by the treated cells or their descendants may yield insights into improving efficacy.

To this end, I have developed two main approaches. Firstly, I have utilised microscopy-based lineage tracing of cells expressing genetically encoded Fluorescent Ubiquitination-based Cell Cycle Indicator (FUCCI) probes with semi-automated image analysis to characterise the response of single cells and their descendants to DNA lesions induced by neocarzinostatin treatment across multiple cell cycle generations. This approach has allowed me to characterise the timing of cell fate determination, the non-genetic heterogeneity in checkpoint responses, correlations between cells, cell cycle timing dependent sensitivities to neocarzinostatin treatment and overall lineage behaviour. This approach along with several novel analyses have allowed the resultant behaviour to be well described and a number of interesting observations to be made. Chiefly amongst which has been the observation of abundant descendant cell death in U2OS cells following the induction of DNA damage, indeed the rate of death in descendant generations typically exceeds the death rate of the cells that actually received the DNA damage. The death of descendant cells, termed ‘delayed death’, subsequently drives the extinction of a great proportion of cell lineages, in effect contributing as much as death of treated cells to eliminating the proliferation of DNA damaged clones. These results suggest that cell cycle checkpoint processes are operating, and possibly co-operating, across multiple cell cycle phases and generations. This provides a new paradigm for how checkpoint mechanisms could restrain the proliferation of DNA damaged cells by considering the behaviour of lineages instead of simply single cells. Further research is merited into how delayed death is triggered in descendant cells and determining whether lineages that show delayed cell death but do not exhaust during the experimental timespan eventually regain typical proliferative capacity. Furthermore this also raises questions about how elimination of cell lineages over multiple generations rather than through the death of the initially DNA damaged cell might influence the evolution of tumours treated with DNA damage.

Secondly, I developed a complementary flow cytometry based method to allow indirect tracing of generations and estimation of cell fate determination. This approach has allowed me to produce corroborating evidence for the delayed death observed by microscopy in the U2OS cell line,

characterise the behaviour of further cell lines and will permit the testing of a greater range of experimental conditions than are practical via microscopy based means. Furthermore, I have observed evidence of the persistent elevated presence of DNA damage in cells following treatment over many days, suggesting a possible explanation for the delayed death observed.

In summary, through single cell based experimental work I have been able to characterise the response of cancer cells to DNA damage over multiple generations demonstrating that descendant cells show dramatically altered cell fate determination in response to DNA damage received by their ancestor, so revealing the importance of considering descendant cell responses. Understanding these responses, namely how, why and when cells die, will have implications for therapeutic approaches.

Microscopy based lineage tracing – cell fate following DNA damage

1.6 The development of a microscopy-based lineage tracing approach

One approach, as demonstrated by the literature discussed previously in 1.4.2, for understanding how DNA damage can have consequences over multiple cell cycle phases and across multiple generations of cells is to follow and track cells as they move and divide via the acquisition of time-lapse microscope images. Several cell measurements can be made from such an approach, including, for example: the duration of its lifetime, so allowing any cell cycle arrests to be inferred; its movement; and its fate, namely whether it divides, dies or does neither during the period of observation. Significantly, this approach allows the tracing of familial relationships between cells, thereby conveying direct information about cell lineages and their component generations of cells, thereby revealing how cells behave when an ancestor has experienced DNA damage. The addition of sensors can provide yet further cellular information, for example, the FUCCI probes discussed previously allow estimation of when the cell transitions from G1 to S phase, granting the ability to infer which cell cycle phase a cell is arrested in, thus giving a more precise description of cell lineage behaviour following DNA damage.

In practical terms however, most mammalian cells in culture are not easy to follow via methods that merely illuminate the cell, for example brightfield, phase contrast and differential interference contrast microscopy (Figure 8). Furthermore, to follow the numbers of cells required to make meaningful biological inferences is extremely laborious. A solution to the former is the use of fluorescent probes with fluorescence microscopy allowing cells to be better identified in a microscope image. The discovery and development of a great many fluorescent proteins has allowed fluorescent species to be genetically encoded in cells and targeted to particular cell locations. The use of nuclear localised fluorescent proteins allows the production of images where cells can be identified by the presence of discrete fluorescent nuclei (Figure 8). This approach lends itself to relatively simple computer-based image analysis whereby these nuclei can be discerned from the background with a reasonable level of accuracy by appropriate segmentation algorithms; these may then be compared to the nuclei identified in previous and

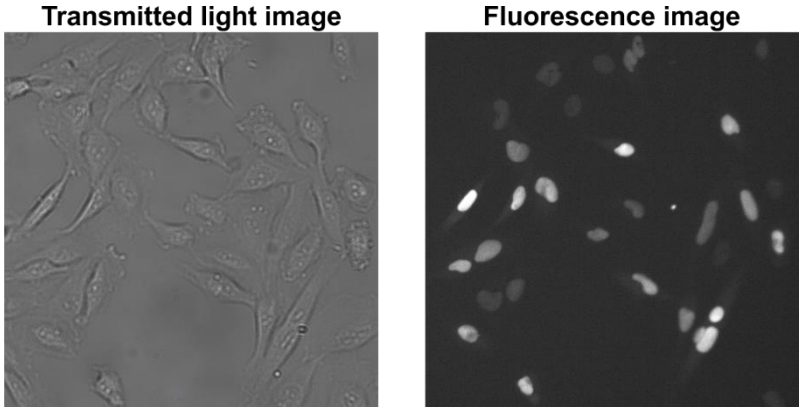

Figure 8: Identifying cells by microscopy
Transmitted light microscopy images allow cell morphology to be visualised. Identifying individual can be difficult by both eye and computational analysis. Nuclear localised fluorescence can be identified via fluorescence microscopy allowing discrete nuclei to be identified relatively easily by computational analysis.

subsequent images allowing automated cell tracking (Figure 9), thus reducing the laborious nature of cell lineage tracing. Segmented cell nuclei also allow the measurement of fluorescent sensors present in a cell, for example FRET based sensors.

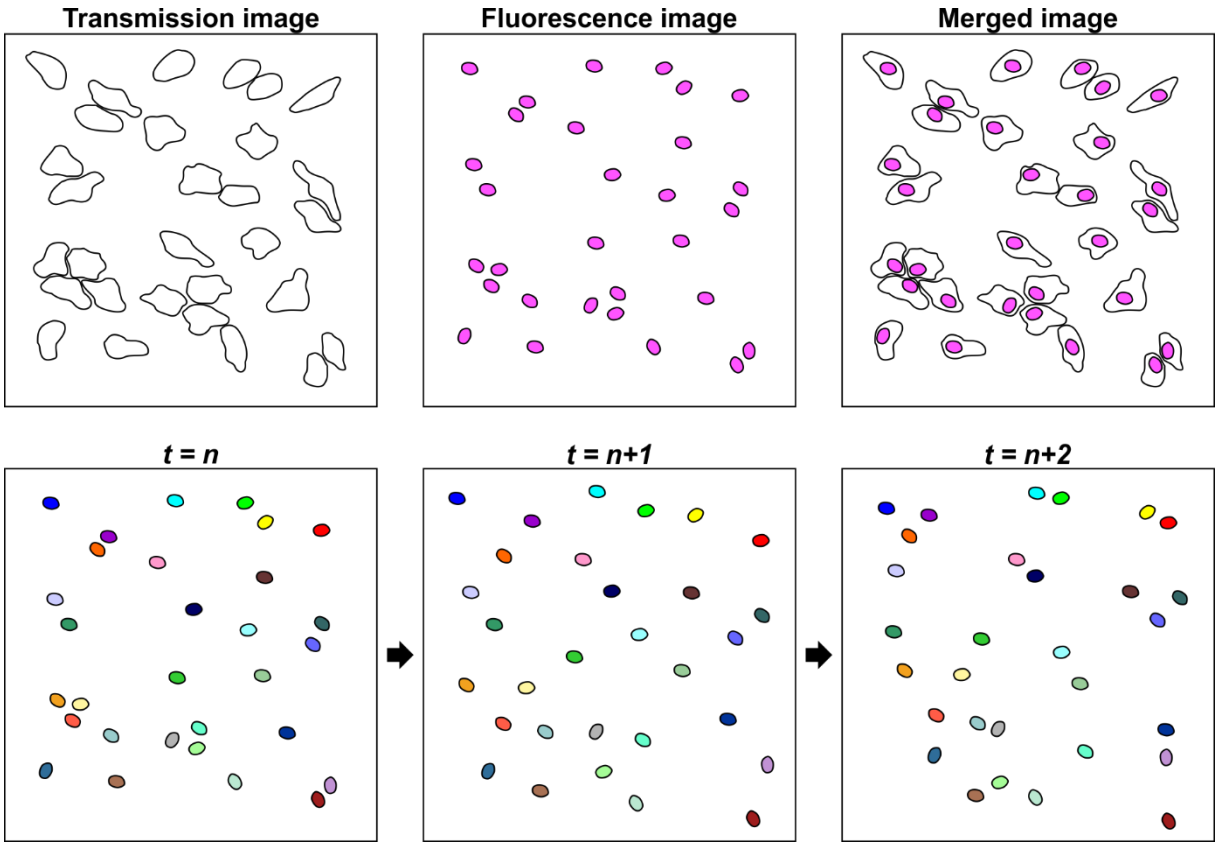

Figure 9: Tracking cells via segmented nuclei
Nuclei identified by fluorescence microscopy can be used as a proxy for the location of cells. Comparison of nuclei identified in multiple time points (t) allows the movement of nuclei, and thus cells, to be tracked over time.

The FUCCI probes are themselves nuclear localised and also convey information about the progression through the cell cycle in the changes in fluorescence intensity over time. This permitted the semi-automated analysis of hundreds of L1210 lymphoblast cells discussed previously in 1.4.2. Nevertheless, it has also been reported that the loss of FUCCI probe fluorescence during mitosis can present difficulty in the continuous tracking of cells and identification of the daughter cells generated by a mitosis. One solution to this problem was the substitution of the S&G2 probe mAG-hGem(aa1-110) with a chromatin, and thus nuclear, localised H2B-eGFP fusion construct producing the 'CycleTrak' system whereby the fluorescence of the G1 probe was used to determine the timing of the G1/S transition and the H2B-eGFP allowed continuous tracking even through mitosis (Ridenour et al. 2012).

Clearly the use of a fluorescence nuclear marker facilitates continuous cell tracking and thus total cell cycle length calculation. Furthermore, a nuclear marker spectrally compatible with co-expression of both FUCCI probes would also permit the use of both probes to identify the timing of transitions between cell cycle phases and correct for the difficulty in cell tracking during mitosis and early G1 when the fluorescence of the FUCCI probes is absent or low (Figure 10).

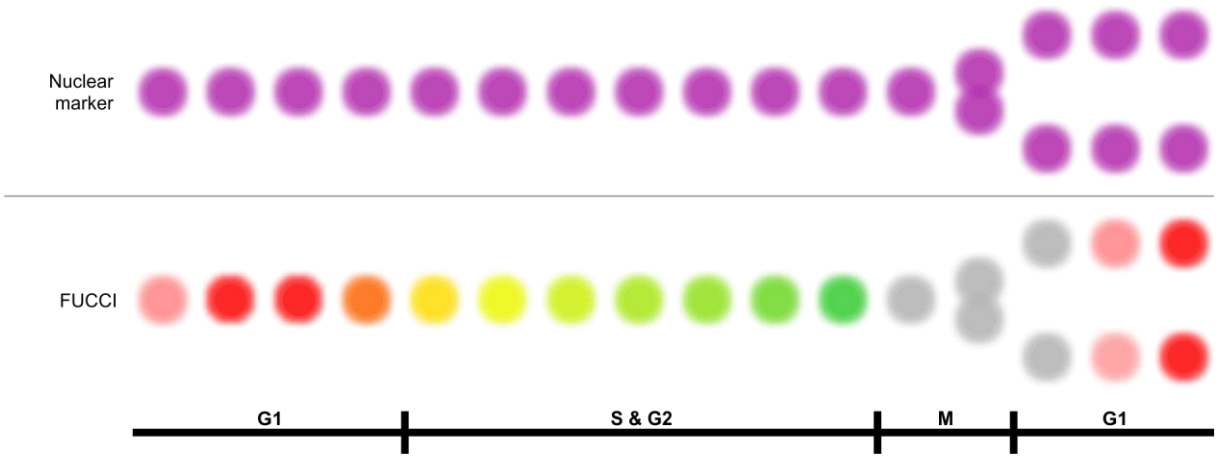

Figure 10: Idealised representation of FUCCI and nuclear marker fluorescence across cell cycle
The FUCCI components vary in nuclear intensity throughout the cell cycle causing red→yellow→green transitions and are typically absent during mitosis and immediately after division (represented as grey). The consistently expressed nuclear marker allows automated cell segmentation and tracking.

1.6.1 Design of a genetically encoded fluorescent nuclear marker

The emission spectra of the two FUCCI probes mAG-hGem(aa1-110) and mCherry-hCdt1(aa30-120) cover a large region of the visible spectrum (Figure 11) leaving the violet, blue, and near-infrared regions of the spectrum available for a third fluorescent component. The use of shorter wavelength light to excite fluorescent species presents a greater risk of phototoxicity during imaging and therefore the use of a far-red fluorescent nuclear marker would be preferable. Similarly to the FUCCI probes, the use of genetically encoded fluorescent proteins would also allow for the creation of stable cell lines and avoid the use of dyes that often cannot be used for extended periods of time without toxic side effects. Several near-infrared fluorescent proteins have been discovered and developed, of which iRFP682 was selected for use on the basis of spectral compatibility with the FUCCI probes and microscopy, and sufficient brightness when expressed in mammalian cells (Shcherbakova & Verkhusha 2013).

Expression of this protein alone will however result in fluorescence throughout the cell, rendering adjacent cells difficult to discern. In order to confer nuclear localisation appropriate amino acid sequences need to be added. In the CycleTrak example (Ridenour et al. 2012) this was achieved by fusion of eGFP to H2B sequences which results in the incorporation of the eGFP into the nucleosomes around which DNA is wrapped to form chromatin. Such an approach results in a fluorescent nucleus during interphase when chromatin is uncondensed and visualisation of the condensed chromatin structures during mitosis. An alternative approach is to tag proteins with a nuclear localisation signal (NLS) to drive nuclear import of the protein. During interphase this also results in a fluorescent nucleus, while during mitosis nuclear envelope breakdown will release the fluorescent protein throughout the rounded-up cell.

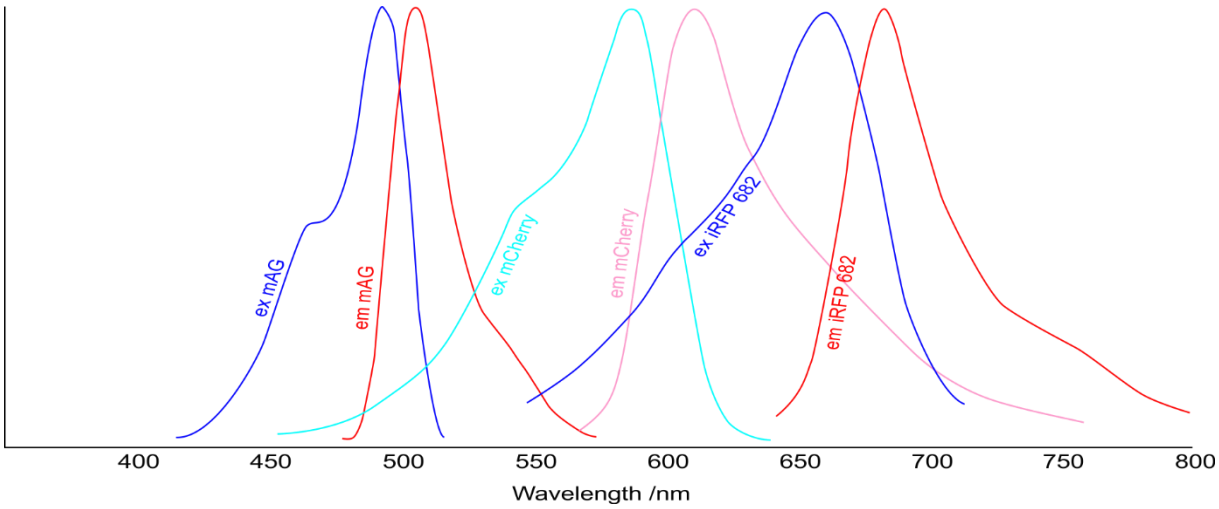

Figure 11: Fluorescence excitation and emission electromagnetic spectra
Three fluorescent markers, mAG-hGeminin (1-110) ***(S&G2 probe)****, mCherry-hCdt1(30-120)* ***(G1 probe)*** *and NLS-iRFP682-NLS* ***(nuclear marker)*** *can be used simultaneously due to the separation of their excitation and emission peaks across the electromagnetic spectrum.*

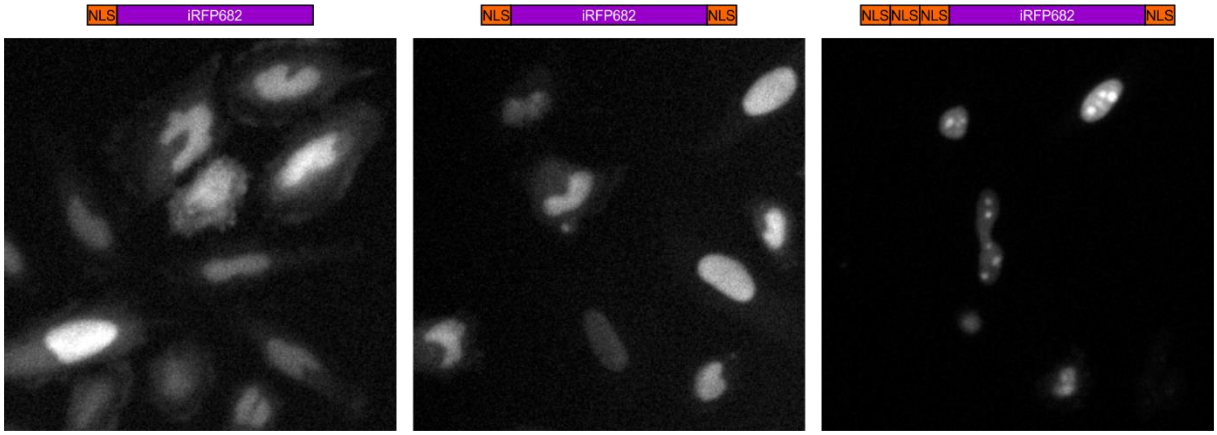

Figure 12: Comparison of nuclear-cytoplasm contrast of variant NLS tagged iRFP682 constructs

As different NLS sequences and NLS combinations can result in varying degrees of nuclear to cytoplasmic contrast several variant NLS fusions to iRFP682 were tested to determine the optimum for image analysis. Microscopic analysis (Figure 12) indicated the best contrast was achieved by tagging iRFP682 N-terminally with an NLS from the Large T antigen of Simian virus 40 (amino acid sequence PKKKRKV) and C-terminally with the human myc NLS (amino acid PAAKRVKLD) hereafter referred to as NLS-iRFP682, had the best nuclear to cytoplasm fluorescence contrast. A single NLS alone was sufficient to drive nuclear import but with a reduced contrast between the nucleus and cytoplasm, while three tandem N-terminal NLS sequences in addition to a C-terminal NLS resulted in very high nuclear import but also caused the appearance of large nuclear foci, possibly indicating this construct tends to localise to the nucleoli.

1.6.2 Construction and validation of stable cell lines for lineage tracing

Monoclonal U2OS cells stably expressing mCherry-hCdt1(aa30-120), mAG-hGem(aa1-110) and NLS-iRFP682 were produced by transfection with a dual promoter plasmid (pBudCE4.1) containing the two

FUCCI probes and with a plasmid (pcDNA3.1(-)) containing the iRFP nuclear marker (see materials and methods). U2OS cells are a bone osteosarcoma derived cell line amenable to genetic manipulation, microscopy imaging and have been previously used in the group to study the role of Plk1 signalling in recovery from the G2/M checkpoint (Liang et al. 2014 discussed previously). Expression of the tripartite nuclear marker and FUCCI system, hereafter FUCCI-NM, resulted in the expected measurable changes in the fluorescence intensities of the FUCCI probes as cells pass through the cell cycle (Figure 13).

1.6.3 Development of an analysis workflow

Time-lapse cell microscopy involves the acquisition of images of cells in the relevant experimental conditions at regular time intervals. At each time point, imaging of the FUCCI-NM cells requires acquisition of multiple image channels, a brightfield channel to indicate cell morphology and a fluorescence channel for each of the three fluorescent proteins expressed. Ultimately a series of image files are produced from which the appropriate data series must be extracted.

In lineage tracing, cells must be identified within each image, accurately tracked through time, and the relevant measurements and observations made to produce the final data series. This was achieved for FUCCI-NM time-lapse series via a semi-automated workflow (Figure 14). Firstly, cell nuclei were identified automatically in each image by segmentation algorithms using the nuclear-localised fluorescence (nuclear segmentation). Nuclei were then tracked automatically from one timepoint to the next by comparing the distances between the nuclei identified in one frame to another. The regions identified as nuclei were then used to measure the fluorescence intensity of the FUCCI probes for each cell through time. Inevitably the automatic segmentation and tracking introduces occasional major errors where cell nuclei are temporarily lost or misidentified necessitating a process of manual validation and correction of the cell traces. Additionally, the time of cell death and division was curated manually as was the assignment of daughter cells to the mother following cell division. Finally, validated cell traces were used to estimate the G1/S transition time by observing where the average fluorescence intensity of the G1 FUCCI probe began to decline. This allows the duration of G1 and the duration of the combined S phase, G2 phase and mitosis, hereafter SG2M, to be calculated. An example of a lineage constructed with G1 and S&G2 and mitosis assignments is given in (Figure 15).

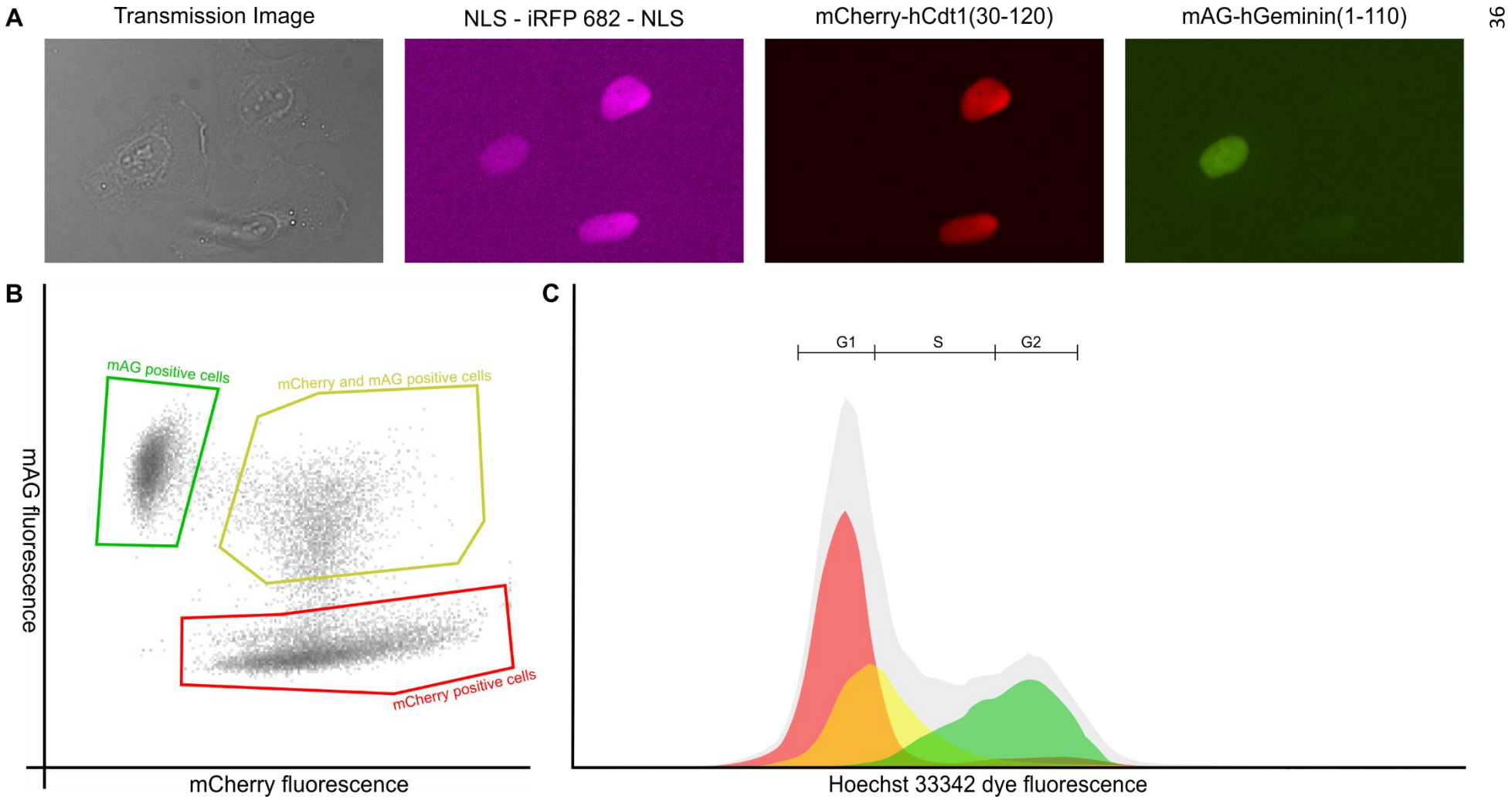

Figure 13: Characterisation of stable FUCCI-NM U2OS cell line
A) *FUCCI-NM U2OS cells stably express three fluorescent probes which can be imaged via fluorescence microscopy alongside transmitted light microscopy indicating cell morphology.*
B) *FUCCI-NM U2OS cells assessed by flow cytometry show three major populations, mCherry positive cells, mAG positive cells and doubly positive cells.*
C) *Cell cycle profiles based on the entire population (grey) and from the three populations identified in B) indicates the FUCCI system is working as expected in separating G1 cells, red, from G2 cells, green, while doubly positive cells are around the G1/S transition.*

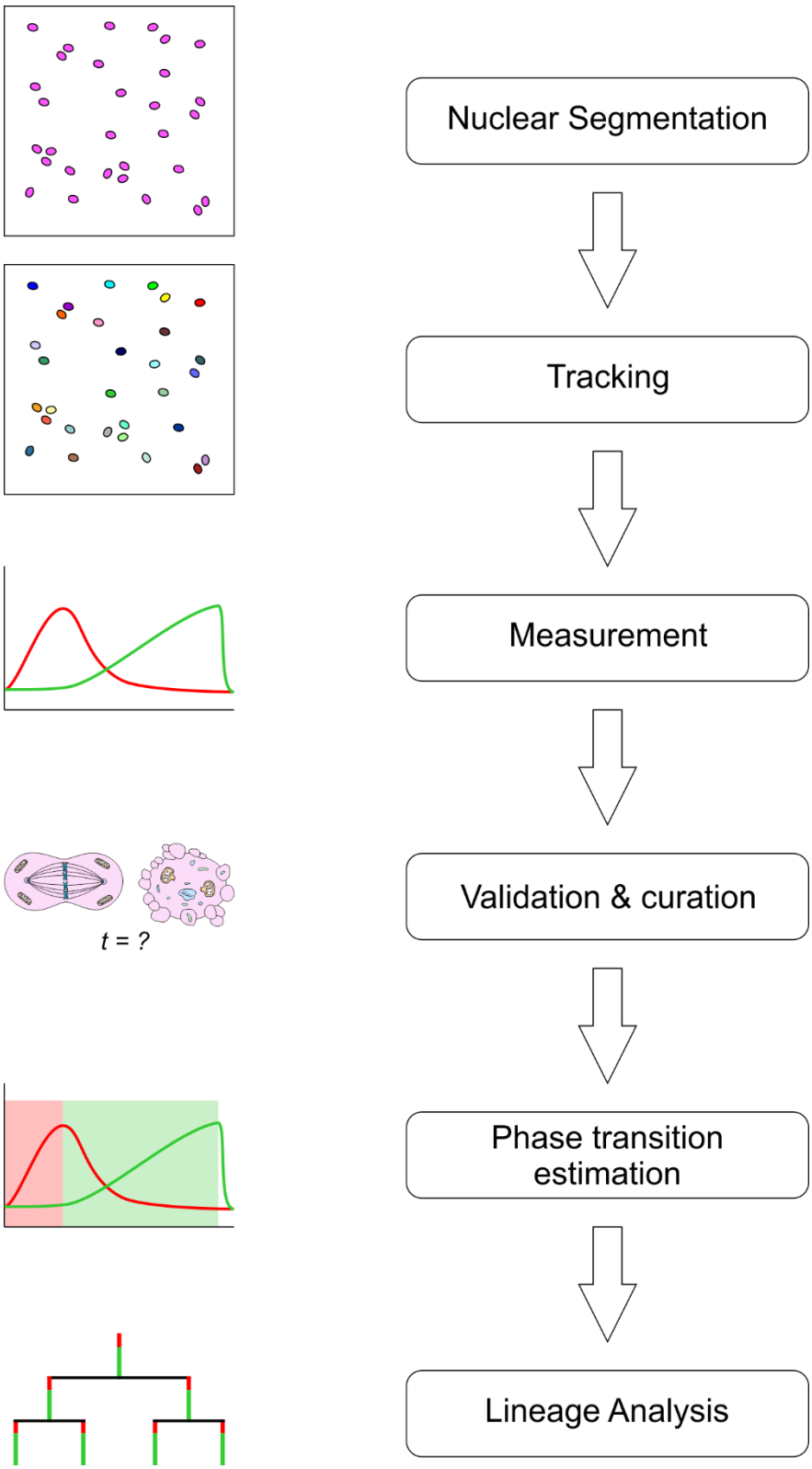

Figure 14: Analytical workflow for analysis of microscopy based lineage tracing

- *Nuclei were identified by automated image segmentation.*
- *Identified nuclei were automatically tracked through time based on distances between nuclei centroids.*
- *Fluorescence was automatically measured for each identified nucleus allowing the changes in FUCCI probe fluorescence to be determined.*
- *Automatically identified cell traces were validated by manual assessment and the timing of division and death assigned based on the cellular morphology.*
- *Validated cell traces were used to determine the approximate timing of G1/S transition.*
- *Fluorescence traces from related cells were collated together as lineages allowing further analyses.*

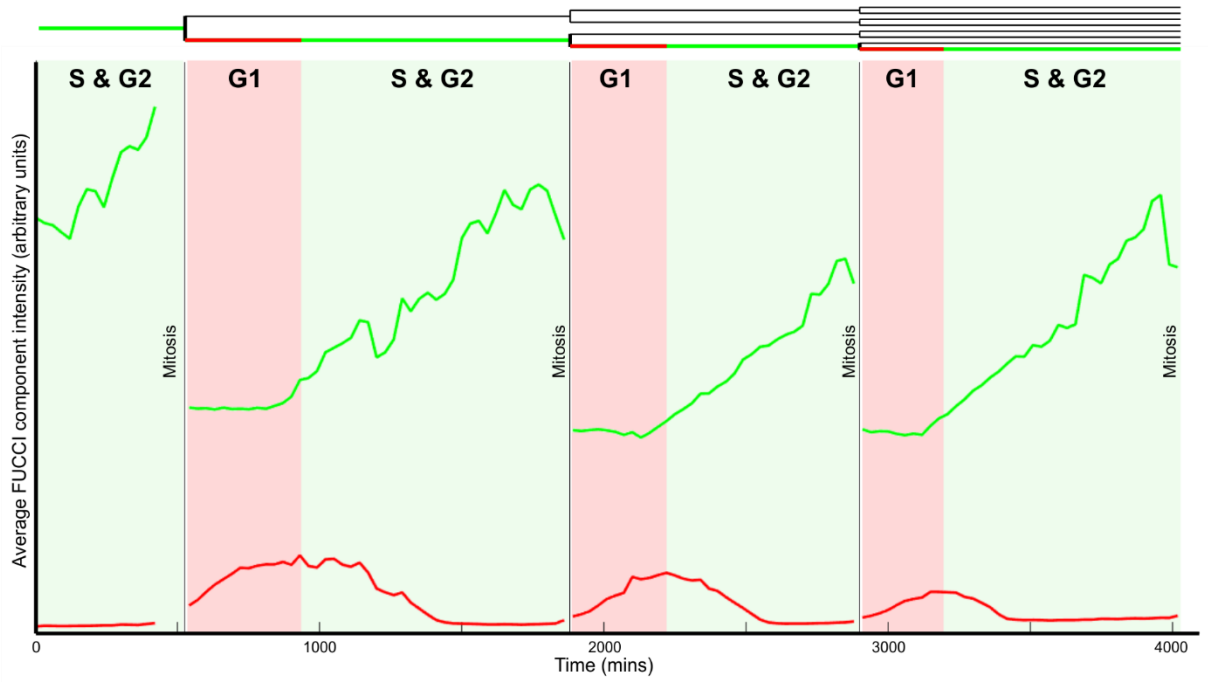

Figure 15: Multigenerational FUCCI lineage tracing
Example of multi-generational FUCCI fluorescent traces of undamaged regularly dividing cells (one cell in each generation shown). The red G1 probe peaks before the green S&G2 probe indicating the end of the G1 phase of the cell cycle. The green S&G2 probe peaks just before mitosis.

1.7 Initial characterisation of lineage and fate tracing using the FUCCI-NM system

As discussed previously, there are a great range of possible DNA lesions to which cell cycle checkpoints are responsive. In terms of the responses of checkpoints DNA strand breaks are amongst the best studied and were used to investigate the checkpoint response in U2OS cells previously (Liang et al. 2014). Of the many agents capable of inducing DNA damage, neocarzinostatin (NCS), an enediyne chromophore bound to a stabilising apoprotein, was selected (Figure 16A). Neocarzinostatin has been characterised as producing both single and double strand breaks via a proposed direct chemical reaction with DNA (Kappen & Goldberg 1997) within minutes of addition to cell media (Figure 16B). Neocarzinostatin has also been characterised as being rapidly inactivated following addition to culture media in the presence of cells, as it is degraded by light, heat and serum containing media, and is consumed in the reaction with DNA (Yoko Kuroda, Takehito Sasaki 1991; Richard M. Burger, Jack Peisach 1978). This property allows the rapid induction of DNA damage over a relatively brief time, which may be advantageous over ionising radiation, which in contrast, has been characterised as potentially having long term consequences via the generation of radical oxygen species that can cause cellular damage long after the initial treatment (Azzam et al. 2012).

I hypothesised that the descendants of cells that received DNA damage but managed to divide would show changes in cell phenotypes and sought therefore to identify using lineage tracing whether NCS-induced DNA damage would induce observable changes in the cell fates and cell cycle durations, not only in the treated cells, which has clearly been done before, but in their descendant cells as well. Furthermore, I sought to establish new analytical methods to explore this data and thus determine

whether these measurements and construction of cell lineages can enable meaningful inferences to be made about the behaviour of these cells and their responses to DNA damage.

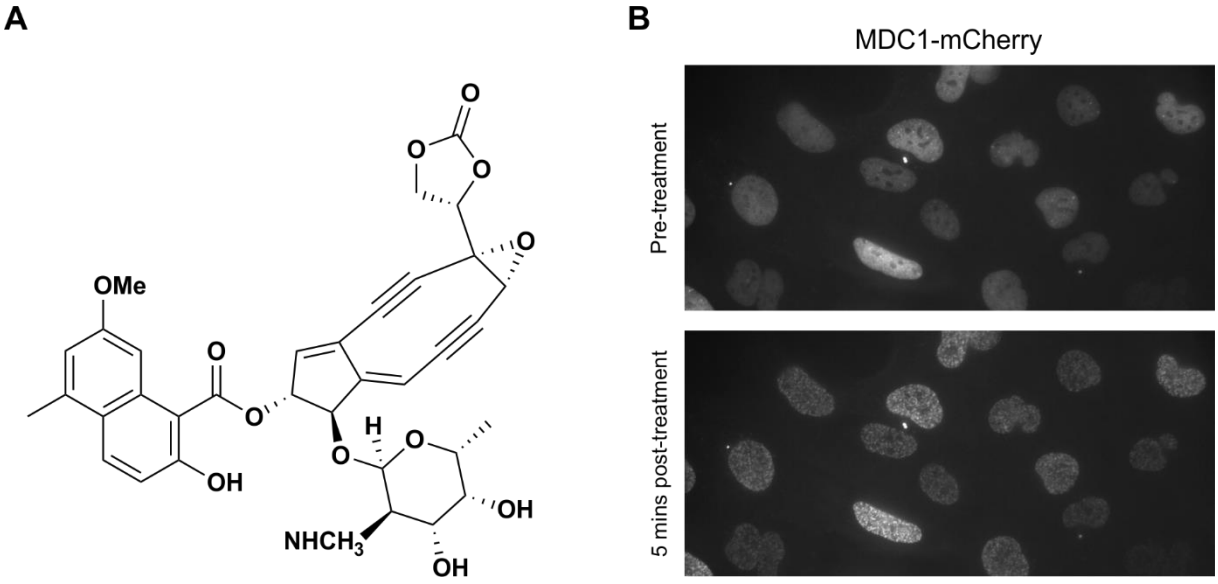

Figure 16: Neocarzinostatin (NCS) induces DNA damage rapidly
A) *The chemical structure of the Neocarzinostatin chromophore responsible for inducing DNA damage. Chemical structure kindly provided by Miss Robyn Hardisty.*
B) *DNA damage is evident by the formation of punctate MDC1 foci as soon as 5 minutes after treatment with NCS. U2OS cells expressing the fluorescent reporter construct MDC1-mCherry.*

Asynchronous cells were therefore given mock or NCS treatment shortly before beginning time-lapse microscopy lasting for five days in an exploratory experiment (protocol: Figure 20A, and further discussed in materials and methods). Lineages were analysed according to the workflow detailed above, Figure 14, to a maximum of three generations, i.e. treated cells, daughters and granddaughter cells. Where possible, lineages were analysed to the full three generations but some cells are lost either due to tracking difficulties or migration out of the microscope field of view and some cells that would have gone on to divide are not recorded as having done so as the experiment ended before they could. Therefore, two important constraints on the lineage analysis are the three generations analysed and the experimental duration, while loss of cells through migration and difficulties in tracking means some lineages will be incomplete.

The resultant lineage data is by its nature complex, containing information about familial relationships, cell fates and cell phase transitions over time. Such complexity presents a challenge for both description and visualisation of the data, and determining the appropriate analyses. Although the problem of describing relationships between cells is aided by the use of terms like ‘mother’, ‘daughter’, ‘sister’ and ‘generation’ borrowed from genealogy these terms are imperfect analogies with important distinctions. For example, in symmetrically dividing cells the division of a mother cell represents the end of its existence and its replacement by its daughter cells. Therefore, unlike in human relationships a descendant cell and its ancestor never coexist. Regarding visualisation, tree diagrams permit the

depiction of lineages in a format that can be read by the human eye and which encapsulates a great range of information, in particular indicating the status and presence of cells at any particular time. An example of such a representation and the associated terminology is shown in Figure 17.

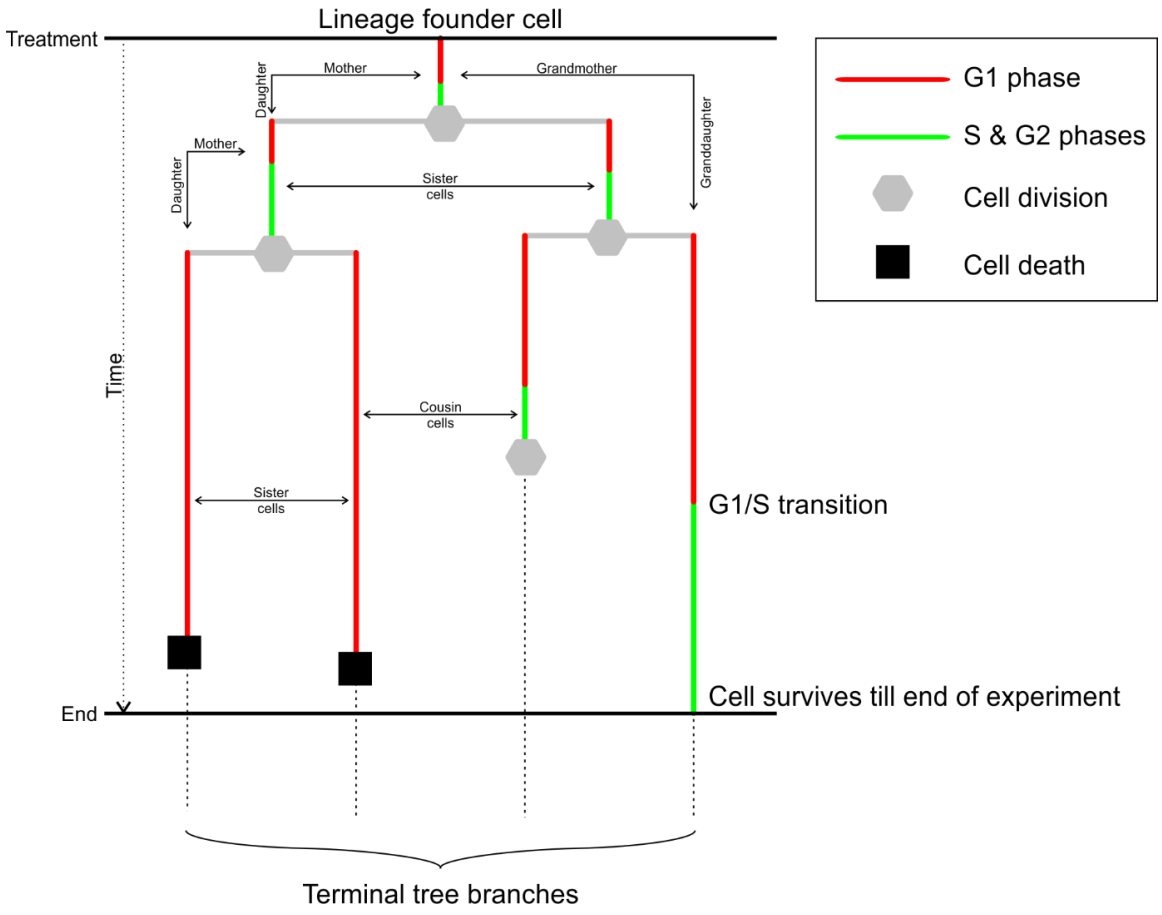

Figure 17: Lineage trees depict familial relations between cells and convey cellular information

Visualising all the analysed lineages together in the form of such family trees (Figure 18) reveals the diversity of lineage behaviour within each experimental condition but also allows the changes that NCS treatment induces in lineages to be observed. Considering only the mock treated lineages shows that even unperturbed cells can lead to very different lineage outcomes. Approximately half of these lineages show what might be considered the ideal behaviour, namely that there are regular cell divisions with each cell having similar total, G1 and SG2M durations, ultimately reaching the maximum expected 4 granddaughter cells in the final generation analysed, which then divide themselves. This lineage behaviour indicates that both the founder cell and the lineage overall can be considered to demonstrate high fitness. High fitness can be defined as a cell or lineage having high proliferative capacity, i.e. multiple divisions taking place regularly without cell cycle delay, and high survival of the lineage where no branches of the family tree terminate in a cell that dies. The remaining lineages show varying degrees of fitness in their behaviour. Some show multiple divisions but have members of the lineage which take abnormally long to divide. Other lineages show regular divisions but occasionally cell death truncates a branch of the tree.

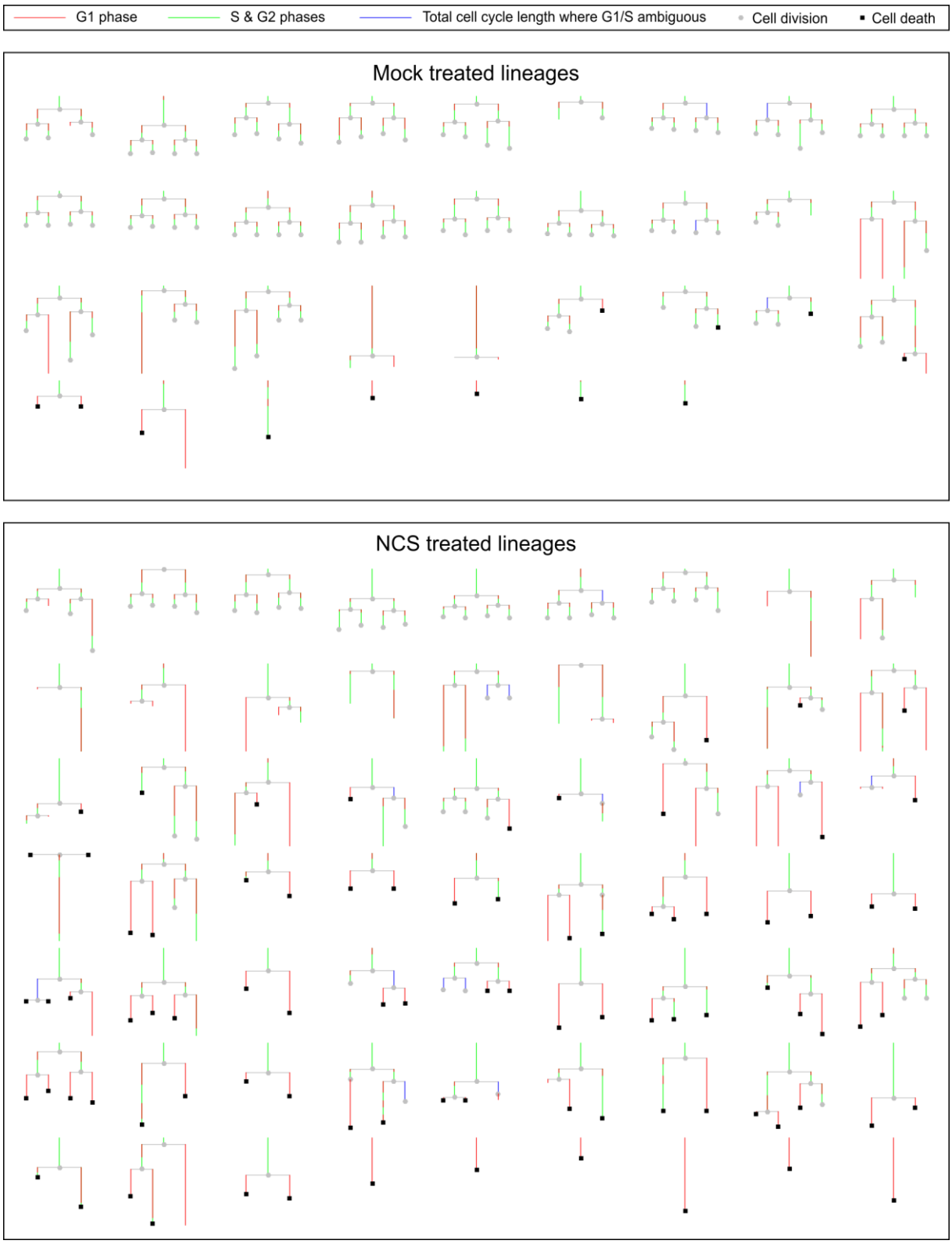

Figure 18: Lineages trees from mock or neocarzinostatin (NCS) treated cells
All lineages analysed from a single experiment can be visualised together in tree diagrams allowing the diversity of lineage behaviour and NCS induced changes to be assessed.

Furthermore a few lineages die out completely, several end with the mock treated cell dying and one dies out when the mock treated cell divides to produce two daughters that die. Clearly even without the perturbation of NCS-induced DNA damage cells show varied fitness in the lineages they give rise to indicating the presence of non-genetic heterogeneity. Such non-genetic heterogeneity in the background fitness of these cancer cells may be an intrinsic property, perhaps given their cancerous origins low levels of spontaneous cell death might be expected to arise if the normal homeostatic regulatory networks that maintain cell fitness have been disrupted during the evolution of the ancestral tumour. Alternatively, it might be a chance effect triggered by stresses placed on the cells by the experimental procedures. In any case, this apparent heterogeneity only becomes clear by taking this single cell lineage tracing approach.

The patterns of lineage behaviour in NCS treated cells obviously differ from those in the mock treated, in particular it is immediately apparent that there is much more cell death, an expected response to DNA damage. Interestingly, the lineage trees reveal that most cell death is not occurring in the NCS treated cells, most cell death is instead occurring in later generations. This observation alone demonstrates the suitability of using NCS-induced damage to probe the consequences of DNA damage for descendant cells.

NCS treated lineage trees are also greatly heterogeneous. Some lineages are very similar to the predominant lineage type in the mock treated sample, i.e. regularly dividing with no cell death, suggesting that the treated cell in the lineage either experienced little DNA damage (later analyses of NCS induced DNA damage suggest this is unlikely) or that it was able to tolerate the damage so no obvious consequences have arisen in its descendant cells. However, these lineages are clearly a minority, in contrast to their predominance in the untreated cells. The remaining lineages all demonstrate to varying degrees defects in their fitness. A subset of archetypal lineages are included in Figure 19, treated cells may themselves die, Figure 19B, but the proportion that do so appears similar to the proportion that do in the mock treated sample, daughter cells may die (Figure 19C), granddaughter cells may die (Figure 19D), cell death may occur in a mixture of generations (Figure 19E) and some cells in a lineage may die while others survive (Figure 19F). This indicates that the DNA damage given to these cells is often capable of exhausting a lineage within three generations but that this exhaustion can occur in different ways. Furthermore, it is clear that cell death can occur in some branches of a lineage while other descendant cells survive. While lineages with surviving members may have eventually been observed to die out if the experiment and analysis had proceeded for longer, it appears reasonable to presume that some would have been able to proliferate indefinitely. These intra-lineage generational differences in when cell death occurs and intra-lineage differences whereby some members of the lineage die while others survive and proliferate indicate that the consequences

of the DNA damage received by the founder cell can trigger different outcomes amongst any descendant cells.

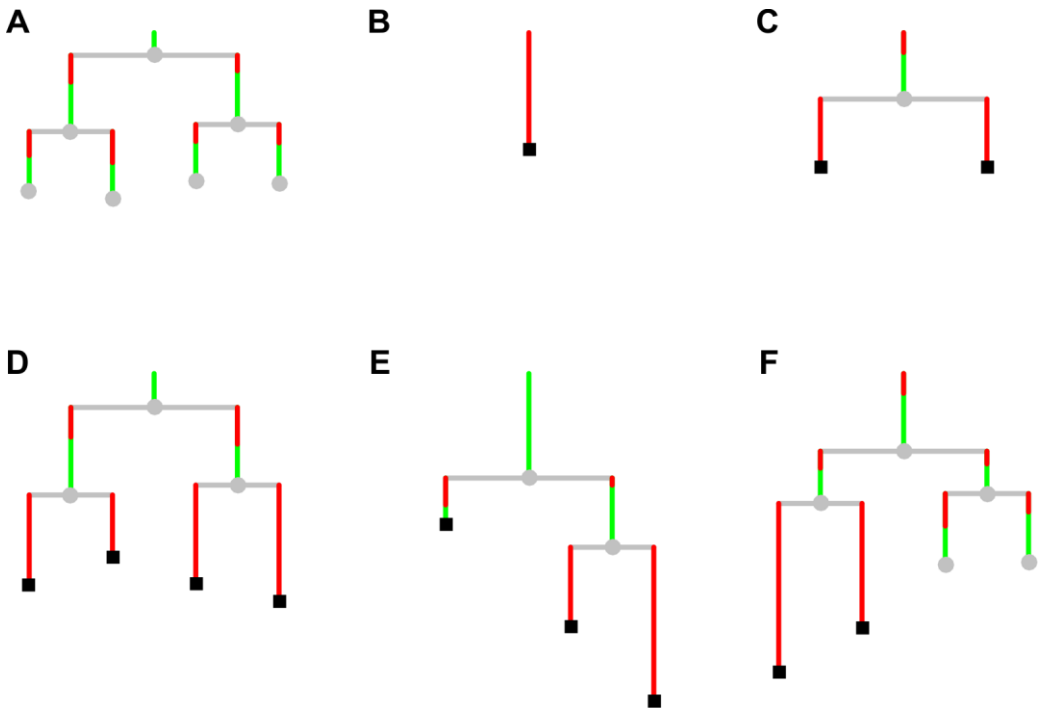

*Figure 19: Depicting lineages as family trees allows the heterogeneity of descendant cell fates to be visualised. Cells treated with Neocarzinostatin to induce DNA double strand breaks show a variety of responses when multiple generations are assessed. Some lineages show regular division with no apparent cell death **(A)** but most feature obvious cell death **(B-F)**. Cell death may occur in the treated cell **(B)** or manifest in daughter and granddaughter cells **(C-F)**.*

To facilitate further analysis of cell cycle durations and cell fates cells were grouped into which generation they belong to and then plotted both as a swarm plot showing the actual data points and as half-violin plots, indicating the distribution of the data (Figure 20). This approach allows cells to be compared regardless of their birth in absolute time, but by what their relative position in the lineage is, namely a treated cell, a daughter or a granddaughter cell. To further aid analysis the data is colour coded with the fate of the cell, i.e. whether it divides, dies or survives until the end of the experiment.

In this experiment, asynchronous cells received mock or NCS treatment shortly before the microscopy began. Therefore, at the time of treatment these cells would be expected to be at various degrees of progression through their cell cycles. Measurements of the treated cell's lifetime during the experiment will thus be an underestimate of the true length as it will have been born before the experiment began. In the mock treated cells, this would be expected to manifest as a distribution of total cell cycle durations for dividing cells predominantly between 0 and the length of a normal cell cycle, while for NCS treated these would be expected to undertake a cell cycle arrest and so should produce a distribution of measured cell cycle lengths reaching longer lengths than the mock. Subsequent generations in contrast should give true measurements of the cell's life time for those cells

that are measured from birth to death or division, while those cells that survive until the end of the experiment will have truncated lifespan measurements.

Indeed, this is evident in Figure 20C, mock treated cells that divide are predominantly measured as having cell lifetimes distributed widely between 0 and around 20 hours, while their daughters and granddaughters that divide have more tightly distributed total cell cycle durations of 20.5hrs±2 (median cell cycle length ± median absolute deviation) for the daughters and 18.5hrs±2.5 for the granddaughters. When considering the NCS treated cells one observes the measured cell lifetimes for cells that divide are mostly between 0 and 60 hours in length, which when compared to the mock treated controls indicates that many of these cells have experienced cell cycle delays. Interestingly, when considering the cell cycle lengths of those daughter (18hrs±4) and granddaughter cells (20.3hrs±4.3) of NCS treated cells which divide, most of these complete their cell cycles within the same distribution of time as the daughter and granddaughters of the mock treated cells. This would suggest that most of these cell cycle lengths should be considered phenotypically normal, in contrast to previous reports, albeit in other cell types, that indicated cell cycle arrests in the descendants of DNA damaged cells could be detected.

Considering cell death (black) yields further insights, inspecting lineage family trees indicated there is some level of death even in the mock treated cells. This, if anything, appears to be greatest in the mock treated generation, which may reflect a stress response to the experimental procedures or may be a product of the smaller sample of cells present for the first generation compared to those of the later. The NCS treated cells appear little different to the mock treated in terms of dying cells indicating that the DNA damage induced in this experiment was not particularly driving cell death in the treated generation. However, as soon as we consider the daughter and granddaughter cells for the mock versus NCS treatments the differences become stark. The proportion of cells dying in the daughter and granddaughter generations of the NCS treated cells is much higher than for their mock treated counterparts. The distribution of dying cell lifetimes is spread over a range of times with some cells dying shortly after birth and others dying three days later. Unlike the dividing cells in these generations this distribution does not have a pronounced clustering about any particular time suggesting that the time for a cell to die is relatively uniformly distributed. As some of the dying daughter and granddaughter cells die after many hours longer than a typical cell division would take, this shows these cells are undergoing active cell cycle arrest mechanisms, perhaps in response to DNA damage or other signals, thus prolonging the cell's lifetime until the cell death process finally begins. I have termed the observation of significant cell death in descendant cells 'delayed death'.

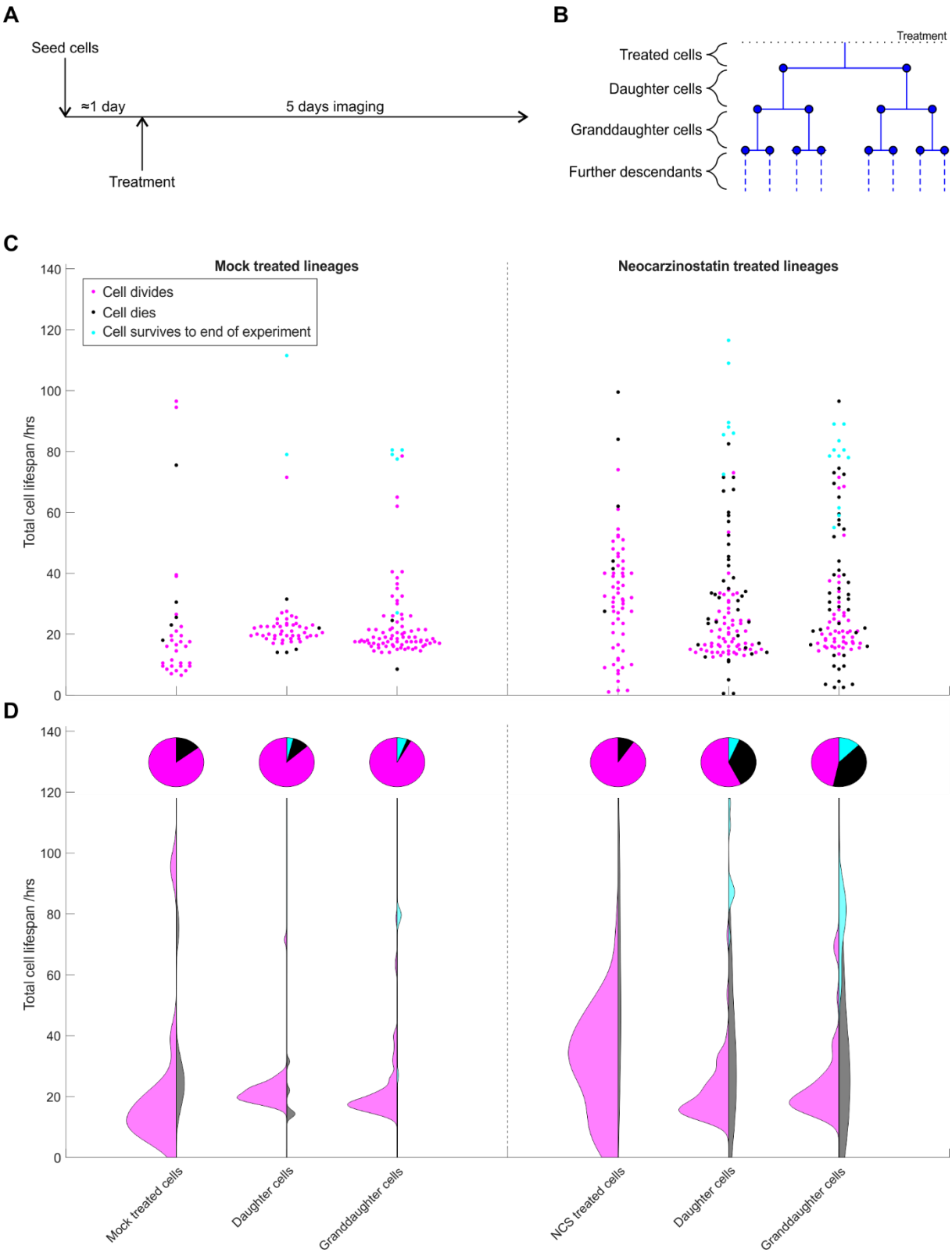

Figure 20: Generational analyses of lineage traced cells

A) *Experimental protocol. FUCCI-NM U2OS cells were seeded in Ibidi 4 well chamber slides and treated with either mock treatment or cell culture media containing either NCS (20ng/ml) followed by timelapse microscopy for 5 days with 30 minute intervals.* ***B)*** *The resultant lineage trees can be divided into treated cells, their daughters, granddaughters and further descendants. Cells were analysed up to the granddaughter generation.* ***C)*** *Swarm plot showing total cell cycle length for FUCCI-NM U2OS cells coloured by cell fate and separated into their generations.* ***D)*** *Half-violin plots show distribution of swarm plot data and pie charts showing proportion of cell fates adopted in each generation. Cell proliferation shown on left hand side, death or survival until the end of the experiment fates shown on right hand side. DNA damage by neocarzinostatin results in increased cell death in Daughters and Granddaughters indicating a delayed death phenotype.*

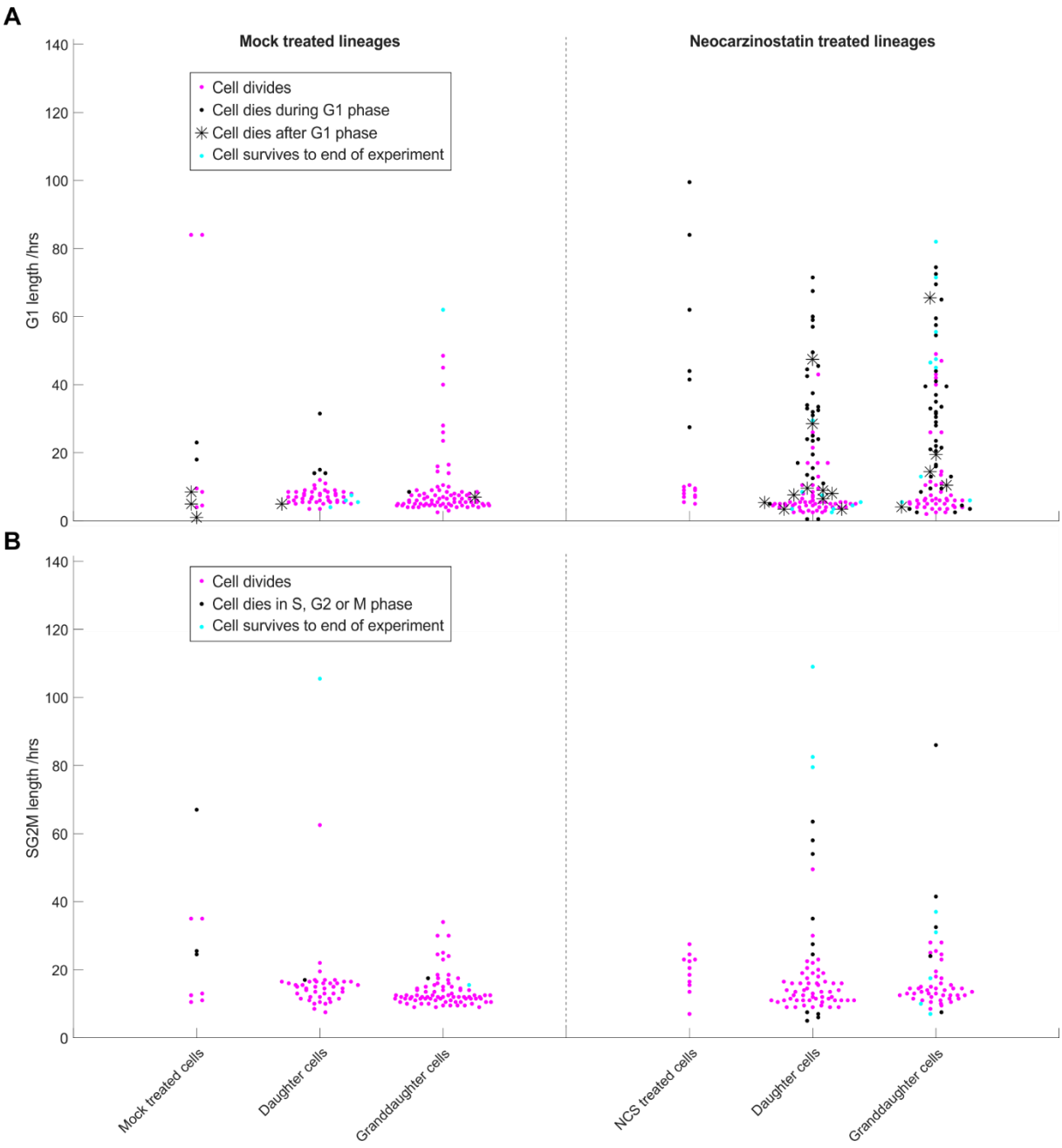

Figure 21 Swarm plots of G1 length and length of combined S, G2, and M (SG2M) phases.
***A)** Swarm plot showing G1 length for FUCCI-NM U2OS cells with identifiable G1/S transitions coloured by cell fate and separated into their generations **B)** Swarm plot showing SG2M length for FUCCI-NM U2OS cells with identifiable G1/S transitions coloured by cell fate and separated into their generations.*

Extending this analysis to the G1 and combined SG2M durations measured with the FUCCI probes permits the determination of the behaviour of the G1 and SG2M cell cycle subdivisions in the mock and NCS treated lineages (Figure 21). Unfortunately, as very few G1/S transitions were observed in the treated population generations, very few cells are represented in this generation and so the results are likely to be artifactual and not worth further analysis. The daughter and granddaughter generations of NCS treated lineages however, do show that both G1 and SG2M durations of most cells which go on to divide appear to be similar to their corresponding generations in the mock treated lineages. This would be expected as the total cell cycle duration did not appear different in these generations following NCS treatment. Cell death in the daughter and granddaughter cells is predominantly, but not

exclusively occurring in G1, suggesting that G1 phase mechanisms may be more important in delayed death. As was observed with total cell cycle duration, the time spent in each phase for those cells that go on to die is very variable with no pronounced clustering.

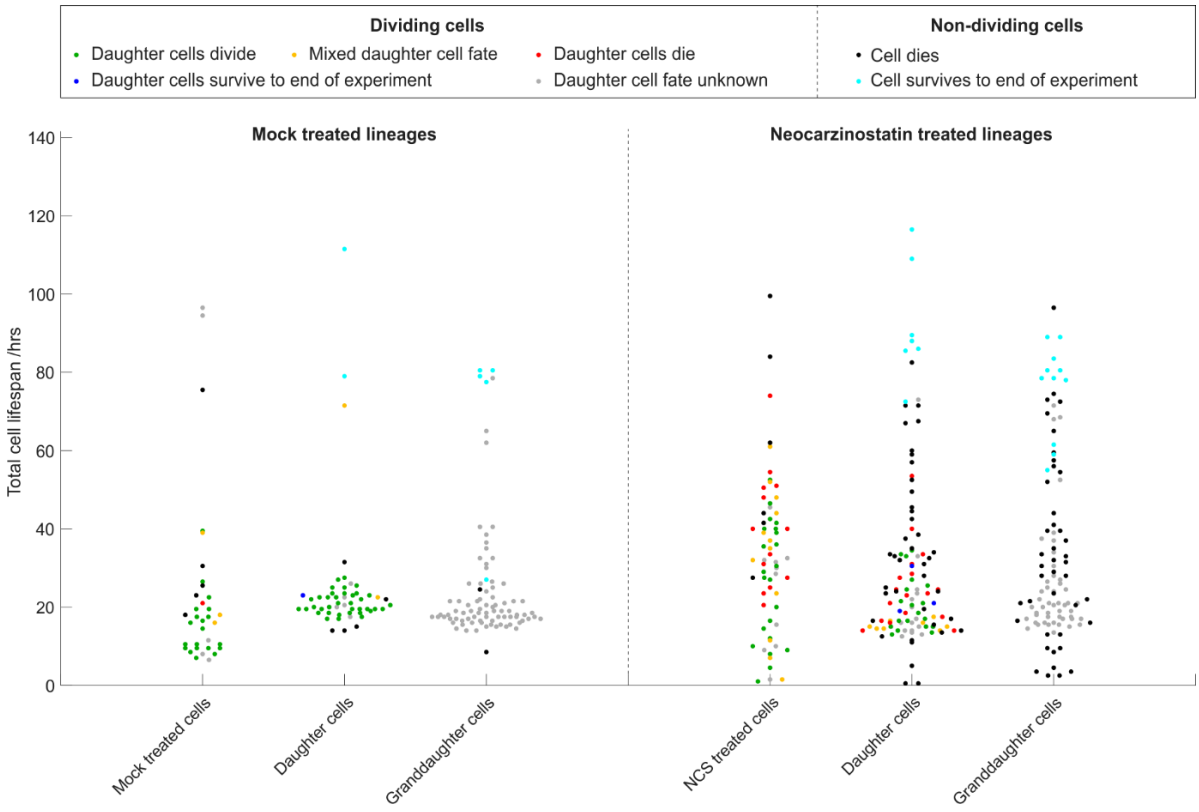

Figure 22: Swarm plots of cells showing total cell cycle length for FUCCI-NM U2OS cells coloured by daughter or own cell fate and separated into their generations.

The observation that death during the granddaughter generation is very abundant is perhaps slightly surprising given the observation that the cells from which they are born (the daughter generation) exhibit an apparently normal cell cycle in the majority of cases. To examine whether this is a correct interpretation of the lineage data, cells of the daughter generation were colour coded by their offspring's fate (Figure 22). This representation confirms that apparently phenotypically normally cycling cells can divide into cells where one or both daughters die. This raises the question of what triggers death in granddaughter cells, if it is remaining DNA damage then why does it not trigger discernible cell cycle arrests in the normally cycling daughter cell and if not then what is the trigger of the delayed death phenotype?

In conclusion, these initial observations were successful in probing the consequences of DNA damage in later generations, having identified the delayed death and lineage heterogeneity. The shortcoming of this approach however, is that there is no information about where the treated cells are in their cell cycle at the time they are exposed to the DNA damaging agent, thus limiting the inferences that can be made, for example, how long any individual treated cell spends in a cell cycle. An improved approach is to treat cells partway through time lapse microscopy, at a point where most of the cells receiving the treatment will have been born during the experiment allowing the full length of their

lifetimes to be determined. In order to confirm the initial conclusions from this preliminary work and examine how the behaviour of descendant cells may relate to the response to treatment of the treated cells several such experiments were undertaken.

1.8 Full characterisation and novel analysis of the response of U2OS cells to DNA damage

1.8.1 Lineage Trees

The optimization of this assay proved technically challenging as it required the integration of long term imaging, fluidic control and the development of experimental strategies aimed to ensure reproducibility; ultimately, an optimal protocol to treat cells partway through time-lapse microscopy was obtained as briefly outlined in Figure 27A and detailed in the Materials and Methods. Initially it was observed that the rate of cell death could be very variable from experiment to experiment even when using the same concentration of NCS. This variability is likely due to a combination of factors that can vary each time the experiment is carried out, the stress the cells experience during the seeding process, the number of cells seeded, the time between preparation of the NCS solution and applying it to the cells during which some of the NCS will degrade, and the amount and flow rate of NCS containing media applied to the cells. These processes were all controlled as carefully as was practical but inevitably some variation remains influencing the severity of the phenotype. To deal with this variability, several concentrations of NCS were given during each experimental attempt. Whichever concentration triggered a clear cell cycle arrest while still allowing most treated cells to complete division qualified for full analysis. These criteria exclude NCS conditions that prevent cell division within the experimental timeframe or are too mild to effectively discern from the untreated control without otherwise biasing the analyses. Qualifying analyses from different experiments can then be compared to see if they demonstrate the same trends in behaviour. Three experimental repeats are presented in this work, each demonstrating the same trends and phenotypes, but differing in the degree of severity. One dataset is presented as the best representative of the trends and observations from Figure 23 to Figure 42, while the remaining two and their associated analyses are presented together from Figure 44 to Figure 59.

Similarly to the preliminary work, cells were tracked from the beginning of the experiment and they and their descendants analysed by constructing lineage trees. However, as the NCS treatments were applied after the experiment began two possibilities now arise for where in the lineage the treated cells are located (Figure 27B). Either the cell tracked from the beginning of the experiment experienced the NCS treatment or, more commonly, descendant cells did, typically the daughter cells of the cell present at the start of the experiment. In the former case then the time of treatment could be calculated relative only to the G1S transition if it occurred before the time of treatment as the birth

time of the cell is unknown. In the latter case, the time of treatment could be determined relative to both the known birth of the cell and relative to the G1S transition. Furthermore, where two known sister cells receive treatment this also allows sister pairwise comparison of the resultant lineages.

The resultant lineage trees are displayed in Figure 23. Mock treated cells show fairly regular division with the large majority of all descendants surviving within the three generations analysed and the experimental timespan. Nonetheless many lineages exhibit some aberrant phenomena, including cell death, lengthened cell cycles, failure to complete cytokinesis and even a few mitoses that produce 3 daughter cells. Aberrant cell cycling can be observed where cells enter multiple apparent G1 phases as measured by the return of the red FUCCI probe in the absence of an intervening mitosis. A plurality of different lineages exists, once again demonstrating significant non-genetic heterogeneity in untreated cycling cells. Similar behaviour is also observed in the other experimental repeats (Figure 44 and Figure 52), albeit these datasets demonstrating a greater proportion of mock treated lineages showing defects in fitness.

The NCS treated lineages, unsurprisingly, exhibit a much higher degree of cell death following DNA damage. Moreover, at the levels of damage used in these experiments, this increase is evident in the treated generation but even more pronounced in the following generations. Visual inspection reveals a great deal of heterogeneity in the behaviour of the lineages, with examples of the different trees possible shown in Figure 24. As in the preliminary data, cell death can take place in any of the three generations analysed and in any particular lineage the cells that die may all belong to the same generation, e.g. both daughters, or may belong to different generations, e.g. daughter and granddaughter cells. Furthermore, the severity of the death varies greatly between lineages, some exhibit complete exhaustion of the lineage wherein all branches of the tree dies out within the three generations analysed. Others show a reduced degree of death ‘penetrance’ whereby some of the branches of the tree are still viable after three generations or at the end of the experiment. There are even some lineages produced from NCS treated cells that feature regularly dividing cells and no cell death, despite all cells being extremely likely to have received damage from the NCS treatment, Figure 26. These lineages may show no defects in fitness due to successful DNA damage repair. The ability to identify sisters at the time of NCS treatment means the pair of lineages they give rise to can also be compared. The lineage trees visualised in Figure 25 show examples of similar and dissimilar pairs, indicating at least that there is no absolute relationship between the sister pairs. One final observation is that somewhat more cells appear to survive without dividing during the experimental timeframe suggesting that these could be either in a state of survival with prolonged arrest or that they simply would have died after the end of the experiment. Similar trends can be observed in the datasets presented in Figure 44 and Figure 52, albeit with varying frequency of cell death following NCS treatment.

Figure 23: All lineages analysed from a single experiment can be visualised together in tree diagrams allowing the diversity of lineage behaviour and NCS induced changes to be assessed.
Treatment was applied partway through the experiment (horizontal black line).

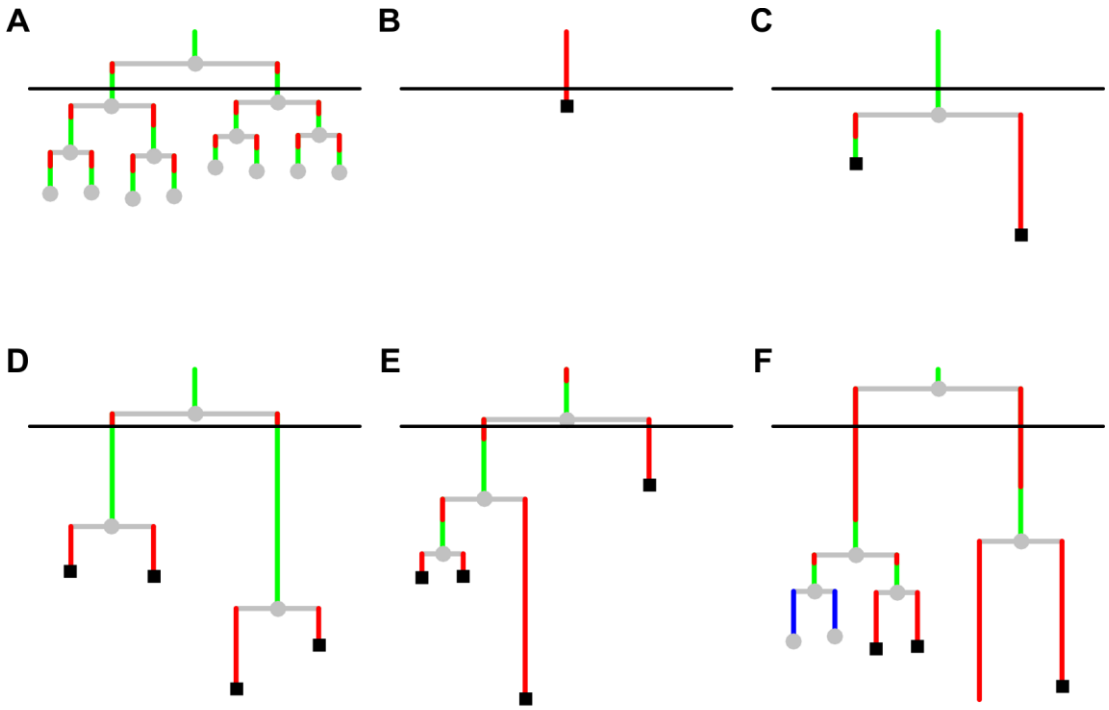

Figure 24: Depicting lineages as family trees allows the heterogeneity of descendant cell fates to be visualised.
A)** Mock treated undamaged cells typically divide regularly **B-F)** Cells treated with Neocarzinostatin to induce DNA double strand breaks show a variety of response when multiple generations are assessed. The treated cell may itself die **(B)** or descendant cells may die in various subsequent generations **(C-F)**. Some descendants will survive and proliferate **(F)

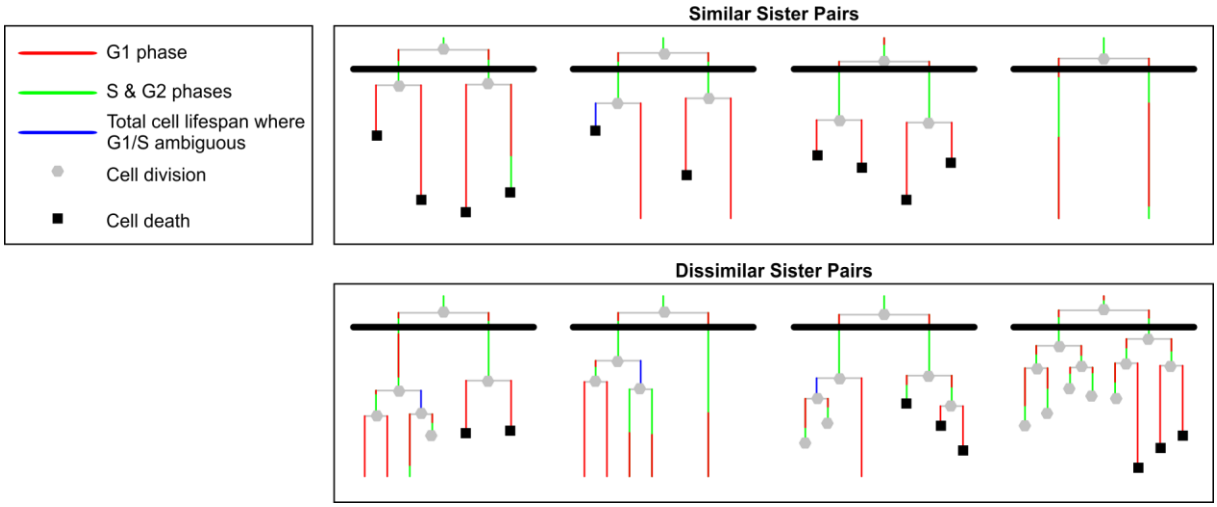

Figure 25: Sister cells both receiving NCS treatment can produce both similar and dissimilar lineages

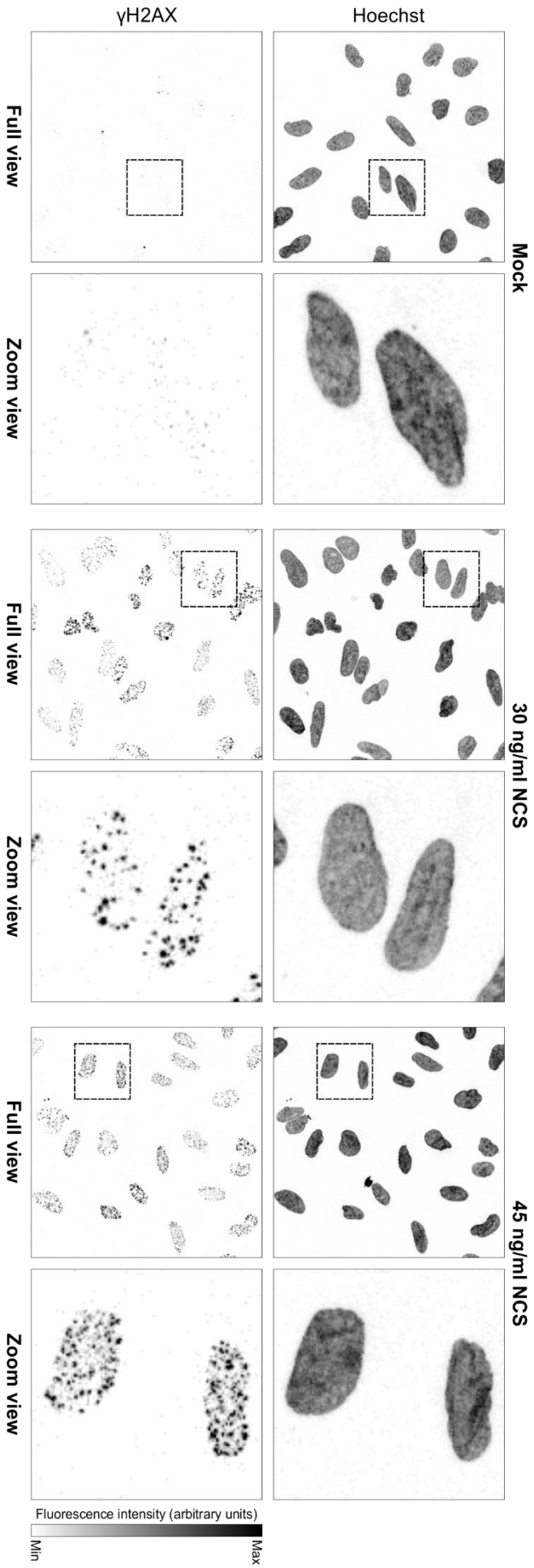

Figure 26: Neocarzinostatin induces the formation of γH2AX foci
U2OS parental cell line cells receiving mock or neocarzinostatin treatments in the same manner as lineage traced cells show DNA damage is evident in all NCS treated cells 1.5 hours after treatment via the formation of γH2AX foci as detected by immunofluorescence. (n=1)

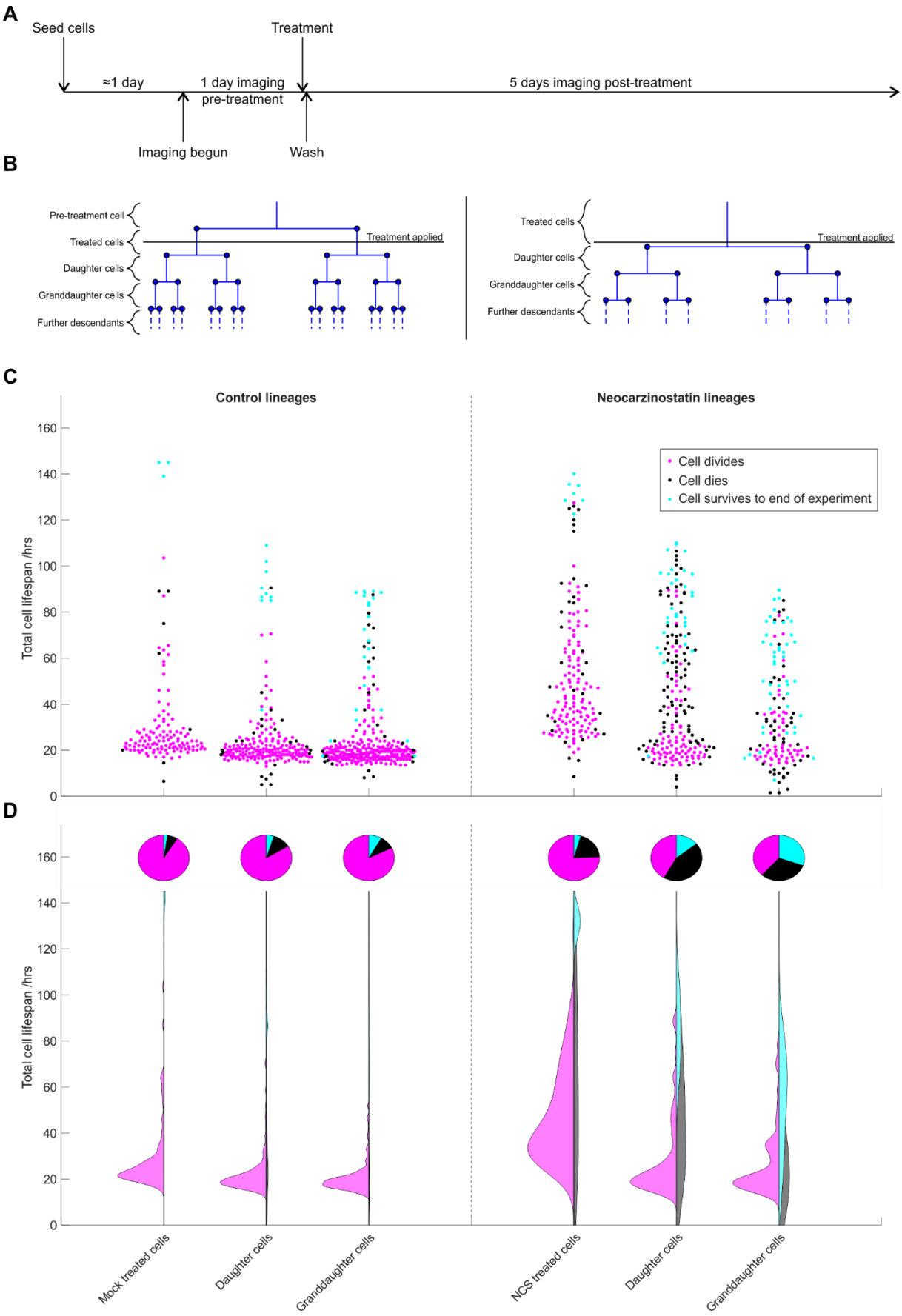
A
Seed cells
Treatment
≈1 day
1 day imaging
pre-treatment
5 days imaging post-treatment
Imaging begun
Wash
B
Pre-treatment cell
Treated cells
Daughter cells
Granddaughter cells
Further descendants
Treatment applied
Treated cells
Daughter cells
Granddaughter cells
Further descendants
Treatment applied
C
Control lineages
Neocarzinostatin lineages
Cell divides
Cell dies
Cell survives to end of experiment
Total cell lifespan /hrs
0
20
40
60
80
100
120
140
160
D
Total cell lifespan /hrs
Mock treated cells
Daughter cells
Granddaughter cells
NCS treated cells
Daughter cells
Granddaughter cells

Figure 27: Generational analyses of mock and NCS treated FUCCI-NM U2OS cells
***A)** Experimental protocol for microscopy-based lineage tracing with treatment part way through timelapse microscopy.*
***B)** Lineage trees can be divided into pre-treatment cells, treated cells, their daughters, granddaughters and further descendants. Depending on whether a cell identified from the start of the experiment dies or divides before or after treatments were applied it will belong to the pre-treatment or treated cell generations respectively. The artifactual population of pre-treatment cells were not further analysed.*
***C)** Swarm plot showing total cell cycle length for FUCCI-NM U2OS cells coloured by cell fate and separated into their generations.*
***D)** Half-violin plots show distribution of swarm plot data and pie charts showing proportion of cell fates adopted in each generation. Cell proliferation shown on left hand side, death or survival until the end of the experiment fates shown on right hand side. DNA damage by neocarzinostatin results in cell cycle arrests in NCS treated cells and increased cell death in Daughters and Granddaughters indicating a delayed death phenotype.*

1.8.2 Generational Analyses

Analysis by visual inspection allows identification of the broad trends in changes in cell fate following DNA damage and allows the heterogeneity of the lineages to be conveyed. To explore the changes further by comparing cells across generations the cells were plotted by generation and cell fate in the swarm and half-violin plots (Figure 27C and D). Hereafter, the treated cells, their daughters and granddaughters for mock and NCS treated lineages are referred to as: $mock^{Treated}$, $mock^{Daughters}$, $mock^{Granddaughters}$, $NCS^{Treated}$, $NCS^{Daughters}$ and $NCS^{Granddaughters}$.

Dividing $mock^{Treated}$, $mock^{Daughters}$ and $mock^{Granddaughters}$ cells predominantly do so after fairly similar cell cycle durations. Each subsequent generation appears to divide slightly faster than the previous ($mock^{Treated}$ 23hrs±3 (median cell cycle length±median absolute deviation), $mock^{Daughters}$ 19.5hrs±2.5, $mock^{Granddaughters}$ 19hrs±2) but only the $mock^{Treated}$ generation shows statistically discernible differences in distribution from the other two (Two-sample Kolmogorov-Smirnov test with 5% significance level: $mock^{Treated}$-$mock^{Daughters}$ p = 7.7E-10, $mock^{Treated}$-$mock^{Granddaughters}$ p = 2.4E-19). Why this is happening is unclear but may reflect differences in the populations that result from changes in the cell culture media over time, increases in cell confluence with time, time since the seeding process, acclimatising to the microscope environment, and the washing of mock treatment in fresh media that the treated cells received and the descendants did not. In any case, the change is relatively small and not particularly concerning. Each generation features a similar small proportion of cells undergoing cell death spontaneously perhaps indicating a background rate of cell death due to endogenous cell processes or any stresses generated by the experimental setup. The proportion of cells surviving to the end of the experiment increases with each generation, as is to be expected given cells in each generation tend to be born later in the experiment than previous generation cells making it more likely each cell in that generation will reach the end of the experiment without dividing or dying. This effect is also visible as a reduction in the maximum cell lifespan recorded with each passing generation (Figure 27C).

The proportion of cells that die is increased in the $NCS^{Treated}$ generation compared with the $mock^{Treated}$ generation, as one might expect from treating cells with DNA damage. The proportion of cells that survive until the end of the experiment without dividing appears little changed suggesting that in this cell type these doses of DNA damage do not trigger prolonged cell cycle arrests of the order of 5 days

in the $NCS^{Treated}$ generation. This would suggest that these doses are predominantly not triggering senescence in this generation. Over 75% of cells divide even after the DNA damage but these typically have longer cell cycle durations, 40.5hrs±12, than the dividing $mock^{Treated}$ cells, 23hrs±3, indicating the activation of cell cycle arrest mechanisms. This arrest can be seen as both an increase in the peak of the half-violin plot indicating where most cells cluster, but also in an increased tail of cells with even longer cell cycle durations. However, the most striking differences between mock and NCS treated lineages are clearly apparent in the daughter and granddaughter generations where the proportion of cells undergoing cell death continues to remain higher than the corresponding generation in the mock treated lineages. Indeed, the increase in cell death relative to the corresponding control generation is much greater in the daughter and granddaughter cells than the increase in cell death in the actual NCS treated cells. The distribution of lifespans of cells that go on to die is much less clustered than the distribution of cell cycle durations of dividing cells, instead showing a more uniform distribution over time. These observations therefore support the previous identification of a delayed death phenotype where cells that survive the DNA damage treatment divide to produce descendants that die instead. In this experiment, in the NCS treated lineages almost half of all daughter cells are observed to die and less than half of the daughter cells are observed to divide leaving the population size of the granddaughter generation actually smaller than the daughter generation. The experiments presented in Figure 45 and Figure 53 while varying in the magnitude of the observable cell cycle arrest and proportion of cell fates in each generation show the same trends and, in particular, similarly show the phenomenon of delayed death being at least as significant as death in the treated generation if not more so. Figure 45B and C indicate that in one experiment the $mock^{Treated}$ cells that divide appeared to have an unusually long cell cycle compared to the later generations indicating that these cells may have experienced a degree of cell cycle arrest for unclear reasons, nevertheless there is still a clear contrast between the NCS and mock treated lineages with the same trends observed above.

Given the increased rate of cell death in the $NCS^{Granddaughters}$ I hypothesised this would be accompanied by the $NCS^{Daughters}$ that divided to produce the $NCS^{Granddaughters}$ having clearly prolonged cell cycles due to the presence of DNA damage that ultimately goes on to cause the death of their offspring. However, comparing the distribution of cell cycle durations of dividing $mock^{Daughters}$ and $NCS^{Daughters}$ shows these distributions peak and cluster in very similar locations, i.e. most cells in both conditions appear phenotypically normal by cell cycle duration. There is however, an increase in the proportion of dividing cells that take longer which can be seen as an increased tail in the half-violin plots which is likely responsible for the two populations distributions appearing to be statistically different (Two-sample Kolgorov-Smirnov test $p = 0.019$). Most dividing $NCS^{Daughters}$ generation cells therefore appear normal, with the differences from its corresponding $mock^{Daughters}$ generation being due to the increased proportion of the minority of cells that take longer. I hypothesised that the daughter cells that take

longer to divide produce the granddaughter cells that die while the daughters with normal cell cycle lengths produce granddaughters that contrinue to cycle. To investigate this, dividing cells were reclassified by their daughter cell fates (for the avoidance of doubt daughter here refers to the daughter of the cell under consideration, not in the sense of $mock^{Daughters}$ and $NCS^{Daughters}$) and redrawn in the swarm plot Figure 28. Here, three different subpopulations are of relevance for comparison, those cells whose daughters also divide, d^{divide} (coded in green), those cells whose daughters all die, d^{die} (coded in red), and those cells who have a mixture of daughters that die and daughters that divide/survive to the end of the experiment, d^{mixed} (coded in yellow). From Figure 28 it is clear that dividing $NCS^{Daughters}$ generation cells with apparently normal cell cycle durations, i.e. between 16-24 hours in length, as compared to the corresponding $Mock^{Daughters}$ generation, can belong to subpopulations d^{die} and d^{mixed}, i.e. produce granddaughter cells that will die. There is clearly no absolute dividing line between d^{divide}, d^{die} and d^{mixed}. However, I hypothesised there could be a more subtle relationship where these populations have different but overlapping distributions of cell cycle duration.

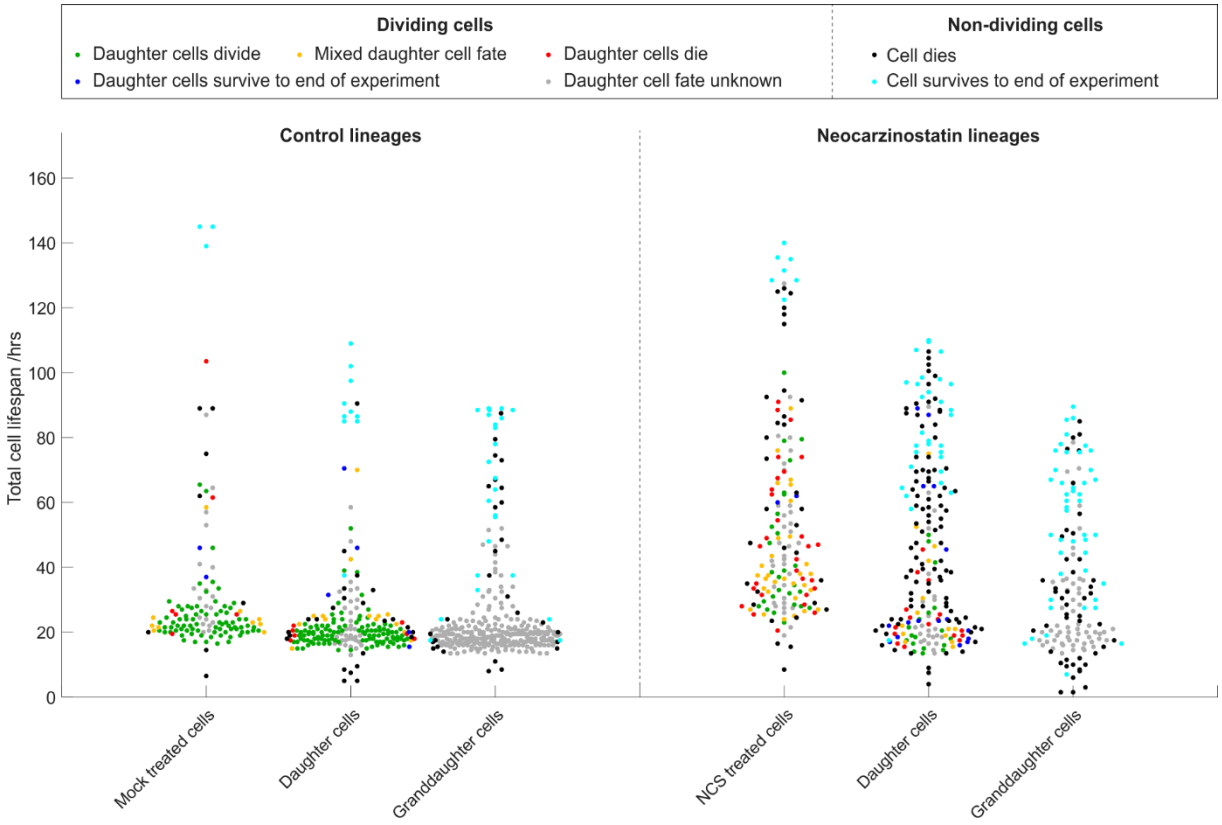

Figure 28: Swarm plot showing total cell cycle length for FUCCI-NM U2OS cells coloured by the fate of their daughter cells if they divide, or by their own cell fate if not.
Daughter cells from NCS treated lineages can produce Granddaughter cells that go on to die after having cycled with apparently normal cell cycle duration when compared to their mock treated counterparts.

Examining the distributions of the cell cycle durations of the d^{divide}, d^{die} and d^{mixed} subpopulations of the $NCS^{Daughters}$ generation allows this comparison to be made. The median cell cycle duration of d^{die}

(18.75hrs) is greater than d^{divide} (22hrs) by 3.25 hrs, while d^{mixed} (21.5 hrs) is greater than d^{divide} by 2.75 hrs suggesting that there could be some difference. Viewing the data in histogram format however, Figure 29, there are no obvious stark differences between the populations, nor does any difference appear to be discernible statistically (Two-sample pairwise Kolmogorov-Smirnov (K-S) test 5% significance level with multiple comparison Bonferroni test). Extending this analysis to the d^{divide}, d^{die} and d^{mixed} subpopulations of the $NCS^{Treated}$ generation does not show any statistically significant differences either between their distributions either. Considering generations from the mock treated lineages as well, the only comparison passing the K-S statistical test (at the 5% statistical significance level with multiple test Bonferroni correction) is the comparison between the d^{divide} and d^{mixed} subpopulations of the $mock^{Daughters}$ generation (p=0.00005). However, when considering the three experimental datasets together neither this nor any of the comparisons had reproducibly statistically discernible differences (data not shown).

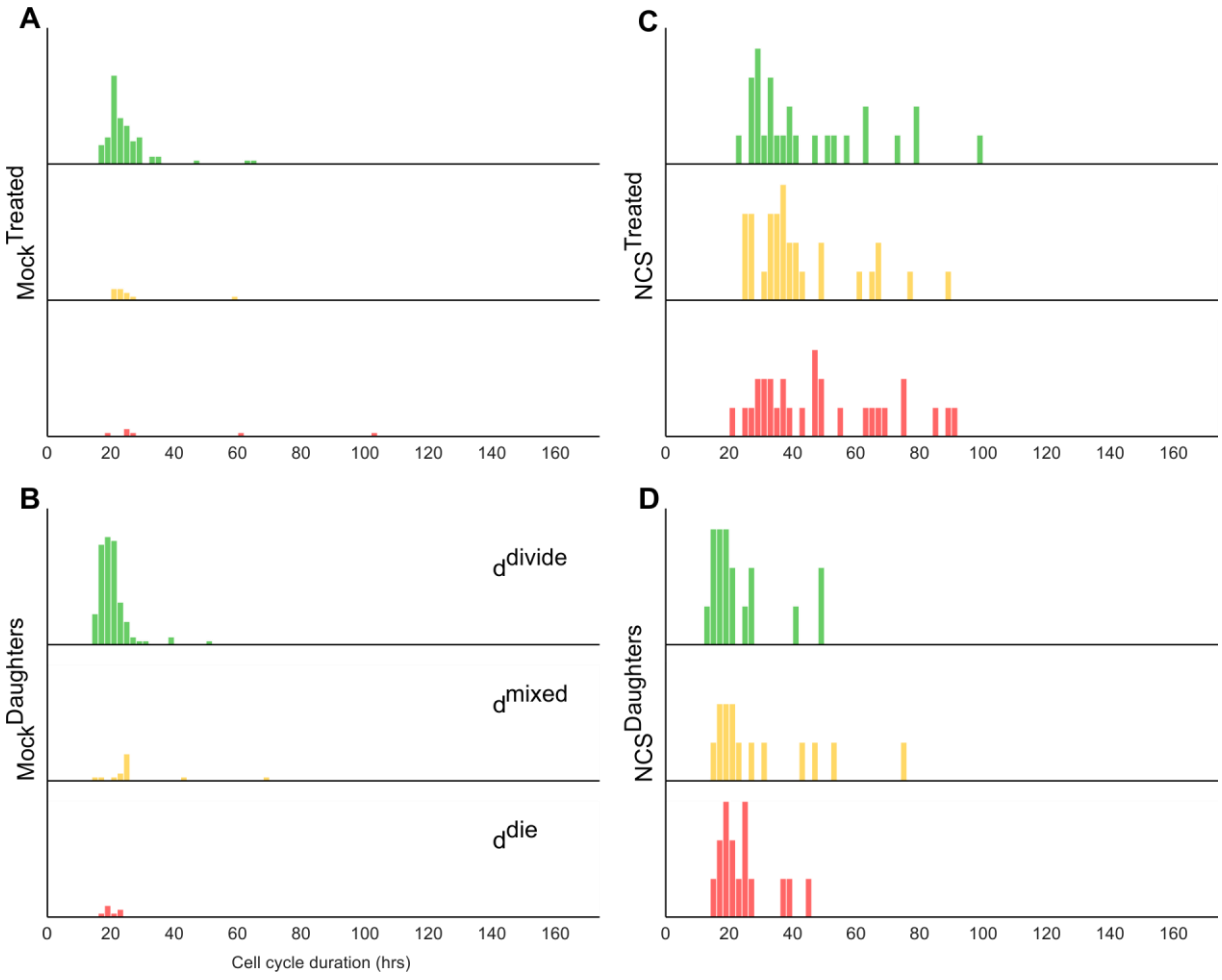

Figure 29: Histograms taken from the indicated generations of cells indicating the cell cycle duration for their subpopulations d^{divide}, d^{mixed} and d^{die}.
***A** and **B)** The highest of the three subpopulations for $Mock^{Treated}$ and $Mock^{Daughters}$ generation cells is d^{divide}. d^{mixed} and d^{die} are much smaller in population but do not appear dramatically different.*
***C)** The NCS induced cell cycle arrest is evident in all three subpopulations of $NCS^{Treated}$ generation cells, there are no stark differences between the distributions three subpopulations.*
***D)** The three subpopulations of the $NCS^{Daughters}$ generation cells all have similar distributions.*

In conclusion, this analysis has two main findings, firstly, $NCS^{Daughters}$ cells that are phenotypically normal with regard to the cell cycle duration can produce descendant $NCS^{Granddaughters}$ cells that die in the next generation. Secondly, although across the three experiments differences can be observed in the median values for the three subpopulations in each generation differences in the distributions of the cell cycle durations of the three subpopulations were not statistically discernible.

These observations are consistent with the preliminary findings and present the interesting conundrum that granddaughter cells that engage cell death mechanisms, and in many cases have prolonged cell lifespans before death, can be born of cells demonstrating no apparent abnormalities in the duration of their cell cycles. If this prolonged lifespan and eventual death is triggered by DDR mechanisms responding to residual inherited DNA damage then one might have expected their parent cell to also show some checkpoint response.

The proportion of cells that survive to the end of the experiment (cyan) also increases in the $NCS^{Daughters}$ and $NCS^{Granddaughters}$ generations compared to the corresponding mock generations $mock^{Daughters}$ and $mock^{Granddaughters}$, possibly suggesting an increase in the number of cells that undergo a prolonged arrest without death or division. However, caution in interpreting this data is necessary as the $NCS^{Daughters}$ and $NCS^{Granddaughters}$ generations are born later in the experiment on average than the corresponding control generations due to the DNA damage induced cell cycle arrest of the treated cells. As discussed above, if a generation is born later in the experiment it would be expected to have a greater proportion of these cells as they have had less time to adopt their final fate.

The FUCCI component of the data allows information about the subdivisions of the cell cycle to be gleaned, I hypothesised that cell cycle delays and cell death may occur predominantly in one of the two subdivisions and so examined the data subdivided into the two measurable phases G1 and SG2M. The contributions of G1 and the combined SG2M phases to the cell lifespans are seen in Figure 30, where all cells for which a G1S transition could be identified are plotted by the duration of the respective G1 and SG2 phases. This reveals that the cell cycle arrests observed in the $NCS^{Treated}$ generation are mostly due to lengthening during S or G2. This is in part because those cells that only received NCS treatment during SG2 would be expected to have normal G1 durations. These plots reveal that death in the $mock^{Daughters}$, $mock^{Granddaughters}$, $NCS^{Daughters}$ and $NCS^{Granddaughters}$ generations occurs more often in G1 than SG2. In contrast death occurs more commonly in SG2M in the cells that actually received the mock and NCS treatments. In the case of the mock treated cells this is likely an issue of sampling, very few cells die and so the sample is unlikely to be representative of what is actually happening. In the case of the NCS treated cells death in SG2M is likely more common because in this experiment most were treated after the G1S transition. These observations indicate that in this cell type death can occur in either part of the cell cycle but that it operates more commonly through G1 based processes. Otherwise, these two subdivisions show similar trends to the total cell lifespan

duration figures, for example the durations of G1 and SG2M in dividing cells in the NCS^{Daughters} generation are comparable to the corresponding mock^{Daughters} generation durations. There is a statistically discernible difference between the distributions of mock^{Daughters} and NCS^{Daughters} SG2 lengths (p=0.0076 Two-sample pairwise Kolmogorov-Smirnov (K-S) test 5% significance level with multiple comparison Bonferroni test), but as for total cell cycle duration it is likely this effect is due to the increased proportion of cells in the distribution's tail, indeed the mean and median values differ only by 2.8 and 0.75 hrs respectively, which are rather subtle changes. There is therefore little evidence that the majority of dividing NCS^{Daughters} cells undertake any obvious dramatic cell cycle arrest behaviour in either phase measured. Similar trends can be observed in Figure 47 and Figure 55.

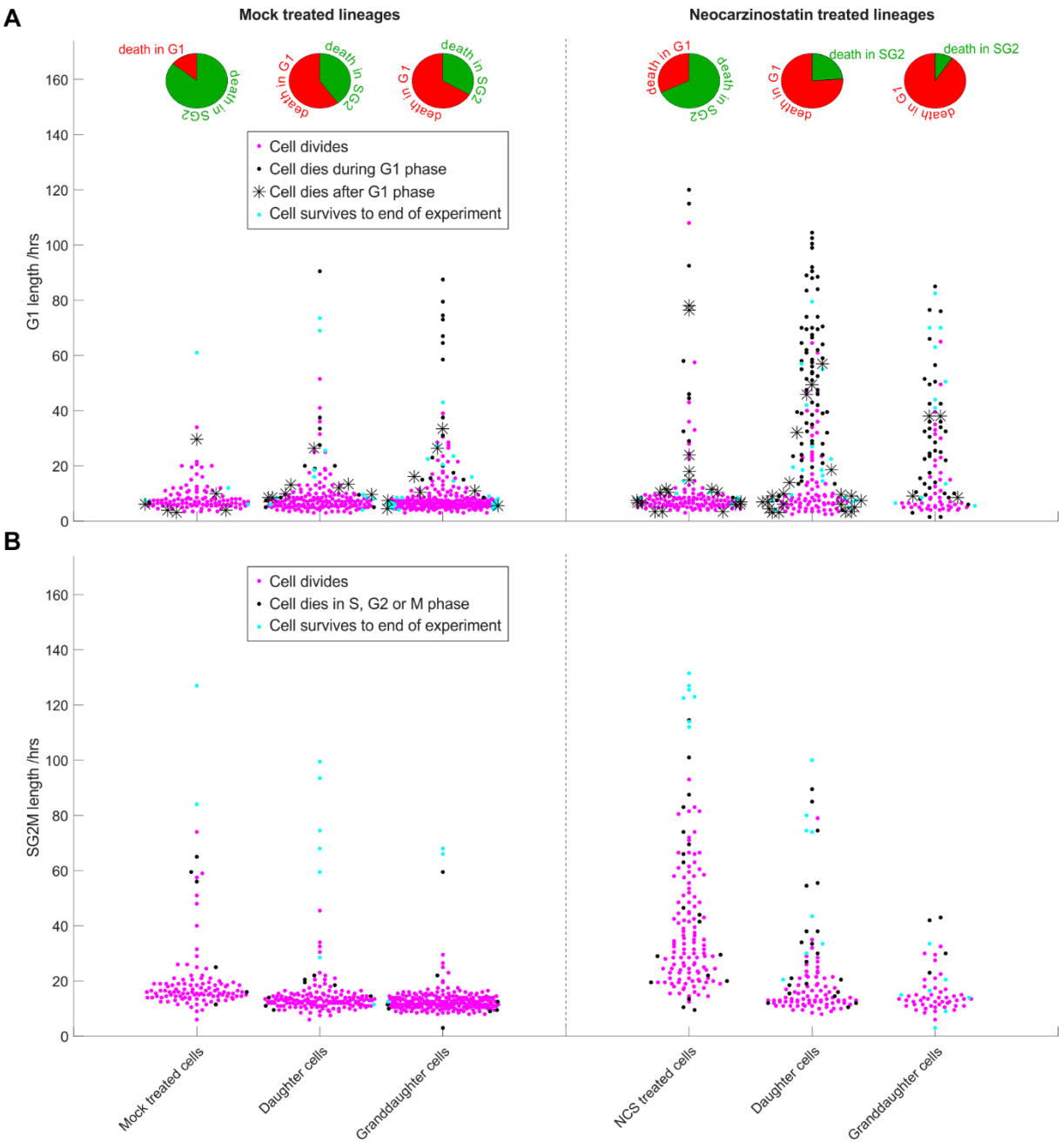

Figure 30: Swarm plots of FUCCI-NM U2OS cells with identifiable G1/S transitions plotted by G1 and SG2M length. NCS induced cell cycle arrests are most evident in the increased SG2M length, in part because many treated cells were treated in SG2M.
***A)** Swarm plot showing G1 length for FUCCI-NM U2OS cells with identifiable G1/S transitions coloured by cell fate and separated into their generations. The proportions of cells dying in G1 or SG2M are indicated in the pie charts. Death occurs most frequently in G1 phase, with the exceptions in $Mock^{Treated}$ generation cells being likely due to small sample size, 7 cells, and in $NCS^{Treated}$ generation cells to the effect that many cells received NCS treatment after successfully completing G1.*
***B)** Swarm plot showing SG2M length for FUCCI-NM U2OS cells with identifiable G1/S transitions coloured by cell fate and separated into their generations.*

1.8.3 Treatment relative to cell cycle position

An alternative depiction of the lineage trees that helps visualise some of these generational findings is given in Figure 31, here the pre-treatment generation of cells are omitted and the resultant lineage trees from cells that received mock or NCS treatment are plotted. These have then been ordered by where the cells were treated in their cell cycle so cells treated at similar times have their lineages drawn together. As cells proliferate the visual density of the tree branches increases and when all three analysed generations are complete the tree terminates leaving blank space in the chart. These plots therefore convey cell proliferation by both how quickly tree density increases over time and how quickly the tree is complete. Furthermore, the death markers indicate the abundance of death and where in the experimental time frame this is occurring. For example, the mock treatment plot shows how cells proliferates quickly with around half of the lineages having completed three generations with little cell death by halfway through the experiment. The NCS treated plot in contrast shows the cell cycle arrests in the lengthening of treated cell traces, particularly evident in the increase in the green SG2 trace when cells are treated in early SG2 (presumably S phase), the greater abundance of cell death markers as cells die and the accumulation of red traces as many of the cells that go on to die do so without a detectable transition from G1. Death can then be seen to occur most abundantly distributed throughout the latter half of the experiment, reflecting that most death is occurring in descendant cells, which are only born later in the experiment. This approach also facilitates comparison between experimental datasets, for example the proportion of G1 cells in the samples in Figure 48 and Figure 56 is higher than the proportion in Figure 31. These sampling differences may contribute to variation between experiments. Another observable difference is in the fitness of the mock treated samples, Figure 48 and Figure 56 show these mock treated lineages tend to have slightly more cell death and cells that survive to the end of the experiment without dividing or dying than shown in Figure 31, as is consistent with the generational analyses shown previously.

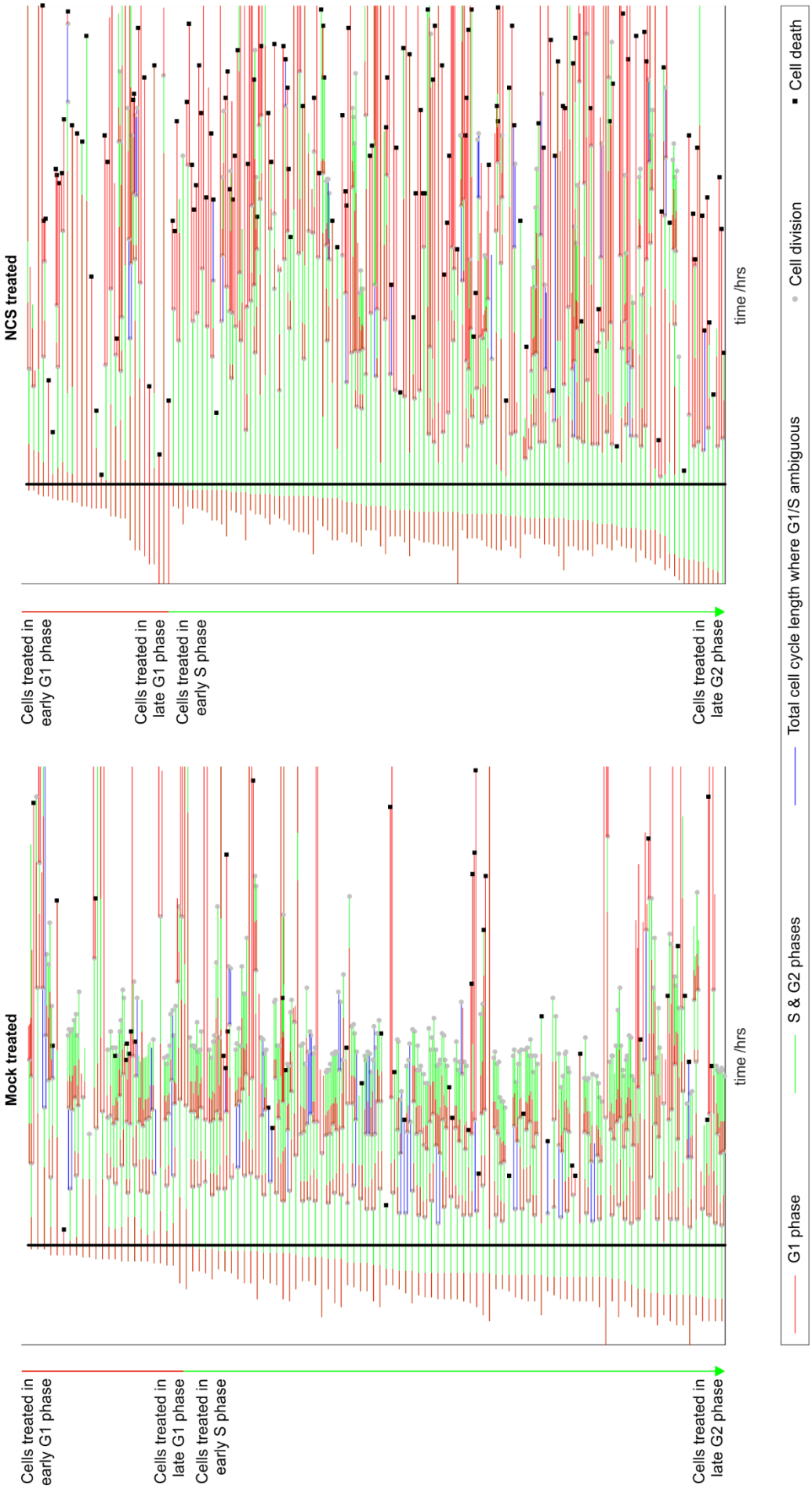

Figure 31: Lineage trees of mock or Neocarzinostatin treated FUCCI-NM U2OS cells ordered with respect to position in cell cycle at the time of treatment. Trees depicted up to the granddaughter generation.

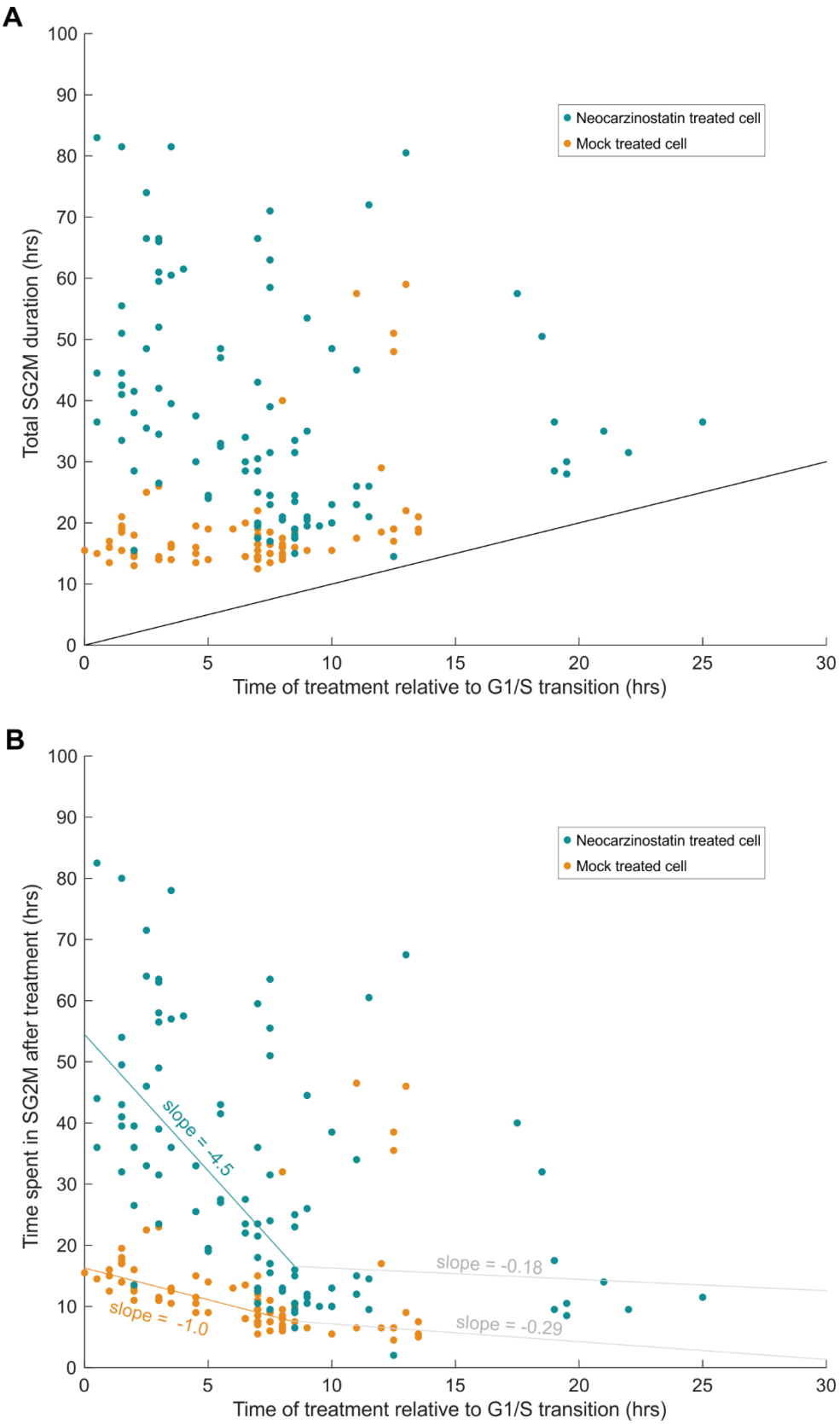

Figure 32: Graphs of cell cycle timing dependencies of the effect of treatments upon SG2M duration
A) *Total duration of SG2M for mock^{Treated} or NCS^{Treated} FUCCI-NM U2OS cells treated during SG2M that subsequently divide against the time of treatment relative to the G1/S transition. Neocarzinostatin treated cells show a cell cycle arrest compared to their mock treated counterparts. This arrest appears to diminish in magnitude the later the treatment time is.* ***B)*** *Time spent in SG2M after treatment for mock^{Treated} or NCS^{Treated} FUCCI-NM U2OS cells that divide. The modelled line of best fits summarise the trends in the data with slopes indicating cell cycle timing dependencies on inducing lengthening of SG2M. Slope values reported to two significant figures.*

These figures give the impression that dividing cells treated with NCS during the green section of their cell cycle, i.e. the combined SG2M phases, tend to spend longer in SG2M the earlier in SG2M the treatment was applied, indicating a possible relationship between the cell cycle timing of treatment and the resultant cell cycle delays. I therefore hypothesised that the earlier NCS treatment was given in SG2M the longer the resultant DNA damage induced cell cycle delay would be. I examined this relationship by plotting the time of treatment relative to the start of SG2M against the length of that SG2M phase indicating the effect that the timing of mock and NCS treatments have on the duration of that phase (Figure 32A). Mock treated cells tend to have quite a flat distribution aside from a few outliers that spontaneously take a long time to progress through the cell cycle, thus indicating, as would be expected, that the timing of mock treatment did not influence the progression through the cell cycle. Cells that received NCS treatment show different behaviour, the SG2M phase length tends to decreases as the time of treatment increases which would suggest that the later the NCS treatment, the shorter the resultant cell cycle arrest. The scatter around this trend appears much larger than the scatter in the mock treated cells which may be due to the variation in arrest that NCS treatment induces even in cells in similar phases of the cell cycle. This downwards trend breaks down for cell treated later in SG2M than around 16 hours. As such cells have already experienced an unusually long SG2M phase this complicates the analysis leading to the effect that after 16 hours the SG2M phase length begins to trend upwards in both conditions. The source of this effect is highlighted by the black line indicating the minimum possible cell cycle phase length for the given treatment time, i.e. a cell cannot have a SG2M phase of length less than 18 hrs if it was treated 18hrs into that phase. From the data here and the data presented in Figure 49 and Figure 57 I surmised that there may be two subpopulations of cells. One population, comprising the majority of cells treated in SG2M, proceeds through SG2M relatively synchronously. In contrast, a minority of cells that have already exhibited an abnormal cell cycle progression at the time of treatment by spending longer than normal in that phase have already become desynchronised relative to other cells. Therefore, the analysis of cell cycle arrest timing will only be meaningful in the former population.

If we were to consider normally cycling cells (median SG2M length 16 hrs) mock treated at 2 hr, 6 hr and 12 hr after the G1/S transition for example, they are likely to progress to mitosis 14 hr, 10 hr and 4 hr after treatment, respectively. Therefore, if plotting the experimental time of treatment against the time since treatment until the transition to mitosis, we should expect a linear trend for the majority of the cells bound by the length of an average SG2M with an approximately -1 slope. The minority of cells with abnormal SG2M progression would not demonstrate this trend and might be expected to show uncorrelated timings. For NCS treated cells, if the duration of the arrest is linked to the time of treatment, as appears evident by eye, we would expect to see a change in the trend, either to a more negative slope or a non-linear relationship, both of which would indicate dependency of the arrest on

the time of treatment. Figure 32B shows the data replotted in this format, where the trends were modelled with two lines, one accounting for the majority population of normally cycling cells and the other for slow cycling cells expected to be uncorrelated and so likely to exhibit shallow slopes.

Here this data indicates that cells treated with NCS soon after the transition from G1 to S phase undergo cell cycle arrests leading to an increase of the remaining phase length to between 35 and 85 hours compared to the approximately 16 hours left in SG2M for mock treated cells treated with equivalent timings. As treatment occurs later in SG2M (indicated by increasing time of treatment) the difference between the NCS treated and the mock declines until the populations start approaching closely to each other around 10 hours into SG2M. At this point it seems that the magnitude of the cell cycle delay following NCS is much diminished and cell cycle phases are starting to approach normal lengths again. Experimentally, the first fitted line for mock treated cells returns a gradient very close to the expected value of -1, i.e. for every hour further into SG2M mock treatment is applied there tends to be one hour fewer left in the phase. In contrast, the data and fitted line for the NCS treated cells shows a clearly stronger negative relationship between the relative time of treatment and the time spent in the phase after treatment, allowing a slope of -4.5 to be determined. This value indicates that every hour later in SG2M NCS treatment is applied the remaining time in the phase will be on average 4.5 hours shorter. This can be phrased alternatively as each hour further a cell progresses into SG2M the duration of the arrest the NCS treatment can induce is reduced by 3.5 hours, once the expected 1 hour decrease is accounted for. The second fitted line provides slopes closer to 0, as expected from a population of that have not passed through SG2M typically and so collectively hold a much weaker relationship between time of treatment and the amount of time remaining in SG2M.

In summary therefore, the earlier NCS treatment occurs in SG2M the greater the extent of the resultant cell cycle delay. This behaviour is also seen in Figure 49, while this behaviour is less obvious in Figure 57, perhaps due to a lower effective dose of DNA damage being received and a less clear arrest, which would be consistent with the reduced severity of the death observed for this experiment. An initial assessment was made similarly of the effect of the timing of treatment relative to the start of G1 in G1 treated cells, however across the three experimental datasets no obvious or reliable trends could be determined (data not shown), likely due to insufficient sample size at this point.

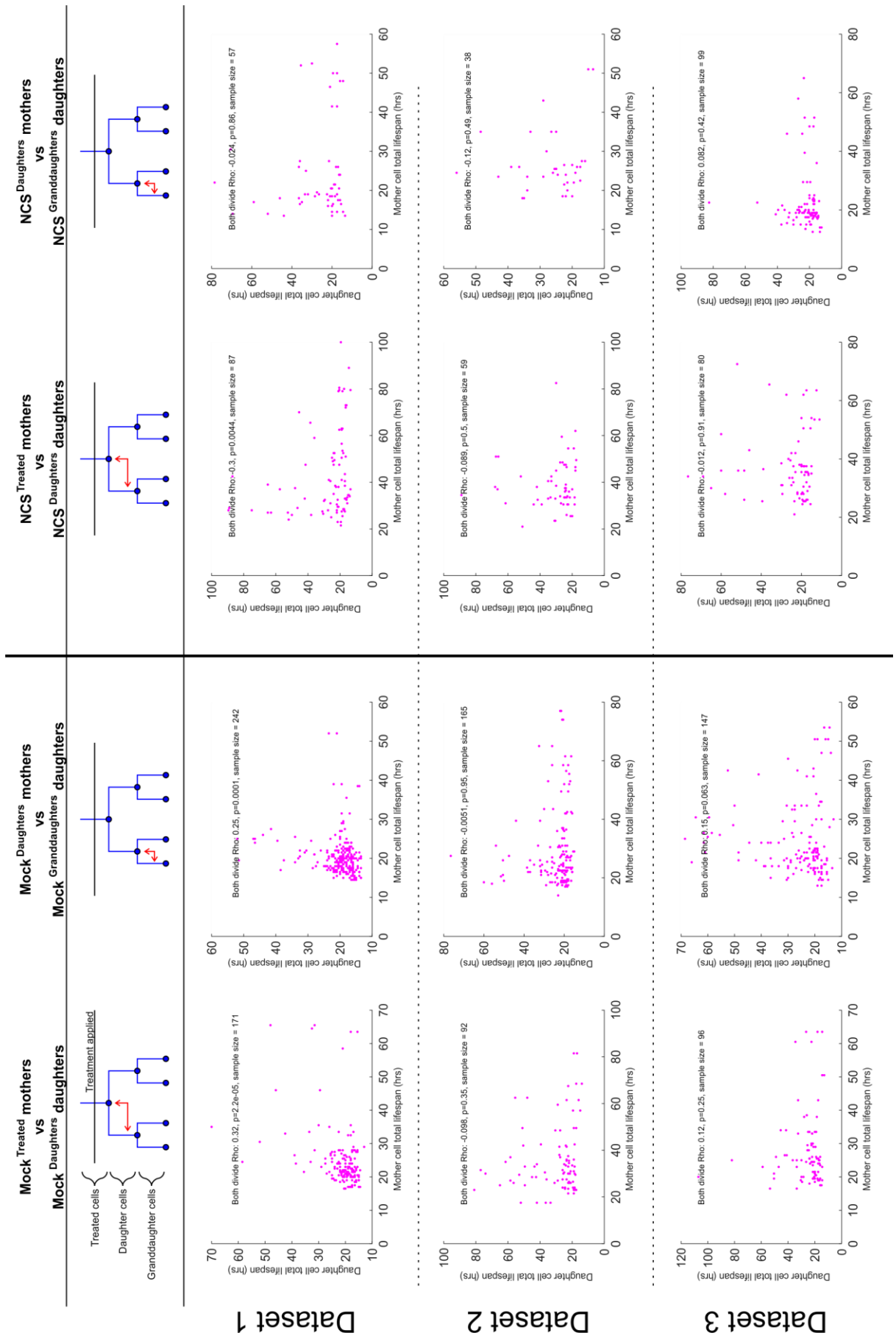

Figure 33: Correlation plots for the four possible Mother-Daughter cell cycle duration comparisons.
Results for three experimental repeats shown. Example lineage trees indicate the familial relationships examined in each plot.

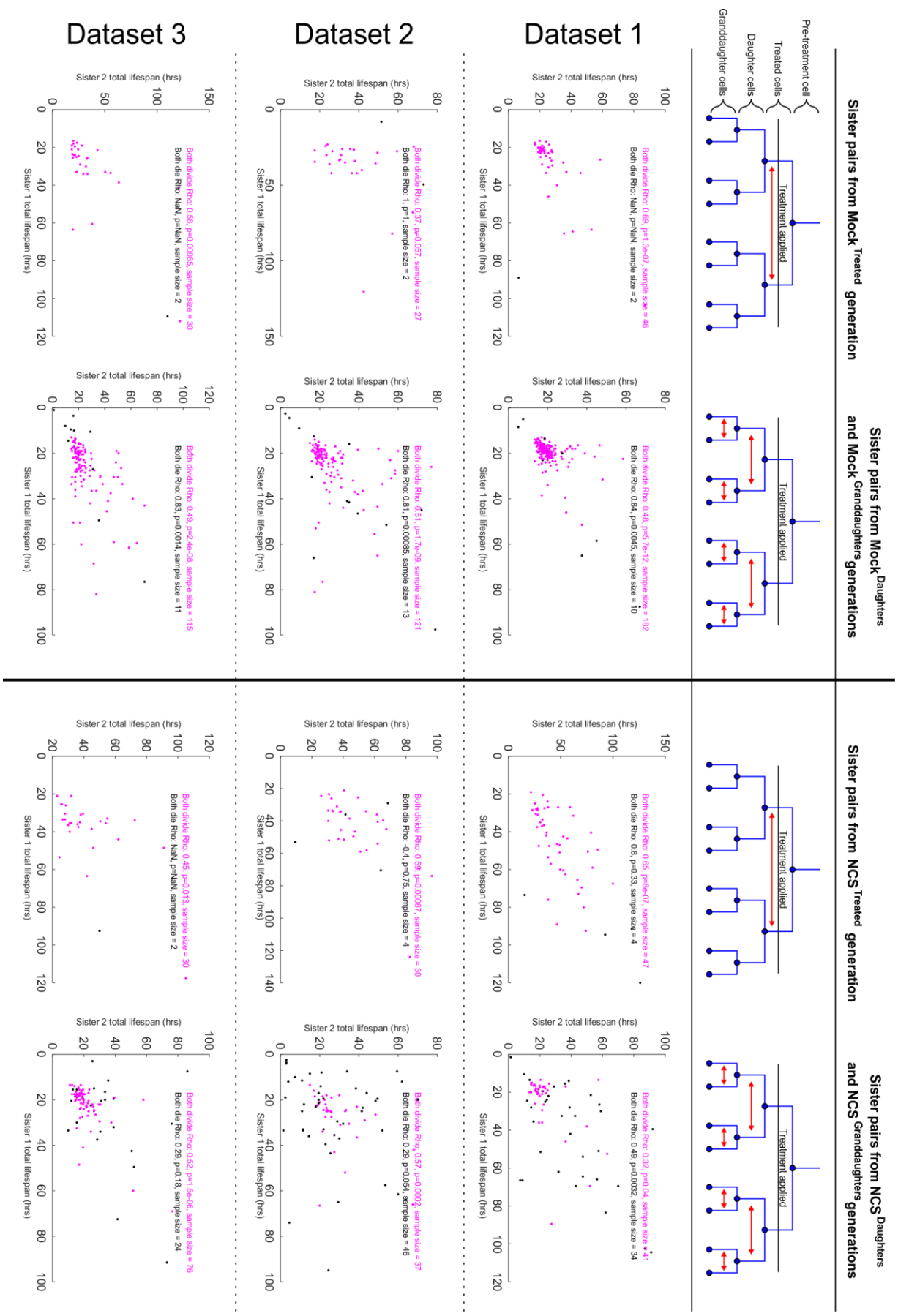

Figure 34: Correlation plots for four Sister-Sister pair cell lifespan comparisons.
Correlations calculated where both sister cells divide (magenta) or both die (black) Results for three experimental repeats shown. Example lineage trees indicate the familial relationships examined in each plot.

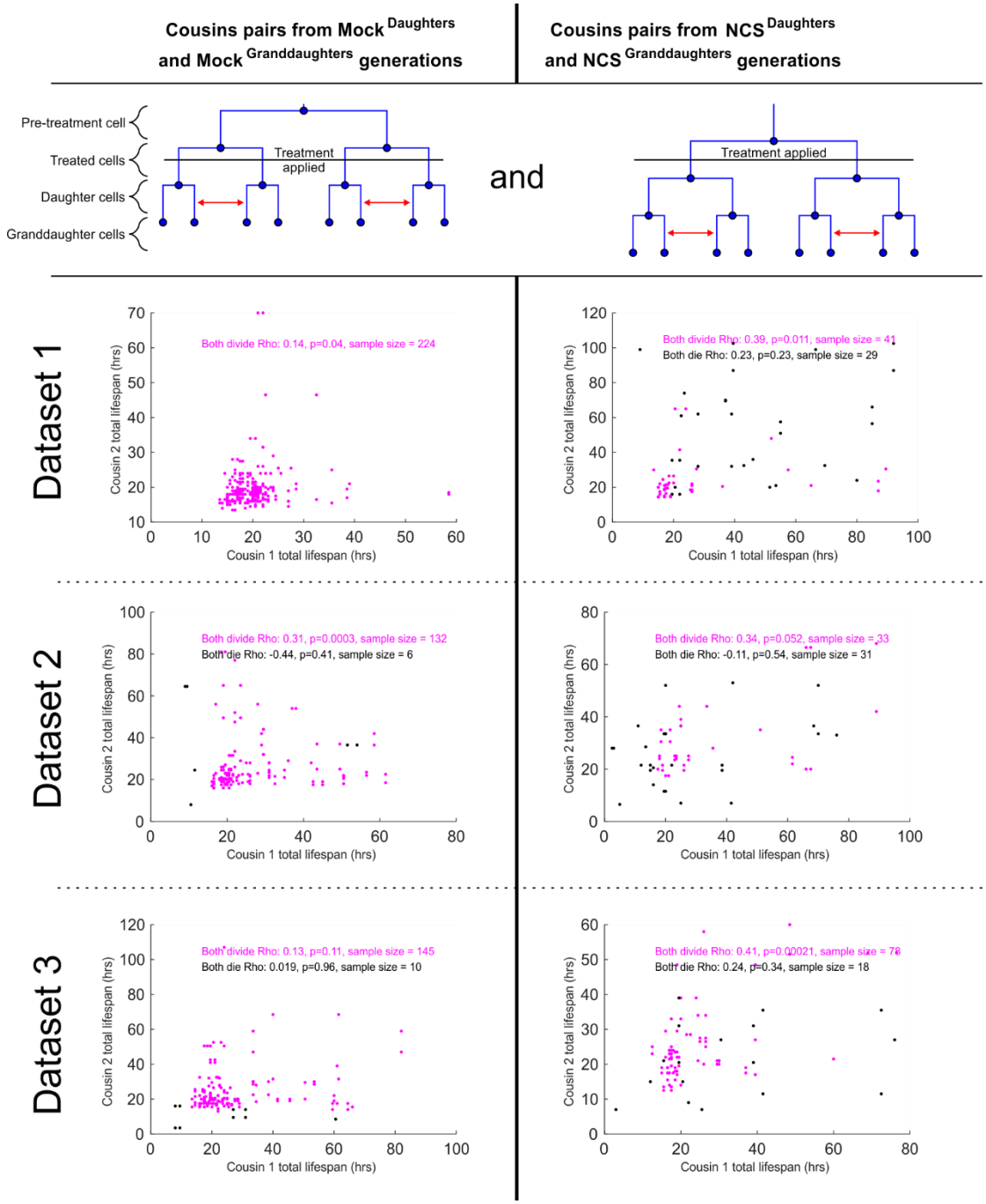

Figure 35: Correlation plots for two Cousin-Cousin pair cell lifespan comparisons.
Correlations calculated where both cousin cells divide (magenta) or both die (black). Results for three experimental repeats shown. Example lineage trees indicate the familial relationships examined in each plot.

1.8.4 Family correlations

The work by (Sandler et al. 2015) discussed in 1.4.2, introduced the use of the FUCCI system and cell tracking across lineages to observe and measure correlations in lengths of the cell cycle, G1 and SG2M between cells of three different particular relationships, i.e. mother-daughter pairs, sister-sister pairs and cousin-cousin pairs. They observed a tendency for sister pairs and cousin pairs to be correlated while mother-daughter pairs were not. I hypothesised that the U2OS cells used here also demonstrate this behaviour and that correlation would change following DNA damage and so I made similar calculations of correlation. In the original Sandler paper there were only three comparisons made, based on dividing cells with the three different relationships analysed. In this work I divide the relationship comparisons into cells from NCS and mock treated lineages and further subdivide these relationships based on whether they feature cells from the $mock^{Treated}$/$NCS^{Treated}$ generations or are derived solely from the post-treatment generations of each lineage, i.e. ^{Daughters} and ^{Granddaughters}. In addition to the cell cycle durations of pairs of dividing cells I also compare the lifespans of pairs of dying cells. The results for all three experimental repeats are presented together in Figures Figure 33 - Figure 35.

The cell cycle duration of dividing mother cells show low to no correlation with the cell cycle durations of their daughter cells in all comparisons made, Figure 33. Across the three experiments and across all mother-daughter cell comparisons the magnitude of the correlation coefficients vary from 0.32 to -0.30 all of which would indicate very low correlation and even this low correlation does not reproducibly pass a statistical test of difference from no correlation. Furthermore, when comparing across different experimental treatments there are no reproducible differences in correlation between:

1) $mock^{Treated}$-$mock^{Daughters}$ and $mock^{Daughters}$-$mock^{Granddaughters}$ mother-daughter pairs.
2) $NCS^{Treated}$-$NCS^{Daughters}$ and $NCS^{Daughters}$-$NCS^{Granddaughters}$ mother-daughter pairs.
3) $mock^{Treated}$-$mock^{Daughters}$ and $NCS^{Treated}$-$NCS^{Daughters}$ mother-daughter pairs.
4) $mock^{Daughters}$-$mock^{Granddaughters}$ and $NCS^{Daughters}$-$NCS^{Granddaughters}$ mother-daughter pairs.

I therefore conclude that there is negligible correlation between mother and daughter U2OS cell cycling durations in all experimental conditions and that NCS treatment, which induces a cell cycle arrest, does not appear to be inducing any changes in correlation either positively or negatively, i.e. the length of cell cycle arrest does not induce a systematic lengthening or shortening of the cell cycle of dividing daughter cells. The observations of the mock treated cells are consistent with the findings of Sandler et al. where the authors observed mother-daughter cells showed very low correlation in otherwise untreated cells. That there is no correlation induced following NCS treatment is, much like the observation that dividing $NCS^{Daughters}$ generation cells do so with fairly normal cell cycle durations,

somewhat surprising based on my initial assumption that DNA damage can be inherited and so affect cell cycle duration in descendant cells.

Dividing sister-sister pairs show more significant levels of correlation, although this too is characterised by variation between experiments, Figure 34. In two out of three experiments the $mock^{Treated}$ generation sister cells show statistically significant moderate correlation (correlation coefficient rho = 0.69 and 0.58, p values < 5% significance with multiple test Bonferroni correction). In all three experiments the correlations between cell cycle durations of sister pairs from either the $mock^{Daughters}$ or $mock^{Granddaughters}$ generations also show statistically discernible correlation and the correlation coefficients are much less variable than other conditions (ranging from 0.48 to 0.51). Sister cells in the unperturbed mock conditions therefore appear to be demonstrating correlation similarly to as reported by Sandler et al. albeit with typically lower magnitude of correlation than the Sandler reported correlation of $\rho = 0.71 \pm 0.07$. Considering dying sister pairs also allows us to observe whether the cell lifespan before death occurs also shows correlation. Very few sister pairs from the $mock^{Treated}$ generation both die in either of the three experimental datasets and so no conclusions can be drawn from this data. 10-13 pairs of sisters that die can be drawn from the $mock^{Daughters}$ and $mock^{Granddaughters}$ generations across the three experimental datasets and these all show high correlation greater than 0.8 and pass the 5% statistical significance test. Thus, spontaneous death that occurs in the mock treated lineages appears to results in highly correlated cell lifespans for those cells that die. This might indicate that the cause of death is inherited and processed in the same way. However, with the small sample sizes of sister pairs that die in mock treated lineages this should be treated cautiously.

The dividing sister pairs taken from the $NCS^{Treated}$ generation of cells also show moderate correlation that passes the statistical test in 2 out of 3 experiments (correlation coefficient rho = 0.65 and 0.59, p values < 5% significance with multiple test Bonferroni correction). These results suggest that when sister cells both received NCS treatment and thus likely experienced some degree of a cell cycle delay, but nonetheless eventually continued to divide they tended to do so with similar cell cycle durations. The lack of obvious decorrelation is consistent with sister cells being typically treated in similar positions in their cell cycle and receiving similar amounts of DNA damage thus undertaking cell cycle arrests that are similar. Nonetheless, it is important to recognise as this is moderate correlation comparable in magnitude to the mock treated lineages, there has been no obvious increase or decrease in correlation that would suggest cell cycle arrests are more or less correlated than unperturbed cell cycle durations. Furthermore, the dividing sister pairs taken from the $NCS^{Daughters}$ and $NCS^{Granddaughters}$ generations show similar degrees of correlation passing statistical significance in 2 out of 3 experiments (correlation coefficient rho = 0.57 and 0.52, p values < 5% significance with multiple test Bonferroni correction). Thus, there appears to be no clear evidence that NCS treatment in ancestors results in changes in the correlation between descendant sister pairs that divide. Dying sister

pairs from the $NCS^{Daughters}$ and $NCS^{Granddaughters}$ generations show either very low correlation or moderate correlation that does not pass the statistical significance test in contrast to the high correlation seen in dying sister pairs drawn from the $mock^{Daughters}$ and $mock^{Granddaughters}$ generations. This would suggest that the NCS driven death of sister pairs is significantly decorrelated with respect to the spontaneous cell death observed in mock treated lineages. Given the small sample size of the dying pairs in mock treated cells this may not be reproducible, but hints at the involvement of stochastic processes in determining cell death timing in the descendant cell death driven by NCS treatment compared to the spontaneous death seen in mock treated lineages.

The final relationship examined was between cousin cells in both mock and NCS treated lineages, Figure 35. There are very few identifiable cousin pairs from the $Mock^{Treated}$ and $NCS^{Treated}$ generations as these can only be born from cells that undergo two divisions between the start of the experiment and the time of treatment, a rare event given this is only 24 hours. Therefore, only cousin pairs from the $Mock^{Daughters}$, $NCS^{Daughters}$, $Mock^{Granddaughters}$ and $NCS^{Granddaughters}$ were examined. Cousin pairs from the mock treated lineages display very low correlation that is statistically indiscernible from no correlation in two out of three experiments and low correlation in the remaining experiment. This is in contrast to the reported findings of Sandler et al. where cousin cells demonstrated correlation of a magnitude only slightly less than sister cells, $\rho = 0.58 \pm 0.08$. This U2OS stable cell line does not appear to demonstrate their observed 'cousin-mother inequality' which may simply reflect a difference in the mechanisms regulating cell cycle progression between the two cell lines. Notably the correlation coefficients between cousin pairs from NCS treated lineages are typically higher than the coefficients for mock lineage cousin pairs in every experiment. However, it is unclear whether these observations are meaningful.

In summary, the mock treated lineages show correlations that broadly recapitulate the sister-sister and mother-daughter correlations reported previously, however cousin-cousin pairs failed to demonstrate meaningful correlation. NCS treatment neither induced correlation in dividing mother-daughter pairs nor did it abolish it in dividing sister pairs. In contrast, there is some evidence from these results that in dying sister pairs correlation is much lower when death is driven by NCS compared to spontaneous cell death in mock treated lineages. Finally, NCS treatment shows a trend to increase correlation in cousin cells but without greater statistical power this observation cannot be confirmed.

1.8.5 Lineage fitness scores

Although limited by the three generations of analysis and the experimental timespan, the lineages presented here can exhibit a great range of outcomes leading to the diversity of lineages depicted previously (Figure 24). This variety arises from differences in the number of generations a lineage passes through, whether different branches of the tree die or survive, and even more unusual

outcomes such as the formation of three cells after a single mitosis. Conceptually, understanding these lineages in terms of their 'fitness' might allow better characterisation of the changes that occur following DNA damage. The extremes of lineage behaviour are easy to conceptualise in terms of fitness, a lineage that features two rounds of division with no cell death will produce 4 viable cells from the original founder cell, suggesting this lineage or indeed the founder cell could be considered to have high fitness. In contrast, a cell that fails to divide at all and then dies could be considered to have very low fitness having given rise to no descendants and failed to survive. Intermediate fitness can be manifested in various ways, a lineage might feature two rounds of division but see two of the resultant granddaughters die. Alternatively, a cell might divide once and then neither of the daughter cells divide, in both cases the same number of cells are alive at the end of the analysis but this has been arrived at by different routes. Understanding how apparently similar endpoints may be reached by different patterns of proliferation and death may have implications for understanding tumour evolution, particularly in response to chemotherapies. To achieve this I developed methods to score the fitness of the lineages, in order to better understand how lineage fitness changes upon NCS treatment and the heterogeneity of the lineages.

A reasonable assumption following DNA damage is that the more generations a lineage passes through the more chances there are for this lineage to survive long term without dying out. Therefore, one measure for how much a DNA damage treatment reduces the fitness of lineages is to compare the maximum number of generations reached by lineages between treatments. In these experiments a maximum of three generations following treatment are analysed, but if a third generation cell, a granddaughter cell, is known to divide the maximum generation a lineage can reach in this analysis is actually the fourth generation. Examples of maximum generation scores are given in Figure 36.

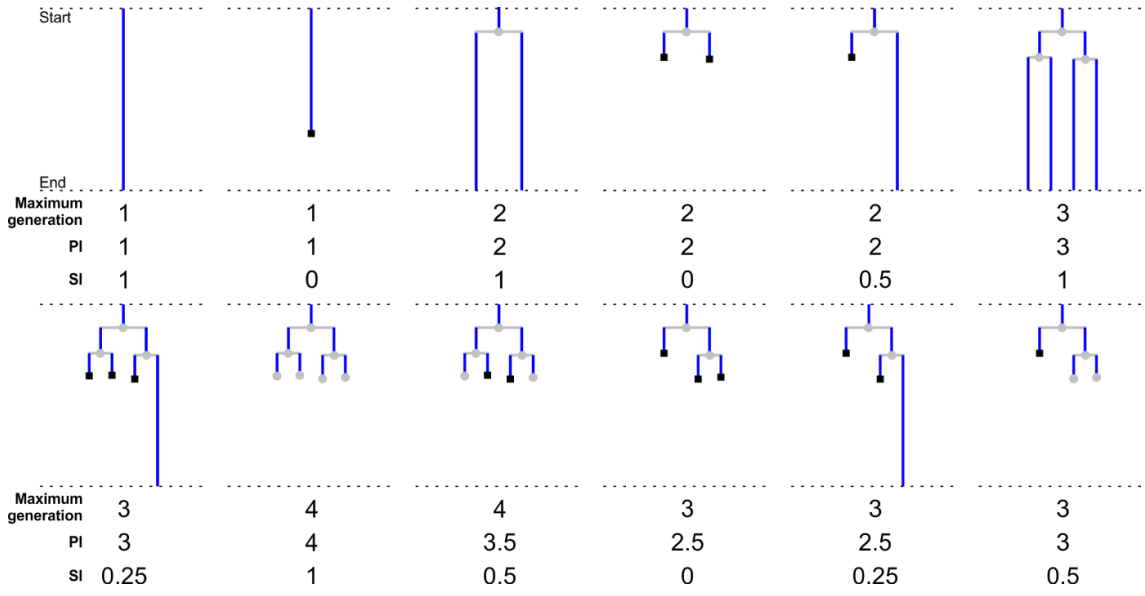

Figure 36: Lineage fitness can be assessed by three different metrics.
Trees can be scored by the maximum generation reached, the Proliferation Index (PI) or the Survival Index (SI). Example lineage trees and their scores for each metric are shown.

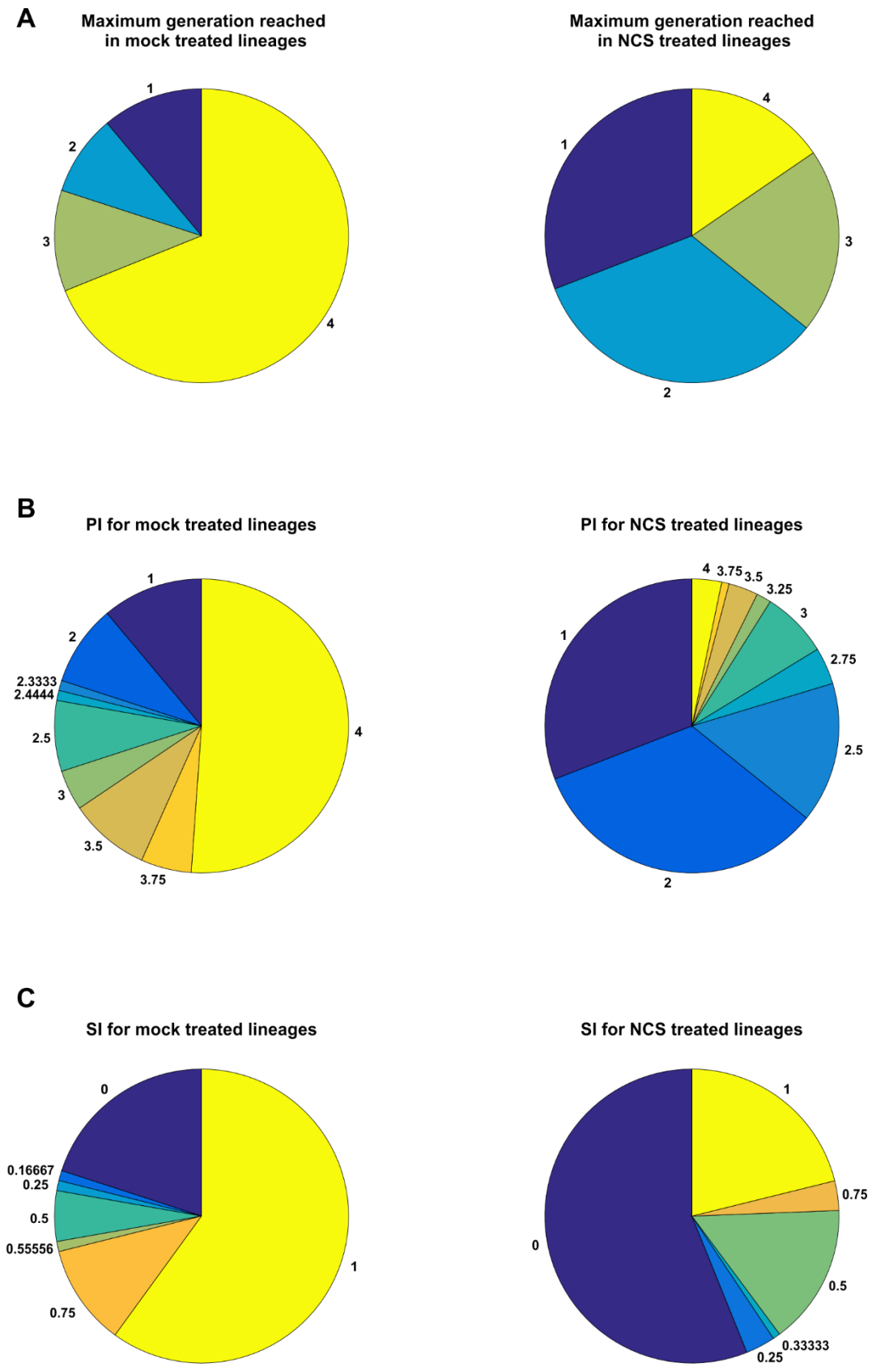

*Figure 37: Heterogeneity and NCS induced changes in lineage fitness can be better understood by scoring lineage fitness Piecharts indicating the proportion of lineages derived from Mock^{Treated} and NCS^{Treated} FUCCI-NM U2OS cells with the given **A)** maximum generation, **B)** PI, or **C)** SI scores.*

Of the mock treated lineages in Figure 24, almost 70% reach the great-granddaughter generation (Figure 37), suggesting the vast majority of lineages have high fitness as one would expect. A further 11% reach the granddaughter generation indicating a reasonable fitness. The remaining 20% of lineages are composed of lineages failing to proceed beyond the lineage founder cell or daughter cells, which given the over five day experimental period clearly shows poor fitness. The change upon NCS treatment is dramatic. Now 30% of lineages fail to proceed beyond the treated generation and a third of lineages do not make it beyond the daughter generation. Only 15% of lineages now reach generation 4, the previously most common score. Broadly, we can see that while there was a degree of heterogeneity in the mock treated lineages there was a dominant class of lineages and that the effect of NCS treatment has been to reduce the number of generations lineages reach within the experimental timespan and also increase the heterogeneity as the four possible classifications become much more evenly spread. These results may be explained by the stochastic nature of DNA damage hits induced by the NCS treatment and stochastic processes in DNA damage signalling leading to a distribution of outcomes following ostensibly the same treatment. Similar trends are observed in the other experiments shown in Figure 50 and Figure 58, with the major differences being the absolute level of fitness for either mock or NCS treated cells. This approach however, while illuminating, does not account for the survival of the cells within the lineage, nor does it account for differences in how many branches of the lineage reach that maximum generation.

Therefore, an alternative measure was derived, termed the proliferation index (PI), which represents an average of the number of generations featuring in the lineage by taking the generation each terminal branch of the tree belongs to and weighting it by the fraction of the tree it represents. Examples of such a scoring system are given in Figure 36. Here the founder cell represents all of the tree, a typical daughter cell represents $\frac{1}{2}$ of the tree and a typical granddaughter cell represents $\frac{1}{4}$. Given the analysis extends to the third generation the terminal branches may have a value of 1 in the case of the founder cell, 2 in the case of the daughter cells, 3 in the case of granddaughter cells that do not divide, and 4 in the case of granddaughter cells which are known to divide. In this case therefore although the great-granddaughters are not analysed they can be accounted for in this score. This includes more information than simply scoring by maximum generation by adjusting for the fact that not all branches may reach the maximum generation.

Applying this method to the same lineages discussed above (Figure 24) allows greater understanding of the variety of lineage behaviour (Figure 37). For instance, now half of the mock treated lineages reach the maximal score of 4, compared to 70% previously. Some lineages previously classed as 3 or 4 by maximal generation now find themselves classed with scores between 2.5 and 3.75 clearly demonstrating how the maximal generation scores overrepresented their fitness. The percentages of lineages scoring 1 and 2 are unchanged by the alternative methodology.

PI values can also better describe the dramatic loss of the highest fitness lineages following NCS treatment, just over 3% score 4 compared to 50% in the mock treated lineages. Thus showing very few lineages now reach the highest possible fitness. The proliferation index also allows a better understanding of the heterogeneity change upon NCS treatment, the large drop in proportion of lineages scoring the maximal PI value of 4 is accompanied by the increased dominance of lineages scoring 1, 2 and 2.5. Therefore, the major change in heterogeneity is from one predominant score to three prominent pluralities. Once again, while Figure 37 shows a single experiment, results from independent experiments (Figure 50 and Figure 58) show very similar trends with the differences mostly being due to a degree of poorer fitness in the mock treated lineages to begin with and variation in how severe the NCS induced fitness reduction is.

Alongside the number of generations a lineage features, another important contributor to assessing lineage fitness is the cell death and survival that occurs. Therefore, I defined a Survival Index (SI) which represents the fraction of the lineage that survives. Each time a member of the lineage dies, ending that branch, a percentage of the lineage is lost depending on how much of the lineage it represents, as was discussed above in the derivation of the proliferation index. Where abnormal numbers of cells result from a mitosis this can lead to abnormal fractions, for example the founder cell dividing to produce three daughter cells will leave each representing $\frac{1}{3}$ of the lineage.

Calculating the survival index for the mock treated lineages, Figure 37C, shows approximately 60% of lineages show no death at all and a further approximately 10% lost only a quarter of the lineage, i.e. one granddaughter cell. Even with only mock treatment, around 20% of the lineages completely die out during the experiment and the remaining approximately 10% of lineages exhibit various intermediate degrees of survival. Similarly to the PI results, it is clear that while there is heterogeneity in the SI scores of mock treated lineages, high survival lineages dominate.

NCS treatment causes a large loss of fitness as assessed by the SI. Over half of all lineages now die out entirely within the three generations analysed leaving no descendants, and around 20% of lineages experience half or more of the tree dying within the three generations analysed. The high fitness lineages of 0.75 SI upwards now represent just a quarter of all lineages compared to around 70% previously. The level of heterogeneity in SI scores does not appear to change dramatically, instead the previously dominant high SI scores have swapped places with the low SI scores. Repeats of this experiment (Figure 50 and Figure 58) show similar trends but with different magnitudes.

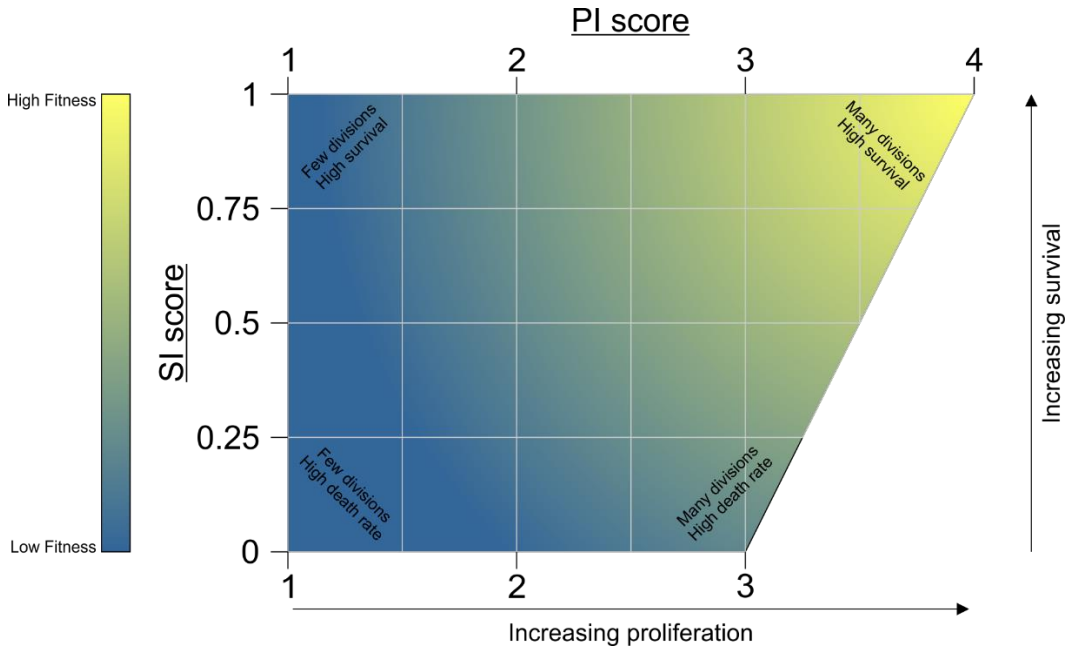

Figure 38: Lineage Fitness Space is defined by the various possible PI and SI scores.
High fitness lineages, i.e. scoring highly for both PI and SI, are found in one corner. As fitness reduces lineages are found further from this corner. The different manifestations of reduced fitness are separated in space facilitating better interpretation of how treatments change lineage fitness.

As the fitness of a lineage depends on both the proliferative capacity and survival of the cells two dimensional plots of PI and SI scores for lineage capture the fitness of lineages better than each alone, diagrams I refer to as 'Lineage fitness space'. This is useful for comparing lineages that by one score appear identical but are clearly very different, for example a lineage which dies out completely and so scores SI=0 may do so by the founder cell dying or it could do so by death of four granddaughter cells. High scores for both proliferation and survival, are found in one corner while lineages with lower fitness populate the remainder of the space. This allows different fitness defects to be visualised in one instructive diagram, lineages featuring few divisions but no cell death (low PI high SI) will be located in a different part of the plot to lineages featuring many divisions but ultimately ending in all cells dying (high PI low SI). Both of these will also be separated from lineages where the founder cell itself dies (low PI low SI). For lineages analysed to three generations the different scores possible for a typical lineage are plotted in Figure 38, which also indicates the differing levels of fitness in the lineage space. Note that some scores are not possible, for example the PI cannot have a value between 1 and 2 as lineages cannot have terminal branches of both 1 and higher generations. Another example is the triangular region between PI scores of 3 and 4 and SI scores between 0 and 1. For a terminal branch of the tree to have a score of 4 it must belong to generation 3 and divide, if it dies instead then it will be scored as generation 3. Thus, as each granddaughter cell dies the maximum PI score possible is reduced by 0.25 from 4. Furthermore, irregular scores are possible when a lineage features abnormal divisions, for example the production of three daughter cells after division gives each daughter cell a weighting of $\frac{1}{3}$ rather than $\frac{1}{2}$, and these are evident where a lineage's PI and/or S.I. score has an unusual fractional component.

Scores were calculated for lineages founded by the mock and NCS treated cells, i.e. ignoring the pre-treatment cells, and the proportions of lineages with each pair of scores plotted in Figure 39. This visualisation permits a number of observations to be made. The most predominant component of mock treated lineages, Figure 39A, at around half of all lineages, are lineages scoring the maximum possible for both PI and SI [4,1], i.e. showing the greatest fitness. The remaining lineages are distributed across various pairs of scores with none forming a particularly large proportion of lineages. NCS treatment causes large changes in the distribution of lineage scores, Figure 39B. The highest fitness collapses to a very small proportion of all lineages and the biggest increases in proportion occurs for lineages dying out entirely through the death of the founder cell [1,0] or through the death of both daughter cells [2,0]. Smaller increases occur for the other possible lineage scores but there is a general shift of density away from the high fitness corner and a shift towards lower PI and SI scores for the intermediate lineages. The advantage of this method of scoring lineages is it permits a more complete understanding of the distributions of lineage fitness both in the mock and NCS treated populations analysed. Mock treated lineages predominantly divide many times to produce descendants which mostly survive. Following NCS treatment lineages are broadly undertaking fewer divisions and experiencing the death of most branches of the lineage as indicated by the shift from high PI high SI lineages being dominant to lower PI, low SI lineages becoming dominant after NCS treatment. There are relatively few lineages following NCS treatment that are high in one index and low in the other, for example [3,0] and [1,1]. This also indicates, consistent with the previous generational analyses, that there appears little evidence for any strong senescence response in these cells at the doses of DNA damage given. If this had occurred it would have been indicated by large increases in the lineages scoring having a low PI score and a high SI score, indicating cells that are alive but have stopped dividing. This scoring system therefore helps separate senescence-like lineage responses (low PI, high SI) from cell death response (low SI). This depiction also indicates how in each condition dominant or more abundant classes of lineage can be identified but that these represent at most half of all lineages, with the rest being distributed amongst various scores. This therefore reflects well the heterogeneity evident by eye from the lineage tree plots discussed earlier and indicates the variability of the underlying biology. Figure 51 and Figure 59 show the same dominance of high fitness lineages in the mock treated sample and the trend towards lineages with low PI and SI scores in the NCS treated samples. As has been commented throughout these other two experiments have tended to demonstrate slightly lower fitness in their mock treated samples and this can be seen in the increased proportions of lineages with slightly lower PI and SI scores. That these still cluster around the high fitness corner of the lineage space indicates that the defects are not very severe and indeed the still stark contrast with changes in distribution of lineages after NCS treatment further supports this.

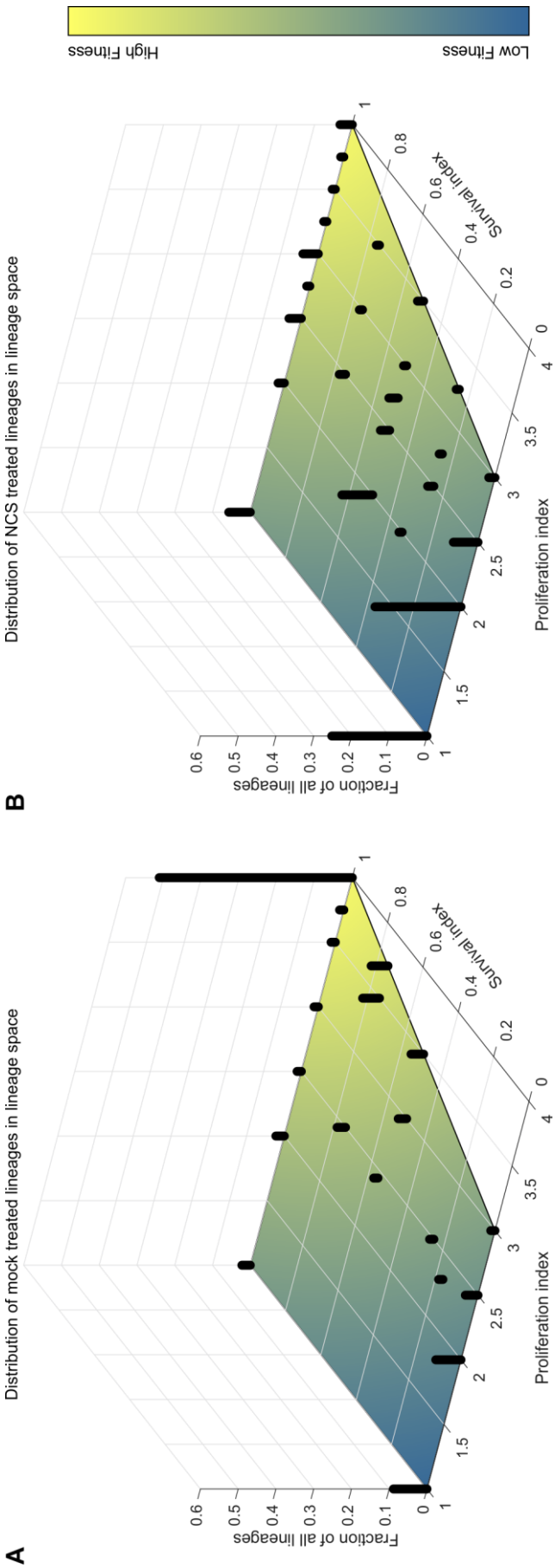

Figure 39: NCS treatment induces a clear shift in lineages away from high fitness and towards low fitness characterised by increased cell death and reduced proliferation
A) Stem plot indicating the proportions of all lineages scoring particular PI and SI scores in mock treated conditions.
B) Stem plot indicating the proportions of all lineages scoring particular PI and SI scores in NCS treated conditions.

In calculating these scores any lineages incomplete due to cells being lost during analysis were discarded. This is likely to have led to a bias towards trees of fewer generations as they will have produced fewer cells to be lost. Nevertheless, even with this bias the results are still illustrative of the changes in lineage fitness that results following NCS treatment.

In summary, the description of lineage tree fitness permits us to better describe the complexity of single cell data. When treated with a DNA damaging agent, U2OS cell lineages experience a dramatic drop of fitness; however, this loss of fitness is experienced both by cells that die immediately upon treatment and by a population of cells that is still cycling leading to a very high degree of heterogeneity. It is also evident that despite this, a small number of NCS treated cells still give rise to reasonably high fitness lineages.

1.8.6 Paired sister lineage comparisons

These experiments were performed with cell lines derived from single clones and at low passage numbers. Therefore, in all effects, the high heterogeneity described is of non-genetic origin. Pairs of sister cells both receiving NCS treatment can be identified, such cells would be expected to be the most similar to each other possible, genetically and epigenetically, having presumably received very similar cell contexts, e. g. proteome composition, upon birth and being likely to have received the NCS treatment during similar periods of their cell cycle. Given this, I hypothesised that these sister lineages would tend to produce lineages that behave similarly, as measured by PI and SI scoring. Paired sister lineages that feature no lost cells, and thus no ambiguity, were identified and their PI and SI scores calculated. Correlation coefficients were then calculated for the PI scores and for the SI scores to examine whether either of the two components of the fitness scoring system demonstrated a degree of correlation. Considering the results across all three datasets together, Figure 40, indicate a moderate level of correlation for both indexes, but with large variation between the experiments in the magnitude of the calculated correlation coefficients for the proliferation index.

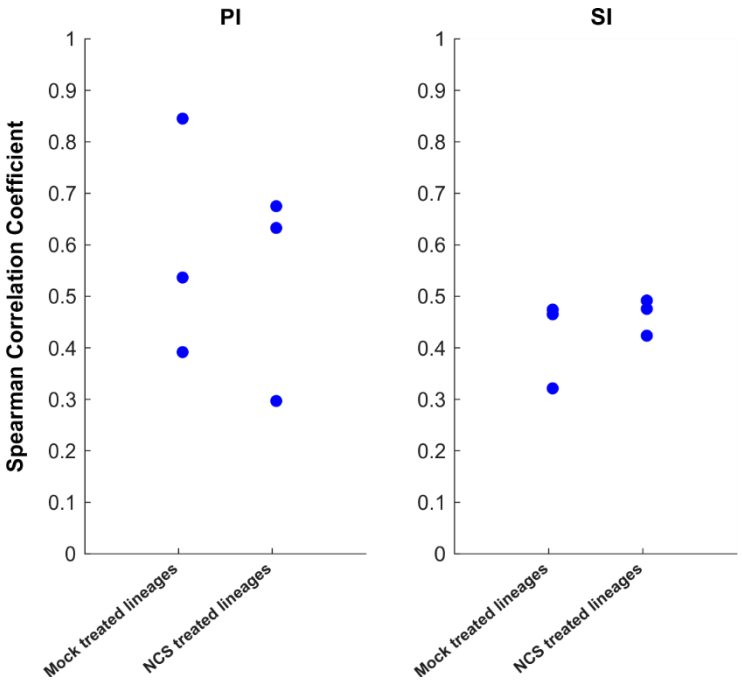

Figure 40: Mock and NCS treated sister lineages appear to moderately correlate in both PI and SI scores to varying extents across experimental repeats.
Results of three experimental repeats shown

To examine this variation the paired sisters were analysed by statistical bootstrapping. In this bootstrapping

analysis, thousands of virtual populations of lineages were created by randomly sampling the sister pairs in the experimental populations. This sampling was with replacement meaning the virtual populations can feature the same sister pairs more than once. Undertaking the calculation of correlation coefficients on each of these virtual populations produces thousands of correlation coefficients. These thousands of calculated correlation coefficients were then used to estimate the average correlation coefficient, its confidence interval and the probability density function describing the distribution of estimates of the correlation coefficient. Furthermore, in order to control for the distribution of correlation coefficients in the case where no correlation due to lineage inheritance could exist, the same bootstrapping analysis was carried out on thousands of virtual populations of cells which had been randomly assigned as 'sisters' to each other, rather than using their actual known sisters. In summary, this statistical method allows the estimation of confidence intervals and probability density functions for the correlation coefficients using only the experimental data. The results for the three experimental repeats examined here are presented as histograms in Figure 41.

These results allow an understanding of why the initially calculated correlation coefficients vary so from experiment to experiment. The probability density function histograms drawn for the PI and SI scores for both the Mock and NCS treated lineages in each of the experimental datasets are broad. This indicates that with these sample sizes and variance of the underlying data the correlation calculated in any experiment is likely to vary from other repeats. It is also clear from the overlap between Mock and NCS treated lineage histograms for both PI and SI scores across the three experimental repeats that there is no reproducible difference between the two conditions. The histograms for the randomised sister pairs for both PI and SI all centre around 0, indicating that the appropriate comparison of correlation for sister pairs is indeed with zero correlation and that the populations are not introducing any background artifactual correlation.

From this I make the following conclusions. Firstly, in mock treatment conditions sister cells give rise to lineages that have low to moderate correlation for both their PI and SI score. That correlation is not higher was somewhat surprising as I expected these cells to be the closest to identical duplicates of each other as is technically possible to achieve and that having received only a mock treatment to have not received an obvious stimulus that would drive them to differ. This result indicates that while they do correlate to a degree there is significant non-genetic heterogeneity between even the cells that one would expect to be the most similar as they can give rise to dissimilar lineages. Secondly and remarkably, addition of the NCS treatment does not appear to change the strength of correlation. This would suggest that the induction of DNA damage in sister cells neither causes dramatic decorrelation between the lineages these cells found, nor does it induce greater similarities. The presence of low to moderate correlation in both mock and NCS treated conditions is consistent with a hereditary component to determining lineage behaviour, but that a great part is still due to chance.

It would be interesting to determining whether greater population sampling is sufficient to reduce the variation in correlation coefficients and thus strengthen these analyses and conclusions.

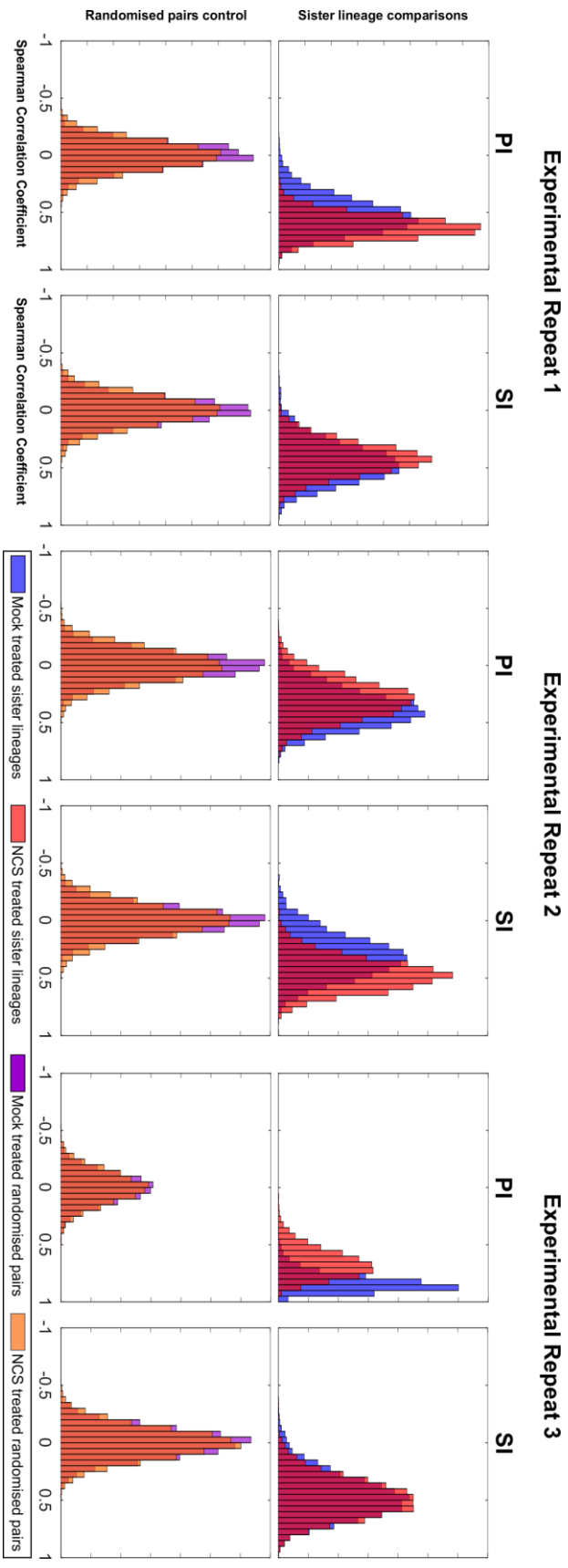

Figure 41:Bootstrapped probability density functions for calculated Spearman Correlation coefficient for sister lineages and control randomised pairs. Results of three experiments shown.

1.8.7 Lineage progression in space and time

During the image analysis and curation the location of each cell nucleus was recorded along with the FUCCI and nuclear marker probe intensities. This data can be used to virtually recreate the experiment for the analysed cells and artificially render cell migration traces through time and convey information via colour coding, such as G1 vs SG2M phases (Figure 42A), cell generation (Figure 42B) and cell lineage (Figure 42C). This can be done for individual lineages (Figure 42A and B) and for entire fields of view (Figure 42C). Spatial correlations were not analysed but may yield further insights.

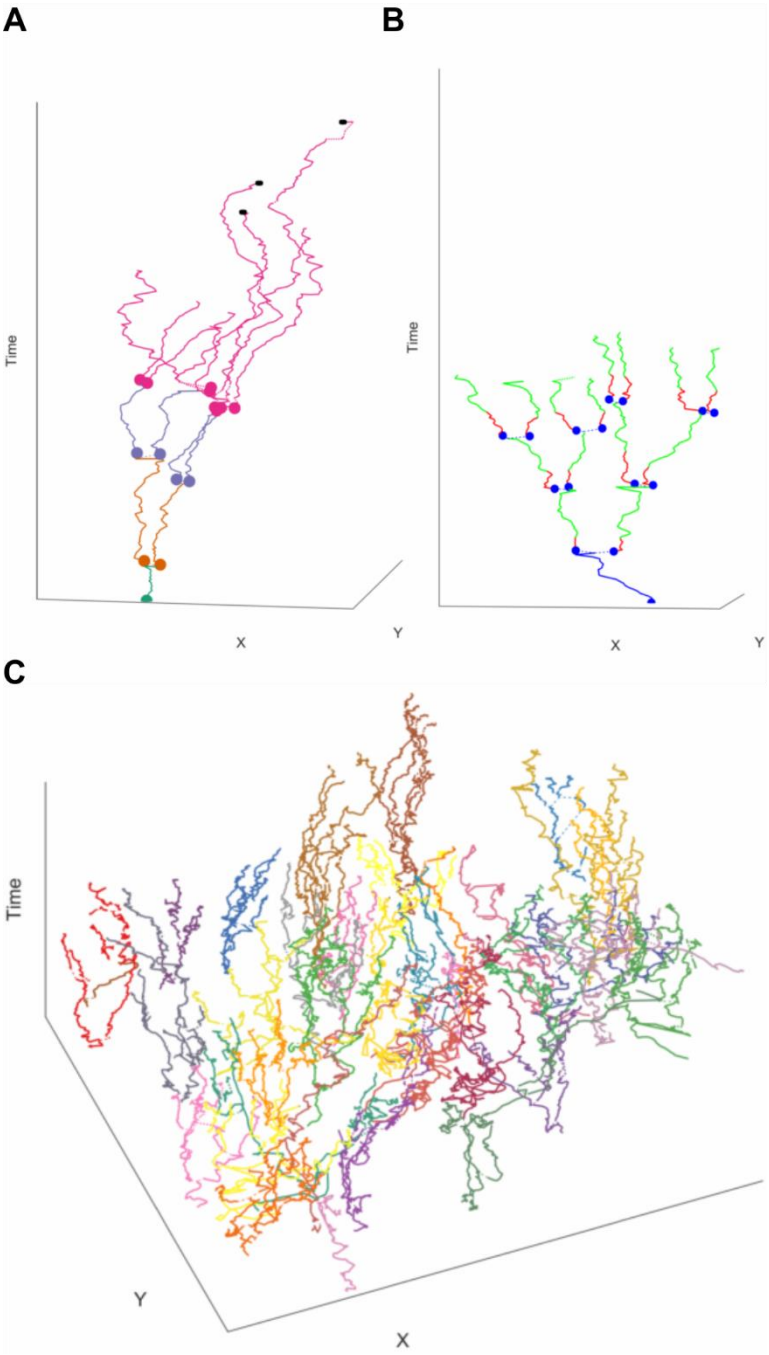

*Figure 42: Cell lineages can be visualised in three dimensions with two-dimensional movement against time. Cells in each lineage may be coloured by which generation they belong to **(A)**, by the FUCCI assigned cell cycle phases **(B)** and by which lineage they belong to **(C)**.*

1.8.8 Other cell lines

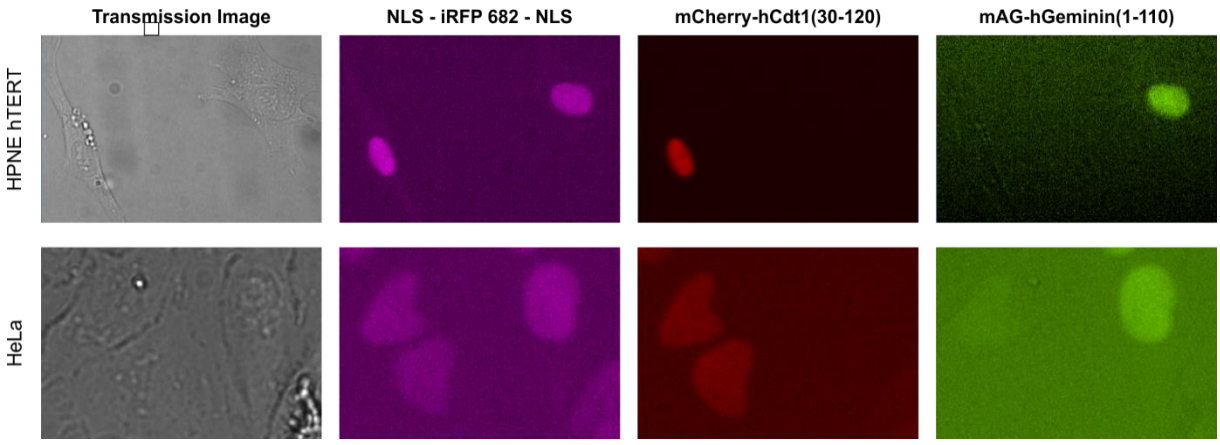

Figure 43: FUCCI-NM in HPNE hTERT and HeLa cell line

The work presented here has featured U2OS cells, a cell line derived from a moderately differentiated sarcoma of the tibia of a 15 year old girl in 1964 (ATCC). These cells have been characterised as being highly altered chromosomally with chromosomal rearrangements and hypertriploid chromosome counts. They have been characterised as possessing wild type p53 but have been reported to lack $p15^{INK4B}$ and $p16^{INK4}$ both of which are involved in cell cycle regulation and a known cancer mutation. These cells are clearly abnormal with respective to a typical cell in the body and so the findings described above are best interpreted with this in mind. These observations are still of great relevance to understanding the biology of checkpoint studies and cancer as such behaviour may be typical of many or certain types of tumour and insights into checkpoint recovery have already been made utilising these cells. In particular, these findings suggest that the observation of G2/M checkpoint negligence reported previously by Liang et al. in this cell line does not simply trigger cell cycle responses in the immediate next G1 phase in the daughter cells as might have been assumed. Instead the responses occur over many cell cycle phases and generations.

Nonetheless, it would be advantageous to characterise more cell lines in order to understand whether phenomenon such as delayed death may also be observed in these, in particular utilising cell lines that have undergone fewer genetic changes and so should be more typical of the cells found in the body. Further cell lines were derived from HeLa and HPNE (Human Pancreatic Nestin-Expressing) hTERT cells expressing either the FUCCI-NM system or simply a nuclear marker amenable to cell tracking. HeLa cells are another cancer cell line that have been studied greatly but are also known to be abnormal in cell cycle regulatory components, for example p53. HPNE cells in contrast are much more normal having been derived from an acinar to ductal metaplasia immortalised through hTERT expression. These feature a relatively normal karyotype, albeit with reports of 50% of cells carrying a derivative chromosome 21, and so are likely to be more representative of human tissues than either U2OS or HeLa cells. Regrettably, HPNE hTERT cells did not prove amenable to microscopy experiments of

multiple days due to much greater cell motility than could be tolerated, resulting in it proving too difficult to track cells and generate lineages. Attempts to manipulate the speed of cell migration with different tissue culture vessel coatings proved unsuccessful. Preliminary data acquisition and analysis of the HeLa cells is ongoing.

1.9 Discussion

In summary, my experiments in lineage tracing have shown that with the levels of DNA damage induced by the concentrations of NCS used here most treated cells can continue to divide and produce descendants, the daughter and granddaughter cells. Interestingly many of these descendants then go on to die, delayed death, which can lead to the extinction of the entire lineage perhaps compensating for the failure of the initially DNA damaged cell to die. Intriguingly granddaughter cells may die even when their mother cell in the daughter generation has cycled with a phenotypically normal cell cycle length, a surprising finding given my initial assumptions that death in later generations would likely be triggered by inherited DNA damage capable of activating both cell cycle arrest and cell death processes. The cause of this delayed death has not been established but the possible causes are discussed further below.

Furthermore, when studying even a comparatively simple phenomenon, such as cell death, at a single cell level, experimental observations become rather complex because of the heterogeneity that cellular behaviour exhibit. This is usually neglected when performing ensemble measurements assuming or trying to establish homogeneous and synchronous responses. Because of this complexity, I have presented here a range of analytical methods to facilitate the description of the experimental observations and to aid their interpretation.

1.9.1 Descendant cell death

The most notable observation has been that delayed death, where cell death most frequently occurs not in DNA damaged cells but in their descendants, is a significant phenomenon within a cancer cell line that has previously been described as having a negligent checkpoint. This confirms previously reported indications that the consequences of DNA damage can extend beyond the cell receiving the damage and raises the possibility that cell cycle checkpoints may operate in a co-ordinated manner whereby subsequent checkpoint processes are influenced by the actions of those previously. Such behaviour might be termed checkpoint cooperation or checkpoint memory. This could provide an explanation for how the apparent negligence of cell cycle DNA damage checkpoints can be tolerated if cell fate decisions are revisited in subsequent phases and generations. Indeed, in the experimental results presented here cell death is relatively uncommon in the $NCS^{Treated}$ generation, increasing to much greater frequencies in the subsequent generations. However, contrary to my initial expectations, rather than observing compensatory checkpoint activation in the first DNA damage checkpoint

following a negligent checkpoint, for example a negligent G2/M checkpoint in a treated cell followed by G1/S in the daughter cells, cell death can occur in granddaughter cells, i.e. having passed through many opportunities for the activation of checkpoint machinery, in many cases with little evidence of such intervening checkpoint activation given the lack of obvious large cell cycle delays.

The analysis of lineage fitness demonstrates that descendant cell death is an important component in the exhaustion of lineages, i.e. where no cells survive. Of all lineages that feature an SI score of 0 just under half of these tend to come from the treated cell dying, the remainder originate from lineages that feature the death of all the descendant cells, predominantly but not exclusively via death of both members of the $NCS^{Daughters}$ generation. As we typically think of the death of a cell that receives DNA damage as an evolutionarily adaptive response that protects the organism via sacrificing a potentially dangerously mutated cell, elimination of a DNA damaged cell's lineage by the death of all its descendants may represent an extension of the same concept. With this in mind therefore, descendant cell death within just three generations is approximately as significant, in terms of percentages of all lineages analysed, as death of treated cells in achieving the exhaustion of the lineage. Furthermore, it is likely that further lineages would have exhausted if the experiment had been longer and more generations been analysed, suggesting the importance of descendant cell death in lineage exhaustion may be greater than observed here. In the first instance, therefore, descendant cell death represents an opportunity to compensate for the failure of DNA damaged cells to die by instead resulting in the death of all the founder cell's descendants.

This raises the question of what the mechanism for triggering death in descendant cells might be. To address this, I have considered three plausible explanations:

1.9.2 Proposed delayed death mechanism: Inherited DNA damage

Inheritance of unresolved DNA damage may simply activate cell cycle checkpoint mechanisms in descendant cells. DNA damage that remains unrepaired despite the activation of cell cycle checkpoint mechanisms for repair might then eventually trigger death in descendant cells. This would be the simplest explanation and does not rely on the existence of unknown mechanisms. However, the observation that $NCS^{Daughters}$ generation cells dividing after phenotypically normal cell cycle durations can produce $NCS^{Granddaughters}$ generation cells that go on to die complicates this explanation. If death is triggered in these $NCS^{Granddaughters}$ generation cells by inherited DNA damage why do their mother cells in the $NCS^{Daughters}$ generation often not show clear evidence of activation of checkpoint arrests?

Checkpoint negligence, as discussed in 1.3.9, has been suggested to operate in two ways, either arising from DNA damage being detected too late for a proper arrest to initiate, timing negligence, or arising from a failure to meet a threshold of activation, threshold negligence. I have observed what might be interpreted as timing negligence where cells treated in late SG2M have typically short arrests. The

simplest assumption therefore might be that a checkpoint that fails to prevent the transmission of DNA damage due to timing negligence will simply recognise it at the next competent checkpoint and address it then, either by arresting and repairing or by dying or senescing. Similarly, a checkpoint that fails to prevent the transmission of DNA damage due to negligence over the threshold of activation, for example a G2/M checkpoint faced with few lesions or high Plk1 activity, might simply result in the activation of the next more sensitive checkpoint, perhaps daughter cell G1/S checkpoints. Some of the delayed death observed here could be explained by this, daughter cells dying in G1 may be activating robust G1 checkpoint responses to inherited DNA damage that passed through their mother cell's G1/S or G2/M checkpoints by one of these kinds of negligence. However, for death in later cell cycle phases and generations to be explained simply by a checkpoint response to persistent DNA damage requires that the intervening checkpoints that permitted continued passage of this DNA damage to also be negligent as they neither robustly induce cell death nor do they show much evidence of a cell cycle arrest.

If this is the case, why are intervening checkpoints sometimes negligent and sometimes not? Timing should no longer be an issue as the damage will be present throughout that cell cycle phase but perhaps checkpoints in U2OS cells have a probabilistic threshold negligence to activation whereby the typical levels of damage inherited in these experiments has a chance of activating a checkpoint response and leading to cell death. However, it does not explain why cell death is the most common effect in later generations, rather than cell cycle arrests followed by a return to cycling.

Another possibility is that cells in the daughter generation that do not die have inherited some DNA damage but not enough to trigger a cell cycle arrest due to checkpoint negligence. The processes of replication and/or mitosis upon damaged DNA in these cells may stochastically trigger a crisis of greatly increased damage so that there is now sufficient damage to trigger checkpoint responses leading to cell death. Micronuclei, for example, are an aberration that result from damaged DNA passing through mitosis.

An alternative speculative explanation is provided by the work on telomere deprotection discussed in the Introduction (Cesare et al. 2013). Here, a particular lesion in the telomeric region of chromosomes was capable of activating some cell cycle checkpoint components leading to stable senescence in descendant cells but fails to trigger an arrest in the original cell. Furthermore, telomeric DNA is known to be resistant to typical DNA repair mechanisms (Fumagalli et al. 2012). This indicates that the cell cycle checkpoint machinery discriminates based on different genomic contexts. An analogous scenario could be happening here where DNA damage in a particular genomic context may fail to be repaired by the initial cell and upon inheritance by descendant cells be capable of triggering cell death responses but not cell cycle arrest. This context may not necessarily be telomeres, a relatively small stretch of the genome (average length in human populations 5-15 kb Samassekou et al. 2010), there may instead be

other undiscovered regions that are treated differentially. If this were the case then clinical interventions could be imagined that preferentially trigger damage in these genomic contexts in tumour cells to trigger high rates of lineage exhaustion and thus tumour regression.

Alternatively, it may be that DNA damage passing through cell cycle checkpoints in the initially treated cell experience some process that leads to residual lesions being marked resulting in differential activation of cell cycle arrest and cell death mechanisms in descendant cells. Such a mark would have to be resistant to erasure by the processes of replication to explain responses beyond the G1 phase of daughter cells. One possible, albeit imperfect, analogy is the way aphidicolin induced partial replication results in the formation of persistent DNA damage and 53BP1-containing OPT domains in the G1 phases of daughter cells (Harrigan et al. 2011) rather than in the G2 of the aphidicolin treated cell.

1.9.3 Proposed delayed death mechanism: Checkpoint memory

An alternative explanation is that cell death in descendant cells is governed instead by non-DNA damage mediated signals that are inherited and predispose cells to engaging cell death mechanisms. A precedent for such a mechanism has been set by the reporting that endogenous replication stress results in DNA damage being inherited by daughters, but importantly, so is hypophosphorylated Rb protein and elevated levels of p21. This then leads to the triggering of quiescence in the daughter cells immediately after birth (Arora et al. 2017). It is possible therefore that during the checkpoint activation in DNA damaged cells certain DDR components, for example p53, experience changes, perhaps in level or post-translational modification, that are inherited by the descendant cells leading to increased predisposition to cell death. It is also possible this effect would work in combination with inherited DNA damage. Inherited changes in the DDR mediators could alter checkpoint responses to favour cell death and disfavour cell cycle arrests in descendant cells. Such an effect would constitute a cellular memory whereby descendant cells 'remember' their ancestor experienced DNA damage.

1.9.4 Proposed delayed death mechanism: DNA damage triggered cell deregulation

A third possibility is that the DNA damage created in the treated cells results in severe consequences for the cell's ability to maintain cellular homeostasis, manifesting as a predisposition to cell death in descendant cells. A plausible suggestion for the type of consequences posited here is structural rearrangement of the DNA during mitosis in cells with residual damage. The formation of micronuclei and chromosome loss/gain in daughter cells would be expected to lead to disruption of typical gene regulation, resulting in gene expression changes and alteration of homeostatic regulatory networks. Such changes might weaken the cell's normally robust ability to respond to typical stresses during the cell cycle and so result in an increased chance of cell death. These changes might not trigger cell cycle arrest mechanisms, especially if the basic lesions themselves have been resolved or silenced in the process of generating these abnormal structural rearrangements, but would bring about an increased

probability of cell death. Delayed death in this case might therefore be triggered in the absence of DDR activation and it may thus be possible to distinguish this experimentally from death triggered by inherited DNA. This scenario would not represent a deliberate reassessment of inherited damage by later checkpoints, i.e. checkpoint cooperation, instead being the consequence of permanent damage to the genome.

In conclusion, there are a number of possibilities for how cell death could be triggered in later generations and it should be possible in future to interrogate these experimentally, for example by searching for evidence of persistent DNA damage, by screening for the presence of aberrations such as micronuclei and by determining the activity of checkpoint machinery in cells over time and generations.

1.9.5 Checkpoint negligence in U2OS cells

Human and cancer cell checkpoint negligence has been increasingly studied in the past decade, as discussed in 1.3.9, and my analysis of the DNA damage based checkpoint responses in SG2M of the U2OS cells provides further characterisation of the checkpoint behaviour previously assessed by (Liang et al. 2014). I found that following transition into S phase the capacity for cell cycle arrests following DNA damage decreases as cells progress further into the combined SG2M phases, with arrests close to the normal time of mitosis approaching zero in length. Part of this explanation might be that cells damaged in S phase can experience elongation of the cell by the actions of the replication, intra-S-phase and G2/M checkpoints, while cells irradiated in G2 can only experience cell cycle elongation by the G2/M checkpoints. This can be further explained, as the work by Liang et al suggested, by cells accumulating commitment to mitosis during G2 in the form of increasing Plk1 activity. The typically higher levels of Plk1 likely to be encountered when damage is induced in cells that have already progressed far into SG2M could then limit the extent of possible arrest relative to cells treated early in G2, i.e. a form of timing negligence.

1.9.6 Correlations analysis

I have here presented work that shows U2OS cells demonstrate similar correlation trends between mother-daughter and sister-sister cell pairs to the observations made by Sandler et al. Interestingly, I did not observe the same cousin-cousin pair correlation suggesting that these cells differ in that regard.

Against my initial expectations I observed no clear trend of changes in correlation being induced by NCS treatment. I had expected that DNA damaged mother cells might pass on DNA damage to their daughters and in so doing induce correlation, for example mother cells with short arrests, and thus little time to repair damage, due to treatment late in G2 would tend to pass on more DNA damage to their daughter cells who might then be expected to have longer cell cycles than other cells inheriting less damage due the triggering of checkpoint responses. That this does not appear to be clearly

happening may reflect the previous observation that most daughter cells cycle with normal or near-normal durations. These observations may be informative in future studies to determine the mechanism of this behaviour.

Similarly, the lack of significant change in PI and SI correlations upon NCS treatment was also surprising. NCS treatment represents a strong perturbation to normal cell behaviour but it would appear the determinants of lineage behaviour are just as correlated after NCS treatment as they are in unperturbed mock treated lineages.

1.9.7 Conclusions

In conclusion, this work has analysed the scope and significance of responses to DNA damage both in treated cells and their descendants enabling the characterisation of the significant multigenerational consequences of DNA damage discussed above. Altogether this work has also presented a number of innovative and novel ways to describe, analyse and model the behaviour demonstrated by cells and lineages following treatment with DNA damage. These have enabled trends and concepts that may appear evident to the eye to be quantified and explored, for example both the heterogeneity in lineages and the changes induced by NCS treatment are well characterised by lineage fitness scoring.

Characterisation of additional cell lines to establish whether delayed death is a more widespread phenomenon will be necessary to determine its wider biological relevance. Given the technical difficulty of generating large numbers of transgenic cell lines and analysing them via microscopy-based lineage tracing. Furthermore, microscopy is ill suited to probing the mechanistic basis of delayed cell death and it will be necessary to adopt other means to distinguish between the mechanistic possibilities outlined here. Once aware of the level of non-genetic heterogeneity and the observation of ‘delayed death’ that can be misinterpreted as prolonged cell arrest in population measurements, alternative assays to characterise lineage behaviour in different cell lines and begin to address mechanistic insight were developed as described in chapter 0.

1.10 Supplementary Figures

1.10.1 Experimental repeat 2

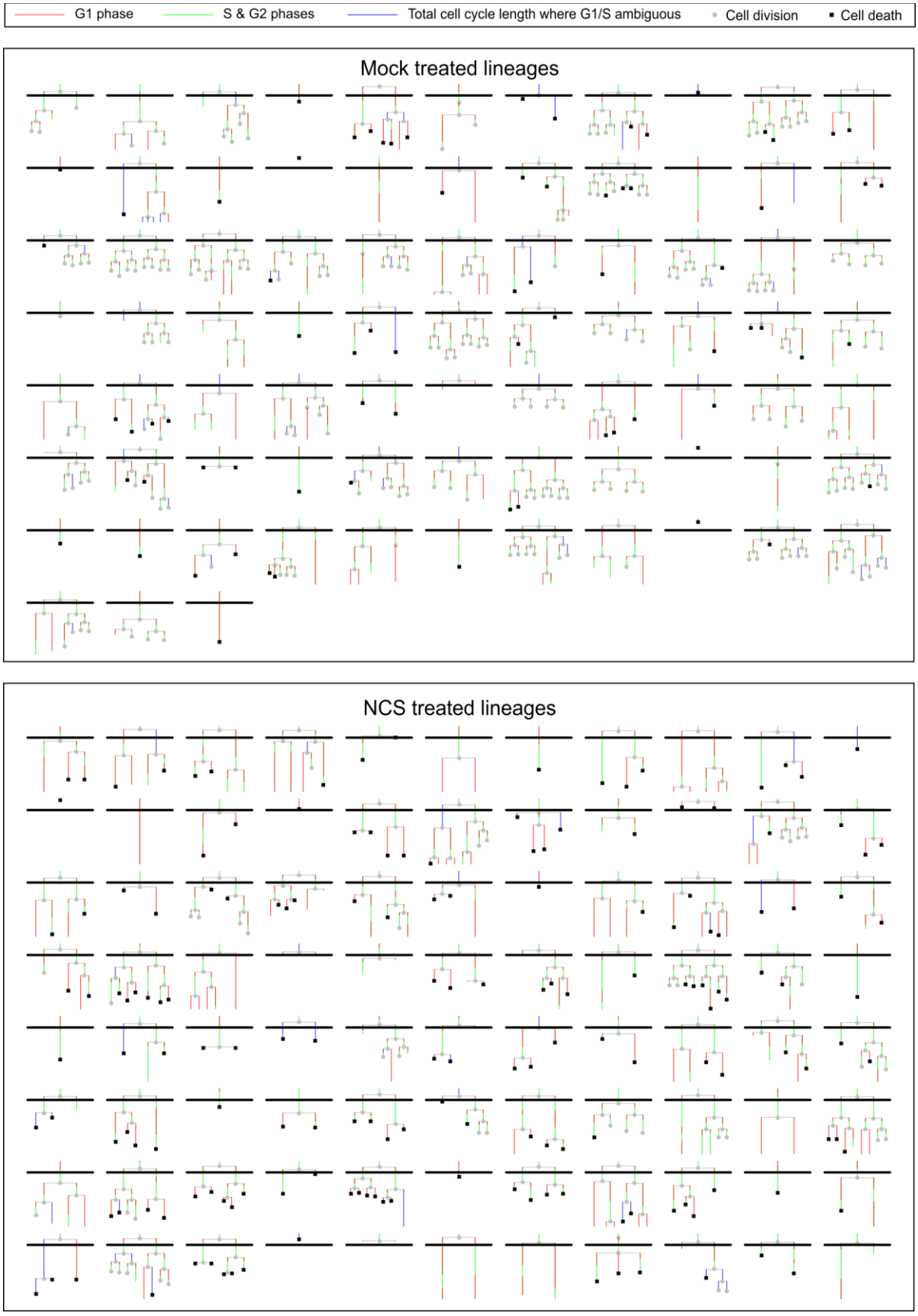

Figure 44: Lineage trees from experimental repeat 2

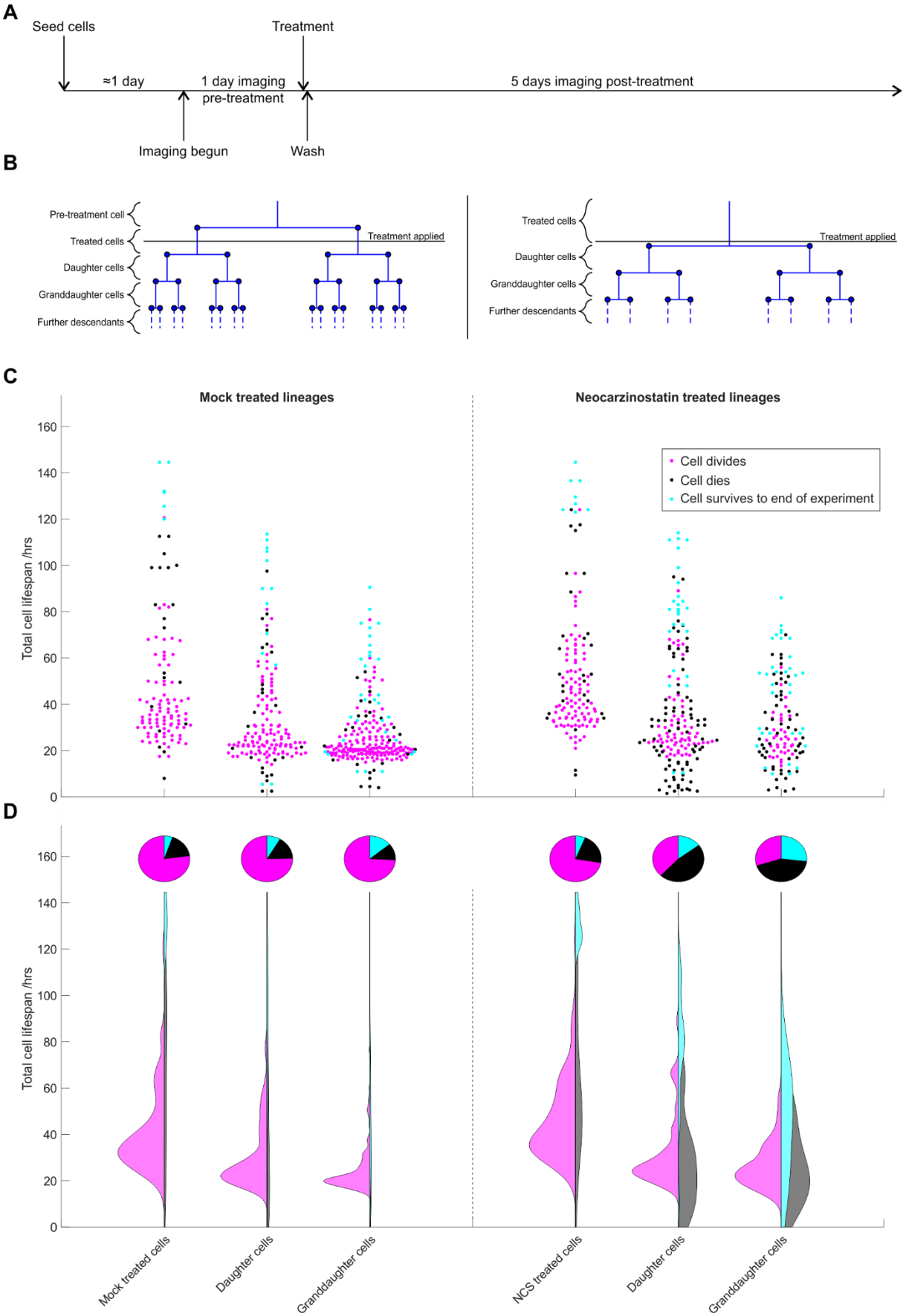

Figure 45: Generational analyses of experimental repeat 2
***A)** Protocol, **B)** Generational terminology of lineage trees **C)** Swarm plot of generations analysed **D)** Half-violin plot*
For unknown reasons the median cell cycle duration of dividing $Mock^{Treated}$ (34.75 hrs) is considerably elevated compared to $Mock^{Daughters}$ and $Mock^{Granddaughters}$ median cell cycle durations, (24.25 and 21 respectively).

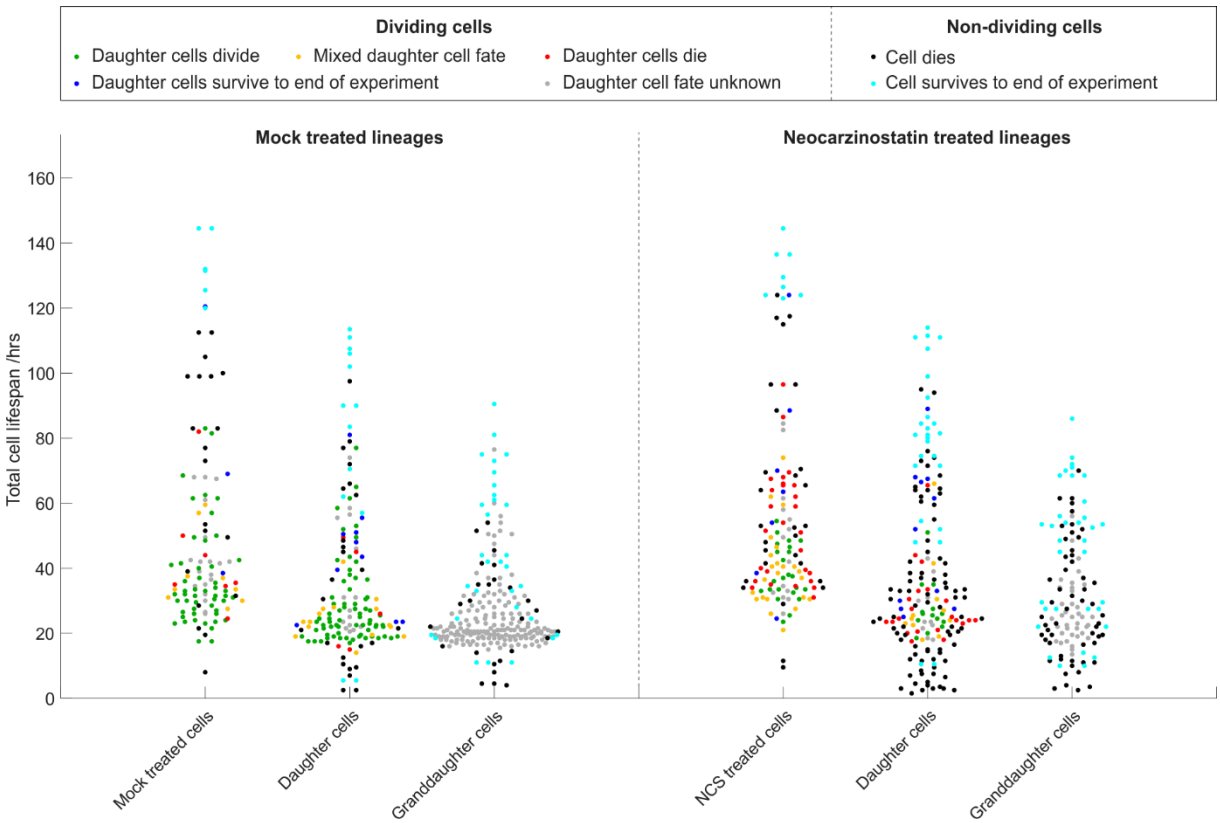

Figure 46: FUCCI-NM U2OS total cell cycle length swarm plot with dividing cells colour coded by daughter cell fates, data from experimental repeat 2.

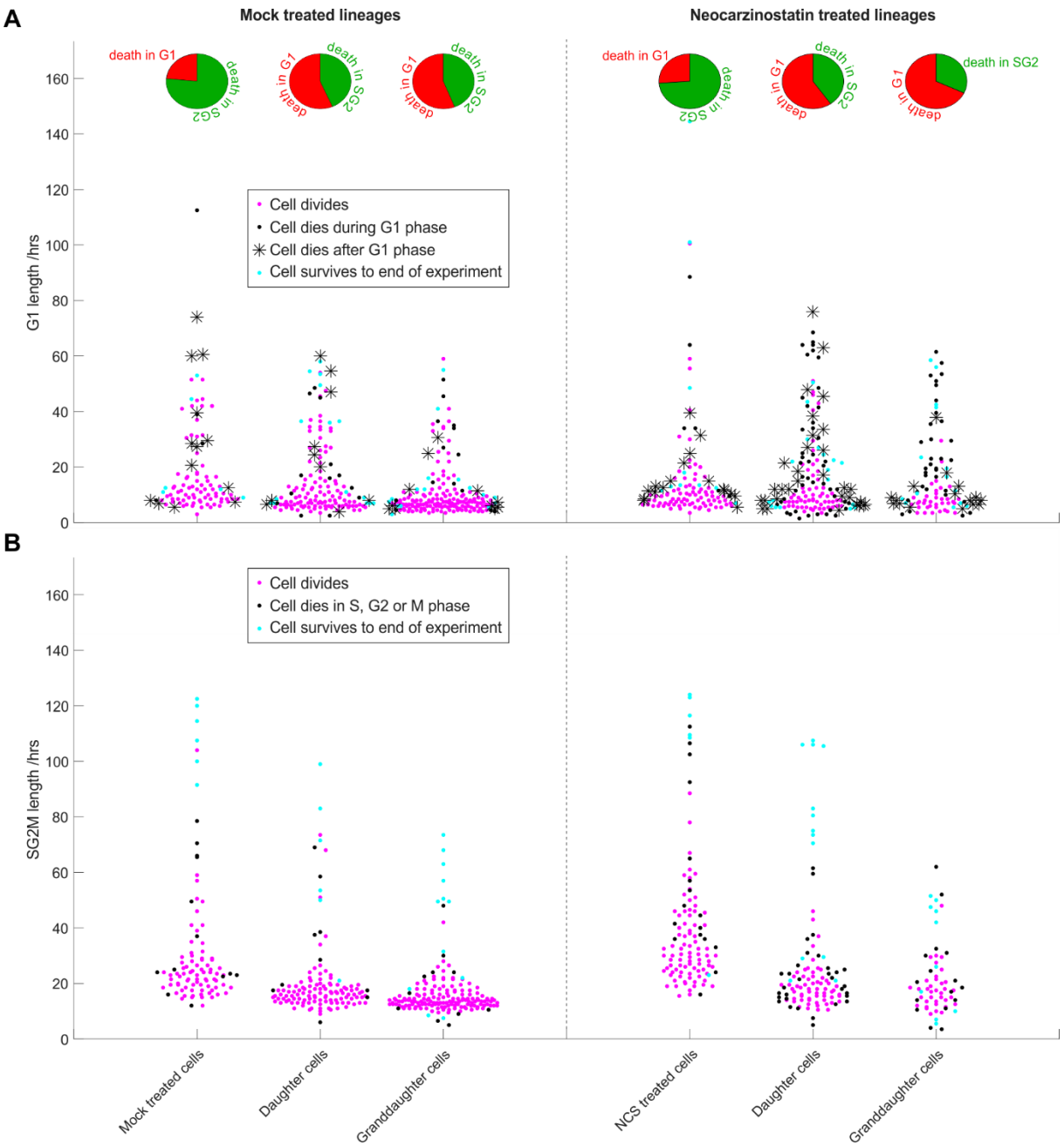

Figure 47: G1/SG2M duration swarm plots of FUCCI-NM U2OS cells with identifiable G1/S transitions, data from experimental repeat 2.
***A)** G1 duration swarm plot coloured by cell fate and separated into their generations.*
***B)** SG2M duration swarm plot coloured by cell fate and separated into their generations.*

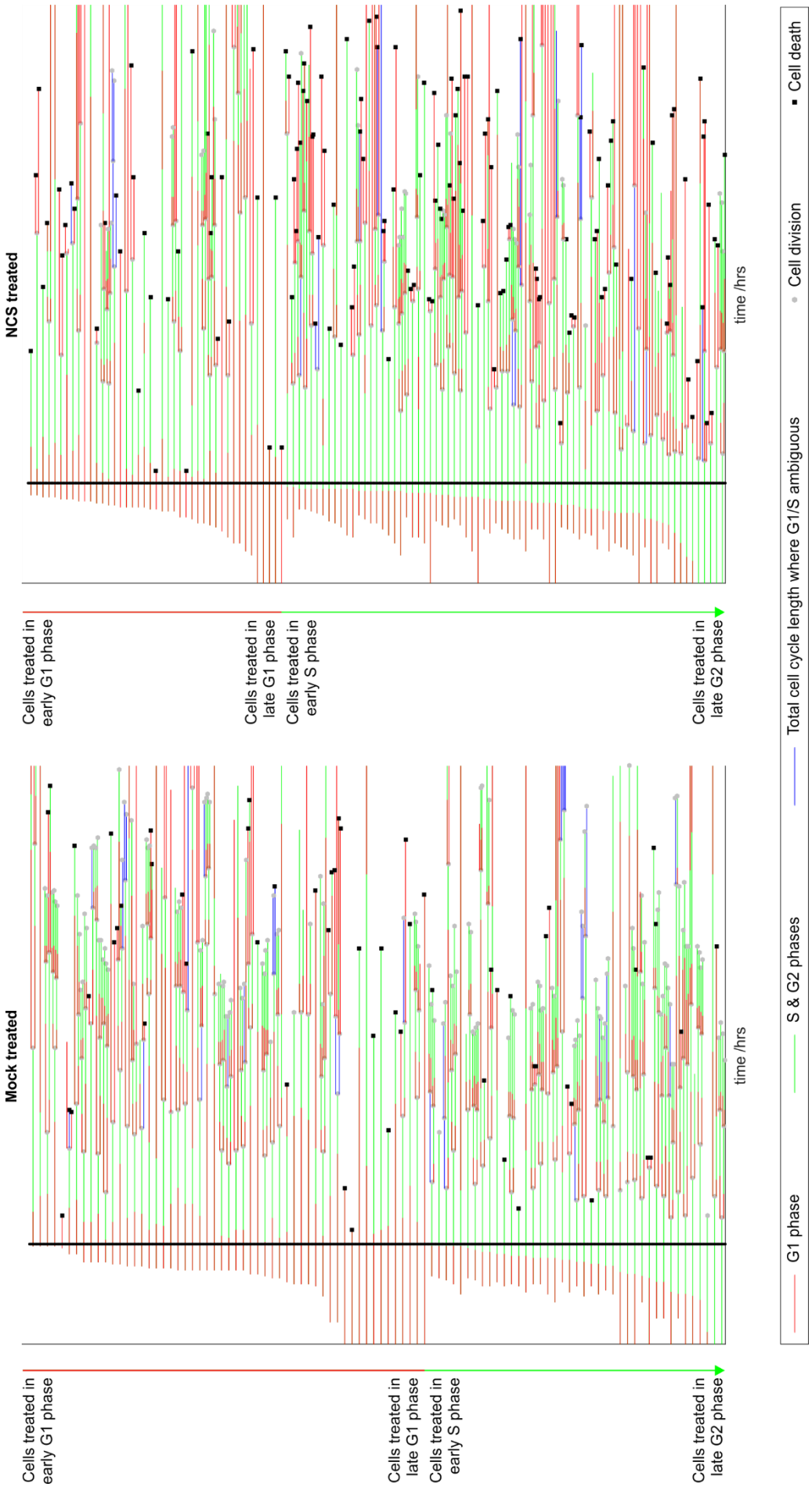

Figure 48: Lineage trees of mock or Neocarzinostatin treated FUCCI-NM U2OS cells ordered with respect to position in cell cycle at the time of treatment, data from experimental repeat 2. Trees depicted up to the granddaughter generation.

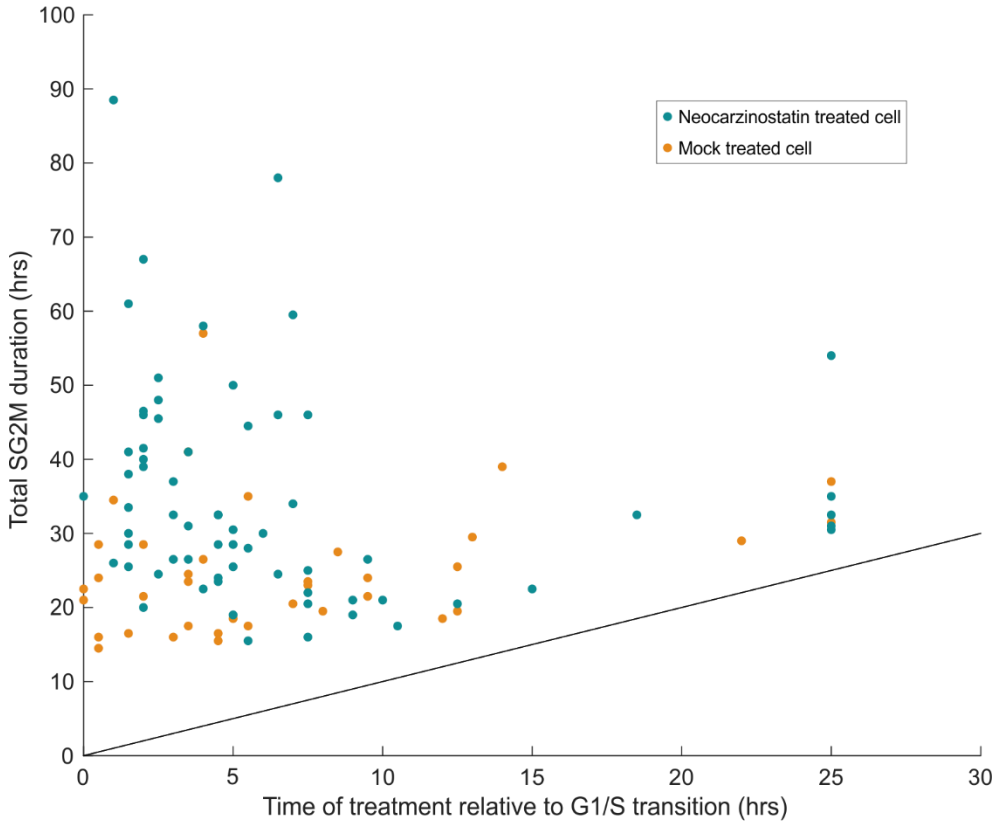

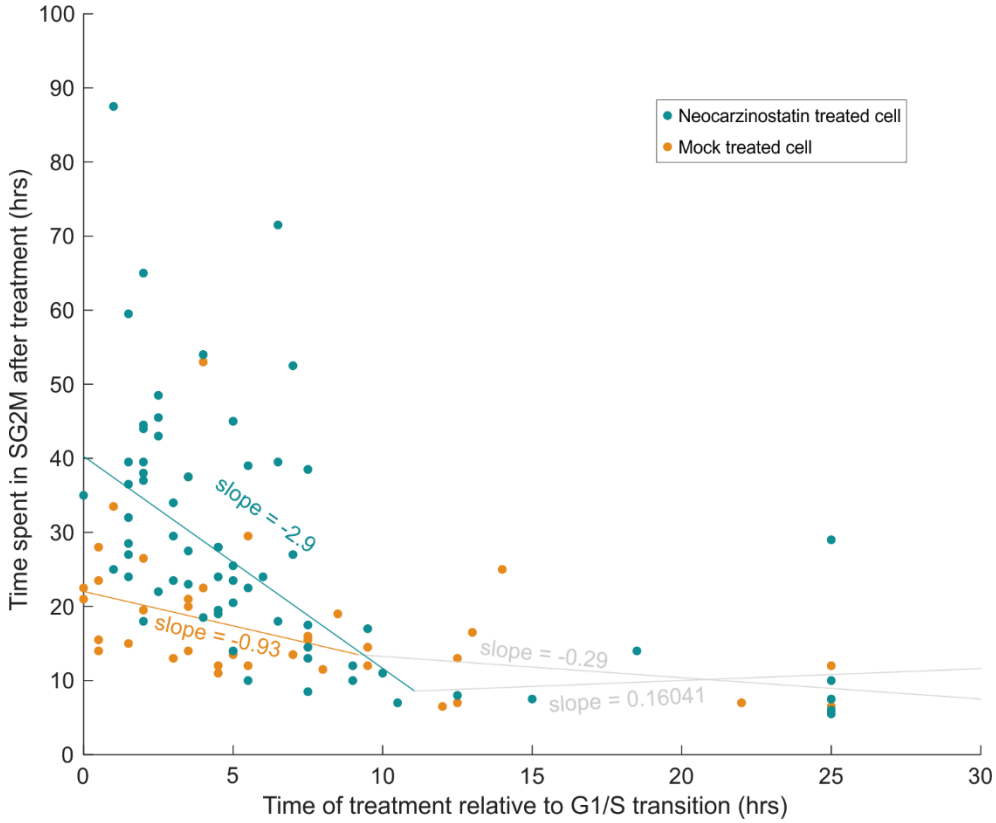

Figure 49: Graphs of cell cycle timing dependencies of the effect of treatments upon SG2M duration, data from experimental repeat 2

***A)** Total duration of SG2M for mockTreated or NCSTreated FUCCI-NM U2OS cells treated during SG2M that subsequently divide against the time of treatment relative to the G1/S transition. **B)** Time spent in SG2M after treatment for mockTreated or NCSTreated FUCCI-NM U2OS cells that divide. The modelled line of best fits summarise the trends in the data with slopes indicating cell cycle timing dependencies on inducing lengthening of SG2M.*

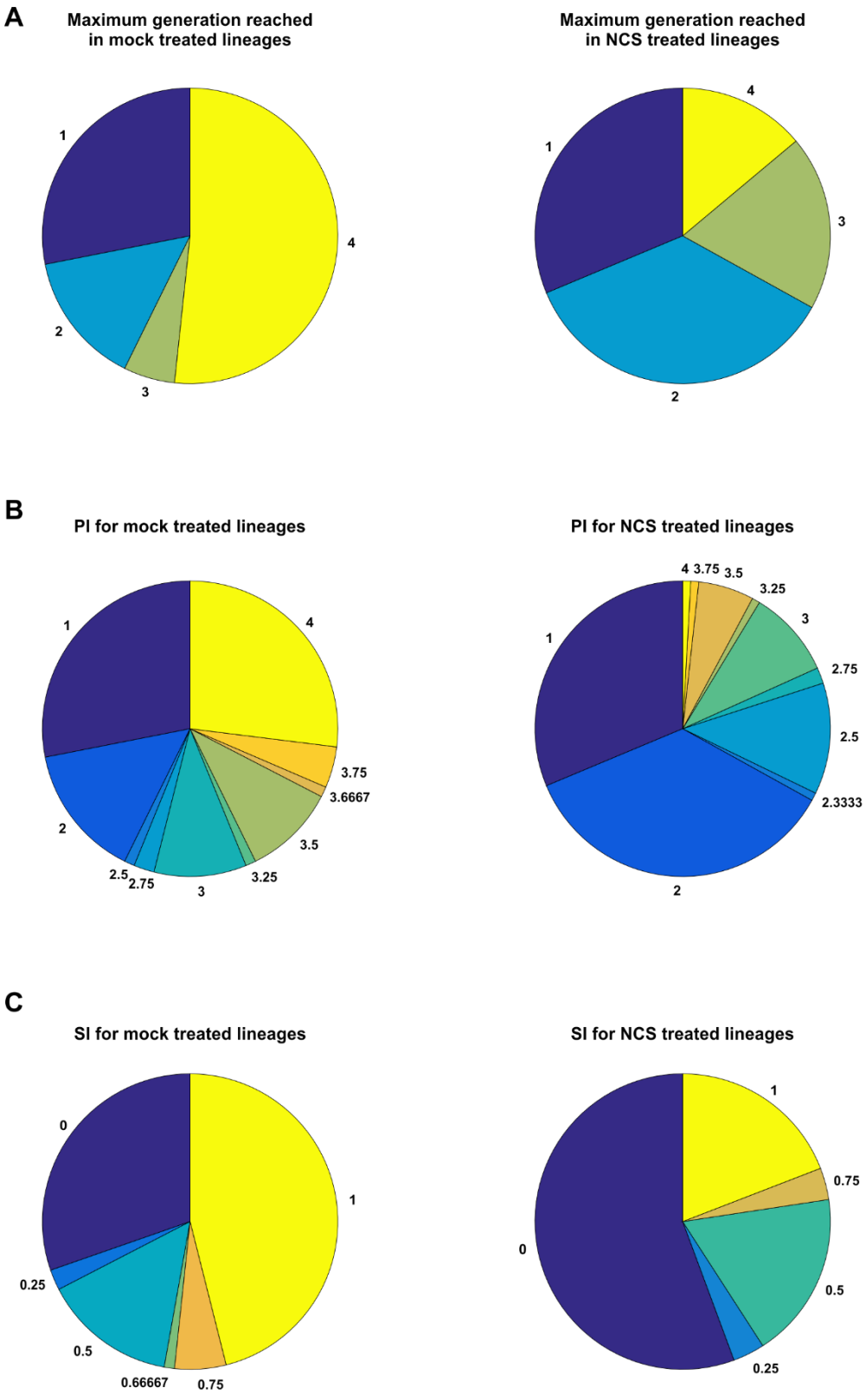

Figure 50: Lineage fitness as assessed by three different metrics, data from experimental repeat 2
*Piecharts indicating the proportion of lineages derived from Mock^{Treated} and NCS^{Treated} FUCCI-NM U2OS cells with the given **A)** maximum generation, **B)** PI, or **C)** SI scores.*

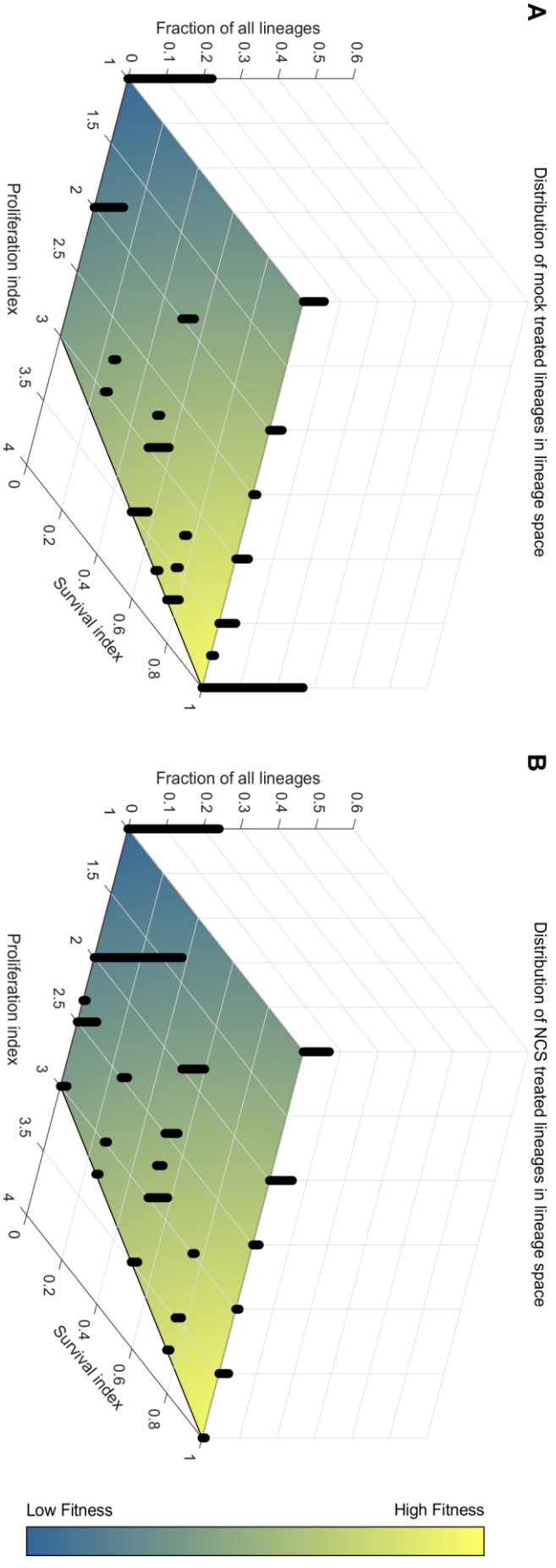

Figure 51: Stem plots indicating the proportion of all lineages with the given combination of PI and SI score in each experimental condition, data from experimental repeat 2
A) *Mock treated condition*
B) *NCS treated condition*

1.10.2 Experimental repeat 3

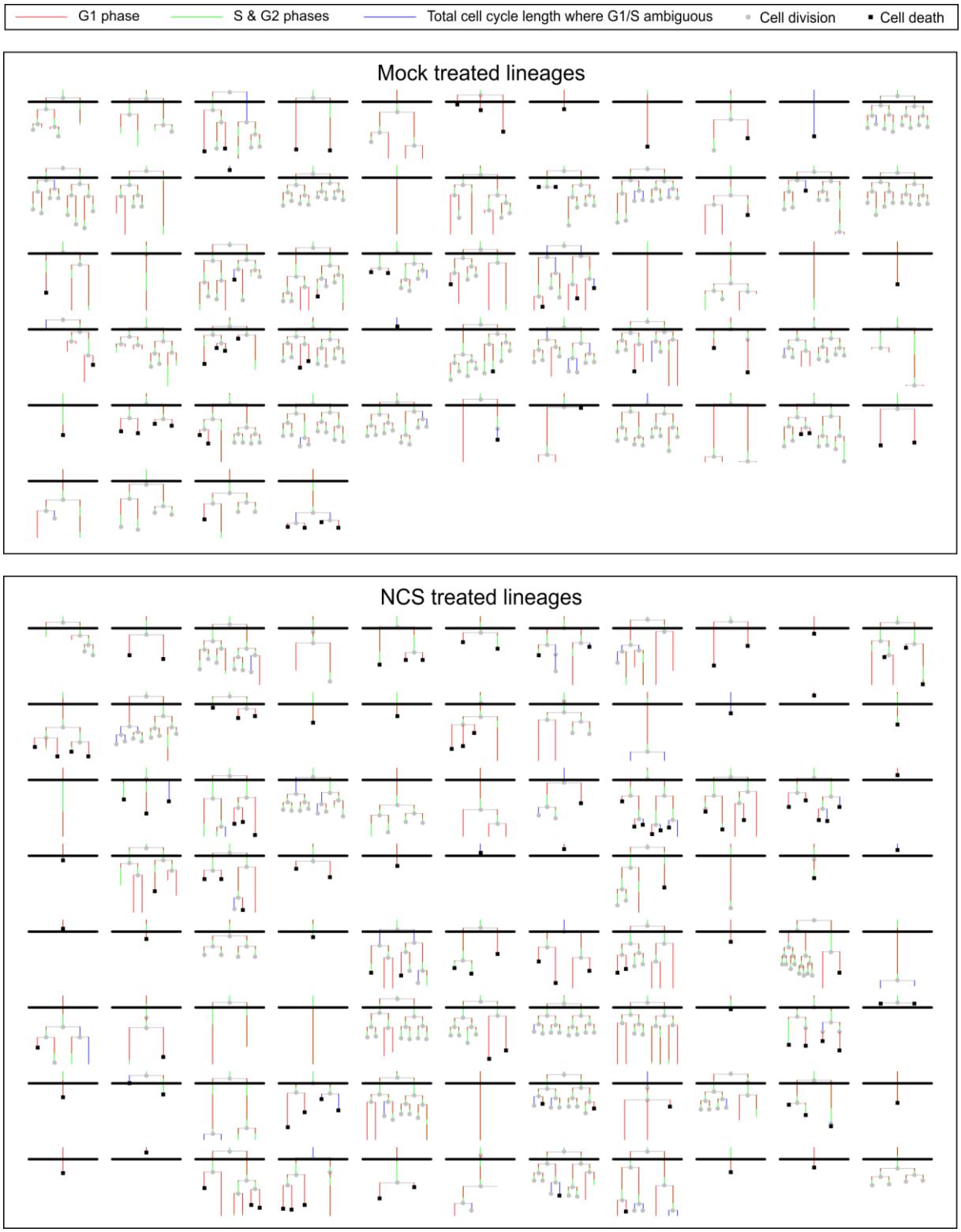

Figure 52: Lineage trees from experimental repeat 3

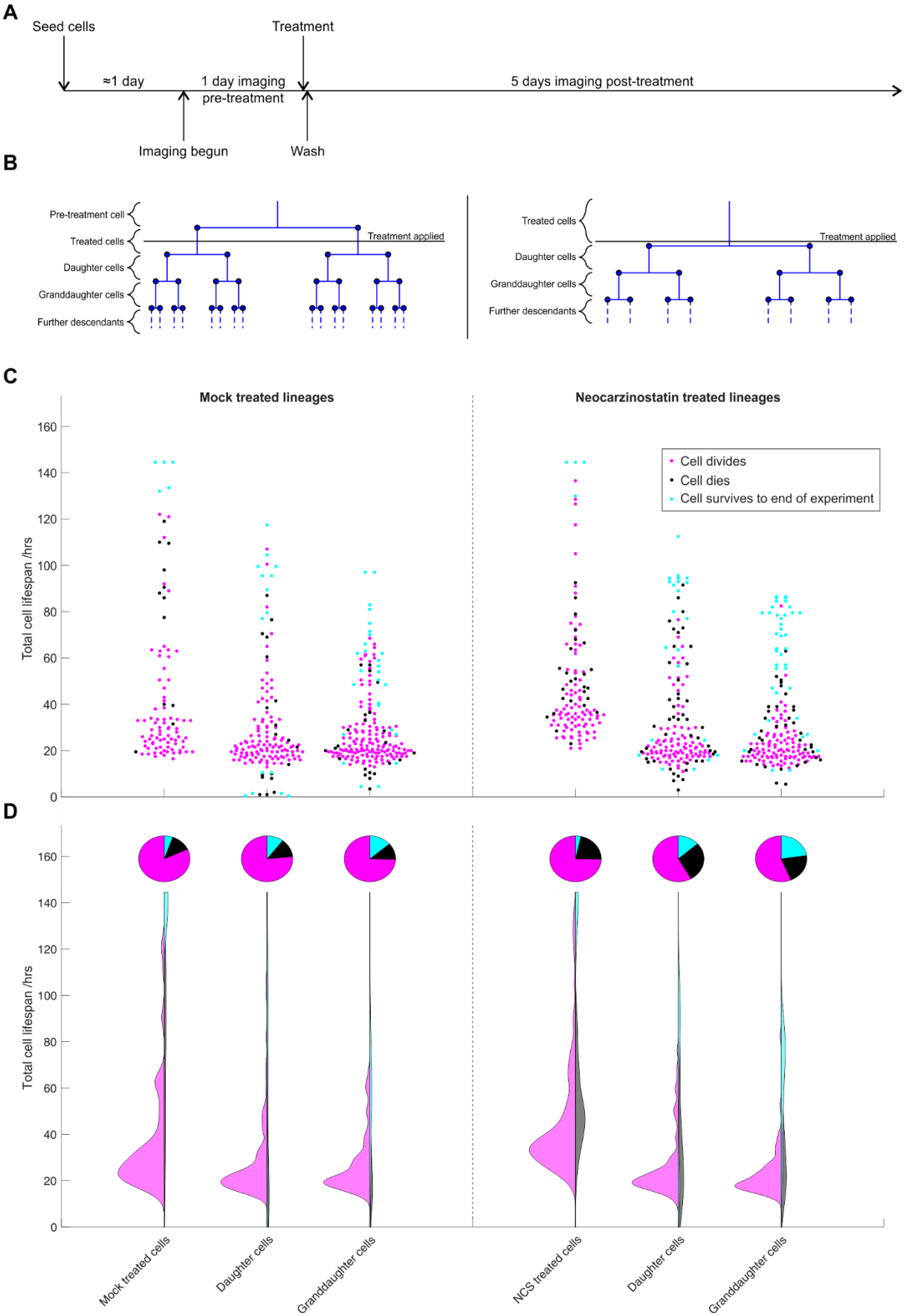

Figure 53: Generational analyses of experiment repeat 3
***A)** Protocol, **B)** Generational terminology of lineage trees **C)** Swarm plot of generations analysed **D)** Half-violin plot*

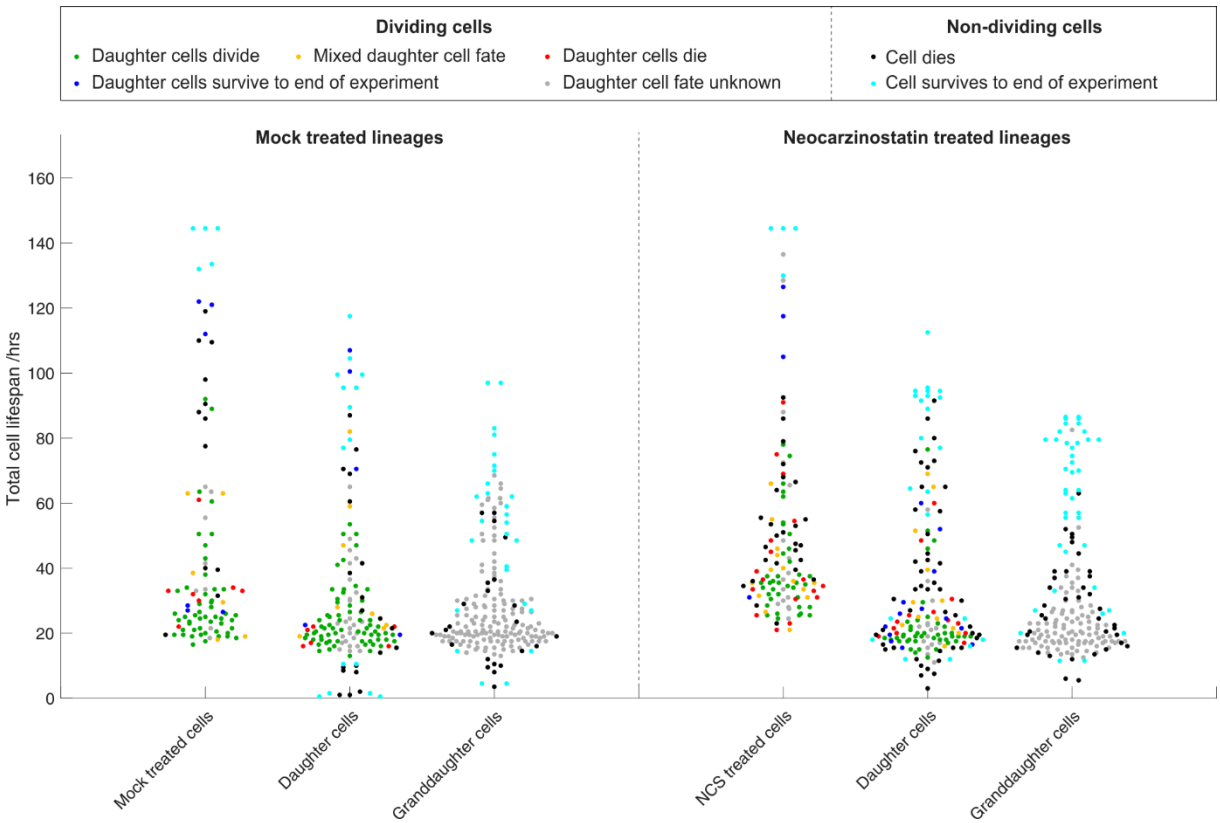

Figure 54: FUCCI-NM U2OS total cell cycle length swarm plot with dividing cells colour coded by daughter cell fates, data from experimental repeat 3.

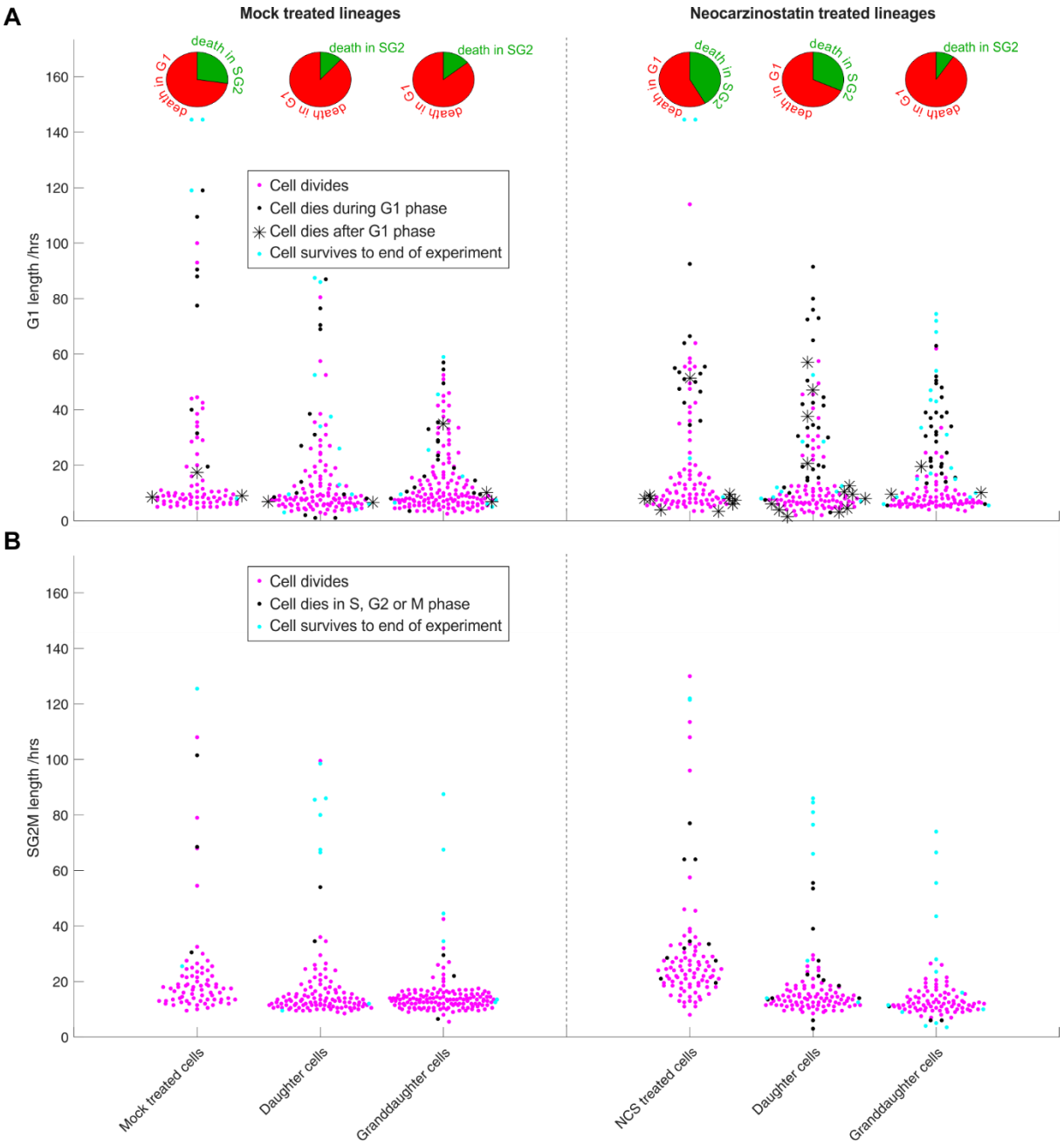

Figure 55: G1/SG2M duration swarm plots of FUCCI-NM U2OS cells with identifiable G1/S transitions, data from experimental repeat 3
A) *G1 duration swarm plot coloured by cell fate and separated into their generations.*
B) *SG2M duration swarm plot coloured by cell fate and separated into their generations.*

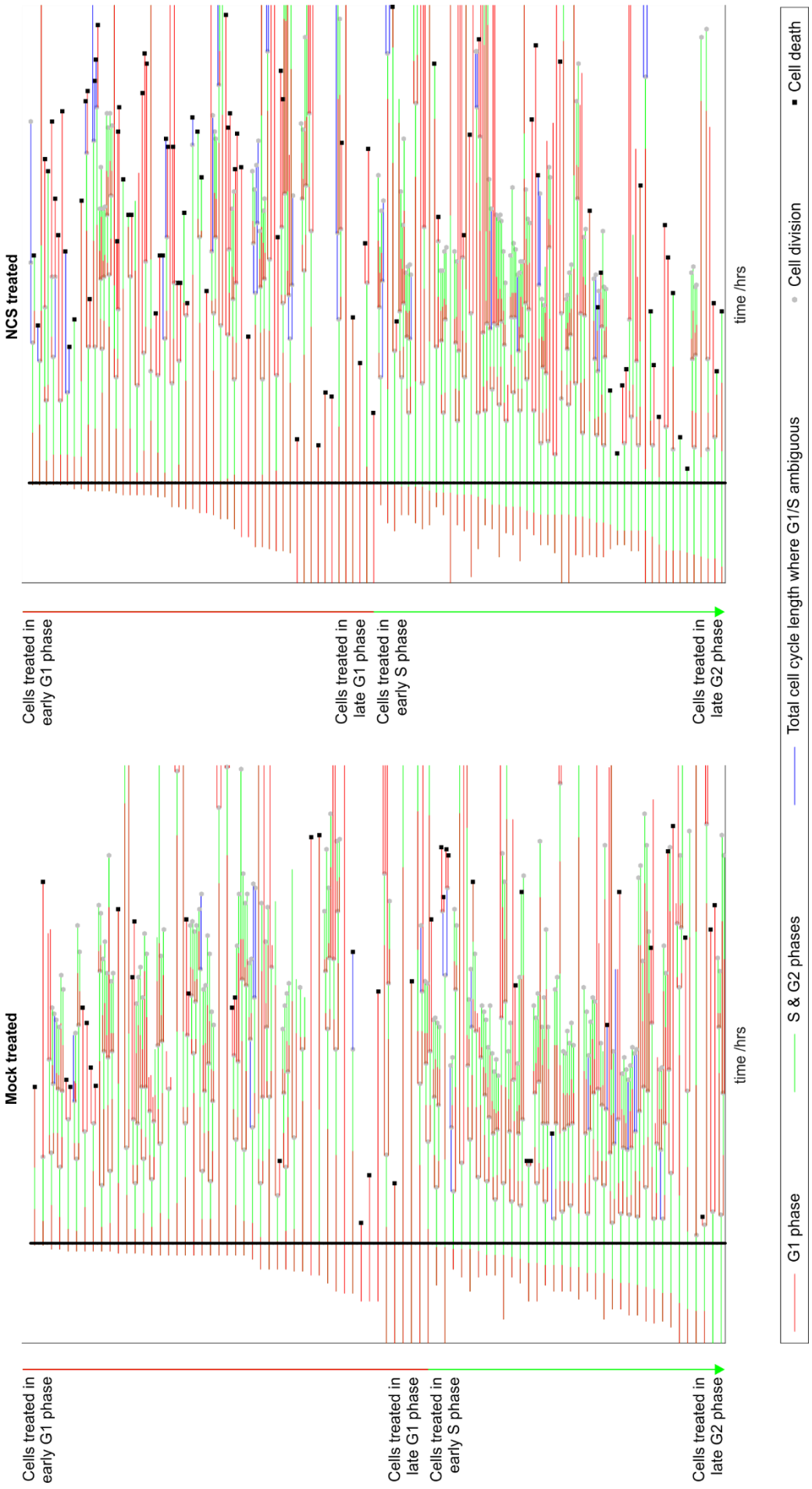

Figure 56: Lineage trees of mock or Neocarzinostatin treated FUCCI-NM U2OS cells ordered with respect to position in cell cycle at the time of treatment, data from experimental repeat 3. Trees depicted up to the granddaughter generation.

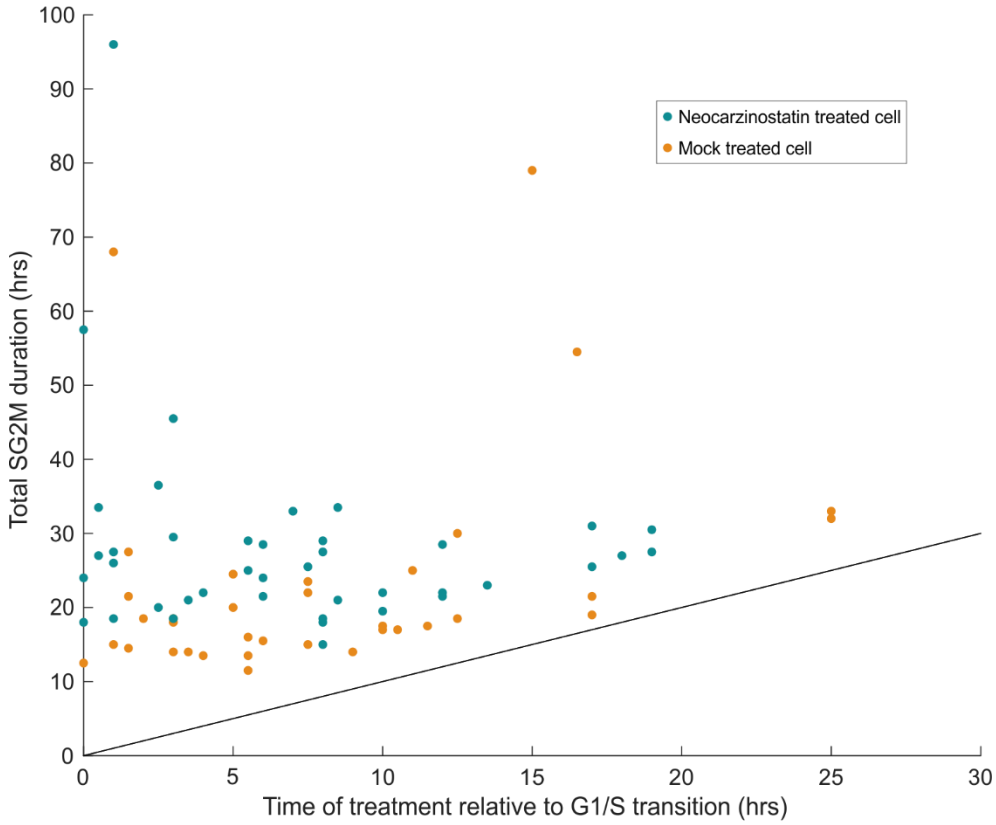

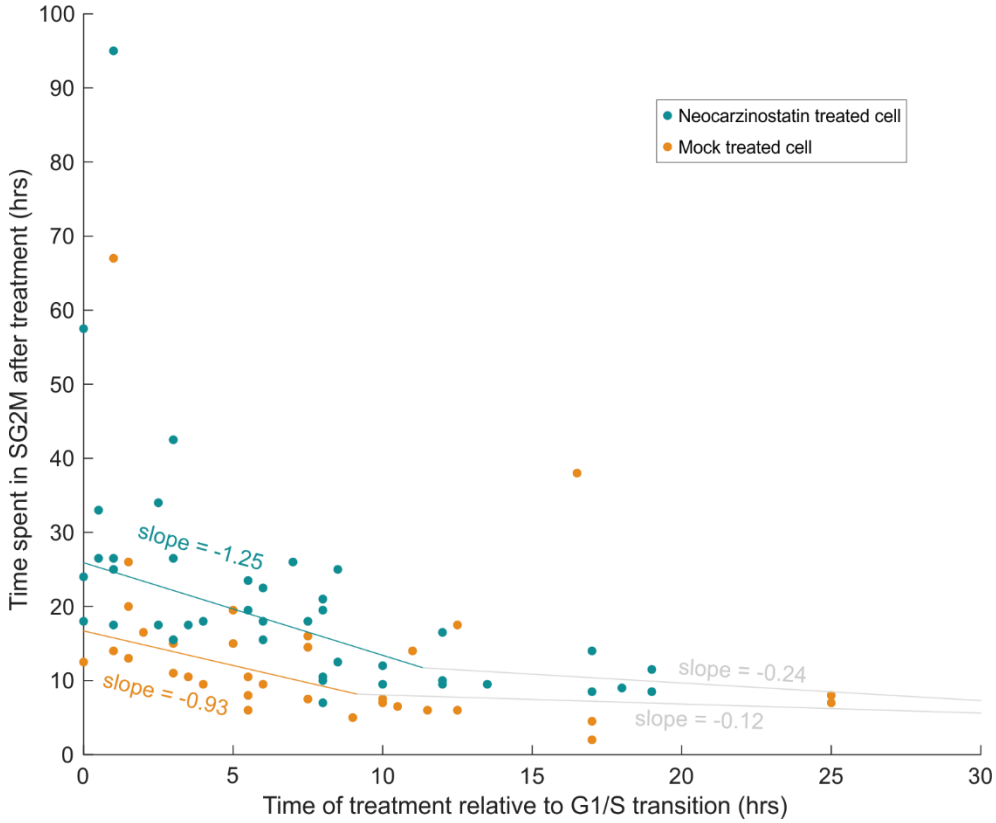

Figure 57: Graphs of cell cycle timing dependencies of the effect of treatments upon SG2M duration, data from experimental repeat 3

***A)** Total duration of SG2M for mockTreated or NCSTreated FUCCI-NM U2OS cells treated during SG2M that subsequently divide against the time of treatment relative to the G1/S transition. **B)** Time spent in SG2M after treatment for mockTreated or NCSTreated FUCCI-NM U2OS cells that divide. The modelled line of best fits summarise the trends in the data with slopes indicating cell cycle timing dependencies on inducing lengthening of SG2M.*

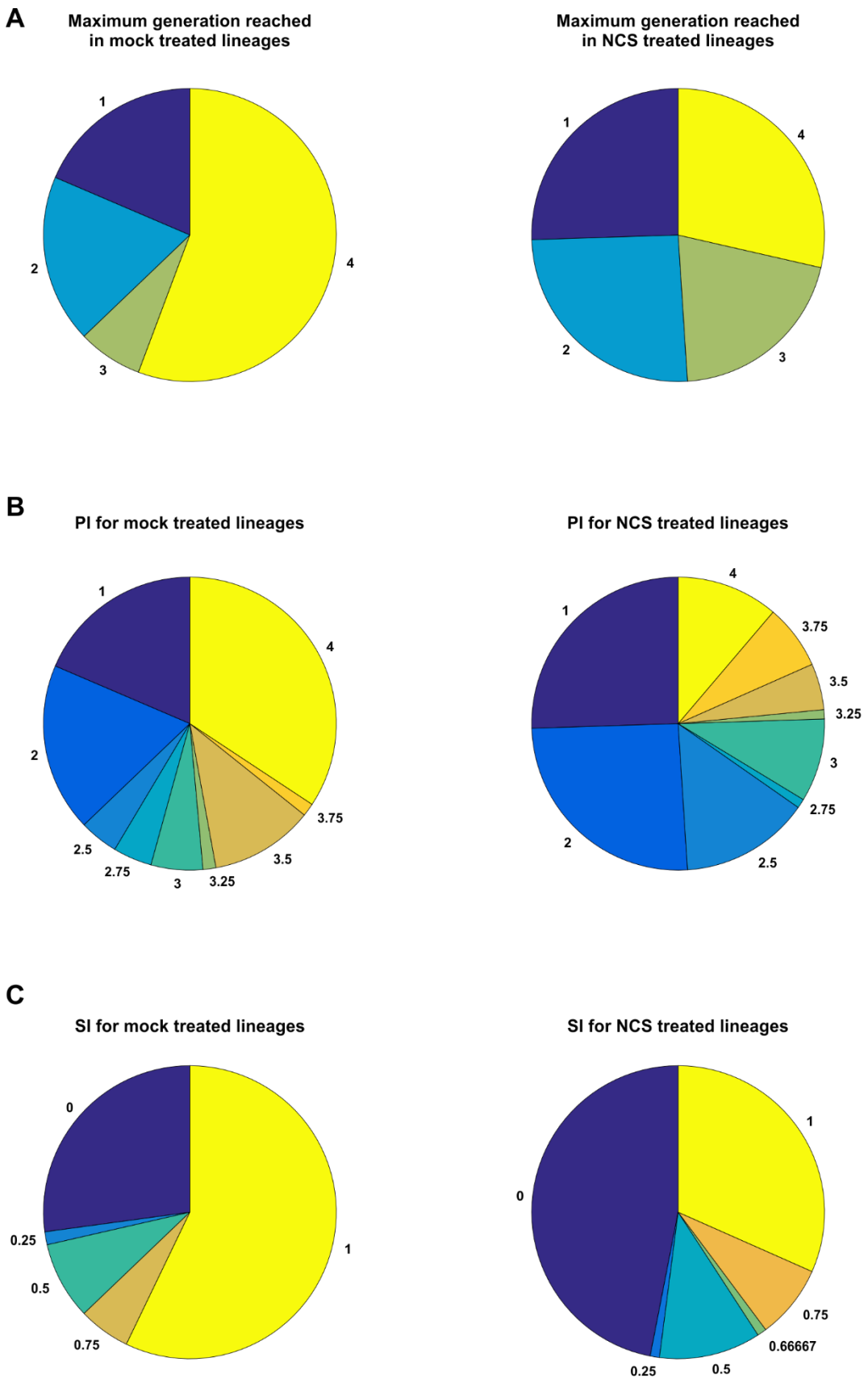

Figure 58: Lineage fitness as assessed by three different metrics, data from experimental repeat 3
*Piecharts indicating the proportion of lineages derived from Mock^{Treated} and NCS^{Treated} FUCCI-NM U2OS cells with the given **A)** maximum generation, **B)** PI, or **C)** SI scores.*

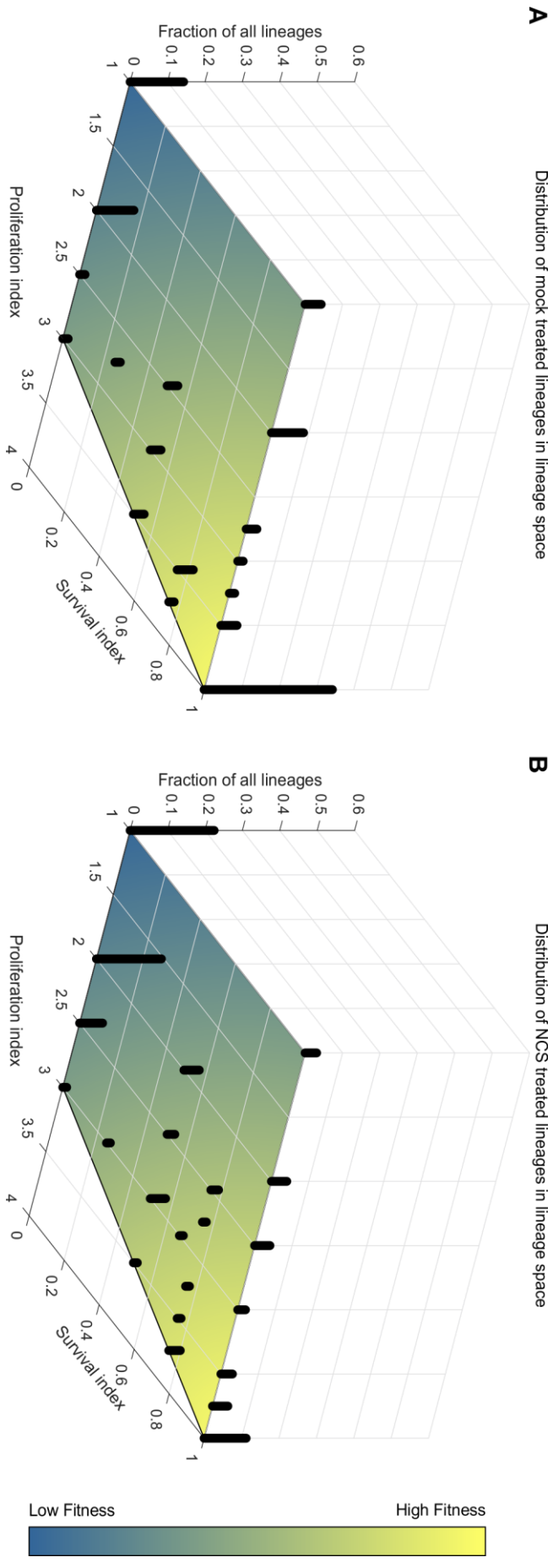

Figure 59: Stem plots indicating the proportion of all lineages with the given combination of PI and SI score in each experimental condition, data from experimental repeat 2
A) *Mock treated condition*
B) *NCS treated condition*

Generational tracing by flow cytometry

1.11 Assay development

Data provided by time-lapse microscopy has the great advantages of providing single cell resolution and lineage based information allowing the in-depth analyses and characterisation presented in the previous chapter. Nonetheless the technical constraints limiting which cell lines are suitable for such microscopy, the need to generate stable reporter cell lines and the laborious curation required even with semi-automated analysis place limits on the experimental conditions that can be tested. In order to provide corroborative evidence for the findings already observed, probe possible mechanisms and provide the opportunity to interrogate a greater range of cell lines it would be advantageous to develop alternative assays. I therefore sought to identify an assay that might allow descendant cell death to be inferred and compared across different conditions and cell lines.

Such an assay should allow the ability to measure or infer information about cell generations and death, and be amenable to taking place over comparable timescales to the microscopy assay. Flow cytometry permits single cell resolution and is amenable to processing large samples quickly, and so provides a suitable basis for an alternative assay where cells can be harvested at various time points, fixed and analysed together. In order to confer the ability to infer generational information cells can be stained with CellTrace™ dye (ThermoFisher), a cell-permeable chemical that permanently labels amine groups in proteins via covalent reaction with a non-fluorescent ester that is converted to its fluorescent derivative by cellular esterases. With each cell division each daughter cell will inherit around half of the labelled amines and so have half the fluorescence of its mother cell (Figure 60). In this manner, the number of divisions undertaken since the cell was labelled can be inferred. This dye is reportedly suitable for experiments taking place over multiple days (ThermoFisher Scientific). Thus, cells can be stained and samples collected at time intervals over several days allowing the progression of the population through multiple generations to be identified.

Once progression through generations can be identified the expected relative change in population can be calculated given each dividing cell typically produces two daughter cells, aside from rare abnormal mitoses. By estimating the population size of each collected sample with cell counting technology the measured value can be compared to the expected over time. Significant deviations between the two will result from cells dying, causing the measured population to be lower than expected. This could be used to estimate differences in cell death between different conditions. For example, greater divergence from the expected population in particular experimental conditions would indicate greater cell death than in less divergent experimental conditions. Furthermore, with the use of fluorescent DNA intercalating dyes cell cycle distributions can be measured allowing changes to be identified, for example those resulting from cell cycle arrests after DNA damage.

In principle therefore, using the CellTrace dye, DNA intercalating fluorescent dyes and population counts should allow the changes in cell populations to be characterised over time, potentially allowing the indirect observation of phenomena such as descendant cell death.

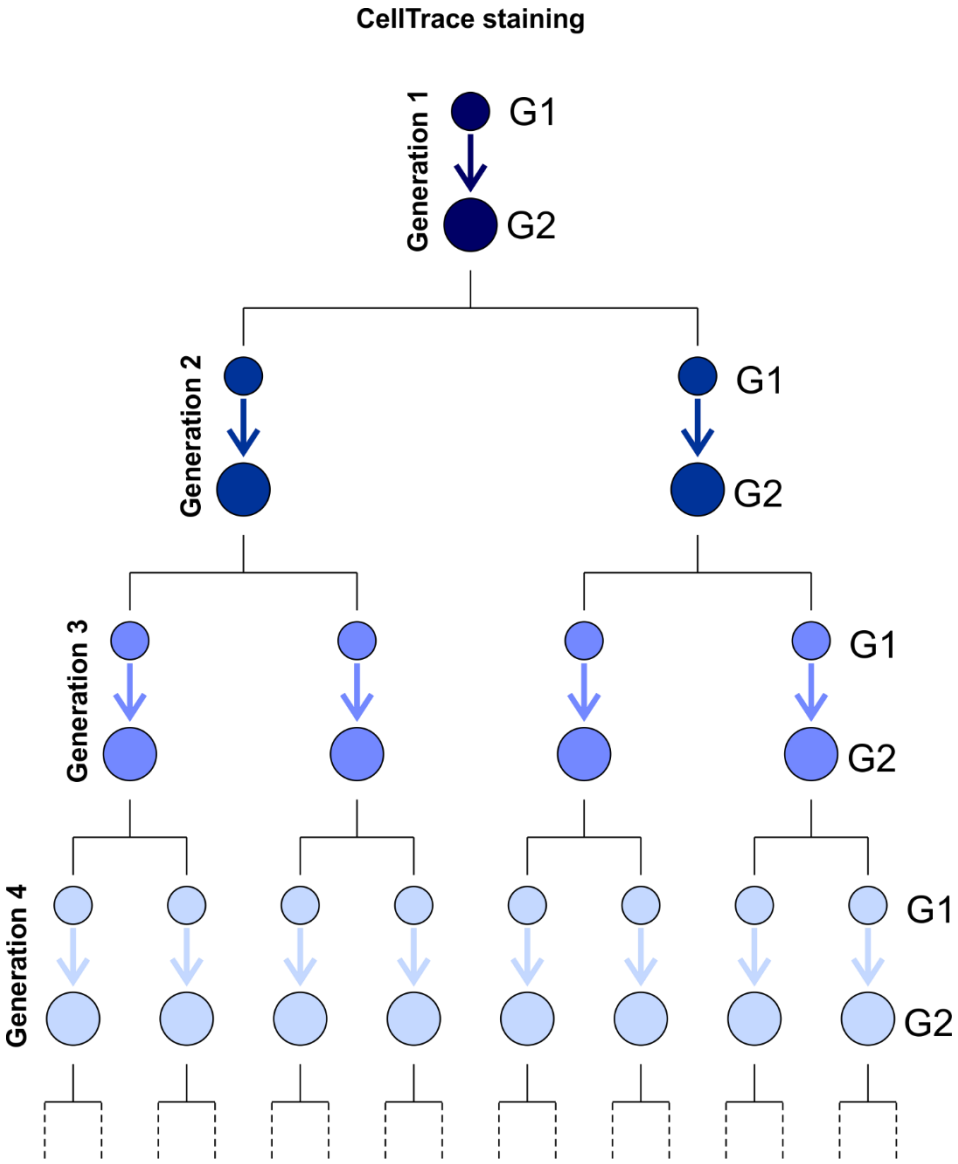

Figure 60: CellTrace dyed cells halve in fluorescence with each cell division allowing generational progression to be inferred via flow cytometric measurements.

1.12 Generational tracing in U2OS cells

1.12.1 Experimental setup

In order to determine whether this approach could indirectly infer some of the observations made directly from microscopy, U2OS cells were perturbed with NCS or mock treatments according to the protocol outlined in Figure 61. The different cell culture vessels and ratio of culture media to cells presents a difficulty in determining equivalent NCS treatments in different assays. In microscopy, large volumes of NCS-containing media were washed over a small cell growth area whereas here an entire

dish of cells is treated with the typical volume of media required for the dish size. As NCS is a chemical that reacts with the DNA the number of NCS molecules per cell may be more important than simply the concentration of NCS in the culture media. Therefore, in these experiments one of the concentrations established successfully in microscopy experiments, 45 ng/ml NCS, was tested alongside a higher concentration of 100 ng/ml NCS to determine whether either was suitable. The results of a representative U2OS experiment are presented in Figure 62.

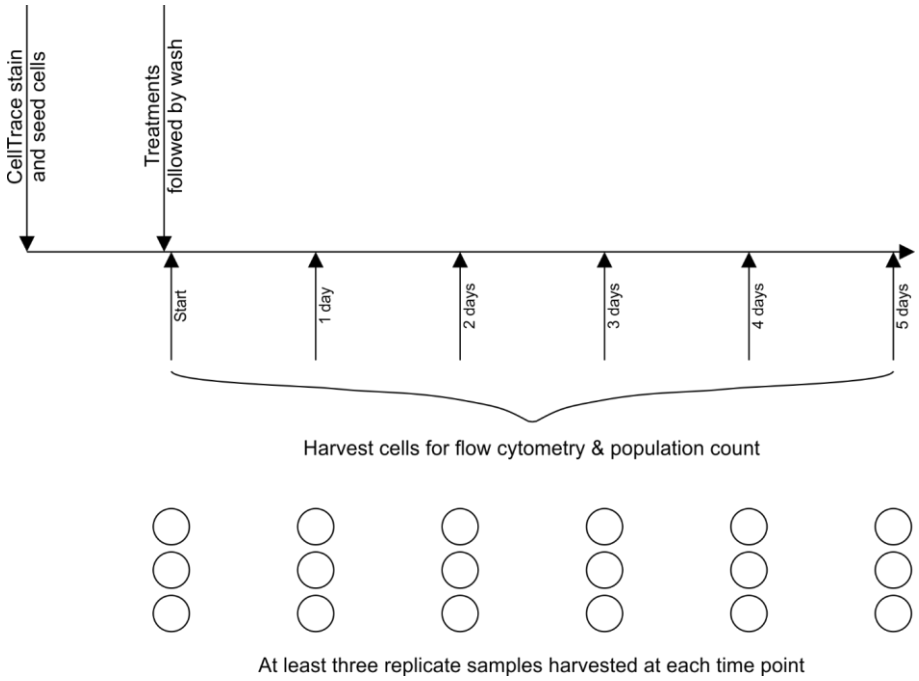

Figure 61: Experimental protocol for generational tracing by flow cytometry

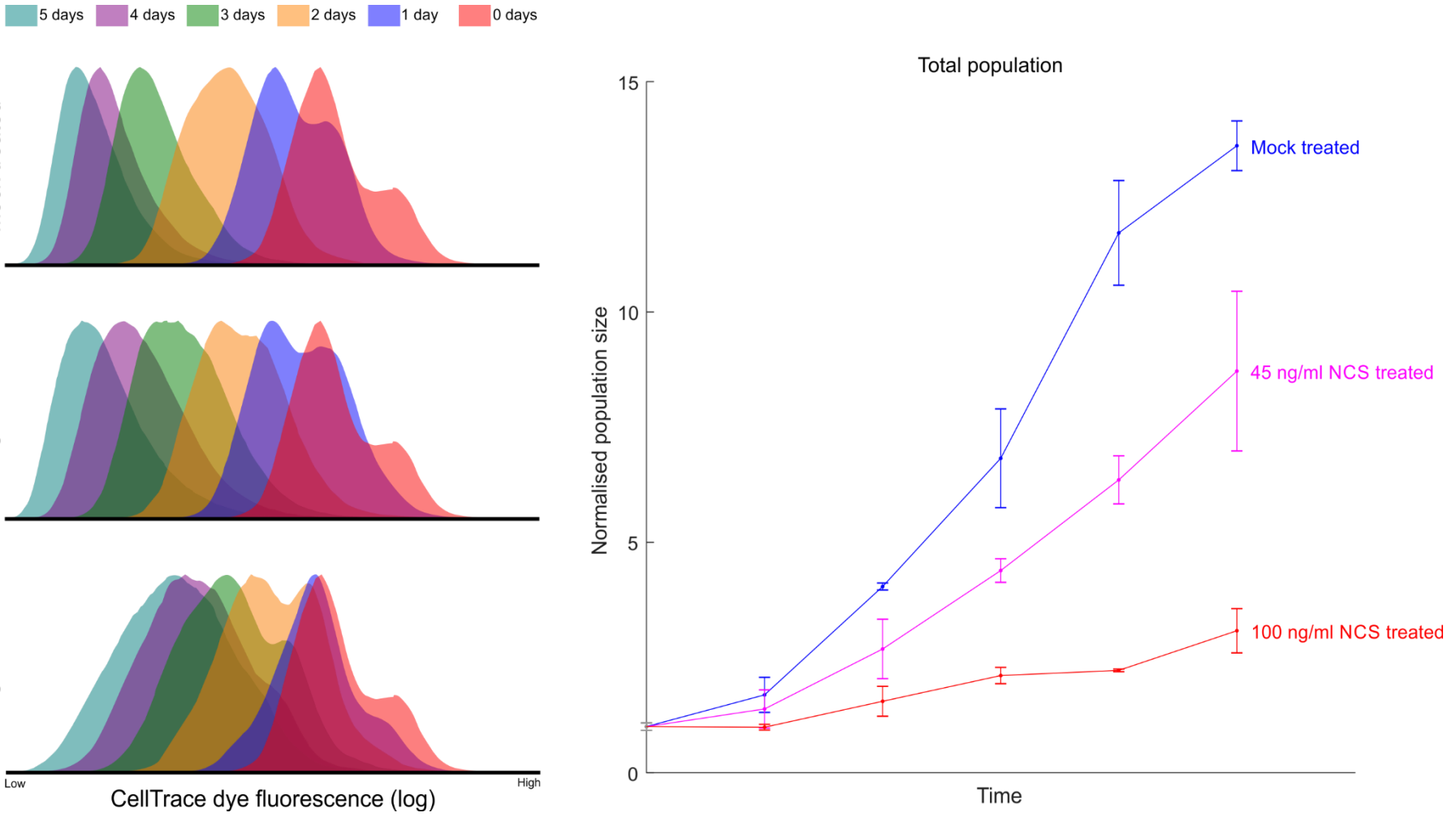

Figure 62: CellTrace profiles and total population graphs for U2OS cells.
Cells treated with mock (n=3), 45 ng/ml NCS (n=2) and 100 ng/ml NCS (n=3) conditions. Results from one representative experiment shown. ***Left)*** *Measured CellTrace Fluorescence curves for each timepoint for each condition. Logarithmic scale of fluorescence, one representative curve from each timepoint triplicate shown.* ***Right)*** *Measured total population changes over time for each experimental condition. Average of timepoint triplicates shown with standard deviation error bars.*

1.12.2 CellTrace dilution characterisation

CellTrace staining of the mock treated samples, despite optimisation, was unable to resolve generations into well separated peaks at each time point, instead producing unimodal or bimodal distributions, as indicated in Figure 62. Each distribution curve observed is likely the product of overlapping generation curves. This prevented determination of the proportion of cells belonging to any particular exact generation at each time point, but nonetheless still demonstrated the progressive loss of fluorescence with increasing time indicating the continued division of cells over the duration of the experiment. That the curves do not appear to broaden over time suggests that the cells are proceeding relatively synchronously through the generations, with the majority of cells at any particular time point belonging to a similar generation.

The 45 ng/ml NCS treated cells show a visible decrease in the rate of loss of fluorescence compared to the mock treated, but cells are clearly continuing to divide as by the final time point the CellTrace fluorescence distribution is shifted far to the left of the initial time point curve. There is no evidence of a prolonged arrest in the cells at this concentration. A slight broadening of the curves suggests that with this treatment progression through the generations becomes less synchronous with greater differences between the cells at later time points, for example the broader 3 days curve.

At the higher 100 ng/ml NCS concentration greater differences are evident. The 1 day time point CellTrace curve overlaps considerably more with the initial time point revealing that this dose of NCS has triggered a prolonged cell cycle arrest with far fewer cells having divided 1 day after treatment. After 2 days however, it is apparent that much cell division has resumed by the greater leftward shift of the peak. This continues with the 3, 4 and 5 days peaks each continuing to reduce in fluorescence indicating that cells continue to cycle throughout the experiment. These peaks are now considerably broader than in the mock treated, which may be a product of the initial cell cycle arrest. Some cells may have arrested for much longer than others, as observed via microscopy, and so the population may have become relatively less synchronous overall in the progression of through the generations. Alternatively, this could be due to an increase in the heterogeneity of cell cycle durations in descendant cells achieving the same result in desynchronising progression through generations. Nonetheless, by the end of the experiment, although not having lost as much fluorescence as the control, we see that the final time point curve only slightly overlaps with the initial time point, approximately 15% of final time point cells, suggesting few cells have arrested for the entirety of the experiment following the DNA damage at the beginning.

1.12.3 Population size

Examining the changes in population size over time indicates that, as one would expect, the mock treated cells population increases considerably, reaching around 14 times the starting population.

There is some evidence that at the last two time points the rate of growth begins to slow down, which at this point is likely due to the high confluency of the dish and consumption of growth factors and nutrients in the growth medium. The lower NCS concentration shows considerably reduced proliferation, having typically lower populations at each time point than the mock treatment and ending up around 9 times greater than the initial population. The higher NCS concentration again shows more distinct differences, the 24hr time point is slightly lower than the initial, which is consistent with the majority of cells having undergone a prolonged cell cycle arrest and possibly some cell death over this period. After this however the population begins to rise indicating they are cycling, albeit at a much slower rate than the mock treated eventually reaching a final population of around just 3 times greater than the initial population. Viable population, a measure of viable cells based on trypan blue viable cell discrimination, see Materials and Methods, is plotted in Figure 80 and shows similar trends.

1.12.4 Comparing CellTrace dilution with population size

Clearly there are differences between the treatments in both the CellTrace profiles and the population growth measured. However, it is difficult to link the progression of CellTrace curves with changes in population by eye. The high NCS dose results in dramatically fewer cells by the end of the experiment which could indicate that cells are dying throughout the experiment, or alternatively, is simply due to cells having gone through fewer divisions as the CellTrace profiles indicate has happened. To relate the two observations together I designed a simple model. If we assume a population of CellTrace stained cells divide regularly without cell death then by sampling this at time intervals approximating the duration of the cell cycle we would expect to see the population double and the CellTrace fluorescence to halve between each time interval, Figure 63A. This would be expected to manifest as CellTrace curves that on a logarithmic plot move from high fluorescence to low fluorescence with regular spacing, Figure 63B, similarly to what is observed for mock treated cells. Plotting the number of population doublings against the number of CellTrace halvings, i.e. taking a logarithmic value for each parameter, could allow a linear relationship to be obtained between the two, Figure 63C. For these idealised cells, this line would have a slope of 1, where each halving of the CellTrace fluorescence is accompanied by a doubling of the population. For more realistic populations where some cells die rather than divide each generation, a line drawn through such data would still show a linear relationship but have a shallower slope as each CellTrace halving would be accompanied by a smaller number of population doublings. Therefore, if each generation shows an increased rate of death following NCS treatment, i.e. a form of the delayed death observed previously, this might be evident by this form of analysis. However, if the death rate varies considerably within the experimental timeframe or changes significantly between generations a linear relationship would likely prove a poor fit for the data. In order to achieve such a modelling of the data it is necessary to derive a number that

describes the rate of CellTrace loss for each CellTrace distribution. This was served by using the median value of fluorescence for each distribution.

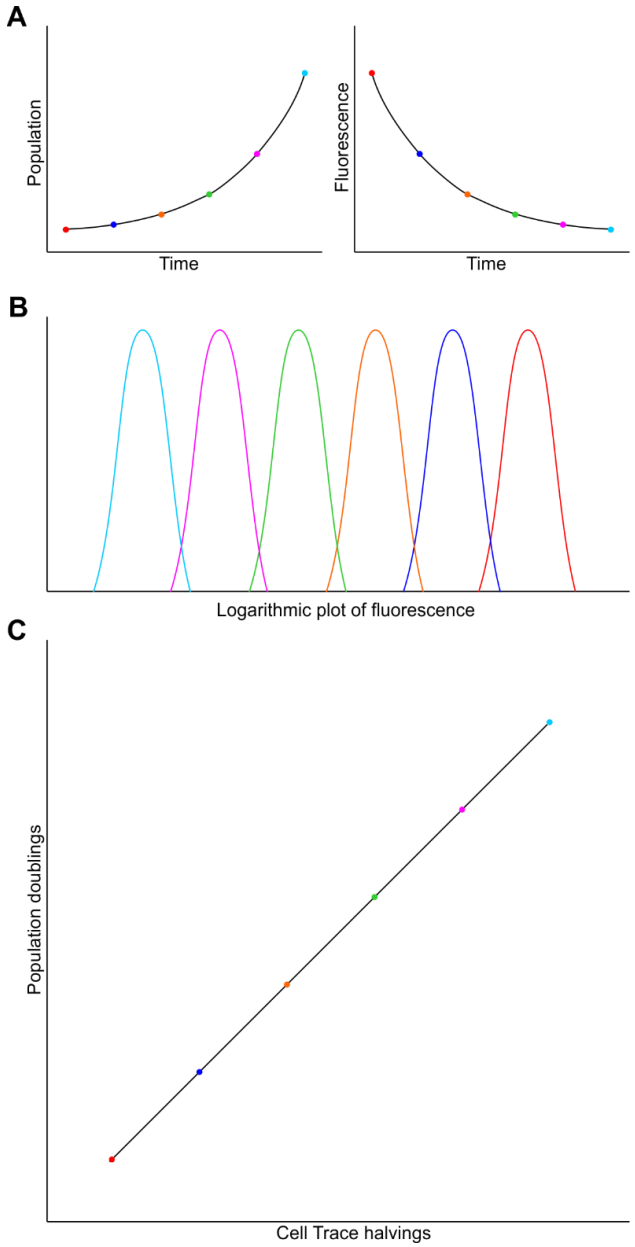

*Figure 63: Changes in CellTrace fluorescence and population size can be compared to infer generational behaviour. In principle as cells divide, the population should double while the fluorescence halves **(A)**. This would be expected to manifest as movement of measured fluorescence curves from high fluorescence to low with each increasing timepoint **(B)**. In this idealised scenario measured population doublings should have a linear relationship of slope 1 with CellTrace halvings **(C)**.*

Therefore, the population estimate and median CellTrace fluorescence for each replicate in each time point were normalised to the mean of the initial timepoint and converted to logarithmic values that represented the number of population doublings and CellTrace halvings with representative results plotted in Figure 64. Each experimental condition demonstrates a reasonably linear relationship between the two variables suggesting that modelling the data as having a reasonably similar rate of cell death per generation during this experiment is appropriate.

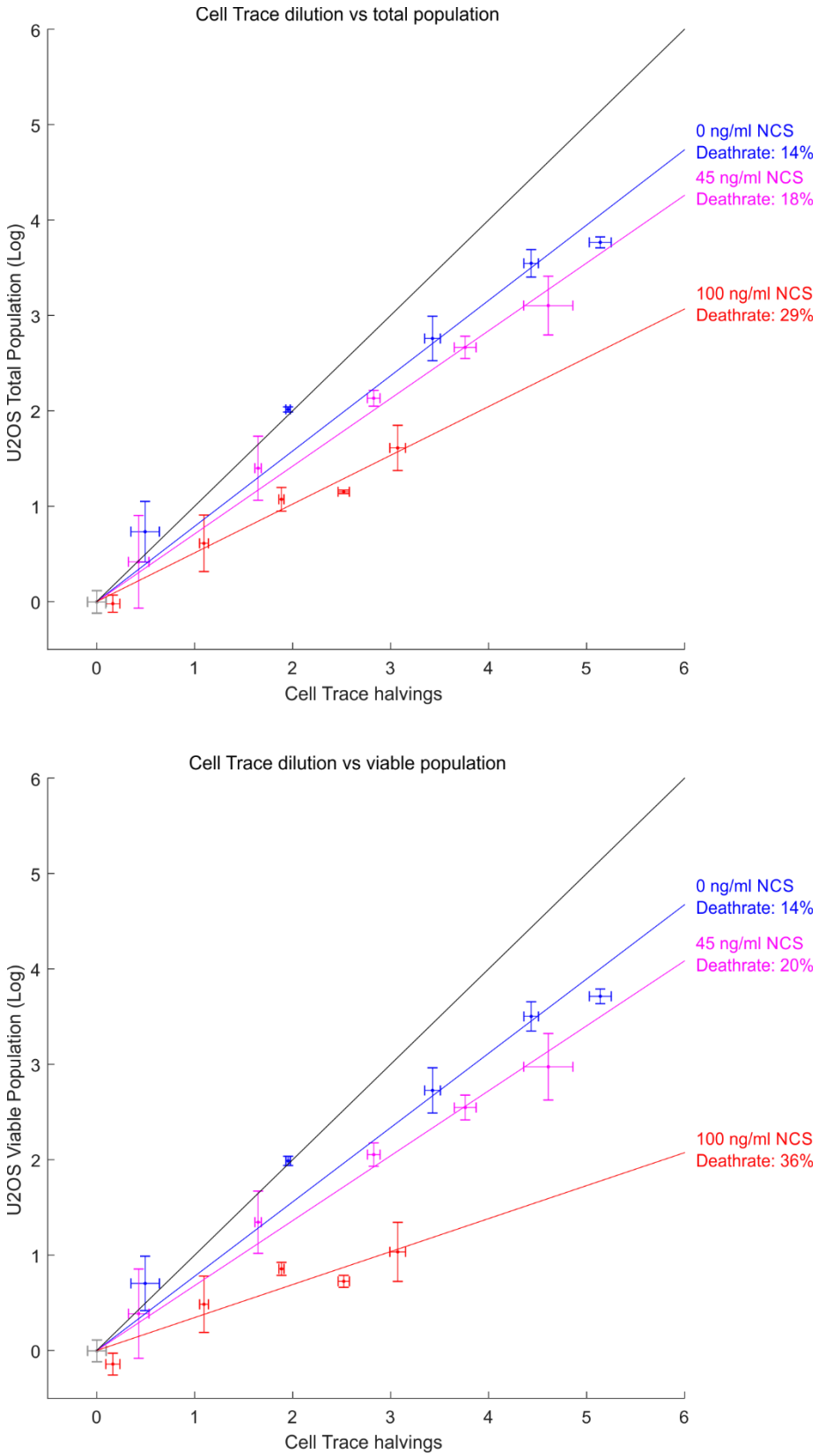

Figure 64: Comparing population changes to the dilution of CellTrace fluorescence allows generational death in U2OS cells to be inferred.
One representative experiment with three conditions shown, mock (n=3), 45 ng/ml NCS (n=2) and 100 ng/ml NCS (n=3).Averages of triplicate measurements from each timepoint are shown with vertical and horizontal standard deviation errors bars. The approximately linear relationship for each condition suggests a constant death rate per generation. Linear regression through the origin allows approximation of this rate. ***Top)*** *Using total population ViCell counts,* ***Bottom)*** *Using viable population ViCell counts.*

As described previously we can see that the mock treated achieves both the greatest number of population doublings and the highest number of CellTrace halvings during the experiment. A line of best fit drawn through the origin has a shallower slope than the idealised 1:1 ratio of CellTrace halvings to population doublings. This would suggest that a small proportion of cells are dying in each generation. The 45 ng/ml NCS treated samples show a slightly smaller gradient in their line of best fit suggesting that the slightly reduced CellTrace dilution is not sufficient to explain the smaller population growth seen compared to the mock treated. This would indicate a greater rate of cell death per generation than in the mock treated, but not by a great deal.

The 100 ng/ml NCS treated samples show the greatest difference to the mock treated. Here the line of best fit is considerably shallower than the mock treated, indicating the reduced progression through generations as shown by the CellTrace fluorescence is far from sufficient to explain the much reduced population relative to the mock treated. This suggests a much larger rate of death in these cells throughout the experiment than the mock treated and is supportive of the idea that delayed death occurs throughout the timespan of the experiment corroborating the findings from direct microscopy observation. Repeat experiment results are shown in Figure 81.

1.12.5 Estimation of death rate

This analysis may prove suitable for estimation of the proportion of cell death in each generation if the rate is assumed to be reasonably constant throughout the experiment, as a good linear fit would suggest. To achieve this estimation a mathematical derivation was determined by Dr Alessandro Esposito which allowed estimation of this generational cell death rate, see materials and methods 1.30.

Using this on the data presented in Figure 64, gives an estimate of cell death per generation using the total population count in the mock treated condition of 14% cell death and 29% for the 100 ng/ml NCS treated samples. If the viable population count is used in the calculation instead of the total population count we see a greater estimate of cell death for the 100 ng/ml NCS treated samples of around 36%. Comparing across repeated experiments in Figure 81, shows that all three estimate reasonably similar values. These numbers are reasonably comparable to the microscopy data, the mock treated value is higher than expected but not alarmingly so. This may be a product of neglecting the ρ value or may represent higher cell death in this assay. The generational death proportion in the 100 ng/ml NCS treated samples is consistent with being a slightly milder version of the phenotype demonstrated in the NCS treated lineages in the microscopy experiments. Therefore, with a number of assumptions, it would appear that the results from the flow cytometry experiments are consistent with the delayed death observed previously. The NCS concentrations required to demonstrate this are higher, but as addressed previously, this is likely due to the same concentrations of NCS not being comparable across different assays, necessitating the titration of NCS with new experimental setups.

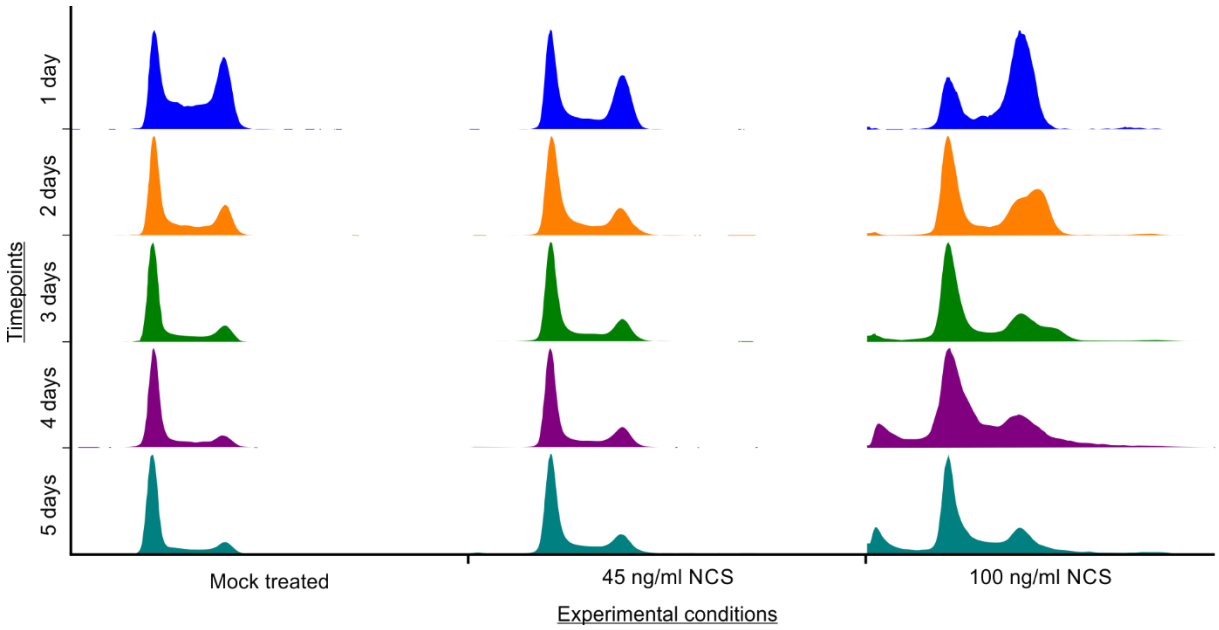

Figure 65: Cell cycle distributions over time of U2OS cells receiving mock or NCS treatments.

1.12.6 Cell Cycle analysis

Samples taken at each time point following treatment were also analysed for changes in the cell cycle distribution, Figure 65, from which cell cycle arrests and cell death could be inferred. Mock treated samples show a normal cell cycle distribution 24 hours after mock treatment, the highest peak is the G1 peak but the G2 peak is only slightly smaller and a great many cells are in the intermediate S phase region. Very few cells are in the sub-G1 region indicating few cells are dying or hypoploid. Similarly, very few cells are in the hyperploid region beyond the G2 peak, indicating few cells are polyploid, relative to this cell line's normal ploidy. With each later time point the G1 peak becomes more dominant relative to S and G2 indicating more and more cells are in G1. This is likely due to the depletion of nutrients and growth signalling factors over time and possibly due to effects of increasing confluency. U2OS cells are a cancer line and therefore unlikely to demonstrate typical contact inhibition but some changes may still occur. There is no apparent increase in irregular cells, either hypo or hyperploid, over the timespan of the experiment.

45 ng/ml NCS treatment results in few changes to the cell cycle profiles at each timepoint. 24 hours after treatment there are fewer cells in S phase relative to the mock treated control which may indicate that cells are still arresting in G1 and G2 phase at this point causing relative accumulation in these phases of the cell. At subsequent time points the only difference appears to be a slightly less dominant G1 peak, likely due to the population being lower relative to the control at every time point and so will have experienced fewer media and confluency related changes.

At 100 ng/ml NCS the differences are much starker. 24 hours after treatment cell cycle profiles are now greatly shifted to the G2 phase of the cell. This is consistent with the dominance of the G2 arrest

seen with the FUCCI microscopy. The subsequent time points show a return to a larger G1 peak suggesting, as the CellTrace dye results indicate, that cells have resumed cycling by this time. The G2 peak demonstrates an unusual humped distribution at the 48 and 72 hour time points which disappears by later time points. Further abnormalities are the increase in cells in the sub-G1 region and the small increase over time in cells with hyperploid DNA staining. The increase in sub-G1 cells is consistent with the inferred cell death and the hyperploid cells may have failed to carry out mitosis properly and acquired more copies of chromosomes than typical for this cell line. This may be via uneven segregation of chromosomes or the formation of binucleate cells after failed cytokinesis, as was occasionally observed by microscopy. Such abnormalities might drive death in these cells eventually, but are also a potential source of genomic instability which could allow, in a tumour setting, the selection of clones that acquire pro-survival mutations.

1.12.7 The persistence of DNA damage

As discussed previously, one possible cause of delayed death could be inherited DNA damage that fails to be adequately resolved by the descendant cells, ultimately leading to activation of cell death mechanisms. To investigate whether this is plausible, cells were also collected and fixed on coverslips at each time point to allow for detection of the presence of the DNA damage marker γH2AX (Löbrich et al. 2010) via immunofluorescence. Representative images from the mock treated and 100 ng/ml NCS treated cells are shown in Figure 66 and Figure 67.

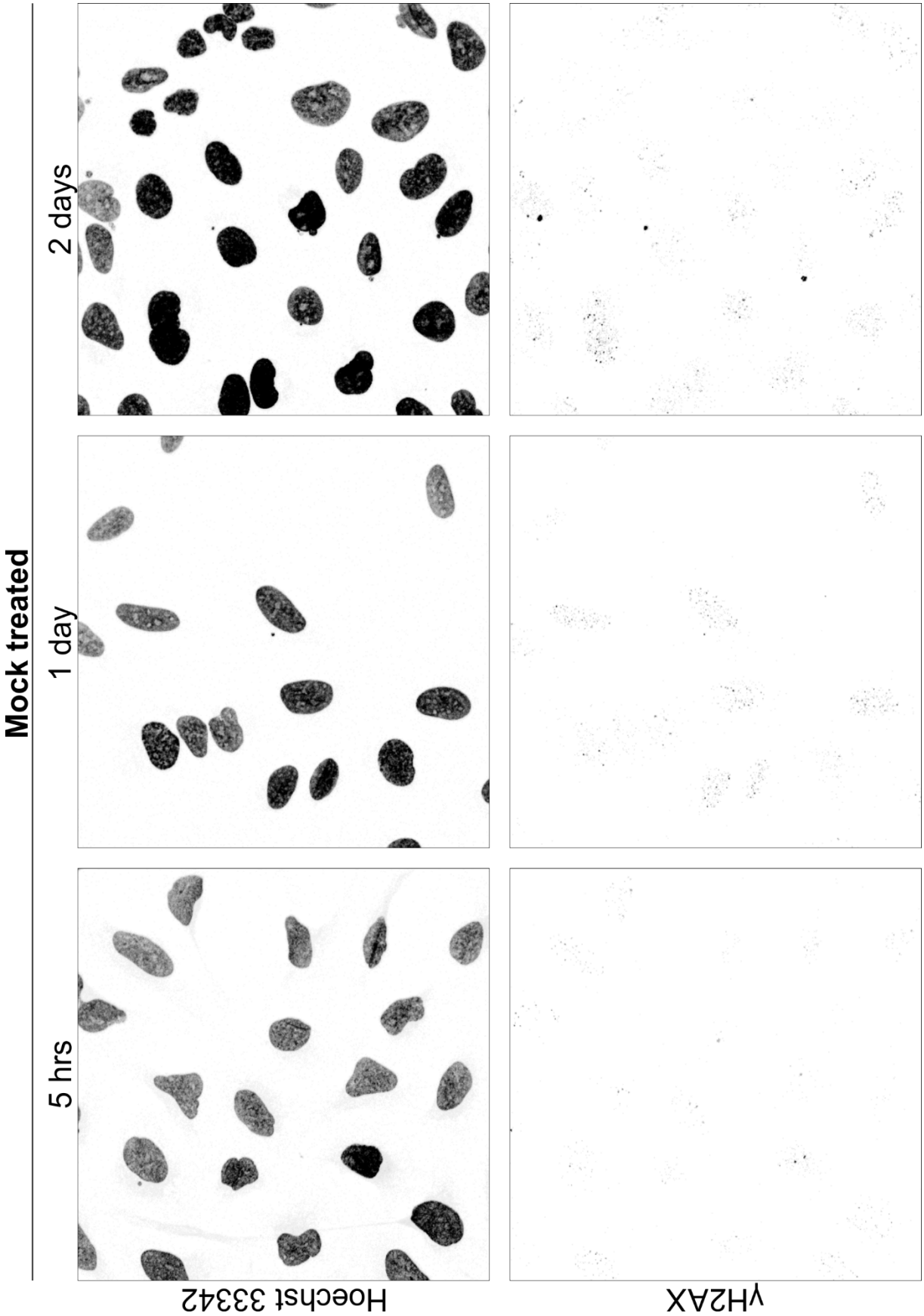
Mock treated
2 days
1 day
5 hrs
Hoechst 33342
γH2AX

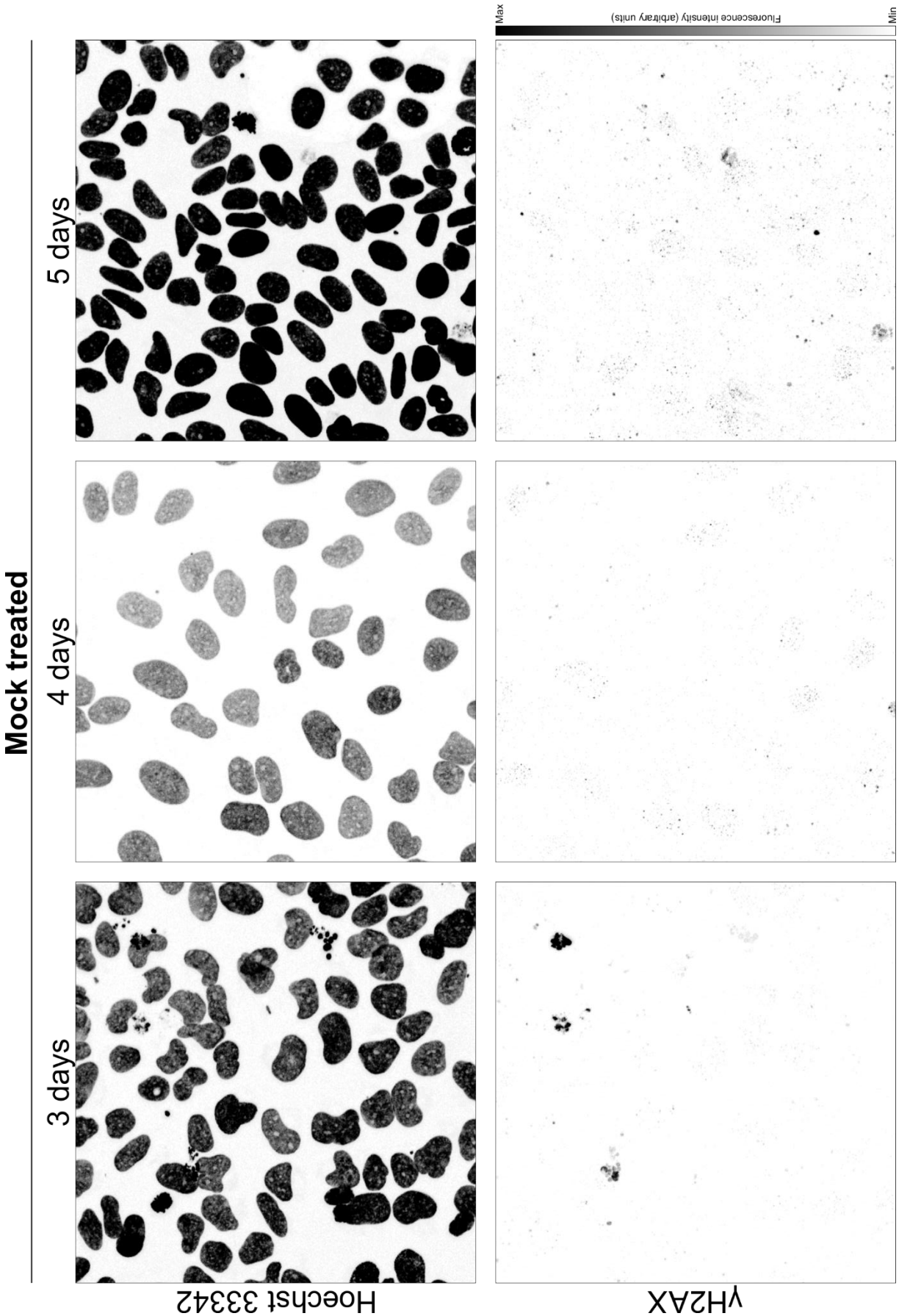

Figure 66: Mock treated cells show few γH2AX foci across the course of the experiment
γH2AX foci visualised by immunofluorescence for mock treated cell samples harvested at each timepoint. Representative experiment of two repeats shown.

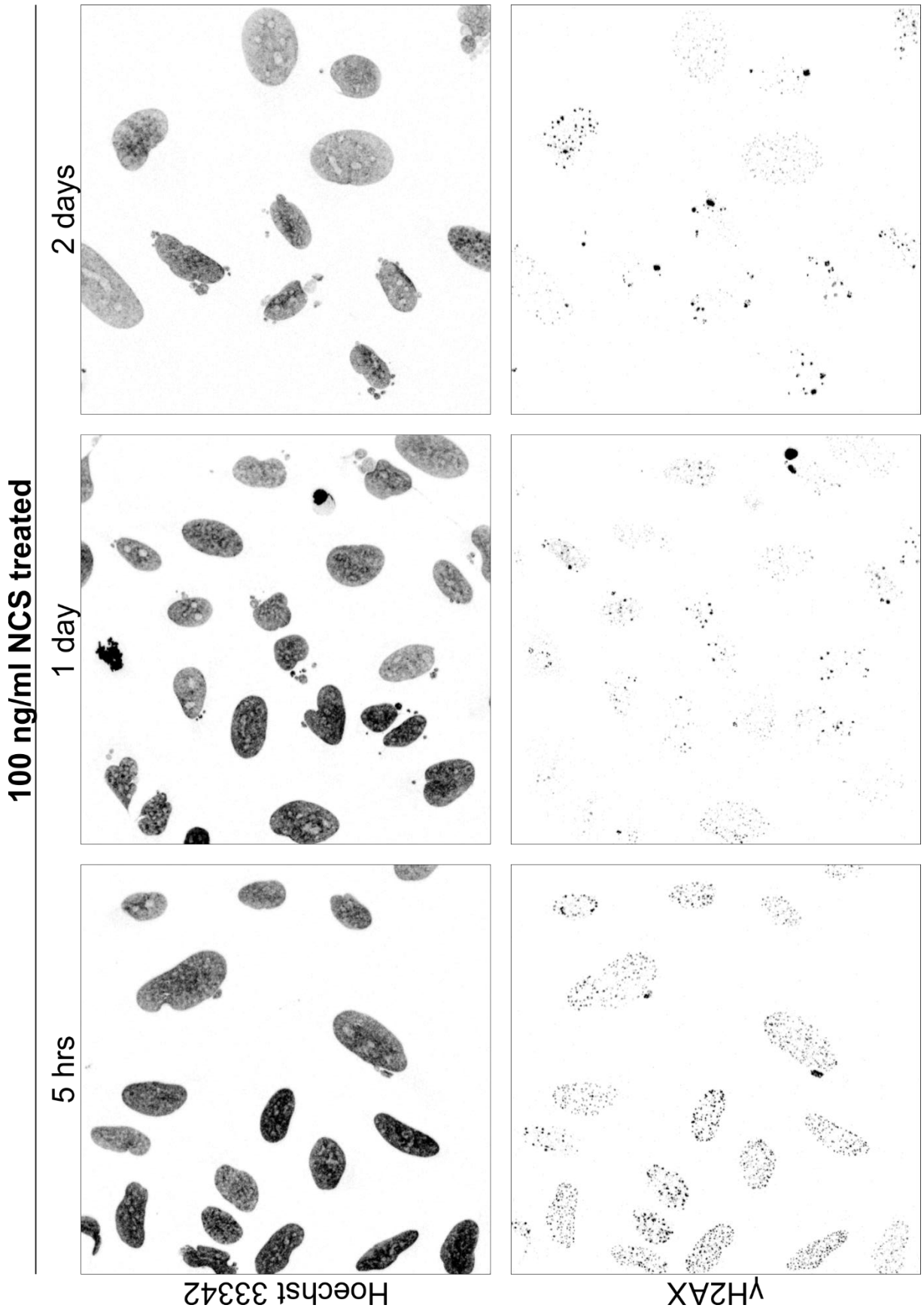
100 ng/ml NCS treated
2 days
1 day
5 hrs
Hoechst 33342
γH2AX

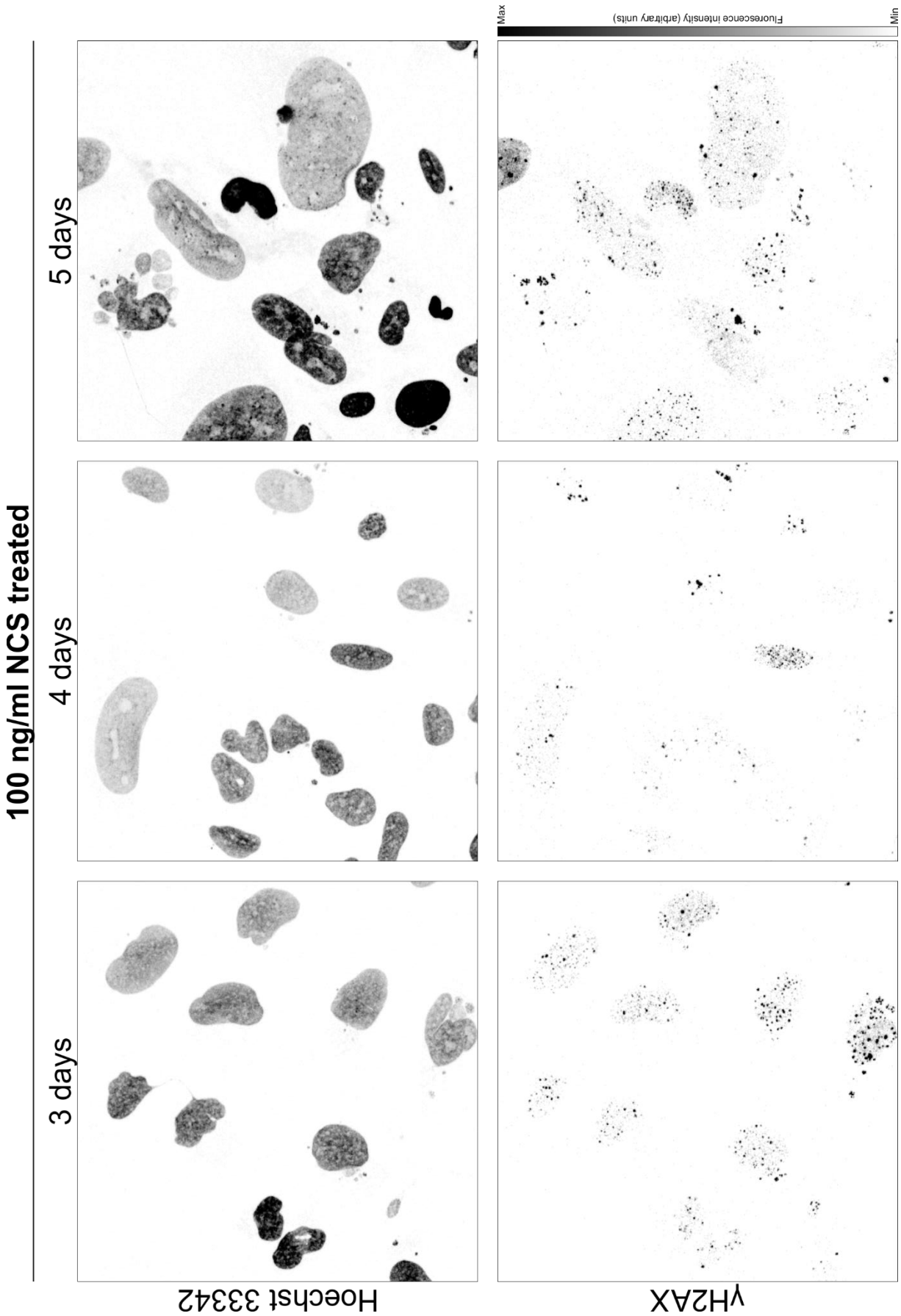

Figure 67: 100ng/ml NCS treated cells show induction of DNA damage that persists over the five days of the experiment. γH2AX foci visualised by immunofluorescence for 100ng/ml NCS treated cell samples harvested at each timepoint. Representative experiment of two repeats shown.

At all time points, mock treated cells exhibit few obvious DNA damage foci suggesting the presence of low endogenous levels of DNA damage and/or unspecific faint nuclear background staining. Furthermore, DNA stained by Hoechst shows little change in nuclear morphology across the course of the experiment, only the expected increase in cell density.

5 hours after 100 ng/ml NCS treatment, all cells exhibit bolder and a far greater number of γH2AX foci compared to the control images, confirming that NCS treatment has induced damage in all cells treated. Differences in the survival of cells or their descendants are unlikely therefore to be due to simply not being damaged to begin with.

Many NCS treated cells exhibit DNA damage in all of the timepoints of the full 5 days span of the experiment even though the vast majority of cells appear to be cycling, based on the CellTrace dilution, Figure 62. Taken together, the data confirms that many descendant cells carry DNA damage and so DNA damage can be inherited by following generations, which die at a higher rate compared to control. By the final time point, treated cells display high heterogeneity in gH2AX staining and in nuclear morphology as indicated by the Hoechst stain. Some nuclei are rather large in size, some appear more ragged and irregular than normal, while others are indistinguishable from controls. NCS treated cells also exhibit an abundance of micronuclei, i.e. small clusters of DNA visible in close proximity to the nucleus, suggesting the presence of significant chromosomal abnormalities. These micronuclei typically stain highly for γH2AX. To depict the high variability in morphology and staining at the end of the experiment, a collection of images from the final NCS treated time point is given in Figure 68.

To quantify these differences γH2AX foci were counted by computer software, with the results presented in Figure 69. As the images suggested the foci counts are similar across the mock treated cells representing endogenous damage and background staining. The 100 ng/ml NCS 5 hr time point in contrast shows the induction of DNA damage in all cells, albeit with a large range. By 24 hours after NCS treatment the number of foci is much reduced with many cells now comparable to the mock treated timepoint indicating that DNA repair is taking place in these cells and the damage being resolved. However, this reduction does not continue to completion. Instead elevated levels of DNA damage remain in some cells to the end of the experiment.

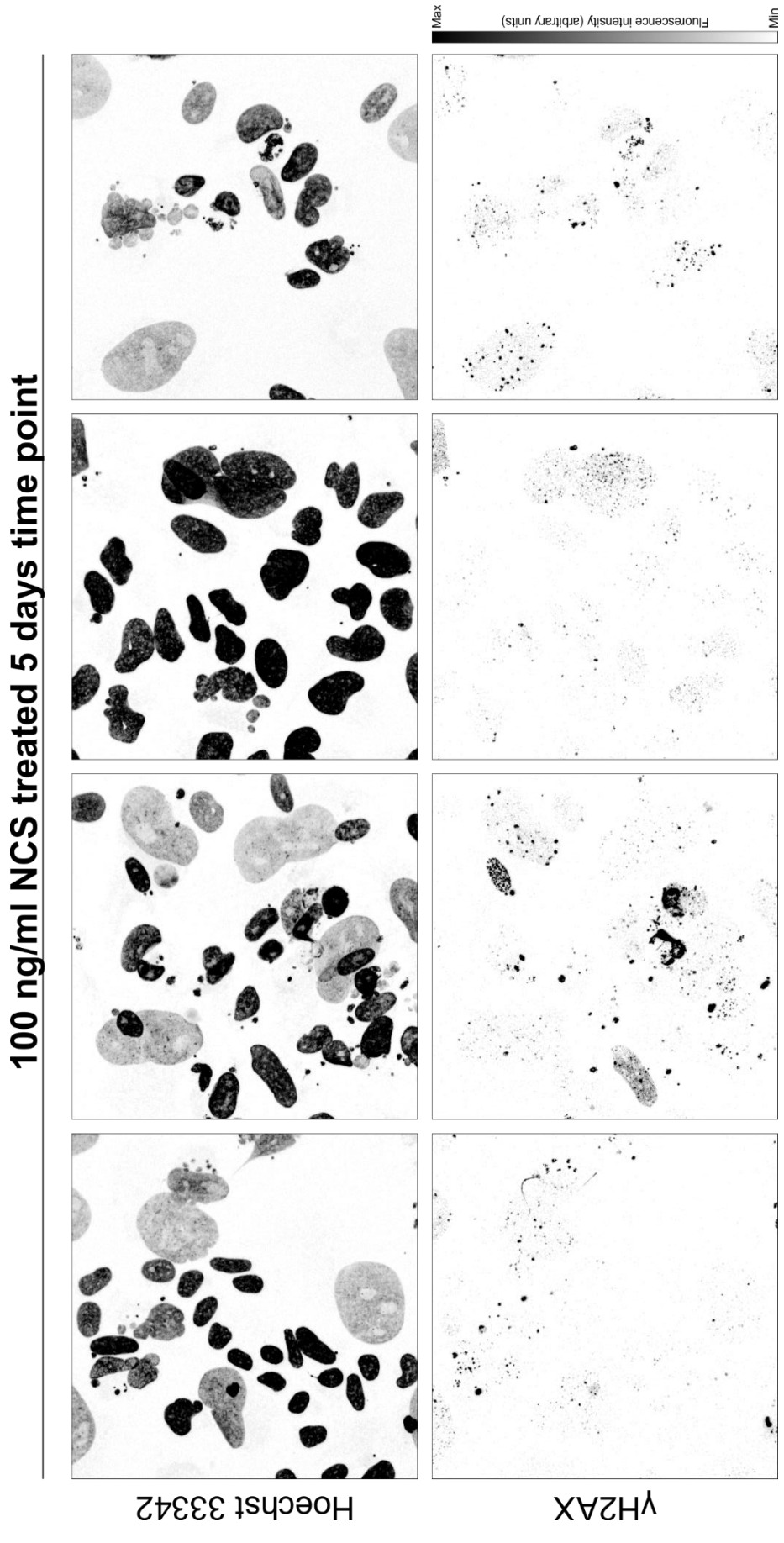

Figure 68: Further examples of immunofluorescence images taken from the NCS treated (100ng/ml) 5 days sample show the range of residual DNA damage (γH2AX foci) and the diversity of nuclear morphology (Hoechst 33342 stained DNA).

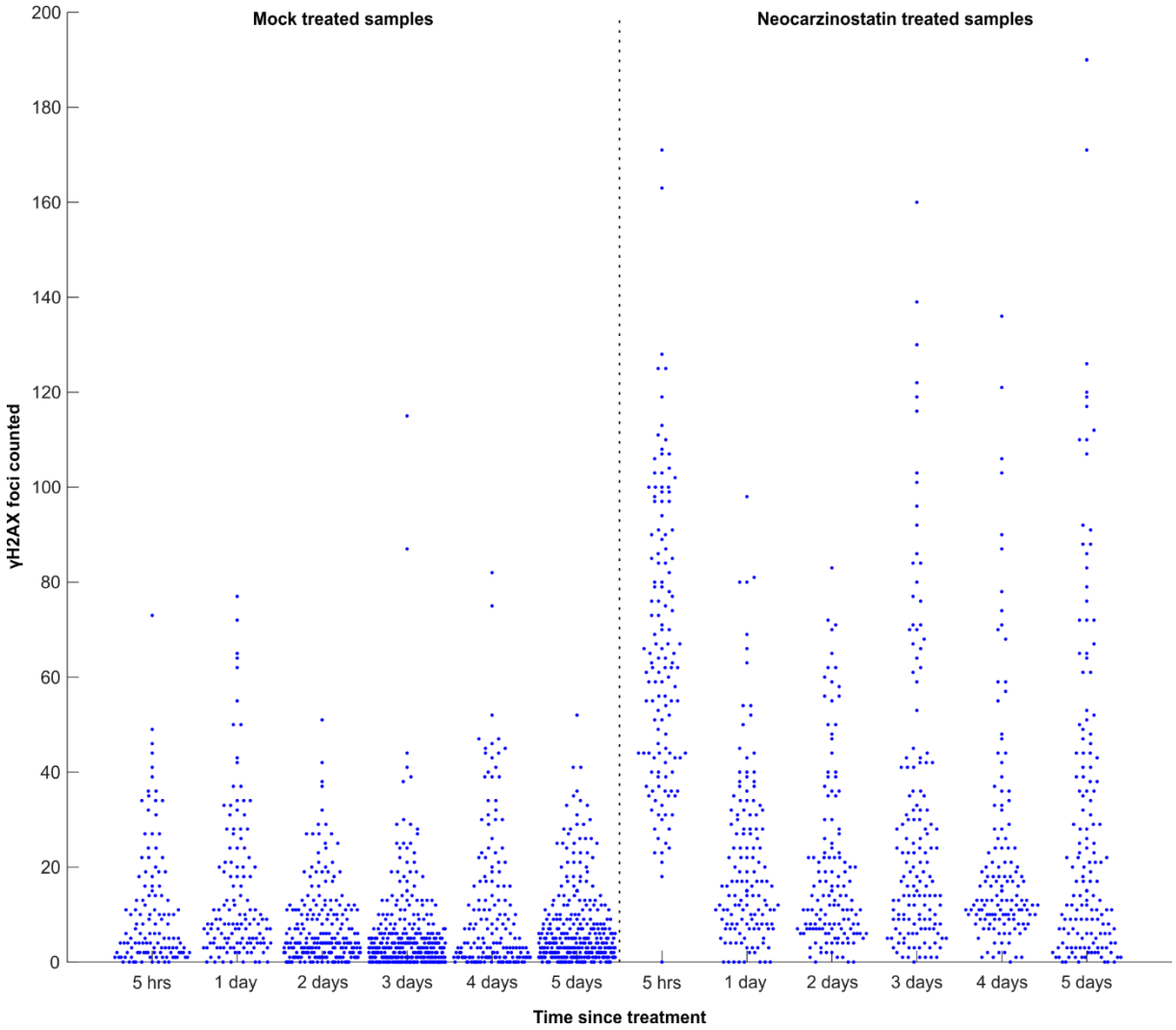

Figure 69: Automatic γH2AX foci counts for each timepoint for mock and 100ng/ml NCS treated samples
Mock treated samples show similar distributions of γH2AX foci across the experimental timepoints representing endogenous damage and background staining. 5 hours after NCS treatment γH2AX foci are elevated compared to mock treated cells. γH2AX foci initially decrease in abundance by the 1 day timepoint but thereafter remain consistently higher than their mock treated counterparts. Representative experiment of two repeats shown.

1.13 Generational tracing in HeLa cells

1.13.1 Initial HeLa comparison to U2OS

So far, the consequences of DNA damage on subsequent generations have only been examined in U2OS cells. I sought to determine whether this assay could be used to make insights into the behaviour of other cell lines. HeLa cells are a very commonly used cancer line, suitable for many cell assays for which we also have multiple transgenic strains. If generational tracing by flow cytometry proves successful on the parental cell lines it should in principle be possible to probe pathways using existing mutant HeLa cell lines. Generational Tracing flow cytometry experiments were therefore conducted upon a HeLa strain called HeLa TetOn. As an untested cell line, it was therefore still necessary to titrate NCS treatments.

The results of the CellTrace dilution are presented in Figure 70. The mock treated samples form a series of regular unimodal distributions that show progressively less fluorescence with each time point. The rate of fluorescence loss with each time point appears to decrease, indicating that by the later time points cell division is slowing. As in the U2OS cells these indicate cells moving relatively synchronously through multiple generations over the course of the experiment.

The CellTrace dilution curves of the NCS treated samples show that these cells demonstrate an initial cell cycle arrest following DNA damage, evident as an increase in overlap between the 0 and 24 hour sample fluorescence distributions, but that division subsequently resumes with fluorescence being lost with each time point. Indeed, the peaks of each curve are almost as far to the left as in the mock treated suggesting a great many cells are dividing almost as much as the cells in the mock treated condition. Differences in the curves are more apparent in the size of the tail of cells with higher fluorescence. This tail increases for each time point with increasing doses of NCS treatment. Similarly to the broadening of peaks seen in the U2OS cells, this may indicate that cells have become relatively desynchronised with each other over the progression through generations. Importantly however, it is not the case that this is just due to the initially DNA damaged cells arresting permanently. The tail of cells stretches across a range of fluorescence with much of it lower than the 0 days distribution, indicating these cells are descendants of the damaged cells.

The total population graph indicates similar trends to the U2OS cells, the mock treated cells divide abundantly, reaching population sizes much larger than at the start of the experiment. At all NCS concentrations the population does manage to grow but with increasing NCS doses this is reduced more and more. Viable population, a measure of viable cells based on trypan blue viable cell discrimination, see Materials and Methods, is plotted in Figure 82 and shows similar trends.

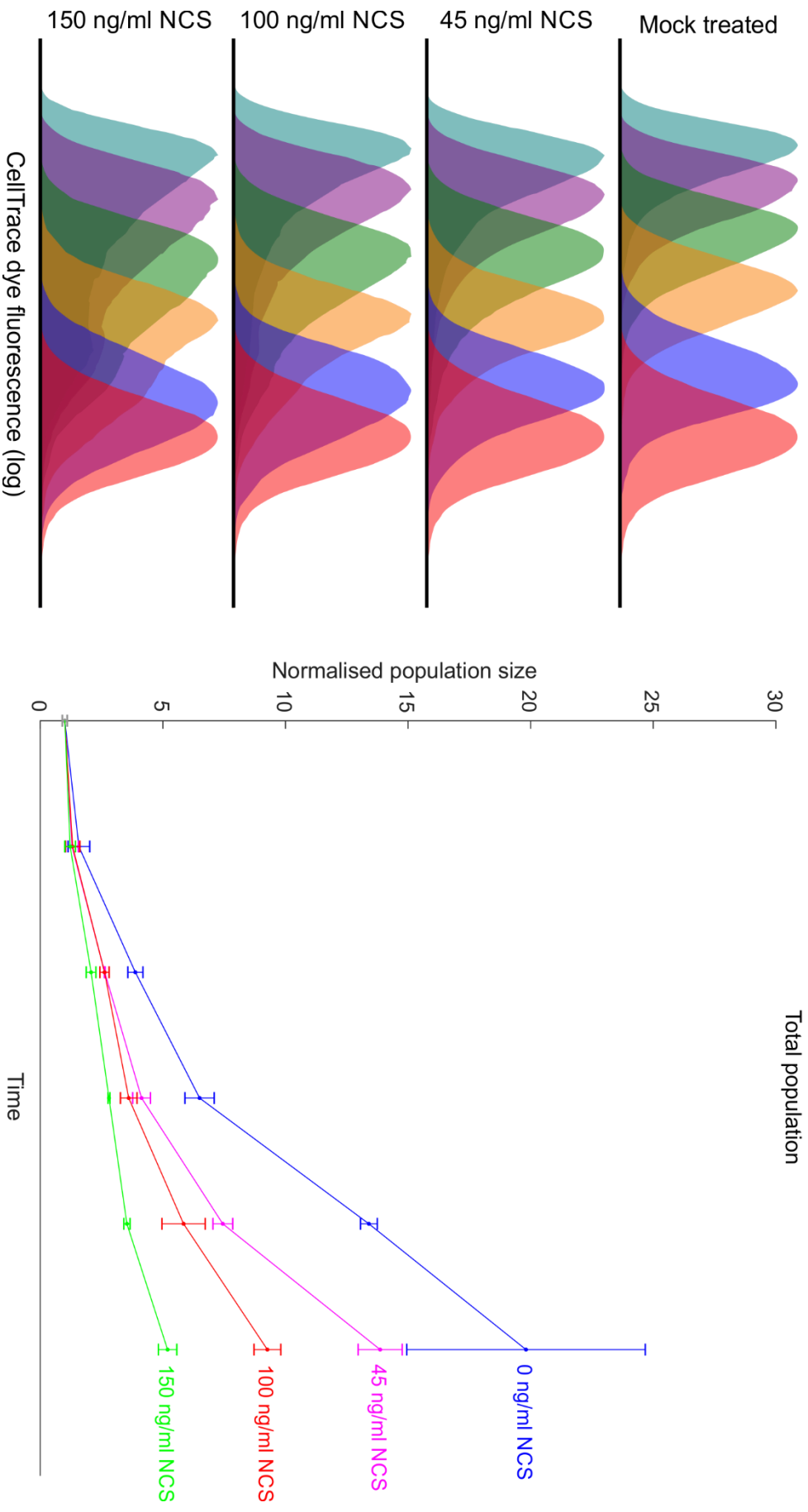

Figure 70: CellTrace profiles and total population graphs for HeLa TetOn cells. Cells treated with mock, 45 ng/ml NCS, 100 ng/ml NCS and 150 ng/ml NCS conditions. (n=1) ***Left)*** *Measured CellTrace Fluorescence curves for each timepoint for each condition. Logarithmic scale of fluorescence, one representative curve from each timepoint triplicate shown.* ***Right)*** *Measured total population changes over time for each experimental condition. Average of timepoint triplicates shown with standard deviation error bars.*

Undertaking the population growth vs CellTrace dilution analysis, Figure 71, reveals that all four experimental conditions demonstrate a linear relationship between the two measurements and that, as with the U2OS cells, increasing NCS concentrations, and thus increasing DNA damage, results in a shallower line of best fit slope. This suggests that NCS treatment increases the proportion of death in each generation and estimating the death rate per generation using the equation derived previously yields the indicated death rates. The estimates for mock treated and 45ng/ml treated cells are very similar to the U2OS cells, while the rate for 100 ng/ml is lower suggesting that 100ng/ml induced a milder increase in death in HeLa cells. The highest tested concentration of 150 ng/ml in HeLa cells gave a death rate similar to the 100 ng/ml in U2OS.

Examining the cell cycle profiles of these cells, Figure 72, shows that the mock treated behave similarly to the U2OS cells, exhibiting a predominant G1 peak that grows larger relative to G2 as the experiment proceeds. The cell cycle arrest induced by the DNA damage is most evident in the 150 ng/ml 1 day time point where the G2 peak has become much larger indicating a strong G2 arrest. This arrest is however no longer present by 2 days after treatment and the majority of cells are now in a more normal G1, S phase and G2 peak pattern, suggesting they have resumed cycling. Cell death is more apparent in the NCS treated samples based on the increased sub-G1 fraction. There is also a larger tail of hyperploid abnormal cells compared to the mock treated cells. The profiles and the changes NCS induces are quite similar to the profiles obtained from the U2OS experiments.

Overall, HeLa TetOn cells appear very similar in behaviour to the U2OS cells tested earlier, which indicates that they probably also feature an increase in cell death in descendant cells following DNA damage.

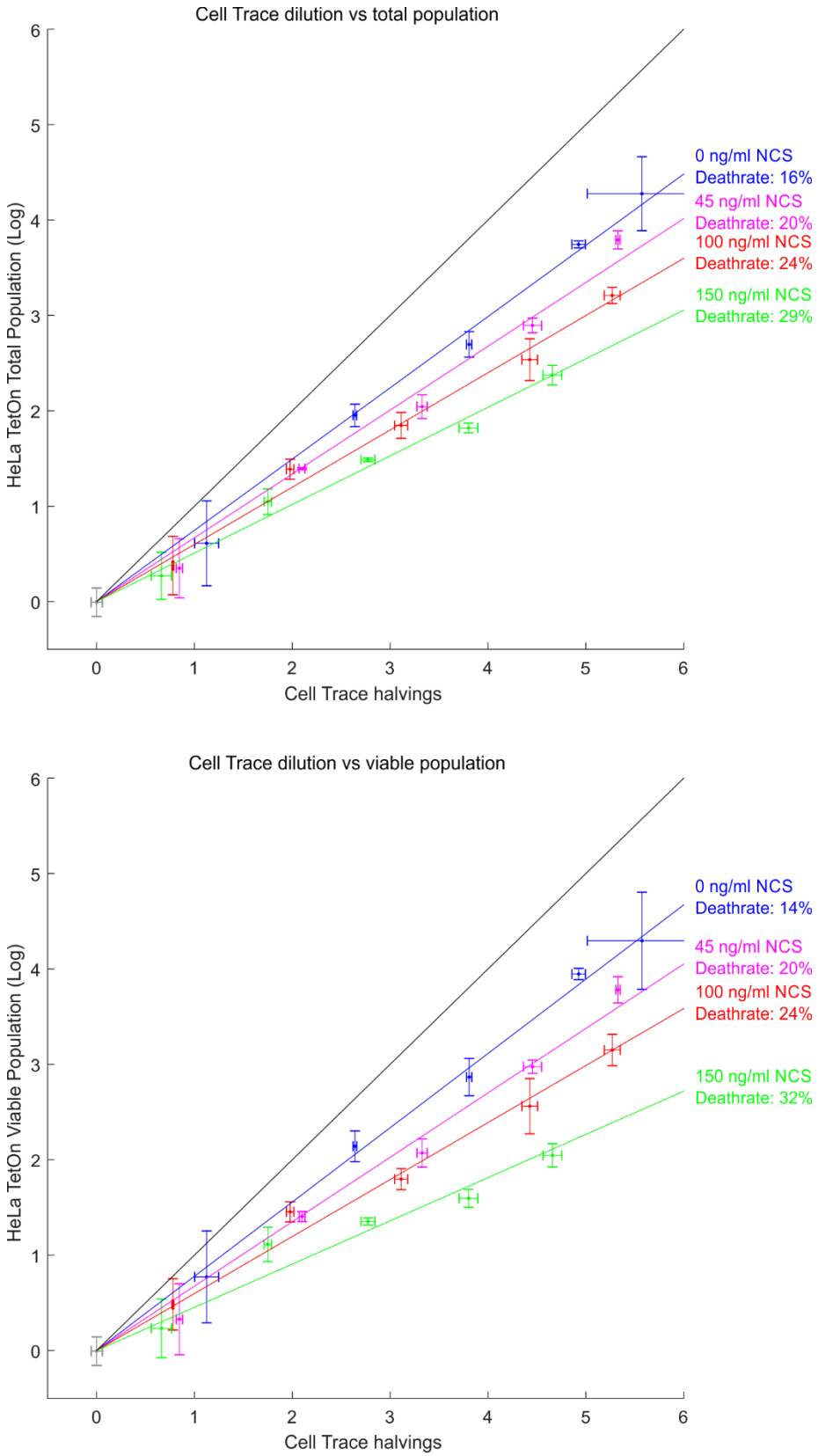

Figure 71: Comparing population changes to the dilution of CellTrace fluorescence allows generational death in HeLa TetOn cells to be inferred
Mock, 45 ng/ml NCS, 100 ng/ml NCS and 150 ng/ml NCS conditions evaluated. Averages of triplicate measurements from each timepoint are shown with vertical and horizontal standard deviation errors bars. The approximately linear relationship for each condition suggests a constant death rate per generation. Linear regression through the origin allows approximation of this rate. ***Top)*** *Using total population ViCell counts,* ***Bottom)*** *Using viable population ViCell counts. (n=1)*

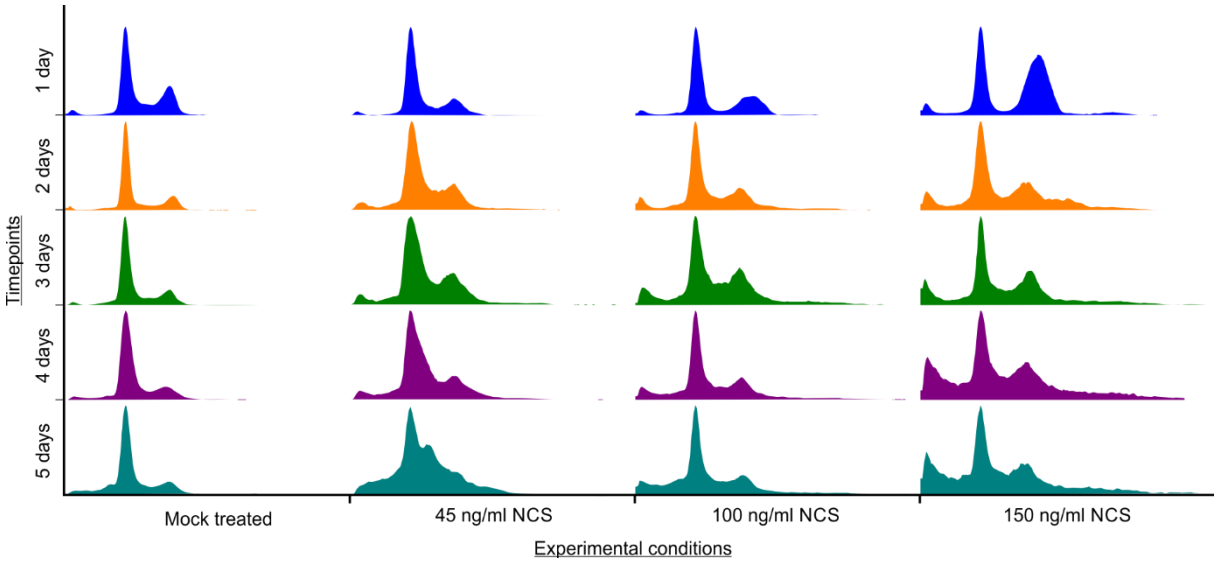

Figure 72: Cell cycle distributions over time of HeLa TetOn cells receiving mock or NCS treatments

1.13.2 Interrogating the response of later generations to DNA damage

This assay presents the opportunity to probe the progression through generations and cell death following DNA damage with a greater range of conditions than are feasible in a microscopy experiment. This could be done using chemical probes, for example inhibitors of checkpoint signalling, or through the use of transgenic cell lines that express molecular species that interfere with typical cell function. Once such cell line, HeLa BRC4.23, has been derived previously from the HeLa TetOn cell line allowing the controllable induction of a fragment of the tumour suppressor BRCA2 termed BRC4 (aa 1517-1551). This fragment has previously been described as binding strongly to RAD51 and so inhibiting the interaction between the full length BRCA2 and RAD51, thus preventing the assembly of RAD51 at the site of DNA damage and interfering with the process of homologous recombination. Induction of this fragment was therefore used to test whether homologous recombination or other unknown processes disrupted by BRC4 play a role in generational progression and cell death. Cells were treated with mock or NCS treatment and 24 hours after this treatment cell samples were then split into two populations, one of which was treated with doxycycline to induce transgene expression, Figure 75. Induction of the BRC4 fragment was confirmed to occur in the induced, and not the uninduced, populations by Western blot, Figure 76. Induction of the transgene 24 hours after the initial treatment permits the initial period of DNA damage repair to proceed as normal without interference while probing the later time points for effects of BRC4 expression on delayed death and inherited DNA damage.

The CellTrace dilution and population growth results are presented in Figure 73. The mock treated induced and uninduced samples are broadly similar in the shape of the fluorescence distributions at each time point, but differ slightly in how much the CellTrace dye is diluted. Induced samples show greater fluorescence for each timepoint following induction (i.e. after 1 day timepoint) suggesting

these cells have been slowed in progression through their generations. The NCS treated induced and uninduced samples show similar trends having curves of similar shapes but differing in the degree to which the dye has been diluted. The population curves show that the treatment with doxycycline reduces the population growth over the experiment, with this effect being most evident in the mock treated populations. Compared to the parental cell line experiment Figure 70, the 100 ng/ml NCS treatment was capable of inducing a greater arrest in this experiment, perhaps due to experimental variation or greater sensitivity of this derived cell line. Viable population counts are shown in Figure 83.

Comparing population growth against CellTrace dilution, Figure 74, shows that, as in the parental cell lines, the two measurements have a broadly linear relationship over the timespan of this experiment and that NCS treatment results in a much shallower slope in the line of best fit. It is also clearly apparent that although doxycycline treatment resulted in lower population growth, this is nearly completely explained by reduced progression through generations as the near identical linear relationships indicate. The lack of any observable difference between the induced and uninduced NCS treated samples suggests that disruption of the interaction between RAD51 and BRCA2 causes no consequences for delayed death, neither apparently increasing nor decreasing it. This would suggest that functional homologous recombination plays little role in the determination of cell death in later generations.

The cell cycle profiles from this experiment, Figure 77, broadly recapitulate the findings from the parental cell line. Mock treatment results in normal cell cycle profiles that become more G1 dominated as time passes. Treatment with NCS results in an apparent cell cycle arrest visible 1 day later, resumption in cycling is apparent by the 2 day time point, and accumulation of dying cells and hyperploid cells evidenced by the increasing sub-G1 and super-G2 cells with time. There are no stark differences between the induced and uninduced samples suggesting that any cell cycle distribution changes resulting from transgene induction or doxycycline are relatively small.

This assay has allowed me to identify changes in generational progression and population growth that occur following induction with doxycycline, either due to the presence of the transgene or the doxycycline itself, but show that these changes do not appear to operate on the processes that determine cell death in later generations following DNA damage.

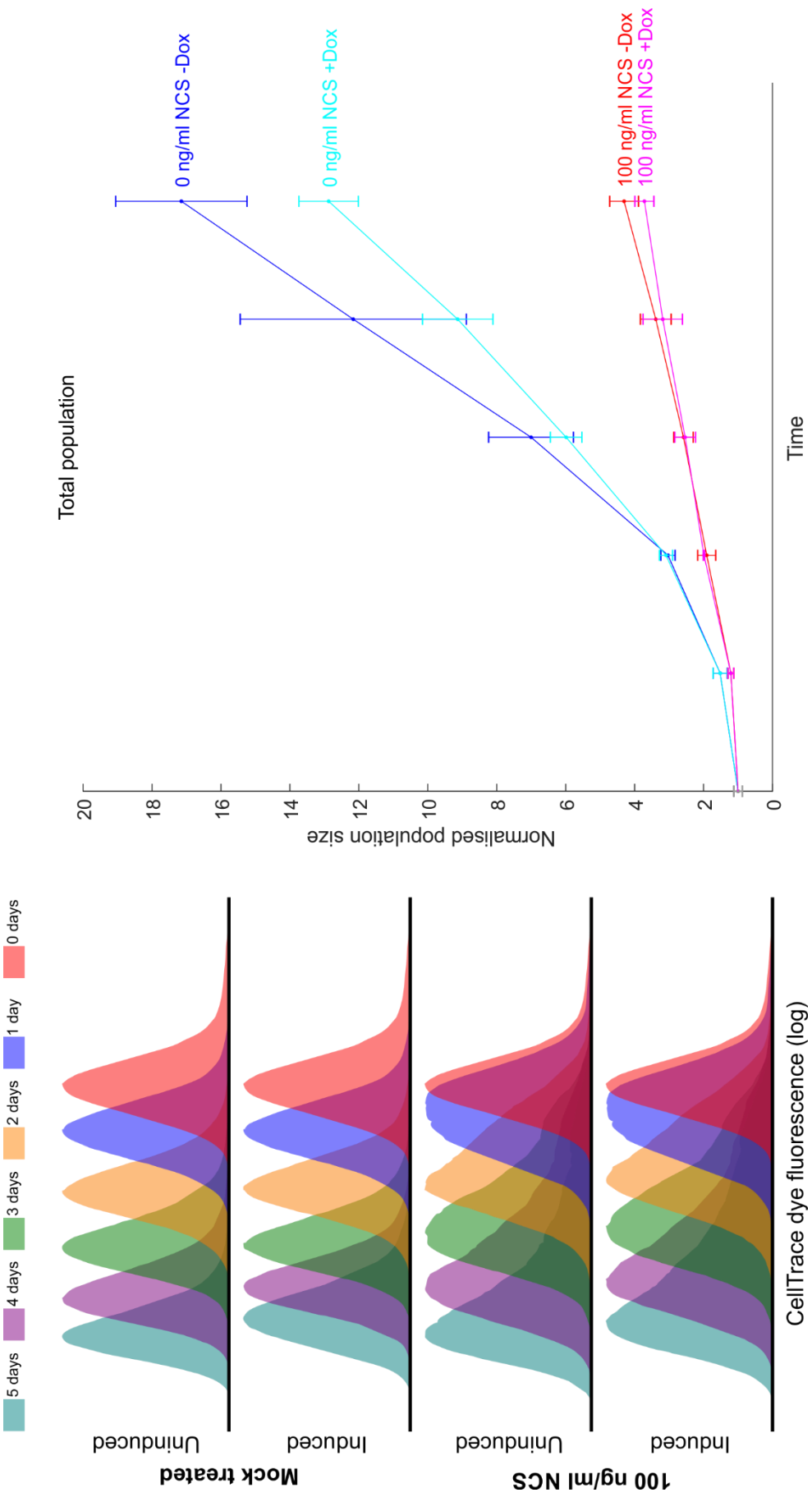

*Figure 73: CellTrace profiles and total population graphs for HeLa BRC4.23 cells. Cells were treated with mock or 100 ng/ml NCS, and are split into induced and uninduced pairs after 24 hours (n=1). **Left)** Measured CellTrace Fluorescence curves for each timepoint for each condition. Logarithmic scale of fluorescence, one representative curve from each timepoint triplicate shown. **Right)** Measured total population changes over time for each experimental condition. Average of timepoint triplicates shown with standard deviation error bars.*

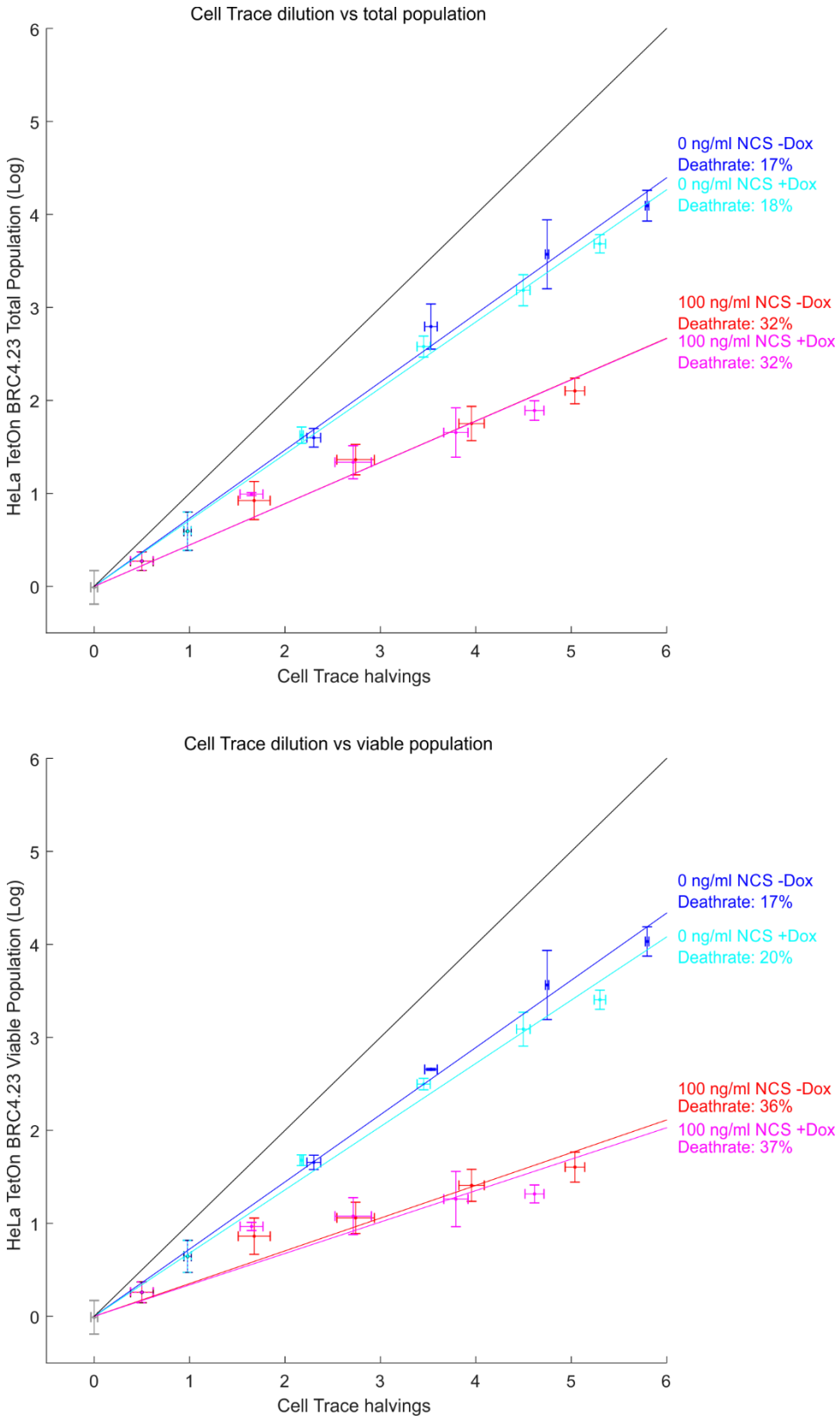

Figure 74: Induction of BRC4 expression appears to have little effect on generational death in NCS treated HeLa BRC4.23 cells Cells were treated with mock or 100 ng/ml NCS, and are split into induced and uninduced pairs after 24 hours (n=1). Averages of triplicate measurements from each timepoint are shown with vertical and horizontal standard deviation errors bars. The approximately linear relationship for each condition suggests a constant death rate per generation. Linear regression through the origin allows approximation of this rate. ***Top)*** *Using total population ViCell counts,* ***Bottom)*** *Using viable population ViCell counts.*

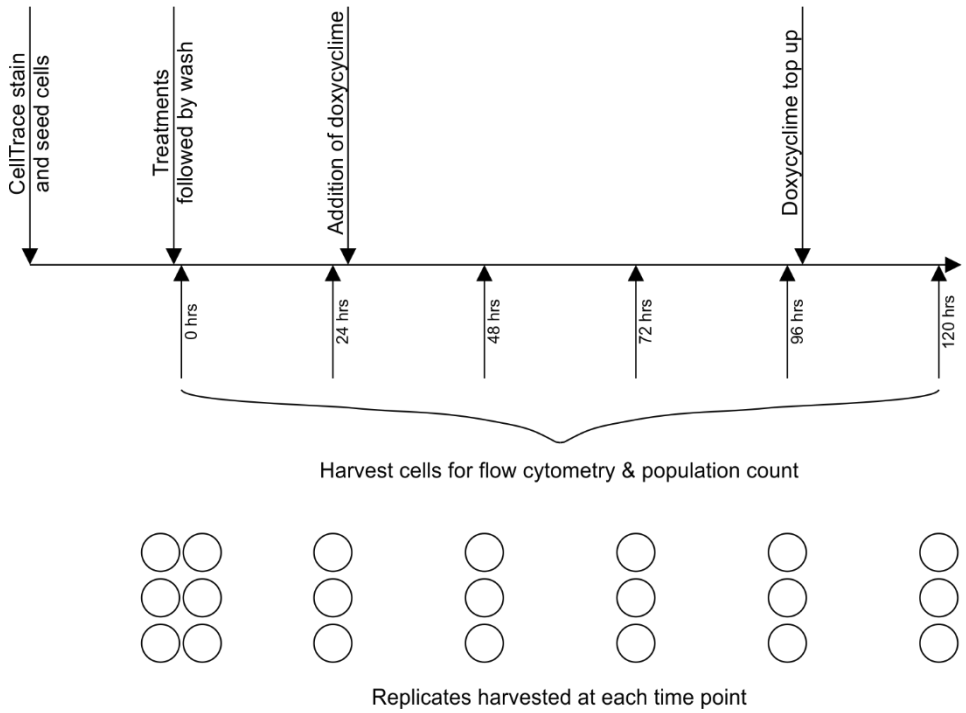

Figure 75: Experimental protocol for testing whether the induction of the BRC4 fragment alters death in descendant cells as inferred by flow cytometry generational tracing

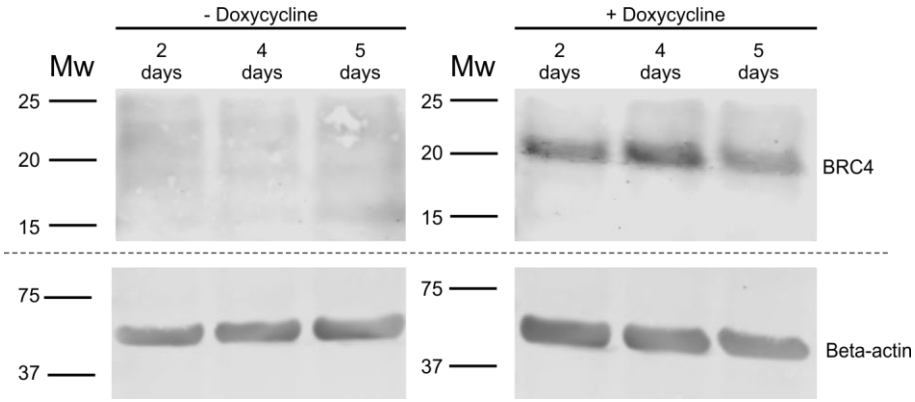

Figure 76: Western blot confirming induction of HeLa BRC4 fragment in dox treated samples after dox/control media addition after the 1 day timepoint
BRC4 is tagged with the myc epitopeand was detected using the antibody 4A6, see Materials and Methods. Equal lane loading (40µg of protein lysate per lane) was confirmed with blotting for Beta-actin.

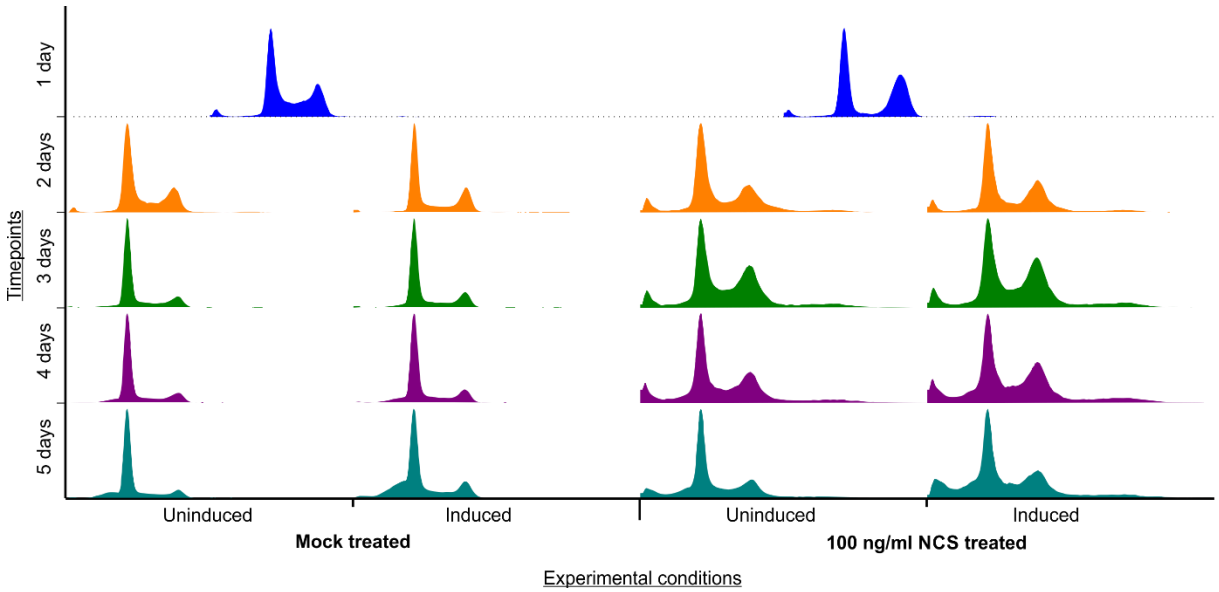

Figure 77: Cell cycle distributions over time of HeLa BRC4.23 cells
Distributions shown for populations receiving mock or NCS treatment and whether they experienced BRC4 induction 1 day after the mock/NCS treatments

1.14 Generational tracing in HPNE cells

HeLa cells are useful to establish that other cancer cell lines may exhibit a similar 'delayed cell death' phenotype but provide no information on the behaviour of non-cancerous cells. To probe if cells more representative of normal tissue exhibit the same phenotype, HPNE hTERT cells, were examined.

The CellTrace dilution and population growth for this experiment are presented in Figure 78. The mock treated samples show similar progression through the generations to the two cancer cell lines for the first 48 hours but after this appear to slow down considerably, with very little difference between the last two time points. Both NCS treatments show a degree of cell cycle arrest in the 1 day sample having fluorescence distributions that are more overlapping with the initial timepoint. These too then appear to resume cycling but after 2 days show much reduced progression through generations. Clearly these cells are behaving in a distinct way to the previously interrogated cell lines. The population measurements show very different behaviour to previously observed, the mock treated cells initially grow in population, peaking at 3 days after mock treatment, then thereafter declining. The NCS treated cells peak 1 day later at 4 days after NCS treatment and then also decline in population. The 100 ng/ml NCS treatment does appear to cause a population drop over the first 24 hours indicating a degree of cell death being triggered initially. When considering population growth against CellTrace dilution it is clearly apparent that these cells do not demonstrate a linear relationship, as would be expected given the initial growth of population and then crash. In all three conditions it appears that cells initially divide but then this cell cycle progression slows and cells begin to die off. Given that it occurs in all conditions this behaviour does not appear to have been dramatically altered by the NCS treatment and may reflect an experimental difficulty in growing these cells without passaging. Why this is occurring is unclear and merits further investigation.

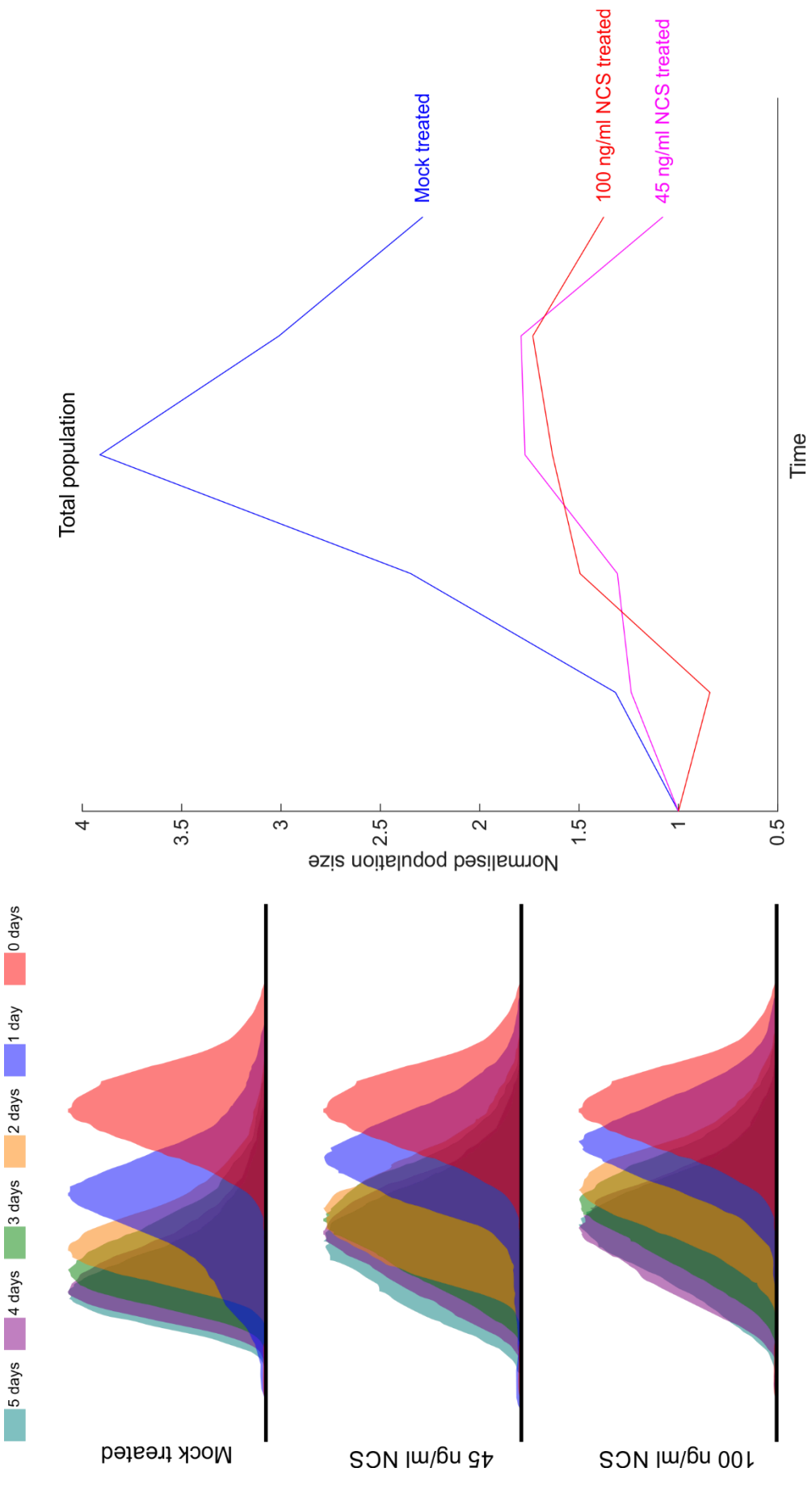

Figure 78: HPNE hTERT show very different behaviour to U2OS and HeLa cells.
***Left)** Measured CellTrace fluorescence curves for each timepoint for each condition. Logarithmic scale of fluorescence.*
***Right)** Measured total population changes over time for each experimental condition. (n=1)*
Only a single measurement was taken of each experimental condition at each timepoint rather than the three replicates in previous experiments

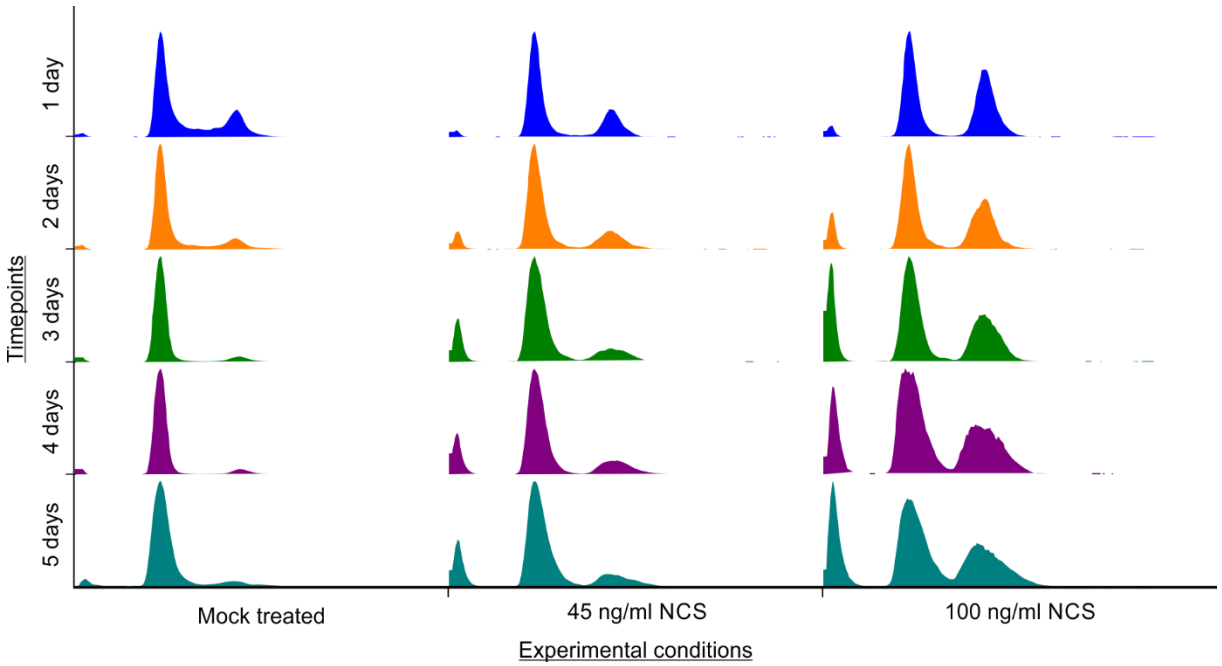

Figure 79: Cell cycle distributions over time of HPNE hTERT cells receiving mock or NCS treatment

The cell cycle distributions of the HPNE hTERT cells indicate an increasing predominance of G1 cells with time in mock treated conditions similarly to the other tested cell lines. NCS treated conditions induce large increases in the sub G1 population which would suggest cell death is occurring in response to the treatment. It is unclear why the drop in population evident after 3 days in the mock treated condition does not manifest as a similarly dramatic increase in the sub-G1. The 100 ng/ml NCS treatments induce a clear arrest visible in the 24 hours sample as a reduced S phase proportion and greater G2 peak compared to the mock treated control. This pattern remains similar across time which may suggest the treatment triggers persistent changes in the cell cycle distribution, unlike in the U2OS and HeLa cell lines which return to a more normal cell cycle distribution by the second day.

1.15 Discussion

The results presented here have supported the use of generational tracing via flow cytometry to further characterise and probe the response of cells and their descendants in a complementary indirect way to the microscopy experiments.

With this approach, the findings concerning delayed death in U2OS cells via microscopy based lineage tracing have been corroborated with reproducible trends across several generational tracing by flow cytometry experiments and new analyses have been designed to determine approximate death rates without direct observation. Furthermore, the combination of understanding generational progression via CellTrace dilution and the immunostaining for the DNA damage marker γH2AX allows us to indirectly infer that descendant cells can exhibit DNA damage markers and abnormal nuclear morphology. Possible mechanisms for triggering delayed death were discussed in the previous chapter,

one such possibility being the presence of persistent DNA damage triggering checkpoint mechanisms in descendant cell deaths and thereby causing cell death. Another possibility is that the initial DNA damage triggered severe consequences for the cell's ability to maintain cellular homeostasis, for example via disrupting normal mitotic function and leading to abnormalities such as aneuploidy and micronuclei that deregulate normal programmes of cell behaviour. The results presented here provide evidence that both are plausible. DNA damage remains abundant for many days after the initial treatment and micronuclei and otherwise irregular nuclei are frequently observed. Why the apparently persistent DNA damage does not appear to trigger cell cycle arrests that can be observed in the cell cycle profiles measured is unclear and may be related to the previously identified question of why apparently normally cycling cells can frequently produce daughter cells that die. Characterising the sensitivity of checkpoint mechanisms to inherited DNA damage may well be essential for understanding why descendant cells die. Furthermore, understanding the immediate consequences of genomic rearrangements and micronuclei formation may also yield insights into descendant cell death.

Beyond U2OS cells, preliminary findings indicating HeLa cells also display significant descendant cell death suggest that this phenomenon may not be specific to U2OS cells, but representative of cancer cells more generally, or those cancer cells that have experienced similar changes to checkpoint regulation by common mutations in oncogenes and tumour suppressors. It will be necessary to confirm this behaviour with repeated experiments. These results indicate that is of fundamental importance to understand how exactly cells die in response to DNA damaging treatments. Furthermore, preliminary work to utilise this assay to probe further experimental conditions was successfully undertaken using the HeLa BRC4.23 cell line.

In summary, this approach has provided a novel alternative to the laborious microscopy approach to identifying behaviour across generations after DNA damage treatment. The resultant data is not as rich and complex but still allows meaningful comparisons to be made between different conditions.

1.16 Supplementary figures

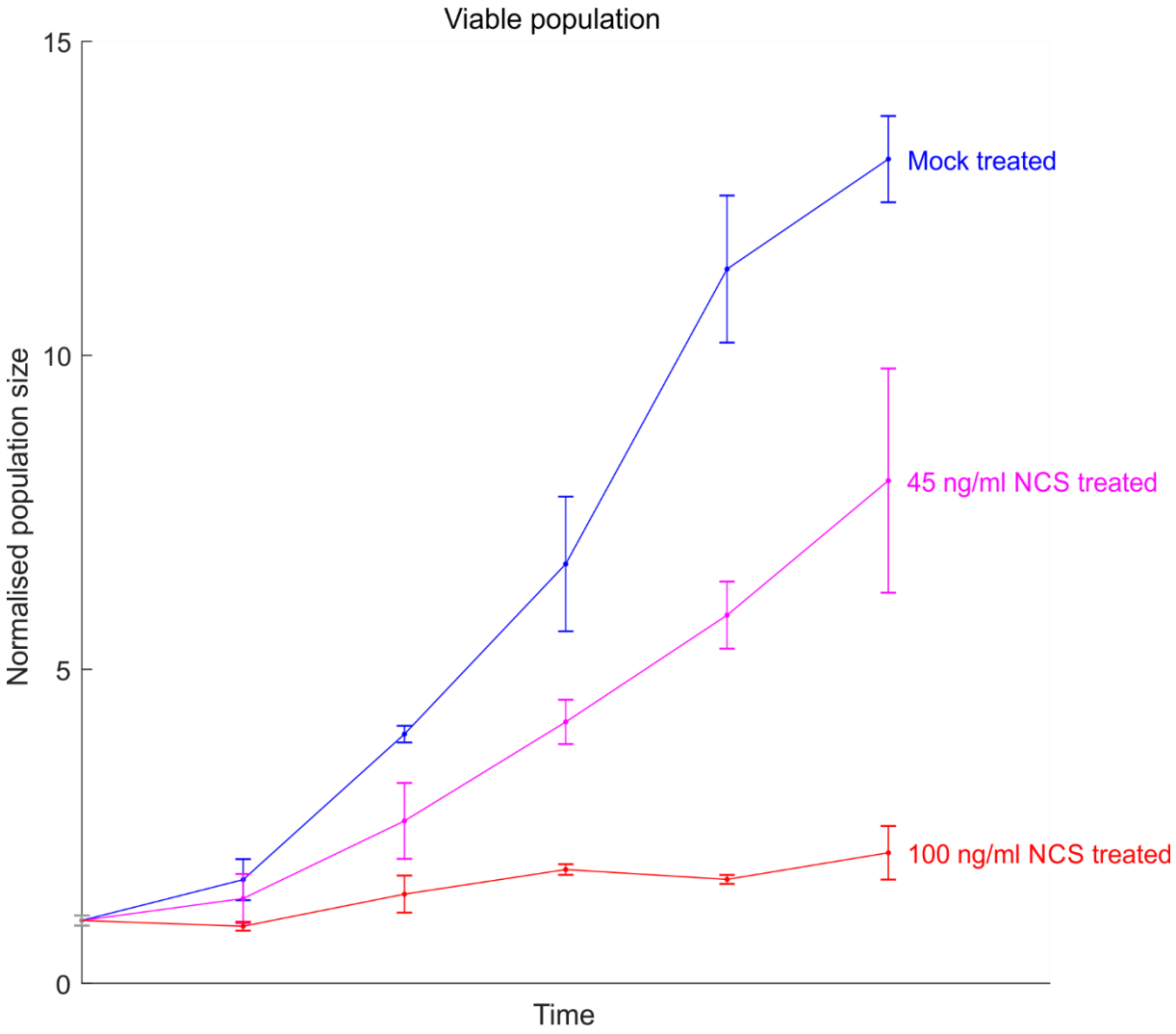

Figure 80: Measured U2OS viable population, as determined by ViCell trypan blue discrimination, changes over time for each experimental condition
Average of timepoint triplicates shown with standard deviation error bars. Representative experiment shown (n=3).

Experimental repeat 2

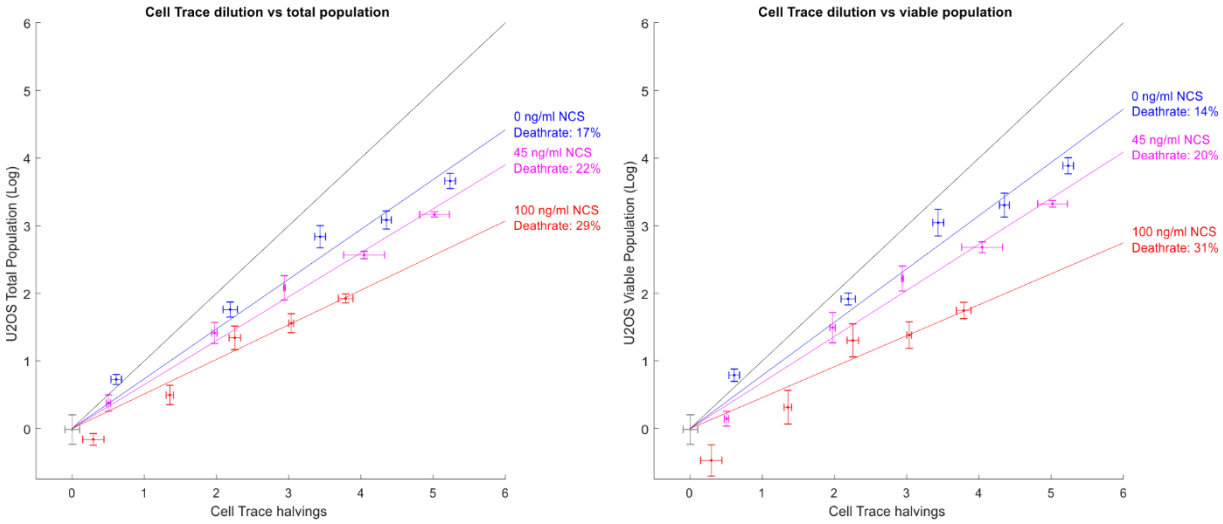

Experimental repeat 3

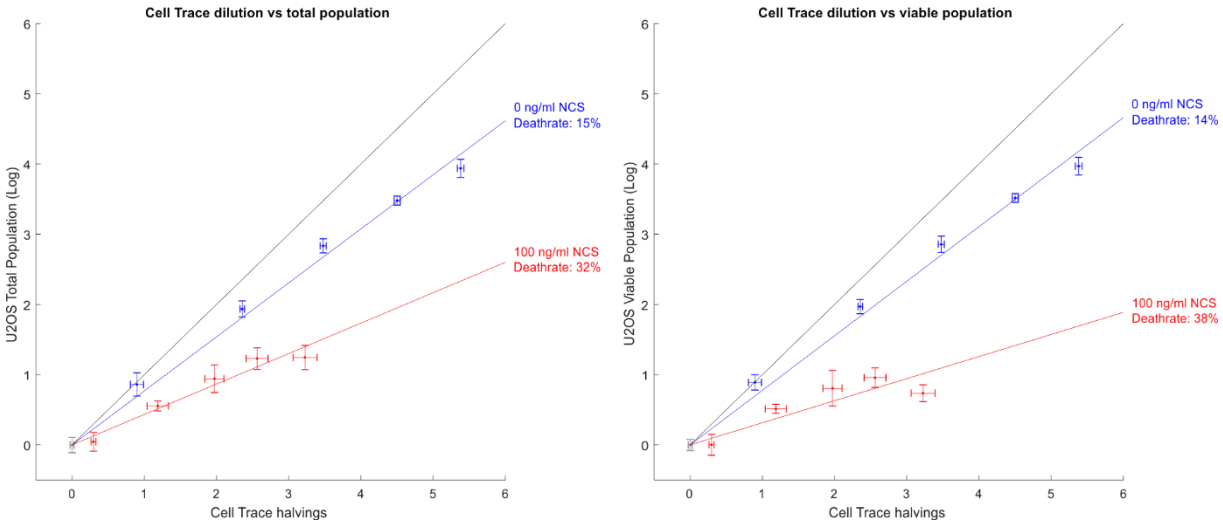

Figure 81: Generational tracing with flow cytometry of U2OS cells experimental repeats show similar trends

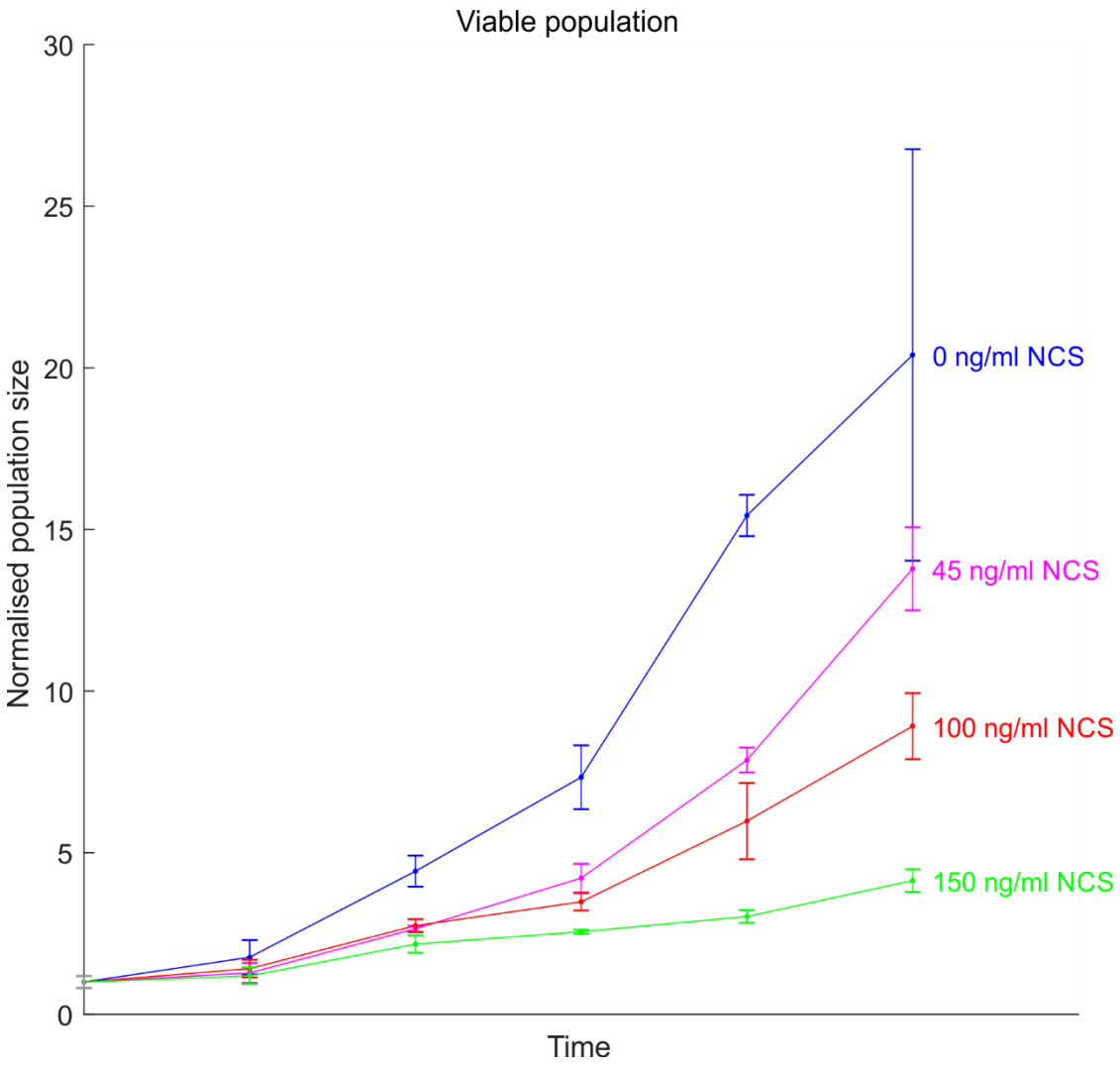

Figure 82: Measured HeLa TetOn viable population, as determined by ViCell trypan blue discrimination, changes over time for each experimental condition
Average of timepoint triplicates shown with standard deviation error bars. (n=1)

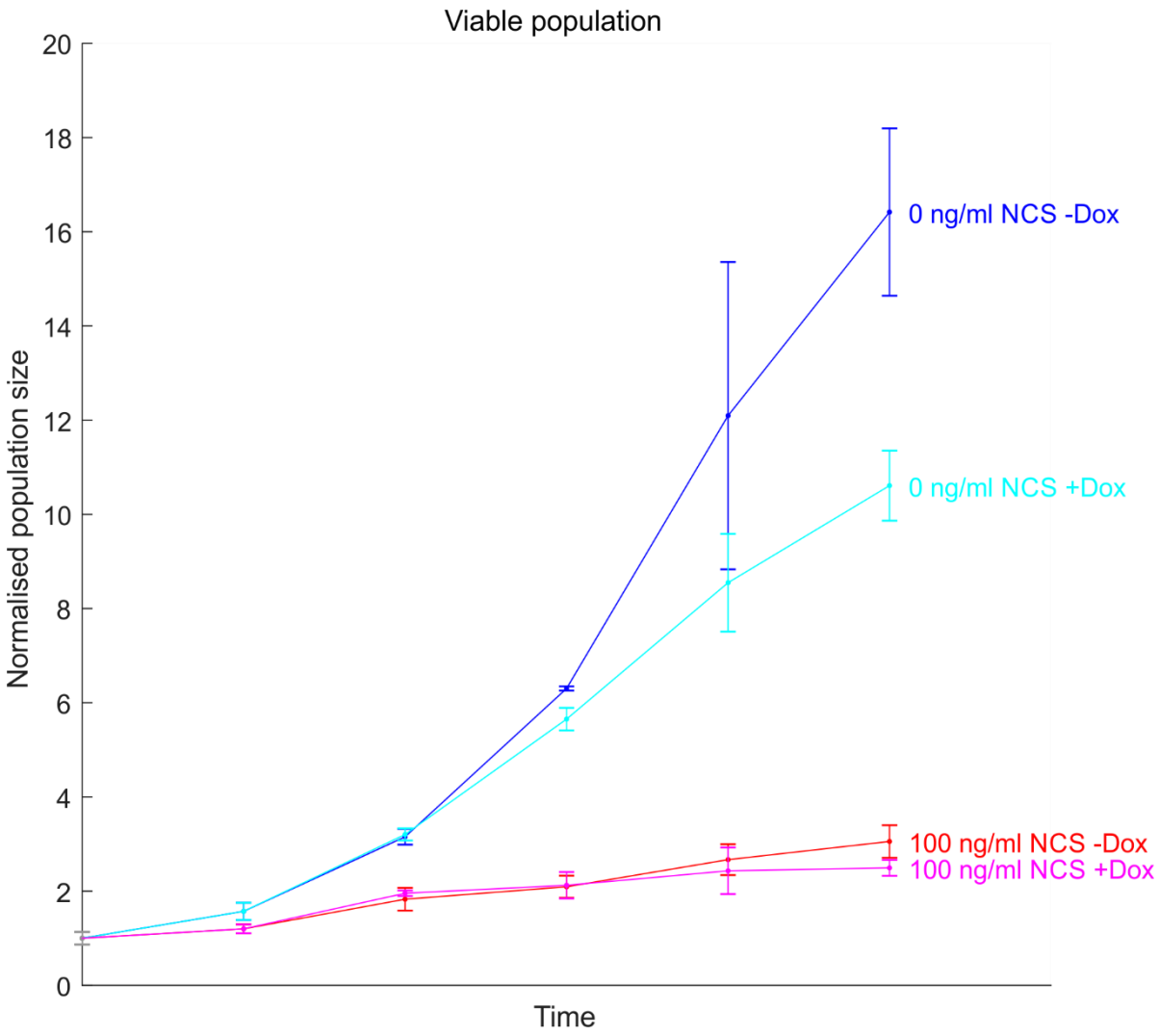

Figure 83: Measured HeLa BRC4.23 viable population, as determined by ViCell trypan blue discrimination, changes over time for each experimental condition
Average of timepoint triplicates shown with standard deviation error bars. (n=1)

Discussion

This work exemplifies how the study of biological phenomena at single cell level is fundamental. When studying even simple phenomena, such as cell death in response to DNA damage, single cell information can reveal biological insight that would otherwise remain hidden potentially leading to misinterpretation of data. In this instance, treatments that induce DNA damage could appear to be cytostatic in ensemble measurements, disguising the reality, for cancerous U2OS and HeLa cells at least, that cells continue cycling with the cellular choice between proliferation and cell death apparently being revisited in each subsequent generation. This delayed death response to DNA damage has been the most notable observation of this work and represents a facet of cell behaviour that has to date been only poorly studied.

It will be important to characterise whether cells from normal human tissue also demonstrate a delayed death response, thus indicating it plays a role in normal tissue physiology. Alternatively, normal cells may show different responses, perhaps initiating more robust arrests, senescence or apoptosis following damage. In this scenario, delayed cell death may only emerge prominently following the abrogation of typical tumour suppressive mechanisms and the selection of proliferative oncogenic mutations during tumour evolution. Understanding this will allow us to contextualise the importance of delayed cell death in restraining carcinogenesis.

As discussed previously in Chapter 0 if delayed cell death is present in normal cells this provides a method of potential checkpoint cooperation by which the negligence of cell cycle checkpoints can be resolved in later generations by eliminating descendant cells. Why cell death does not occur in the first generation is unclear but it has been postulated that in a mutagenic environment stopping indefinitely to repair DNA damage can be more disadvantageous than simply continuing progression through the cell cycle (Breivik 2001). In these cases, it would be advantageous to revisit cell fate decisions in later cell cycles reaching an appropriate balance between cell death and proliferation for that tissue. If delayed death is not evident in normal cells then it would be interesting to determine whether it emerges as a ‘back-up’ tumour suppressive mechanism following the abrogation of more robust checkpoint behaviour in cancer evolution, or if delayed death simply emerges as cancer cells select more negligent checkpoints that allow larger amounts of DNA damage into descendant cells which then die stochastically as the ramifications of inherited DNA damage arise. Fully characterising the delayed death phenomenon will be necessary to more accurately model and understand the role of cell cycle checkpoints in carcinogenesis.

Whether delayed death emerges as a by-product of carcinogenesis or is characteristic of normal human tissue cells this phenomenon is likely to be relevant to cancer treatment. Given the use of DNA damaging radio- and chemotherapy, understanding the delayed death phenomenon will have relevant

clinical implications, much as the current characterisation and understanding of checkpoint mechanisms influences therapies now. If the mechanisms governing and determining this behaviour were identified it could be possible to design more effective therapeutic interventions, perhaps either by finding combinations of existing therapies and identifying dosing regimens, or even by finding new drug targets. It is possible to imagine using these to shift cancer cells to higher rates of descendant cell death or in earlier generations and thus promote lineage exhaustion to cause greater tumour regression.

Furthermore, it has recently become apparent that the formation of micronuclei, which form after DNA damage is passed through mitosis and which I have observed here to accompany delayed cell death, may allow stimulation of the innate immune system (Mackenzie et al. 2017). Thus, the mechanisms we have described of checkpoint negligence and checkpoint cooperation could serve the purpose of generating immune stimulation within nascent tumours in the body for tumour suppression.

Understanding how and when cells die may also have fundamental implications for tumour evolution upon treatment with DNA damaging agents. Continued cell cycling in the presence of damage may generate mutations and provide genetic material for the selection of clones more resistant to DNA damage induced cell death. Furthermore, in the context of genetically heterogeneous tumours, stochastic elimination of lineages via delayed cell death may trigger genetic drift. With high average cell death rates per generation of just under 50%, most lineages will die out and individual clones that survive merely by chance can repopulate an entire tumour (modelled by Dr Alessandro Esposito - data not shown). The resultant fixing of allelic frequencies may produce tumours that differ greatly from the pre-treatment tumour. The implications of delayed cell death on tumour evolution following treatments deserve further investigation.

Cancers in the human body present as collections of cells heterogeneous in their responses to treatment due to both genetic and non-genetic causes. Treatments often cause fractional killing where even apparently very successful degrees of tumour regression can subsequently be undone by proliferation of the surviving clones. My work here has presented evidence that studying even something as simple as when cells dies, but at a single cell level rather than on cell populations, reveals behaviour that has to date not been properly characterised. Understanding how cells die is of fundamental importance in improving the success of treatments, and the phenotype of delayed cell death described here is likely to play a role.

Materials and Methods

1.17 Cell culture

1.17.1 Pre-existing cell lines

U2OS (ATCC® HTB-96™) were obtained from ATCC.

U2OS MDC1-mCherry were developed in our lab to stably express an MDC1-mCherry fusion construct.

HeLa cells (CCL 2, ECACC #93021013) were obtained from the European Collection of Cell cultures.

HeLa TetOn Advanced cells were obtained from Clontech.

HeLa BRC4.23 were developed in our lab from the HeLa TetOn Advanced cell line as described in (Lee et al. 2011).

hTERT-HPNE (ATCC® CRL-4023™) were obtained from ATCC.

1.17.2 Cell culture media

HeLa and U2OS cells were grown in DMEM+GlutaMAX™-I supplemented with 10% fetal bovine serum (FBS) and Pen Strep. HPNE cells were grown in 75% low glucose (1g/ml) DMEM supplemented with 2mM L-Glutamine and 1.5g/L sodium bicarbonate and 25% Medium M3 Base (Incell Corp Cat No. M300F-500) supplemented with human recombinant EGF (10ng/ml), puromycin (CONC), Pen Strep and FBS (ratio 20:1 media to FBS).

During microscopy HeLa and U2OS cells were cultured in phenol-red free DMEM supplemented with 10% FBS, sodium pyruvate, Glutamax and Pen Strep or CO_2-independent Leibowitz L15 medium supplemented with 10% FBS and Pen Strep.

1.17.3 Cell culture vessels

Cell cultures were maintained in Nunclon™ delta treated flasks, dishes and plates.

Cells for imaging were grown in various dishes: poly-D-lysine-coated 35 mm glass bottom No. 1.5 MatTek dish chambers, IbiTreat coated Ibidi 4-well Glass Bottom µ-slide (Catalogue numbers: 80427/80447), IbiTreat coated 8-well Glass Bottom µ-slide and IbiTreat coated Ibidi III 3D perfusion µ-slides.

The preliminary FUCCI microscopy lineage tracing experiment was carried out in an Ibidi 4-well Glass Bottom µ-slide, while follow-up FUCCI microscopy lineage tracing experiments were carried out in Ibidi III 3D perfusion µ-slides and associated flow accessories from Ibidi. (Luer Lock Connector Female, Elbow Luer Connector, y tube fitting, Silicone Tubing. Catalogue numbers: 10825, 10802, 10827, 10841). IbiTreat Ibidi µ-Slide VI$^{0.4}$ and poly-L-Lysine coated µ-Slide I$^{0.8}$ Luer (Catalogue numbers: 80606

80194) were tested but found unsuitable for imaging over multiple days and for allowing cells to withstand the high flow rates of treatment.

Cells grown for flow cytometry generational tracing were cultured in Nunclon Delta surface 6cm dishes.

1.18 Genetic manipulation

1.18.1 Gene synthesis, plasmids and constructs

Gene synthesis was provided by ThermoFisher LifeTechnologies (GeneArt Gene synthesis and GeneArt Strings) and cloning of plasmids was achieved by restriction enzyme, in-fusion and gateway cloning methods.

mKO2-hCdt1(aa30-120) and mAG-hGeminin(aa1-110) gene sequences were synthesised according to the sequences detailed in (Sakaue-Sawano et al. 2008) (Genbank: AB370332.1 AB370333.1). mKO2 was substituted for mCherry and the resultant mCherry-hCdt1(aa30-120) was cloned downstream of the CMV promoter in the dual-promoter plasmid pBudCE4.1 mAG hGeminin(aa1-110) was cloned downstream of the Ef1α promoter.

iRFP682 was synthesised according to the sequences detailed in (Shcherbakova & Verkhusha 2013) (Genbank: KC991143) and NLS tagged variants generated via restriction enzyme cloning into the plasmid backbone pcDNA3.1(-).

Plasmid vector name	Source:
pBudCE4.1	ThermoFisher Scientific
pcDNA3.1(-)	ThermoFisher Scientific
pLenti6/V5-DEST	ThermoFisher Scientific

Table 3: Plasmid vectors used for cloning constructs used in this work

1.18.2 Transfection

Transient transfection of cells was undertaken using JetPrime® (Polyplus) or Effectene® (Qiagen) as directed. DNA concentrations were optimised for gene expression.

1.18.3 Viral particle production and transduction

HEK293T cells were seeded on poly-L-lysine coated Nunclon Delta surface T175 flasks in order to be 40-50% confluent at the time of transfection. Poly-L-lysine coating was applied to flasks using a solution of 0.001% poly-L-lysine in PBS and incubation at 37°C for 1 hour followed by aspiration. HEK293T cells were treated with 25uM chloroquine containing media and transfected by Calcium Phosphate transfection. Lentiviral plasmids were combined with packaging plasmids psPax2 and pMd2.g at a mass ratio of 3:2:1 in a solution of 0.4M CaCl2. This solution was added dropwise to an equal volume of 2x HBS solution while being gently vortexed and the resultant precipitate added to cells. 10 hours after

incubation at 37°C cell media was exchanged. 24 hours after transfection cells were transferred to incubation at 32°C.

Viral particles were harvested by collecting and replacing cell culture media 48 hrs, 60 hrs and 72 hrs after transfection. Debris was removed from the collected media by pelleting or filtering through a 0.45 µm filter. The media was then incubated at 4C with Lenti-X concentrator overnight, pelleted (1500 g 45 minutes) and the resultant pellet resuspended in $\frac{1}{100}$ of the original volume of PBS and frozen at -80°C until use.

HPNE cells were treated with cell culture media with 8µg/ml polybrene and viral particle solution added. The optimal amount of virus solution to add was determined by trial and error. These cells were incubated overnight at 32°C, washed with PBS thrice and fresh media replaced. 24 hours later cells were assessed for successful transduction by fluorescence microscopy.

1.18.4 Stable cell line generation

U2OS FUCCI-NM cells were obtained via JetPrime® transfection with pBudCE4.1 mCherry hCdt1(aa) mAG hGem(aa) and pcDNA3.1(-) (1+1)xNLS iRFP682 followed by selection with zeocin and G418. Monoclonal cell populations were obtained via fluorescence activated cell sorting which were then screened by microscopy for successful stable integration of the two plasmids.

Monoclonal HPNE hTERT NM cells were obtained via electroporation (Lonza) with pcDNA3.1(-) (1+1)xNLS iRFP682 followed by selection with G418 and single cell clone picking. HPNE hTERT FUCCI NM cells were obtained by viral transduction of these cells with pLenti6/V5 mCherry hCdt1(aa30-120) IRESk mAG hGem(aa1-110) followed by Blasticidin selection. Monoclonal cell populations successfully expressing the three components were obtained via fluorescence activated cell sorting and transgene expression maintained with G418 and Blasticidin.

Monoclonal HeLa NM cells were obtained via JetPrime® transfection with pcDNA3.1(-) (1+1)xNLS iRFP682 followed by selection with G418 and fluorescence activated cell sorting. Monoclonal HeLa FUCCI NM cells were obtained via JetPrime® transfection with pBudCE4.1 mCherry hCdt1(aa) mAG hGem(aa) and pcDNA3.1(-) (1+1)xNLS iRFP682 and viral transduction with pLenti6/V5 (1+1)xNLS iRFP682 followed by antibiotic selection with G418 and Blasticidin and fluorescence activated cell sorting.

1.19 Cell culture fluorescent dyes

1.19.1 Hoechst 33342

Hoechst 33342 (Sigma-Aldrich Catalogue No. NUMBER) DNA-intercalating dye was used to stain DNA for microscopy and flow cytometry.

1.19.2 CellTrace™ dyes

CellTrace™ Yellow was purchased from ThermoFisher Scientific (Catalogue No. C34567/C34573).

1.20 DNA damage induction

1.20.1 Neocarzinostatin

Neocarzinostatin was purchased from Sigma-Aldrich (Cas No. 9014-02-2, MDL No. MFCD01778130 Catalogue No. N9162) as a 0.5 mg/ml solution in 20 mM MES buffer (pH 5.5). Neocarzinostatin-containing media was prepared to the indicated concentrations while mock treatments were prepared with the equivalent volume of 20 mM MES buffer (pH 5.5).

1.21 Western blotting

1.21.1 Cell harvesting and Lysate preparation

Cell culture media was collected, cells were washed with PBS and trypsinised. Trypsinised cells, PBS washes and culture media were pooled and the cells pelleted and frozen at -80°C until required.

Pelleted cells were then lysed in RIPA buffer (300mM NaCl 1% NP-40, 0.5% sodium deoxycholate, 0.1% sodium dodecyl sulphate, 50 mM Tris-HCl pH8.0, with protease inhibitors (complete EDTA-free Roche: 11873580001), Phosphatase inhibitor cocktail 2 (P5726) and Phosphatase inhibitor cocktail 3 (P0044)) for 30 minutes on ice, spun down and the supernatant taken as the protein solution.

1.21.2 Protein concentration quantification

Protein concentrations were assessed by BCA assay (Pierce).

1.21.3 Polyacrylamide Gel Electrophoresis

Proteins were denatured in NuPAGE LDS buffer (Invitrogen) with 80mM dithiothreitol at 70°C for 10 minutes and loaded on a NuPAGE 4-12% Bis-Tris SDS PAGE gel (Invitrogen).

1.21.4 Western blot protein transfer

Protein samples were transferred to a Hybond ECL (GE Healthcare) nitrocellulose membrane using wet transfer at 30V for approximately 2 hours at 4°C (Transfer buffer 7.5% Methanol solution in NuPAGE Transfer Buffer (Invitrogen)). Protein transfer was verified by Ponceau-S solution (Sigma Catalogue Number: P7170) staining.

1.21.5 Antibody probing

Membranes were blocked with 5% (w/v) milk TBS-T (Tris Buffered Saline with 0.1% Tween-20) for 1 hour before incubation overnight at 4C with primary antibodies at the dilution indicated in Table 4. Membranes were washed 5 minutes with TBST thrice and incubated with fluorescently labelled

secondary antibodies (IRDye Licor) in Odyssey blocking buffer (Catalogue Number. 927-40000) for 1 hour at room temperature. Membranes were then washed with TBST for 5 minutes thrice and scanned with the Licor Odyssey scanner system.

Antibody name/epitope:	Supplier:	Catalogue Number	Species:	Dilution ratio:
Anti myc tag antibody clone 4A6	Millipore	05-724	Mouse	1:2000
Beta-actin	Sigma	A5441	Mouse	1:10,000
IRDye®680RD anti-Mouse	Licor	925-68070	Goat	1:5000

Table 4: Antibodies used

1.22 Immunofluorescence sample preparation

1.22.1 γH2AX staining

Cells were fixed using a solution of 4% paraformaldehyde, permeabilised (0.1% TritonX-100 in PBS 5 mins r.t.), blocked (Blocking solution: 2% BSA, 0.2% Tween, 0.1% Triton X-100 in PBS 60-90 mins r.t.)and incubated with primary antibodies in blocking solution for 1 hour at 37°C (anti-γH2AX (Millipore JBW301) 1:1000). Cells were washed thrice (washing solution: 0.2% Tween, 0.1% Triton X-100 in PBS) and incubated with secondary antibody and Hoechst dye in blocking solution (Hoechst 33342 1:1000, Alexafluor 594 goat anti-mouse IgG 1:500), washed in washing solution twice, washed twice in PBS, left in PBS and imaged on a Leica SP5 confocal microscope.

Images were acquired with a photo-multiplier tube detector using a 40x objective lens and the settings 512x512 pixel image size, 400 Hz scan speed, 2x zoom, 2-4x line or frame averaging with sequential scanning. Laser power was adjusted based on the appropriate level for sample brightness, permitting clear visualisation of fluorophores but avoiding pixel saturation.

1.23 Flow cytometry

1.23.1 Fluorescence-activated cell sorting (FACS)

FACS was used to sort cell lines stably expressed transfected plasmids and transduced DNA using laser lines and gating appropriate for the relevant fluorophores.

1.23.2 Flow cytometry analysis

Flow cytometric analysis was carried out using BD LSR Fortessa flow cytometers. Flow cytometric events were gated for analysis initially based on Forward Scatter vs Side Scatter followed by doublet discrimination by Forward Scatter Height vs Side Scatter Area or DNA-intercalating dye fluorescence Width vs DNA-intercalating dye fluorescence Area.

Data analysis was carried out using Flowing Software version 2.5.1 provided online by Perttu Terho of the Turku Centre for Biotechnology, University of Turku.

1.24 Generational tracing by flow cytometry

1.24.1 CellTrace™ staining and seeding

Cells were trypsinised and strained through a CellTrics filter to produce a population of cells in suspended. A sufficient number of cells for each experiment were pelleted and resuspended in a 37°C 10 µM CellTrace™ Yellow solution in PBS at a concentration not greater than one million cells per ml and incubated at 37°C for 20 minutes. Residual dye was quenched by the addition of 5 volumes of culture media and cells incubated for a further 5 minutes at 37°C. The remaining cells were pelleted and resuspended in complete media, strained through a CellTrics filter again and seeded in 6 cm dishes at a surface density of typically 9000 cells cm^{-2} (approximately 190,000 cells) in a total volume of 4mls of complete culture medium. Cells were left for approximately 24 hours before treatment to allow attachment and recovery from seeding. Sufficient dishes were seeded to permit the harvesting of the desired number of dishes.

1.24.2 Neocarzinostatin treatment

At the start of the experiment cell culture media was aspirated from all dishes apart from the 0 hour samples and replaced treated with 3ml of culture medium containing the desired concentration of NCS or an equivalent volume of 20mM MES buffer (pH 5.5) in the case of control experiments. 1-2 hours later this was removed, dishes were washed with PBS and 4mls of fresh culture medium added. Any residual unreacted and undegraded Neocarzinostatin should therefore have been reduced to negligible levels.

1.24.3 Cell sample harvesting

Dishes were seeded allowing samples to be taken at 24 hour intervals for each condition.

U2OS, HeLa TetOn and HeLa BRC4.23 experiments were conducted with triplicate dishes for each timepoint and condition, while HPNE hTERT experiments were conducted with a single dish per timepoint and condition.

Additional dishes were seeded with coverslips to allow collection of these for immunofluorescence and collection of the cells bound to the dish for cell cycle profiling.

During sample harvesting cells were trypsinised collecting their culture media and PBS washes. Trypsinised cells were then washed off the dish, collected together with culture media and PBS washes and pelleted. Cells were then resuspended in PBS, a fraction of which was taken to be counted, the remainder mixed with formaldehyde in PBS to a final concentration of 2% formaldehyde and incubated

for 15 minutes on ice. Cells were then washed twice in ice-cold PBS and stored at 4°C in PBS until analysis.

In some experiments cell cycle profiles were obtained from separately harvested cells which were fixed in 70% EtOH in water and stored at -20°C until required after which they were washed once in PBS and analysed.

1.24.4 Population Counting

The fraction of the cell samples dedicated to population counting was diluted in PBS or Leibowitz L15 medium supplemented with FBS and Pen Strep, and analysed on a Beckman Coulter "Vi-cell-XR cell viability analyzer" machine using default cell parameters. This machine provides information both on the estimated total cell concentration and the viable cell concentration based on trypan blue based cell viability discrimination. Both measures were subsequently used for analysing the relative changes in population over time.

1.24.5 Data analysis

Flow cytometry events were acquired as above. Following gating, fluorescent curves representing the CellTrace stained cells were obtained for each sample and the median value extracted to permit fluorescence comparison across samples. Fluorescence measurements were paired with their corresponding population estimates and plotted as indicated in the results. Linear regression was carried out by determining the line of best fit constrained by passing through the origin, i.e. the first time point measurements. Where experiments were carried out with multiple replicates per time point the origin was defined by the average of the first time point replicates.

1.24.6 γH2AX foci counting

Coverslips were stained for γH2AX as directed above, mounted on glass slides with Moviol and analysed on an SP5 confocal microscope, acquiring images of the Hoechst 33342 stained nucleus and the Alexa Fluor secondary antibody used. The resultant acquired images were exported and nuclear masks created based on the nuclear stain using custom MATLAB software. These masks were then used with an inbuilt module (CompartmentalAnalysis.V4 Version 6.0) of Cellomics vHCS™ Scan software (Version 6.3.1 Build 6585 ThermoFisher Scientific) to automatically count the number of γh2ax foci present in each nucleus. γH2AX foci were determined by intensity thresholds. The resultant data was examined and exported from Cellomics View (1.6.3.3 Build 6586 ThermoFisher Scientific).

1.25 Microscopy

1.25.1 Widefield microscope

Widefield microscopy was carried out using a Nikon Eclipse Ti inverted microscope controlled by NIS-Elements AR software (Version 4.30.02). Imaging was achieved with a Zyla sCMOS camera (Andors).

1.25.2 Confocal microscope

Confocal imaging was undertaken on a Leica SP5 confocal microscope.

1.25.3 Optogenetic stimulation

The Nikon Eclipse Ti inverted microscope is coupled to a MOSAIC device for patterned illumination enabling stimulation of multiple definable regions of interest (ROI) with light from X-cite XLED devices (Lumen devices) capable of illuminating with one of four wavelength lights (460, 525, 635 and 735 nm) with variable intensity (5-100% in relative terms for each).

1.26 Microscopy based lineage tracing data acquisition and analytical workflow

1.26.1 Pre-imaging sample preparation

Treatment before imaging experiments:

FUCCI-NM cells were seeded in Ibidi 4-well µ-slides (surface density: 9000 cells cm^{-2})

Treatment during imaging experiments:

FUCCI-NM cells were seeded in Ibidi III 3D perfusion µ-slides (30 µl in each well of 30,000 cells per ml media, i.e. surface density: 3600 cells cm^{-2}) and left to attach. The chamber slide was then charged with media.

Approximately a day later flow tubing was attached allowing individual channels to subsequently receive treatment, and fresh media washed through. Slides were then attached to the microscopy stage, fresh media passed through and imaging begun.

1 day after the start of image acquisition sufficient excess volumes of media, containing mock or NCS treatments, to wash through the entire flow tubing and chamber slide system were passed through the tubing (typically 6-10 mls). An hour later similar excess volumes of media was washed through the tubing to remove any residual neocarzinostatin containing media.

1.26.2 Image acquisition

Images were acquired at 30 minute intervals with 20x air objective lens magnification, 2560x2160 pixel size. Four channels were acquired a bright field transmitted light image and three fluorescence images,

far-red (Cy5 filterset), green (FITC filterset) and red fluorescence (TRITC filterset). Time-lapse microscopy continued for 5/6 days.

1.26.3 Image segmentation

Fluorescence images, using either just the nuclear marker or the nuclear marker and the G1 and SG2 FUCCI probes, were segmented using the NIS-Elements AR built in segmentation function followed by morphological opening using the command: “OpenBinaryND(8,3,1,1,1);” and separation of objects using: “MorphoSeparateObjectsND(15,7,1,1,1);”

The resultant image overlays were exported as tif files and nuclear masks extracted from these. Where three fluorescent channels were used independently for segmentation the resultant three masks were combined to create a single final mask.

1.26.4 Image tracking

The nuclear masks produced from image segmentation were then tracked through time by custom MATLAB software. The centroids of each nucleus identified were compared to previous images and tracking achieved by comparing the distances between them.

1.26.5 Nuclei measurements and curation

The resultant tracked nuclei were used to make measurements of average FUCCI probe fluorescence for each cell. The resultant fluorescence traces were then corrected by manual validation to account for erroneous segmentation and tracking. Cell death and division were assessed by eye and their timings and identities of daughter cells recorded. Cell lineages were analysed to the third generation, the Granddaughter cells, following treatment.

1.26.6 G1/S phase transition estimation

The G1/S phase transition was estimated based on the peaking of the red fluorescent G1 probe mCherry-hCdt1(aa30-120). This was done by assessing both the raw fluorescence measurements and a median filtered version of the data that smoothed experimental noise. Multiple apparent G1 phases could be determined in cells where green SG2 probe fluorescence declined and red G1 probe fluorescence increased without the cell having gone through mitosis.

1.26.7 Data annotation

Cells could also be labelled with text annotations for later analysis.

1.27 Numerical precision

Reported values with many decimal places were typically rounded to an accuracy of one decimal place or two significant figures.

1.28 Modelling the effect of time of treatment relative to SG2M phase start

The remaining time spent in SG2M for populations of dividing cells treated after their G1/S transition were modelled in MATLAB by two linear fits described below. These lines were defined by four variables, a, m, n and c, of which a, the time of treatment at which the two lines meet, was constrained to be at least 8 hours.

```
equation = 'heaviside(a-x)*m*(x-a)+heaviside(x-a)*n*(x-a)+c';
fo_ =
fitoptions('method','NonLinearLeastSquares','Robust','Bisquare','Startpoint
',[10 -1 0 4], 'Lower', [8 -inf -inf -inf], 'MaxFunEvals', 2000, 'MaxIter',
3000);
ft_ = fittype(equation, 'dependent', {'y'}, 'independent', {'x'},
'coefficients', {'a','m','n','c'});
```

1.29 Correlation analysis

1.29.1 Correlations between paired sister lineages

Paired sister lineages were identified by finding all known sisters cells present at the time of treatment that produced lineages with no ambiguity, i.e. no cells lost during analysis. PI and SI scores were calculated and the correlation coefficients and associated p values of these paired values calculated in MATLAB:

```
[rho,p] = corr(sister1PI,sister2PI,'Type','Spearman');
```

```
[rho,p] = corr(sister1SI,sister2SI,'Type','Spearman');
```

Probability density functions describing these correlation coefficients were then calculated by bootstrap analysis of 5000 populations randomly resampled from the original pairs of sister lineages with replacement. The probability density functions describing the level of correlation of randomly paired cells were obtained similarly, but after scrambling sister lineages.

1.29.2 Familial relationship correlations

Spearman's Rank correlation coefficients and associated p values for each familial relationship of interest were calculated using the MATLAB command:

```
[rho,p] = corr(x,y,'Type','Spearman');
```

1.30 Modelling generational rate of cell death from CellTrace vs population growth plots

Assuming that cellular fluorescence is determined by three factors, the initial fluorescence, f_0, the number of cell generations that have taken place, d, and degradation of the probe over time, $\delta(t)$, for example as labelled proteins are turned over in the cells, then fluorescence is given by:

$$f = \frac{f_0}{2^d}\delta(t)$$

If probe degradation is approximated as a linear decay of fluorescence with time where r represents the fraction of fluorescence lost per unit time, t, the following function results.

$$\delta(t) \sim 1 - rt$$

Introducing t_d as the doubling time of cells we can rewrite this as:

$$\delta(t) \sim 1 - rt_d d$$

Rewriting the initial fluorescence equation with this gives

$$f \sim f_0 2^{-d}(1 - rt_d d)$$

The x component in these graphs already represents a logarithmic value of the loss of fluorescence relative to the start of the experiment. This can be expressed as:

$$x = -\log_2 \frac{f}{f_0}$$

Which using the equations above can be expressed as:

$$x \sim -\log_2[2^{-d}(1 - rt_d d)] = d - \log_2(1 - rt_d d)$$

Where probe degradation contributes relatively small losses in fluorescence relative to cell division we can approximate, using $\rho = rt_d$ as the loss of fluorescence per doubling time, x as:

$$x \sim d(1 + \rho)$$

Considering now the number of cells in the sample if we assume a constant rate of cell death in each generation, the number of cells will be determined by the initial size of the population, n_0 number of generations that have taken place, again d, and the proportion of cells dying in each generation, α.

$$n \sim n_0 2^d (1 - \alpha)^d$$

The y component of the graphs already represents a logarithmic value of the increase in cell population relative to the start of the experiment, which can be expressed as

$$y = \log_2 \frac{n}{n_0}$$

Using the equations for n above we can express y as:

$$y \sim \log_2[2^d(1 - \alpha)^d = d[1 + \log_2(1 - \alpha)]$$

y and x can now be related to each other as:

$$y \sim \frac{x}{1+\rho}[1+\log_2(1-\alpha)]$$

Using linear regression where $y = mx + c$, we can use the slope of the line of best fit, m, to estimate the rate of cell death, α.

$$m \sim \frac{1+\log_2(1-\alpha)}{1+\rho}$$

$$\alpha \sim 1 - 2^{m(1+\rho)-1}$$

ρ could be calibrated by measurement, but if we assume ρ is low we can neglect it to give

$$\alpha \sim 1 - 2^{m-1}$$

Bibliography

Acosta, J.C. et al., 2013. A complex secretory program orchestrated by the inflammasome controls paracrine senescence. *Nature Cell Biology*, 15(8), pp.978–990.

Acosta, J.C. et al., 2008. Chemokine Signaling via the CXCR2 Receptor Reinforces Senescence. *Cell*, 133(6), pp.1006–1018.

Agami, R., 2000. Distinct Initiation and Maintenance Mechanisms Cooperate to Induce G1 Cell Cycle Arrest in Response to DNA Damage. , 102, pp.55–66.

Ames, B., 1989. Endogenous oxidative DNA damage, aging and cancer. *Free Radical Research Communications*, 7(3–6), pp.121–128.

Arora, M. et al., 2017. Endogenous Replication Stress in Mother Cells Leads to Quiescence of Daughter Cells. *Cell Reports*, 19(7), pp.1351–1364.

Artandi, S.E. et al., 2000. Telomere dysfunction promotes non-reciprocal translocations and epithelial cancers in mice. *Nature*, 406(6796), pp.641–645.

Azzam, E.I., Jay-Gerin, J.P. & Pain, D., 2012. Ionizing radiation-induced metabolic oxidative stress and prolonged cell injury. *Cancer Letters*, 327(1–2), pp.48–60.

Bartek, J., Lukas, C. & Lukas, J., 2004. Checking on DNA damage in S phase. *Nature Reviews Molecular Cell Biology*, 5(10), pp.792–804.

Bartek, J. & Lukas, J., 2003. Chk1 and Chk2 kinases in checkpoint control and cancer. *Cancer cell*, 3(5), pp.421–9.

Bianconi, E. et al., 2013. An estimation of the number of cells in the human body. *Annals of Human Biology*, 40(6), pp.463–471.

Blanpain, C. et al., 2011. DNA-damage response in tissue-specific and cancer stem cells. *Cell Stem Cell*, 8(1), pp.16–29.

Booher, R.N., Holman, P.S. & Fattaey, A., 1997. Human Myt1 is a cell cycle-regulated kinase that inhibits Cdc2 but not Cdk2 activity. *Journal of Biological Chemistry*, 272(35), pp.22300–22306.

Branzei, D. & Foiani, M., 2005. The DNA damage response during DNA replication. *Current Opinion in Cell Biology*, 17(6), pp.568–575.

Breivik, J., 2001. Don't stop for repairs in a war zone : Darwinian evolution unites genes and environment in cancer development. *PNAS*, 98(10), pp.5379–5381.

Brown, E.J. & Baltimore, D., 2000. ATR disruption leads to chromosomal fragmentation and early embryonic lethality ATR disruption leads to chromosomal fragmentation and early embryonic lethality. , (626), pp.397–402.

Bruno, T. et al., 2006. Che-1 phosphorylation by ATM/ATR and Chk2 kinases activates p53 transcription and the G2/M checkpoint. *Cancer Cell*, 10(6), pp.473–486.

Bulavin, D. V et al., 2004. Inactivation of the Wip1 phosphatase inhibits mammary tumorigenesis through p38 MAPK–mediated activation of the p16Ink4a-p19Arf pathway. *Nature Genetics*, 36(4), pp.343–350.

Bunz, F., 1998. Requirement for p53 and p21 to Sustain G2 Arrest After DNA Damage. *Science*, 282(5393), pp.1497–1501.

Cai, D. et al., 2013. Improved tools for the Brainbow toolbox. *Nature Methods*, 10(6), pp.540–547.

Caldecott, K.W., 2008. Single-strand break repair and genetic disease. *Nature Reviews Genetics*, 9(6), pp.619–631.

Calonge, T.M. & O'Connell, M.J., 2008. Turning off the G2 DNA damage checkpoint. *DNA Repair*, 7(2), pp.136–140.

Campisi, J. & d'Adda di Fagagna, F., 2007. Cellular senescence: when bad things happen to good cells. *Nature Reviews Molecular Cell Biology*, 8(9), pp.729–740.

Cann, K.L. & Hicks, G.G., 2006. Absence of an Immediate G1 / S Checkpoint in Primary MEFs Following γ -Irradiation Identifies a Novel Checkpoint Switch. Cell Cycle , (August), pp.1823–1830.

Carrano, A. V. & Heddle, J. a., 1973. The fate of chromosome aberrations. *Journal of Theoretical Biology*, 38(2), pp.289–304.

Cesare, A.J. et al., 2013. The telomere deprotection response is functionally distinct from the genomic DNA damage response. *Molecular cell*, 51(2), pp.141–55.

Chandler, H. & Peters, G., 2013. Stressing the cell cycle in senescence and aging. *Current Opinion in Cell Biology*, 25(6), pp.765–771.

Chaturvedi, P. et al., 1999. Mammalian Chk2 is a downstream effector of the ATM-dependent DNA damage checkpoint pathway. *Oncogene*, 18(28), pp.4047–4054.

Chen, Q.M., Liu, J. & Merrett, J.B., 2000. Apoptosis or senescence-like growth arrest: influence of cell-cycle position, p53, p21 and bax in H2O2 response of normal human fibroblasts. *The Biochemical journal*, 347(Pt 2), pp.543–51.

Childs, B.G. et al., 2014. Senescence and apoptosis: dueling or complementary cell fates? *EMBO reports*, 15(11), pp.1139–1153.

Chipuk, J.E., 2004. Direct Activation of Bax by p53 Mediates Mitochondrial Membrane Permeabilization and Apoptosis. *Science*, 303(5660), pp.1010–1014.

Cho, S.W. et al., 2013. Targeted genome engineering in human cells with the Cas9 RNA-guided endonuclease. *Nature biotechnology*, 31(3), pp.230–2.

Chou, D.M. et al., 2010. A chromatin localization screen reveals poly (ADP ribose)-regulated recruitment of the repressive polycomb and NuRD complexes to sites of DNA damage. *Proceedings of the National Academy of Sciences*, 107(43), pp.18475–18480.

Chowdhury, D. et al., 2005. γ-H2AX Dephosphorylation by Protein Phosphatase 2A Facilitates DNA Double-Strand Break Repair. *Molecular Cell*, 20(5), pp.801–809.

Ciccia, A. & Elledge, S.J., 2010. The DNA Damage Response: Making It Safe to Play with Knives. *Molecular Cell*, 40(2), pp.179–204.

Coppe, J.P. et al., 2010. The senescence-associated secretory phenotype: the dark side of tumor suppression. *Annu Rev Pathol*, 5, pp.99–118.

Costanzo, V. et al., 2000. Reconstitution of an ATM-Dependent Checkpoint that Inhibits Chromosomal DNA Replication following DNA Damage. *Molecular Cell*, 6(3), pp.649–659.=

Crasta, K. et al., 2012. DNA breaks and chromosome pulverization from errors in mitosis. *Nature*, 482(7383), pp.53–8.

CRUK, 2016. All Cancers Excluding Non-Melanoma Skin Cancer (C00-97 Excl. C44): 2012-2014 Average Number of New Cases Per Year and Age-Specific Incidence Rates per 100,000 Population, UK. *Cancer Research UK*.

d'Adda di Fagagna, F., 2008. Living on a break: cellular senescence as a DNA-damage response. *Nature Reviews Cancer*, 8(7), pp.512–522.

Davidovic, L. et al., 2001. Importance of poly(ADP-ribose) glycohydrolase in the control of poly(ADP-ribose) metabolism. *Experimental cell research*, 268(1), pp.7–13.

Debacq-Chainiaux, F., 2005. Repeated exposure of human skin fibroblasts to UVB at subcytotoxic level triggers premature senescence through the TGF- 1 signaling pathway. *Journal of Cell Science*, 118(4), pp.743–758.

Deckbar, D. et al., 2007. Chromosome breakage after G2 checkpoint release. *The Journal of cell biology*, 176(6), pp.749–55.

Deckbar, D. et al., 2010. The limitations of the G1-S checkpoint. *Cancer research*, 70(11), pp.4412–21.

Deckbar, D., Jeggo, P. a & Löbrich, M., 2011. Understanding the limitations of radiation-induced cell cycle checkpoints. *Critical reviews in biochemistry and molecular biology*, 46(4), pp.271–83.

Delacroix, S. et al., 2007. The Rad9-Hus1-Rad1 (9-1-1) clamp activates checkpoint signaling via TopBP1. *Genes and Development*, 21(12), pp.1472–1477.

Demaria, M. et al., 2014. An essential role for senescent cells in optimal wound healing through secretion of PDGF-AA. *Developmental cell*, 31(6), pp.722–33.

Dick, A.E. & Gerlich, D.W., 2013. Kinetic framework of spindle assembly checkpoint signalling. *Nature cell biology*, 15(11), pp.1370–7.

Diehl, J.A., Zindy, F. & Sherr, C.J., 1997. Inhibition of cyclin D1 phosphorylation on threonine-286 prevents its rapid degradation via the ubiquitin-proteasome pathway. *Genes and Development*, 11(8), pp.957–972.

Dimitrova, D.S. & Gilbert, D.M., 2000. Temporally coordinated assembly and disassembly of replication factories in the absence of DNA synthesis. *Nature cell biology*, 2(10), pp.686–694.

Dotto, G.P., 2000. p21(WAF1/Cip1): More than a break to the cell cycle? *Biochimica et Biophysica Acta - Reviews on Cancer*, 1471(1).

Elkind, M.. & Redpath, J.., 1977. *Molecular and cellular biology of radiation lethality. In Cancer: A Comprehensive Treatise. Volume 6* F. . Becker, ed., New York: Plenum Press.

Falck, J. et al., 2002. The DNA damage-dependent intra-S phase checkpoint is regulated by parallel pathways. *Nature Genetics*, 30(3), pp.290–294.

Feng, Q. et al., 1996. Human L1 Retrotransposon Encodes a Conserved Endonuclease Required for Retrotransposition. *Cell*, 87, pp.905–916.

Fraga, C.G. et al., 1990. Oxidative damage to DNA during aging: 8-Hydroxy- 2'-deoxyguanosine in rat organ DNA and urine (cancer/mutation/endogenous DNA adducts/8-hydroxyguanine/oxygen radicals). *Medical Sciences*, 87(June), pp.4533–4537.

Fumagalli, M. et al., 2012. Telomeric DNA damage is irreparable and causes persistent DNA-damage-response activation. *Nature cell biology*, 14(4), pp.355–65.

Furnari, B., 1997. Cdc25 Mitotic Inducer Targeted by Chk1 DNA Damage Checkpoint Kinase. *Science*, 277(5331), pp.1495–1497.

Gadbois, D.M. & Lehnert, B.E., 1997. Temporal position of G1 arrest in normal human fibroblasts after exposure to gamma-rays. *Experimental cell research*, 232(1), pp.161–6.

Gagné, J.P. et al., 2008. Proteome-wide identification of poly(ADP-ribose) binding proteins and poly(ADP-ribose)-associated protein complexes. *Nucleic Acids Research*, 36(22), pp.6959–6976.

Gartel, a L. & Tyner, a L., 2002. The role of the cyclin-dependent kinase inhibitor p21 in apoptosis. *Mol Cancer Ther*, 1(8), pp.639–649.

Gasiunas, G. et al., 2012. Cas9-crRNA ribonucleoprotein complex mediates specific DNA cleavage for adaptive immunity in bacteria. *Proceedings of the National Academy of Sciences of the United States of America*, 109(39), pp.E2579-86.

Griffith, J.D. et al., 1999. Mammalian telomeres end in a large duplex loop. *Cell*, 97(4), pp.503–514.

Griffiths, A., Miller, J. & Suzuki, D., 2000. *An Introduction to Genetic Analysis* 7th Editio., New York.

Guo, Y. et al., 2002. Caspase-2 induces apoptosis by releasing proapoptotic proteins from mitochondria. *Journal of Biological Chemistry*, 277(16), pp.13430–13437.

Haffner, M.C. et al., 2010. Androgen-induced TOP2B-mediated double-strand breaks and prostate cancer gene rearrangements. *Nature Genetics*, 42(8), pp.668–675.

Hahn, K.M. & Kuhlman, B., 2010. Hold me tightly LOV. *Nature methods*, 7(8), pp.595, 597.

Hall, E.J. & Giaccia, A.J., 2006. *Radiobiology for the Radiologist*, Philadelphia: Lippincott Williams & Wilkins.

Hanahan, D. & Weinberg, R.A., 2011. Hallmarks of cancer: The next generation. *Cell*, 144(5), pp.646–674.

Harper, J.W. et al., 1995. Inhibition of cyclin-dependent kinases by p21. *Molecular biology of the cell*, 6(4), pp.387–400.

Harper, S.M., Neil, L.C. & Gardner, K.H., 2003. Structural basis of a phototropin light switch. *Science (New York, N.Y.)*, 301(5639), pp.1541–4.

Harrigan, J. a et al., 2011. Replication stress induces 53BP1-containing OPT domains in G1 cells. *The Journal of cell biology*, 193(1), pp.97–108.

Hayward, R.L. et al., 2003. Antisense Bcl-xl down-regulation switches the response to topoisomerase I inhibition from senescence to apoptosis in colorectal cancer cells, enhancing global cytotoxicity. *Clinical Cancer Research*, 9(7), pp.2856–2865.

Hecht, F. & Hecht, B.K., 1990. Cancer in Ataxia-telangiectasia patients. *Cancer Genetics and Cytogenetics*, 46(1), pp.9–19.

Hoeijmakers, J.H.J., 2009. DNA damage, aging, and cancer. , 361(15), pp.1475–1485.

Huang, L.C., Clarkin, K.C. & Wahl, G.M., 1996. Sensitivity and selectivity of the DNA damage sensor responsible for activating p53-dependent G1 arrest. *Proceedings of the National Academy of Sciences of the United States of America*, 93(10), pp.4827–32.

Huen, M.S.Y. et al., 2007. RNF8 Transduces the DNA-Damage Signal via Histone Ubiquitylation and Checkpoint Protein Assembly. *Cell*, 131(5), pp.901–914.

Jares, P., Donaldson, a & Blow, J.J., 2000. The Cdc7/Dbf4 protein kinase: target of the S phase checkpoint? *EMBO reports*, 1(4), pp.319–22.

Jiang, P. et al., 2006. The Bad guy cooperates with good cop p53: Bad is transcriptionally up-regulated by p53 and forms a Bad/p53 complex at the mitochondria to induce apoptosis. *Molecular and cellular biology*, 26(23), pp.9071–9082.

Jinek, M. et al., 2012. A programmable dual-RNA-guided DNA endonuclease in adaptive bacterial immunity. *Science (New York, N.Y.)*, 337(6096), pp.816–21.

Johmura, Y. et al., 2014. Necessary and sufficient role for a mitosis skip in senescence induction. *Molecular cell*, 55(1), pp.73–84.

Johnson, A. & Skotheim, J.M., 2013. Start and the restriction point. *Current Opinion in Cell Biology*, 25(6), pp.717–723.

Ju, B.-G. et al., 2006. A Topoisomerase IIβ-mediated dsDNA break required for regulated transcription. *Science*, 312(June), pp.1798–1802.

Jun, J. Il & Lau, L.F., 2010. Cellular senescence controls fibrosis in wound healing. *Aging*, 2(9), pp.627–631.

Kamihara, J., Rana, H.Q. & Garber, J.E., 2014. Germline TP53 mutations and the changing landscape of Li-Fraumeni syndrome. *Human Mutation*, 35(6), pp.654–662.

Kaminaga, K. et al., 2014. Time-lapse study on cell cycle modifications of irradiated and non-irradiated bystander HeLa-Fucci cells with X-ray microbeam Noriko Usami and Akinari Yokoya. , 31, pp.2013–2014.

Kaminaga, K. et al., 2015. Visualisation of cell cycle modifications by X-ray irradiation of single HeLa cells using fluorescent ubiquitination-based cell cycle indicators. *Radiation Protection Dosimetry*, pp.1–4.

Kang, T.-W. et al., 2011. Senescence surveillance of pre-malignant hepatocytes limits liver cancer development. *Nature*, 479(7374), pp.547–551.

Kappen, L.S. & Goldberg, I.H., 1997. Characterization of a covalent monoadduct of neocarzinostatin chromophore at a DNA bulge. *Biochemistry*, 36(48), pp.14861–14867.

Karasawa, S. et al., 2003. A Green-emitting Fluorescent Protein from Galaxeidae Coral and Its Monomeric Version for Use in Fluorescent Labeling. *Journal of Biological Chemistry*, 278(36), pp.34167–34171.

Kawano, F. et al., 2016. A photoactivatable Cre–loxP recombination system for optogenetic genome engineering. *Nature Chemical Biology*, 12(12), pp.1059–1064.

Kawano, F. et al., 2015. Engineered pairs of distinct photoswitches for optogenetic control of cellular proteins. *Nature Communications*, 6, p.6256.

Kim, S. et al., 1999. Substrate Specificities and Identification of Putative Substrates of ATM Kinase Family Members. *The Journal of Biological Chemistry*, 274(53), pp.37538–37543.

Kirschner, K. et al., 2015. Phenotype Specific Analyses Reveal Distinct Regulatory Mechanism for Chronically Activated p53. *PLoS Genetics*, 11(3), pp.1–28.

De Klein, a. et al., 2000. Targeted disruption of the cell-cycle checkpoint gene ATR leads to early embryonic lethality in mice. *Current Biology*, 10(8), pp.479–482.

Klungland, a et al., 1999. Accumulation of premutagenic DNA lesions in mice defective in removal of oxidative base damage. *Proceedings of the National Academy of Sciences of the United States of America*, 96(23), pp.13300–5.

Kolas, N.K. et al., 2007. Orchestration of the DNA-Damage Response by the RNF8 Ubiquitin Ligase. *Science*, 318(5856), pp.1637–1640.

Komatsu, K. et al., 2000. Human homologue of S. pombe Rad9 interacts with BCL-2/BCL-xL and promotes apoptosis. *Nature cell biology*, 2(January), pp.1–6.

Kortlever, R.M., Higgins, P.J. & Bernards, R., 2006. Plasminogen activator inhibitor-1 is a critical downstream target of p53 in the induction of replicative senescence. *Nature Cell Biology*, 8(8), pp.878–884.

Krizhanovsky, V. et al., 2008. Senescence of Activated Stellate Cells Limits Liver Fibrosis. *Cell*, 134(4), pp.657–667.

Kuilman, T. et al., 2008. Oncogene-Induced Senescence Relayed by an Interleukin-Dependent Inflammatory Network. *Cell*, 133(6), pp.1019–1031.

Kumagai, A. et al., 2006. TopBP1 activates the ATR-ATRIP complex. *Cell*, 124(5), pp.943–55.

Kumagai, A. & Dunphy, W.G., 1999. Binding of 14-3-3 proteins and nuclear export control the intracellular localization of the mitotic inducer Cdc25 service Binding of 14-3-3 proteins and nuclear export control the intracellular localization of the mitotic inducer Cdc25. *Genes and Development*, (626), pp.1067–1072.

De Lange, T., 2010. How shelterin solves the telomere end-protection problem. *Cold Spring Harbor Symposia on Quantitative Biology*, 75, pp.167–177.

Lara-Gonzalez, P., Westhorpe, F.G. & Taylor, S.S., 2012. The spindle assembly checkpoint. *Current biology : CB*, 22(22), pp.R966-80.

Latella, L. et al., 2004. Differentiation-Induced Radioresistance in Muscle Cells Differentiation-Induced Radioresistance in Muscle Cells. *Molecular and cellular biology*, 24(14), pp.6350–6361.

Laurent, J. et al., 2013. Multicellular tumor spheroid models to explore cell cycle checkpoints in 3D. *BMC cancer*, 13(1), p.73.

Lawton, J.S., 2016. A fate worse than death. *Journal of Thoracic and Cardiovascular Surgery*, 152(1), pp.97–98.

Lee, J.-H., 2005. ATM Activation by DNA Double-Strand Breaks Through the Mre11-Rad50-Nbs1 Complex. *Science*, 308(5721), pp.551–554.

Lee, J., Kumagai, A. & Dunphy, W.G., 2007. The Rad9-Hus1-Rad1 checkpoint clamp regulates interaction of TopBP1 with ATR. *Journal of Biological Chemistry*, 282(38), pp.28036–28044.

Lee, M. et al., 2011. A mitotic function for the high-mobility group protein HMG20b regulated by its interaction with the BRC repeats of the BRCA2 tumor suppressor. *Oncogene*, 30(30), pp.3360–9.

Leu, J.I.-J. et al., 2004. Mitochondrial p53 activates Bak and causes disruption of a Bak–Mcl1 complex. *Nature Cell Biology*, 6(5), pp.443–450.

Levskaya, A. et al., 2009. Spatiotemporal control of cell signalling using a light-switchable protein interaction. *Nature*, 461(7266), pp.997–1001.

Li, F.P. & Fraumeni Jr, J.F., 1969. Soft-Tissue Sarcomas, Breast Cancer, and Other Neoplasms: A Familial Syndrome? *Annals of Internal Medicine*, 71, pp.747–752.

Li, H. et al., 2000. Cytochrome c Release and Apoptosis Induced by Mitochondrial Targeting of Nuclear Orphan Receptor TR3. *Science*, 289(5482), pp.1159–1164.

Li, T. et al., 2012. Tumor suppression in the absence of p53-mediated cell-cycle arrest, apoptosis, and senescence. *Cell*, 149(6), pp.1269–1283.

Liang, H. et al., 2014. Homeostatic control of polo-like kinase-1 engenders non-genetic heterogeneity in G2 checkpoint fidelity and timing. *Nature communications*, 5(May), p.4048.

Lindahl, T., 1993. Instability and decay of the primary structure of DNA. *Nature Letters*, 363(April).

Lindahl, T. & Barnes, D., 2000. Repair of Endogenous DNA Damage. *Cold Spring Harbor Symposia on Quantitative Biology*, 65, pp.127–134.

Linke, S.P. et al., 1997. p53-mediated accumulation of hypophosphorylated pRb after the G1 restriction point fails to halt cell cycle progression. *Oncogene*, 15(3), pp.337–45.

Linke, S.P., Clarkin, K.C. & Wahl, G.M., 1997. p53 Mediates Permanent Arrest over Multiple Cell Cycles in Response to γ -Irradiation. *Cancer research*, pp.1171–1179.

Liu, F. et al., 1997. The human Myt1 kinase preferentially phosphorylates Cdc2 on threonine 14 and localizes to the endoplasmic reticulum and Golgi complex. *Molecular and cellular biology*, 17(2), pp.571–83.

Liu, J.C., Lerou, P.H. & Lahav, G., 2014. Stem cells: Balancing resistance and sensitivity to DNA damage. *Trends in Cell Biology*, 24(5), pp.268–274.

Liu, Q. et al., 2000. Chk1 is an essential kinase that is regulated by Atr and required for the G 2 / M DNA damage checkpoint. Genes and Development, 2, pp.1448–1459.

Löbrich, M. et al., 2010. gammaH2AX foci analysis for monitoring DNA double-strand break repair: Strengths, limitations and optimization. *Cell Cycle*, 9(4), pp.662–669.

Löbrich, M. & Jeggo, P.A., 2007. The impact of a negligent G2/M checkpoint on genomic instability and cancer induction. *Nature reviews. Cancer*, 7(november), pp.861–869.

Lopez-Girona, a et al., 1999. Nuclear localization of Cdc25 is regulated by DNA damage and a 14-3-3 protein. *Nature*, 397(6715), pp.172–175.

Mackenzie, K.J. et al., 2017. cGAS surveillance of micronuclei links genome instability to innate immunity. *Nature*, 548(7668), pp.461–465.

Macůrek, L. et al., 2010. Wip1 phosphatase is associated with chromatin and dephosphorylates gammaH2AX to promote checkpoint inhibition. *Oncogene*, 29(15), pp.2281–2291.

Mahaney, B.L., Meek, K. & Lees-Miller, S.P., 2009. Repair of ionizing radiation-induced DNA double-strand breaks by non-homologous end-joining. *Biochemical Journal*, 417(3), pp.639–650.

Mailand, N. et al., 2006. Destruction of Claspin by SCFβTrCP Restrains Chk1 Activation and Facilitates Recovery from Genotoxic Stress. *Molecular Cell*, 23(3), pp.307–318.

Mailand, N., 2000. Rapid Destruction of Human Cdc25A in Response to DNA Damage. *Science*,

288(5470), pp.1425–1429.

Mailand, N. et al., 2007. RNF8 Ubiquitylates Histones at DNA Double-Strand Breaks and Promotes Assembly of Repair Proteins. *Cell*, 131(5), pp.887–900.

Marchenko, N.D., Zaika, A. & Moll, U.M., 2000. Death Signal-induced Localization of p53 Protein to Mitochondria A potential role in apoptotic signaling. *The Journal of Biological Chemistry*, 275(21), pp.16202–16212.

Matsuoka, S. et al., 2007. ATM and ATR Substrate Analysis Reveals Extensive Protein Networks Responsive to DNA Damage. *Science*, 316(5828), pp.1160–1166.

Merrick, C.J., Jackson, D. & Diffley, J.F.X., 2004. Visualization of Altered Replication Dynamics after DNA Damage in Human Cells. *Journal of Biological Chemistry*, 279(19), pp.20067–20075.

Mills, E. et al., 2012. Engineering a photoactivated caspase-7 for rapid induction of apoptosis. *ACS synthetic biology*, 1(3), pp.75–82.

Milo, R. et al., 2009. BioNumbers The database of key numbers in molecular and cell biology. *Nucleic Acids Research*, 38(SUPPL.1), pp.750–753.

Miwa, S. et al., 2015. Heterogeneous cell-cycle behavior in response to UVB irradiation by a population of single cancer cells visualized by time-lapse FUCCI imaging. *Cell cycle (Georgetown, Tex.)*, 14(12), pp.1932–7.

Muñoz-Espín, D. et al., 2013. Programmed cell senescence during mammalian embryonic development. *Cell*, 155(5), pp.1104–18.

Nahle, Z. et al., 2002. Direct coupling of the cell cycle and cell death machinery by E2F. *Nature Cell Biology*, 4(11), pp.859–864.

Nakano, K. et al., 2001. PUMA, a novel proapoptotic gene, is induced by p53. *Molecular cell*, 7(3), pp.683–94.

Narita, A. et al., 2015. Real-time observation of irradiated HeLa-cell modified by fluorescent ubiquitination-based cell cycle indicator using synchrotron X-ray microbeam. Radiation Protection Dosimetry, 2, pp.1–5.

Ni, M., Tepperman, J.M. & Quail, P.H., 1999. Binding of phytochrome B to its nuclear signalling partner PIF3 is reversibly induced by light. *Nature*, 400(6746), pp.781–4.

Nihongaki, Y. et al., 2015. Photoactivatable CRISPR-Cas9 for optogenetic genome editing. *Nature Biotechnology*, 33(7).

Niopek, D. et al., 2014. Engineering light-inducible nuclear localization signals for precise spatiotemporal control of protein dynamics in living cells. *Nature communications*, 5, p.4404.

Norbury, C.J. & Zhivotovsky, B., 2004. DNA damage-induced apoptosis. *Oncogene*, 23(16), pp.2797–2808.

Nowsheen, S. & Yang, E.S., 2012. The intersection between Dna Damage Response and cell death pathways. *Experimental oncology*, 34(3), p.243.

O'Connell, M.J. et al., 1997. Chk1 is a wee1 kinase in the G2 DNA damage checkpoint inhibiting cdc2 by Y15 phosphorylation. *EMBO Journal*, 16(3), pp.545–554.

Obaya, A.J. & Sedivy, J.M., 2002. Regulation of cyclin-Cdk activity in mammalian cells. *Cellular and Molecular Life Sciences*, 59(1), pp.126–142.

Oda, E., 2000. Noxa, a BH3-Only Member of the Bcl-2 Family and Candidate Mediator of p53-Induced Apoptosis. *Science*, 288(5468), pp.1053–1058.

Owen-Schaub, L.B. et al., 1995. Wild-type human p53 and a temperature-sensitive mutant induce Fas/APO-1 expression. *Molecular and Cellular Biology*, 15(6), pp.3032–3040.

Ozkan-Dagliyan, I. et al., 2013. Formation of Arabidopsis Cryptochrome 2 photobodies in mammalian nuclei: application as an optogenetic DNA damage checkpoint switch. *The Journal of biological*

chemistry, 288(32), pp.23244–51.

Painter, R.B. & Young, B.R., 1980. Radiosensitivity in ataxia-telangiectasia: A new explanation (genetic disease/cell-cycle delays/replicon initiation/mitotic delay/chromosome aberrations). *Cell Biology*, 77(12), pp.7315–7317.

Parker, L.L. & Piwnica-Worms, H., 1992. Inactivation of the p34cdc2-Cyclin B Complex by the Human WEE1 Tyrosine Kinase. *Science*, 257(1989), pp.1955–1957.

Pediconi, N. et al., 2003. Differential regulation of E2F1 apoptotic target genes in response to DNA damage. *Nature cell biology*, 5(6), pp.552–558.

Peng, C., 1997. Mitotic and G2 Checkpoint Control: Regulation of 14-3-3 Protein Binding by Phosphorylation of Cdc25C on Serine-216. *Science*, 277(5331), pp.1501–1505.

Phillips, D.H. et al., 1988. Correlation of DNA adduct levels in human lung with cigarette smoking. *Nature*, 336, pp.403–405.

Polo, S.E. et al., 2010. Regulation of DNA-damage responses and cell-cycle progression by the chromatin remodelling factor CHD4. *The EMBO Journal*, 29(18), pp.3130–3139.

Poon, R.Y.., 2016. Cell Cycle Control: A System of Interlinking Oscillators. In A. Coutts & L. Weston, eds. *Cell Cycle Oscillators. Methods in Molecular Biology, vol 1342*. New York: Humana Press, pp. 3–19.

Probin, V. et al., 2006. Busulfan selectively induces cellular senescence but not apoptosis in WI38 fibroblasts via a p53-independent but extracellular signal-regulated kinase-p38 mitogen-activated protein kinase-dependent mechanism. *The Journal of pharmacology and experimental therapeutics*, 319(2), pp.551–560.

Purvis, J.E. et al., 2012. P53 Dynamics Control Cell Fate. *Science (New York, N.Y.)*, 336(6087), pp.1440–4.

R., C. & R., S., 1986. The bifurcating autoregression model in cell lineage studies. *Biometrics*, 42(4), pp.769–783.

Rebbaa, A. et al., 2003. Caspase inhibition switches doxorubicin-induced apoptosis to senescence. *Oncogene*, 22(18), pp.2805–2811.

Richard M. Burger, Jack Peisach, S.B.H., 1978. Effect of light and oxygen on neocarzinostain stability and DNA cleaving activity. *Journal of Biological Chemistry*, 253(14), pp.4830–4832.

Ridenour, D. a et al., 2012. CycleTrak: a novel system for the semi-automated analysis of cell cycle dynamics. *Developmental biology*, 365(1), pp.189–95.

Rieder, C.L. et al., 1995. The checkpoint delaying anaphase in response to chromosome monoorientation is mediated by an inhibitory signal produced by unattached kinetochores. *The Journal of cell biology*, 130(4), pp.941–8.

Rogakou, E.P. et al., 1998. Double-stranded Brekas Induce Histone H2AX phosphorylation on Serine 139. *The Journal of Biological Chemistry*, 273(10), pp.5858–5868.

Rogakou, E.P. et al., 1999. Megabase Chromatin Domains Involved in DNA Double-Strand Breaks In Vivo. , 146(5), pp.905–915.

Ruijtenberg, S. & van den Heuvel, S., 2016. Coordinating cell proliferation and differentiation: Antagonism between cell cycle regulators and cell type-specific gene expression. *Cell Cycle*, 15(2), pp.196–212.

Saitou, T. & Imamura, T., 2016. Quantitative imaging with Fucci and mathematics to uncover temporal dynamics of cell cycle progression. *Development, Growth & Differentiation*, 58(1), pp.6–15.

Sakaue-Sawano, A. et al., 2008. Visualizing spatiotemporal dynamics of multicellular cell-cycle progression. *Cell*, 132(3), pp.487–98.

Salomon, M. et al., 2000. Photochemical and Mutational Analysis of the FMN-Binding Domains of the

Plant Blue Light Receptor, Phototropin. *Biochemistry*, 39(31), pp.9401–9410.

Samassekou, O. et al., 2010. Sizing the ends: Normal length of human telomeres. *Annals of Anatomy*, 192(5), pp.284–291.

Sanchez, Y., 1997. Conservation of the Chk1 Checkpoint Pathway in Mammals: Linkage of DNA Damage to Cdk Regulation Through Cdc25. *Science*, 277(5331), pp.1497–1501.

Sandler, O. et al., 2015. Lineage correlations of single cell division time as a probe of cell-cycle dynamics. *Nature*.

Savitsky, K. et al., 1995. A single ataxia telangiectasia gene with a product similar to PI-3 kinase. *Science*, 268(5218), pp.1749–1753.

Sax, J.K. et al., 2002. BID regulation by p53 contributes to chemosensitivity. *Nature cell biology*, 4(11), pp.842–849.

Schneider, L., Fumagalli, M. & d'Adda di Fagagna, F., 2012. Terminally differentiated astrocytes lack DNA damage response signaling and are radioresistant but retain DNA repair proficiency. *Cell Death and Differentiation*, 19(4), pp.582–591.

Shaltiel, I. a et al., 2015. The same, only different - DNA damage checkpoints and their reversal throughout the cell cycle. *Journal of cell science*, 2, pp.607–620.

Shaner, N.C. et al., 2004. Improved monomeric red, orange and yellow fluorescent proteins derived from Discosoma sp. red fluorescent protein. *Nature biotechnology*, 22(12), pp.1567–72.

Shcherbakova, D.M. & Verkhusha, V. V, 2013. Near-infrared fluorescent proteins for multicolor in vivo imaging. *Nature methods*, 10(8), pp.751–4.

Sherr, C.J. & Roberts, J.M., 1995. Inhibitors of mammalian cyclin-dependent kinases. *Genes & Development*, pp.1149–1163.

Shimizu-Sato, S. et al., 2002. A light-switchable gene promoter system. *Nature biotechnology*, 20(10), pp.1041–4.

Shreeram, S. et al., 2006. Wip1 Phosphatase Modulates ATM-Dependent Signaling Pathways. *Molecular Cell*, 23(5), pp.757–764.

Song, Y.S., Lee, B.Y. & Hwang, E.S., 2005. Dinstinct ROS and biochemical profiles in cells undergoing DNA damage-induced senescence and apoptosis. *Mechanisms of Ageing and Development*, 126(5), pp.580–590.

Stephens, P.J. et al., 2011. Massive genomic rearrangement acquired in a single catastrophic event during cancer development. *Cell*, 144(1), pp.27–40.

Stevens, C., Smith, L. & La Thangue, N.B., 2003. Chk2 activates E2F-1 in response to DNA damage. *Nature Cell Biology*, 5(5), pp.401–409.

Stolze, B. et al., 2015. Comparative analysis of KRAS codon 12, 13, 18, 61, and 117 mutations using human MCF10A isogenic cell lines. *Scientific Reports*, 5(1), p.8535.

Stucki, M. & Jackson, S.P., 2006. γH2AX and MDC1: Anchoring the DNA-damage-response machinery to broken chromosomes. *DNA Repair*, 5(5), pp.534–543.

Swartz, T.E. et al., 2001. The photocycle of a flavin-binding domain of the blue light photoreceptor phototropin. *The Journal of biological chemistry*, 276(39), pp.36493–500.

Syljuåsen, R.G., 2007. Checkpoint adaptation in human cells. *Oncogene*, 26(40), pp.5833–9.

Takai, H. et al., 2000. Aberrant cell cycle checkpoint function and early embryonic death in Chk1(-/-) mice. *Genes and Development*, 14(12), pp.1439–1447.

Taylor, W.R. & Stark, G.R., 2001. Regulation of the G2/M transition by p53. *Oncogene*, 20(15), pp.1803–1815.

Toledo, L.I. et al., 2008. ATR signaling can drive cells into senescence in the absence of DNA breaks.

Genes & development, 22(3), pp.297–302.

Toyoshima-Morimoto, F. et al., 2001. Polo-like kinase 1 phosphorylates cyclin B1 and targets it to the nucleus during prophase. *Nature*, 410(6825), pp.215–220.

Toyoshima-Morimoto, F., Taniguchi, E. & Nishida, E., 2002. Plk1 promotes nuclear translocation of human Cdc25C during prophase. *EMBO Reports*, 3(4), pp.341–348.

Uematsu, N. et al., 2007. Autophosphorylation of DNA-PKCS regulates its dynamics at DNA double-strand breaks. *Journal of Cell Biology*, 177(2), pp.219–229.

Uetake, Y. & Sluder, G., 2010. Prolonged prometaphase blocks daughter cell proliferation despite normal completion of mitosis. *Current Biology*, 20(18), pp.1666–1671.

Vogelstein, B. et al., 2013. Cancer Genome Landscapes. *Science*, 339(6127), pp.1546–1558.

Vogelstein, B., Lane, D. & Levine, a J., 2000. Surfing the p53 network. *Nature*, 408(6810), pp.307–310.

Van Vugt, M. a T.M., Brás, A. & Medema, R.H., 2004. Polo-like kinase-1 controls recovery from a G2 DNA damage-induced arrest in mammalian cells. *Molecular Cell*, 15(5), pp.799–811.

Wade Harper, J. et al., 1993. The p21 Cdk-interacting protein Cip1 is a potent inhibitor of G1 cyclin-dependent kinases. *Cell*, 75(4), pp.805–816.

Wajapeyee, N. et al., 2008. Oncogenic BRAF Induces Senescence and Apoptosis through Pathways Mediated by the Secreted Protein IGFBP7. *Cell*, 132(3), pp.363–374.

Wang, B. & Elledge, S.J., 2007. Ubc13/Rnf8 ubiquitin ligases control foci formation of the Rap80/Abraxas/Brca1/Brcc36 complex in response to DNA damage. *Proceedings of the National Academy of Sciences of the United States of America*, 104(52), pp.20759–63.

Wang, H. et al., 2015. DNA damage checkpoint recovery and cancer development. *Experimental Cell Research*, 334(2), pp.350–358.

Wang, H. et al., 2016. LOVTRAP: an optogenetic system for photoinduced protein dissociation. *Nature Methods*, 13(9), pp.755–758.

Wilson, A.J. et al., 2003. TR3 / Nur77 in Colon Cancer Cell Apoptosis. (October), pp.5401–5407.

Wu, Y.I. et al., 2009. A genetically encoded photoactivatable Rac controls the motility of living cells. *Nature*, 461(7260), pp.104–8.

Xue, W. et al., 2007. Senescence and tumour clearance is triggered by p53 restoration in murine liver carcinomas. *Nature*, 445(7128), pp.656–660.

Yan, Y. et al., 2010. Protein phosphatase 2A has an essential role in the activation of γ-irradiation-induced G2/M checkpoint response. *Oncogene*, 29(30), pp.4317–4329.

Yang, J. et al., 1997. Prevention of Apoptosis by Bcl-2: Release of Cytochrome c from Mitochondria Blocked. *Science*, 275(5303), pp.1129–1132.

Yoko Kuroda, Takehito Sasaki, F.H., 1991. Unusual Survival Kinetics of Neocarzinostatin-treated HeLa Cells: Its Relation to the Drug-inactivation. *Journal of Radiation Research*, 32, pp.191–201.

Yu, J., 2006. Intestinal stem cell injury and protection during cancer therapy. *Cell cycle (Georgetown, Tex.)*, 5(1), pp.35–38.

Yumerefendi, H. et al., 2015. Control of protein activity and cell fate specification via light-mediated nuclear translocation. *PLoS ONE*, 10(6), pp.1–19.

Zemelman, B. V et al., 2002. of Genetically ChARGed Neurons. , 33, pp.15–22.

Zhang, Y. et al., 2011. DNMT3a plays a role in switches between doxorubicin-induced senescence and apoptosis of colorectal cancer cells. *International Journal of Cancer*, 128(3), pp.551–561.

Zhou, B.S. & Elledge, S.J., 2000. The DNA damage checkpoint: putting checkpoints in perspective. *Nature*, 408(November), pp.433–439.

Zou, L. & Elledge, S.J., 2003. Sensing DNA Damage Through ATRIP Recognition of RPA-ssDNA Complexes. *Science*, 300(5625), pp.1542–1548.

Appendix: Optogenetic tool development

Part of my work has involved working with optogenetic tools, in particular I attempted to develop new optogenetic tools to facilitate novel methods of probing cell cycle checkpoints. These were not ultimately very successful but a brief example of this work is included in this appendix.

1.31 Optogenetics

Study of checkpoint signalling typically involve the induction of genomic lesions with chemicals or radiation, resulting in heterogeneity in the damage experienced by individual cells. Such treatments may not be very temporally precise with damage being generated over long timescales following initiation of treatment. Furthermore, the resultant repair of the lesions create difficulty in experimentally controlling the signalling and thus dissection of the checkpoint mechanisms. Optogenetic tools allow the specific control of events within cells by light through the use of genetically encodable light responsive proteins, exploiting the variety of photoresponsive protein domains present in nature. In principle, such systems could allow exquisite spatial and temporal control of activation of checkpoint signalling whilst also being tuneable in nature.

There exist now a great many optogenetic tools, the earliest utilised light responsive photoreceptors that trigger transmembrane currents upon illumination which found great use in neurobiology (Zemelman et al. 2002), and since then a great range of light responsive proteins have been adapted to produce optogenetic tools, these now allow light control over protein interactions and activities. A number of examples are included here.

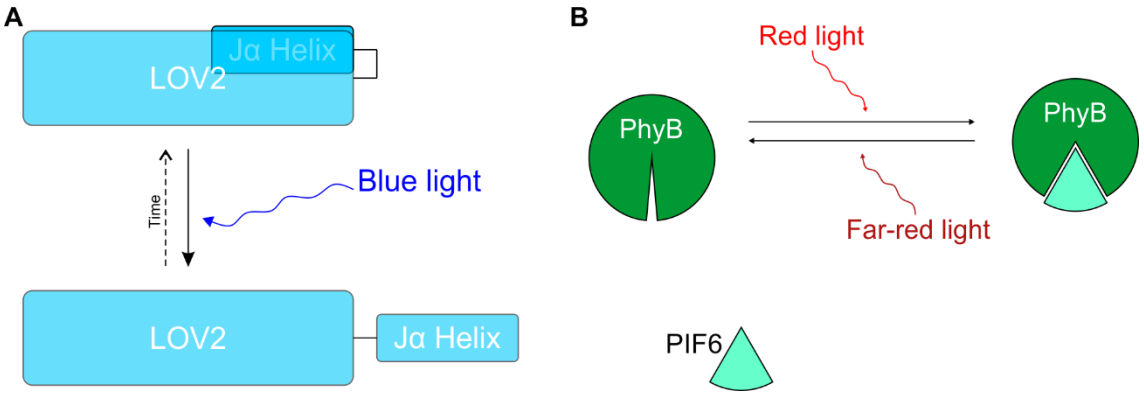

Figure 84: Illustration of principle of use of LOV2 and PhyB-PIF6 light responsive domains
A) The Jα helix of the LOV2 domain is bound closely in the dark state, upon illumination with blue light (<500nm) it is then exposed. Over time it returns to the dark state.
B) Red light promotes the association of PhyB and PIF6 while far-red light reverses this association.

1.32 Optogenetic examples

1.32.1 LOV2

The LOV2 domain from plant phototropins is a blue light responsive (<500nm light) domain that undergoes a photocycle involving a bound chromophore flavin mononucleotide (FMN). Light illumination results in the formation of an adduct between FMN and a cysteine residue (Salomon et al. 2000) which ultimately results in a structural change whereby an amphipathic helix (the Jα helix) undocks from the rest of the domain and is exposed (Harper et al. 2003), Figure 84A. Over a period of time without illumination, depending on the construct, there is spontaneous reversion to the dark/default state so allowing reversal of the effect after illumination. In the natural protein it is thought this undocking prevents an inhibitory association with a kinase so permitting kinase activity. This understanding has allowed the adaptation of the domain into various optogenetic tools. A few examples of which are discussed here.

Fusion of Rac1, a GTPase involved in cytoskeletal regulation, to LOV2 at the Jα helix produced a construct whereby in the dark default state Rac1 activity was sterically blocked by the LOV2 domain. Upon illumination and Jα helix undocking Rac1 was no longer sterically hindered and so could be activated. Locating the activating light to specific regions of the cell allowed localised cell protusions and ruffling to be observed. This allowed investigation of the regulation of RhoA by Rac1 with respect to cell motility. (Wu et al. 2009) A similar use of LOV2 as a steric block allowed the production of a photoactivatable caspase 7 capable of stimulating apoptosis after sufficient period of illumination. (Mills et al. 2012)

The LOV2 domain has the advantages that it is quite small in size and requires no external cofactors. It is also known to be tuneable with certain mutations allowing improvement of dynamic range (Hahn & Kuhlman 2010). The disadvantages of this domain are the necessity of using blue light, which being the most energetic of visible light is more likely to cause phototoxicity and that it is not actively reversible, instead reverting to the dark default state spontaneously. The half-life of reversion in the LOV2 domain from *Avena sativa* is 50 seconds (Swartz et al. 2001), but mutations are known to alter this in both LOV2 domains.

1.32.2 PhyB-PIF3/6

The PhyB-PIF3/6 systems are actively reversible systems of light-dependent binding interactions between two proteins, derived from the interactions between phytochrome B (PhyB) and phytochrome interaction factor 3 (PIF3). The phytochrome protein is capable of photoisomerisation between a Pr and Pfr form, red light will stimulate conversion of the Pr form to Pfr whilst far-red light stimulates the reverse conversion. As it is the Pfr form which is capable of interacting with PIF3, red

light essentially activates the light dependent binding, whilst far-red light reverses this (Ni et al. 1999). This requires the presence of chromophore, phycocyanobilin (PCB), covalently linked to the phytochrome. As this is usually absent in heterologous cells expressing the phytochrome, it must be added (Shimizu-Sato et al. 2002). An optimised version of this for use in optogenetic tools was produced utilising a variant of PhyB and the N terminus of PIF6, creating the PhyB-PIF6 system (Levskaya et al. 2009), Figure 84B. Much like the LOV2 system, this has been utilised in a number of applications, examples of which are given here.

Similarly to the LOV2 example given above, one study created a fusion of the RacGEF Tiam catalytic modules to PIF6, whilst the PhyB component was anchored to the membrane using a KRras(CAAX) membrane anchor. Upon global red light illumination of cells this recruited the RacGEF to the membrane, where it is activated normally and resulted in most co-transfected cells adopting a lamellipodial phenotype. Utilising a system with red light laser stimulation of specific regions and global illumination with far-red light allowed activation of the interaction in one local area, whilst ensuring the rest of the cell had the interaction repressed. This produced a localised lamellipodial 'bloom' which could be drawn out from the main body of the cell (Levskaya et al. 2009).

1.32.3 Magnets

The optogenetic tools pMag and nMag were developed by adapting the homodimerising Vivid system to produce a new system termed Magnets by introducing variants with positively and negatively charged amino acids that can now only heterodimerise with each other. The two components heterodimerise upon blue light illumination and in the dark spontaneously return to the unilluminated state and return to their monomeric state (Kawano et al. 2015). Furthermore, this study was able to show that the kinetics of this ‘switch-off’ process could be altered with certain amino acid substitutions. This tool was then used to control phosphoinositide production by controlling the membrane localisation by fusion of the inter-SH2 domain from the p85 regulatory subunit of PI3K to pMag and expressing nMag fused with a CAAX plasma membrane anchor. Upon illumination the inter-SH2 domain is recruited to the plasma membrane where it stimulates PI3K activity resulting in phosphoinositide production.

1.33 The development of novel optogenetic tools for probing checkpoint biology

I sought to design two kinds of novel optogenetic tools. Firstly, tools that could directly trigger specific DNA lesions that would allow precise interrogation of cells with well-defined DDR stimuli. Secondly, tools to activate the signalling of DDR components in the absence of actual lesions. This approach would allow cellular responses to well defined signalling to be probed, allowing greater dissection of the pathway than that afforded by stimulating with DNA damage which diminishes over time as the cell repairs the lesions.

A general strategy for achieving such control was the creation of a tool that is typically sequestered in the cytoplasm but can be localised to the cell nucleus upon illumination. Fusing this tool to various 'cargo' domains that have a defined activity in the nucleus but little activity in the cytoplasm would control their activity. Possible cargo domains include endonucleases that can induce either single or double strand breaks, or domains that can trigger checkpoint signalling.

A suitable endonuclease for controllable induction of defined doses of DNA lesion is the CRISPR-Cas9 system which triggers DNA breaks at sequences determined by the presence of guide RNAs (Figure 85) (Gasiunas et al. 2012; Jinek et al. 2012; Cho et al. 2013). Whether a double strand break or a single strand results is determined by which variant of Cas9 is used. The wild type causes a double strand break but 'nickase' variants exist that cause only one strand to be broken.

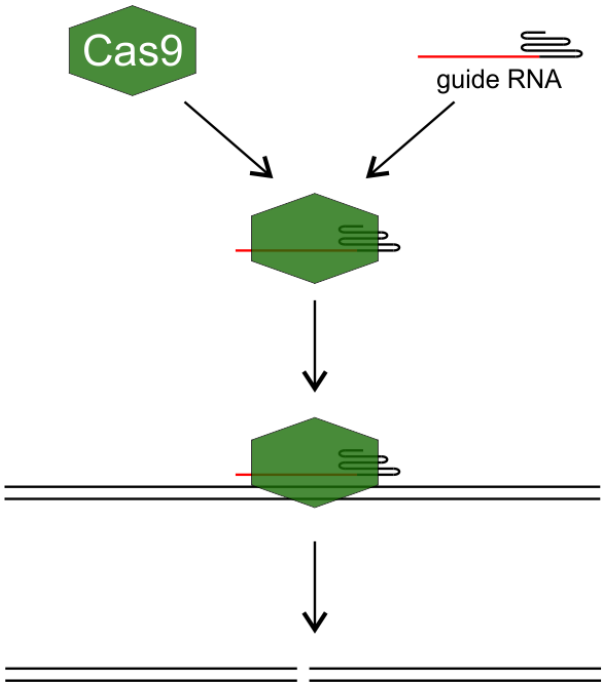

Figure 85: Illustration of Cas9 activity
Specific sequences are cleaved by Cas9 as directed by targeting chimeric guide RNA

An example of a domain that allows artificial stimulation of DDR components is the fragment of TopBP1 covering amino acids 978-1286, hereafter frTopBP1. This fragment has already been used to stimulate ATR signalling upon nuclear import in a chemical induction system (Toledo et al. 2008) and used to stimulate ATR signalling upon nuclear photobody formation in an optogenetic system (Ozkan-Dagliyan et al. 2013).

The proposed nuclear import tool was designed based on the LOV2 domain (Figure 86). A constitutively active NES fused to the protein would drive cytoplasmic sequestration normally while a cryptic Nuclear Localisation Signal (NLS) merged with the Jα helix would be exposed only upon light illumination and subsequently drive nuclear localisation. After light illumination the protein would return to its initial state and the protein returned to the cytoplasm.

Initial attempts to create this construct were not successful as the combinations of NES and NLS sequences used were incapable of triggering the switch in localisation following illumination, likely due to issues with their relative strength (Data not shown). I subsequently became aware that the Kuhlman and Hahn Groups (Department of Biochemistry and Biophysics and Department of Pharmacology, University of North Carolina) were working on the same tool design and had coupled this with another system, LOV TRAP, designed to suppress the background level of nuclear expression by further

sequestering the dark state version of the optogenetic construct on the surface of mitochondria, Figure 87 (Wang et al. 2016). Their LOV2 construct was subsequently published as was another group's similar construct (Yumerefendi et al. 2015; Niopek et al. 2014). With their version of the tool, termed LANS, I was able to reliably induce nuclear localisation of frTopBP1 (Figure 88). Regrettably, preliminary analysis by Western blotting, immunofluorescence and flow cytometry failed to provide reliable evidence that this tool was triggering any ATR signalling upon nuclear translocation (Data not shown). The fusion of Cas9 to the construct similarly failed to demonstrate reliable control of its activity (Data not shown). Nonetheless the merits of attempting to develop such optogenetic tools are demonstrated by the subsequent development of an optogeneti Cas9 tool via light induced dimerisation of two Cas9 fragments. (Nihongaki et al. 2015).

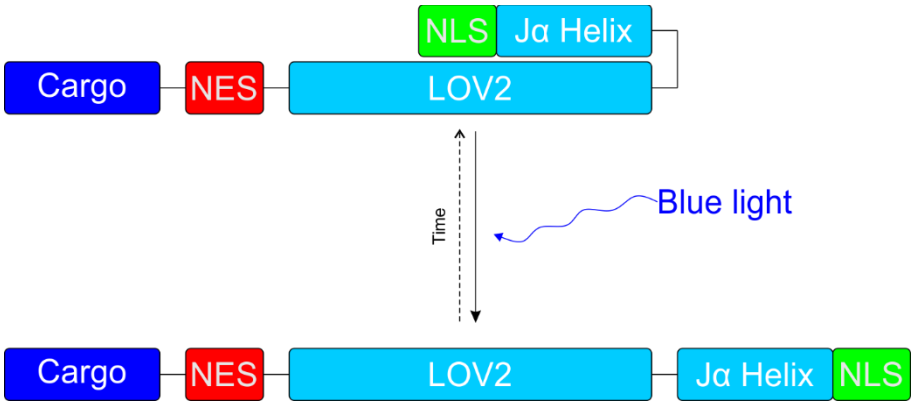

Figure 86: Diagram of nuclear shuttling LOV2 based optogenetic construct

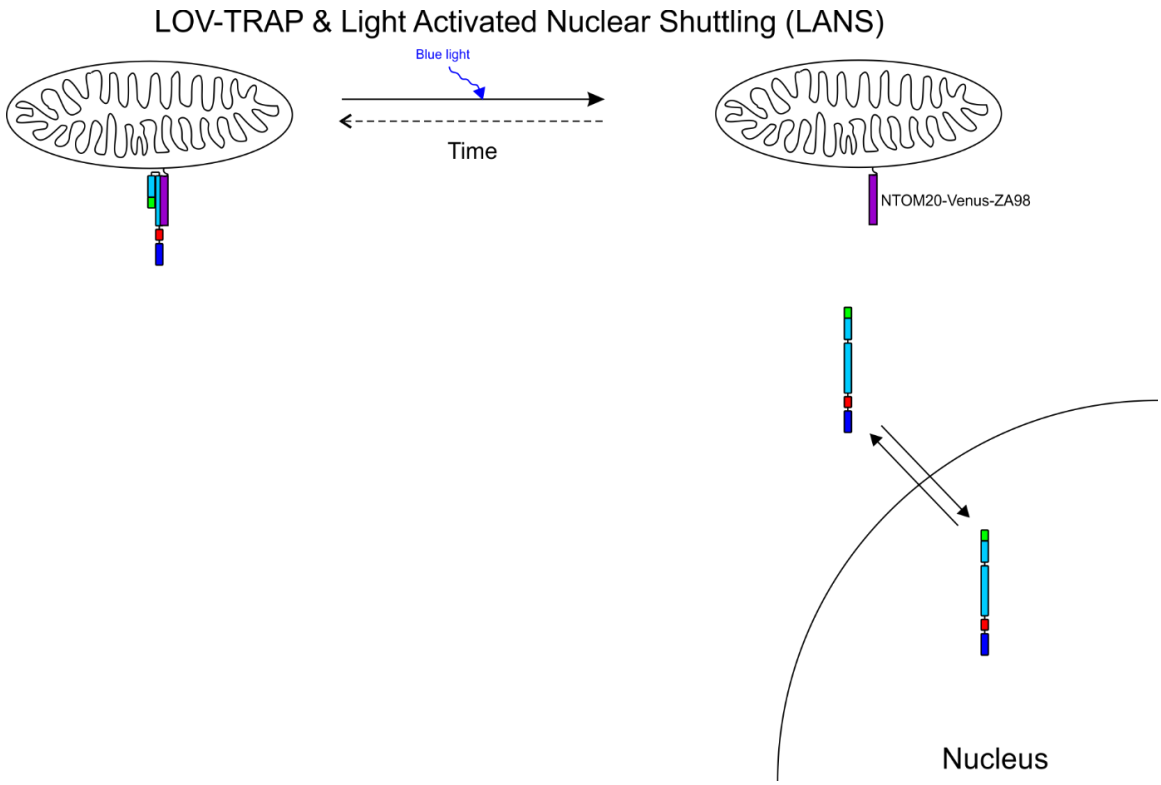

Figure 87: The nuclear import LOV2 optogenetic construct can be further sequestered at the mitochondria
The LOV2 domain binds to NTOM20-Venus-Za98 (LOV TRAP) in its unilluminated state, light illumination disrupts this association releasing it from the mitochondria and allowing it to be imported into the nucleus.

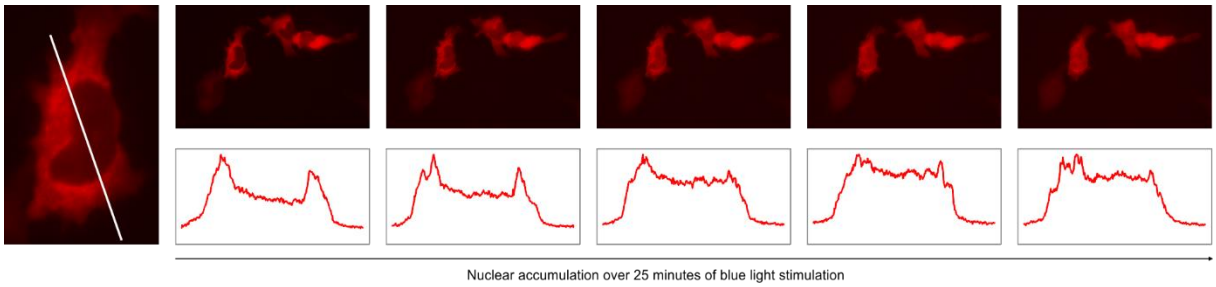

Figure 88: TopBP1-mCherry-LANS construct localises to the nucleus upon blue light stimulation
(Uppermost 5 panes) Over 25 minutes of illumination with blue light (460nm) results in nuclear accumulation of the TopBP1 fragment LOV NLS construct relative to the start. Widefield fluorescence images of mCherry tag (Leftmost pane) Zoom view of cell with line segment region of interest. (Bottommost five panes) Normalised intensity across the line segment region of interest in the corresponding image pane above. Nuclear accumulation can be observed.

1.34 Opto-Cre control of oncogenic signalling

I also assisted in the production of a derivative of the Opto-Cre system (Kawano et al. 2016) that allows simultaneous expression of a fluorescent nuclear marker to facilitate tracing of cells by the addition of an NLS tagged mCherry sequence (Figure 89). This system allows control of Cre recombinase activity by light and will be used to allow the activation of oncogenic signalling in specific cells by triggering recombination to activate gene expression. This system has been tested using derivatives of the Brainbow system to allow visualisation of the activation of Cre in specifically light stimulated cells. The Brainbow system uses cassettes of different fluorescent proteins that recombine in the presence of active Cre causing a change in fluorescence expressed (Cai et al. 2013). Activation of the Opto-cre system triggers brainbow recombination, seen as a change in fluorescence colour, Figure 90. Our addition of a nuclear marker will allow future experiments involving cell tracing of Cre activated cells and their neighbours.

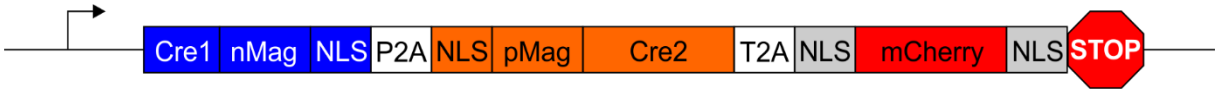

Figure 89: Opto-Cre construct with the addition of an NLS flanked mCherry for cell tracing
A single mRNA encodes three protein constructs that are separated by the self cleaving peptide fragments P2A and T2A. Cre fragments 1 and 2 are fused to nuclear localised Magnet proteins that heterodimerise upon stimulation with blue light. Heterodimerisation reconstitutes fully active Cre recombinase allowing DNA recombination of appropriate Lox sites in the nuclear genome.

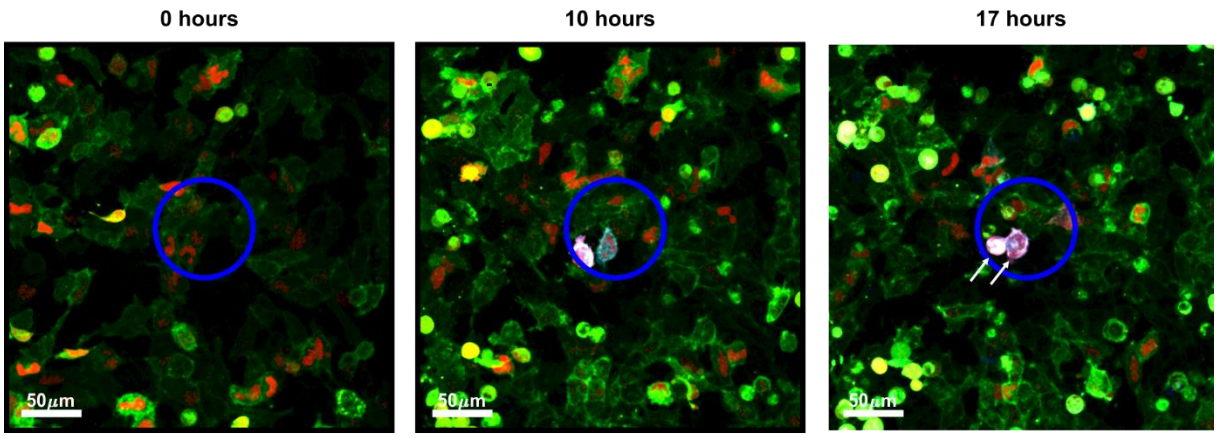

Figure 90: Activation of Opto-Cre in specific cells allows light control over gene expression
Cells expressing nuclear localised mCherry (red) can be traced through time. Cells within the blue circle received stimulatory blue light activating the Opto-Cre which in some cells (indicated by arrows) causes recombination of the Brainbow system causing a change in fluorescence colour.
Experimental work carried out and images provided by Dr Suzan Ber and Dr Alessandro Esposito.

1.35 Conclusion

There have been many exciting developments in the optogenetics field in recent years and the resultant tools have been used to probe interesting biology. Nonetheless it proved difficult in practice for me to develop novel tools even with well-reasoned strategies with experimental precedent. However, given the subsequent publishing of several similar tools to the ideas I had been working on by other research groups it demonstrates that these approaches were valid. As more experience in protein engineering and the suite of protein domains suitable for use in optogenetic constructs is gathered development of new tools is likely to become more successful.

Appendix: Microscopy based lineage tracing computational analysis

A great part of my work involved development of the computational tools necessary to extract cell and lineage information from time lapse microscopy. I present here further detail on the computational steps developed.

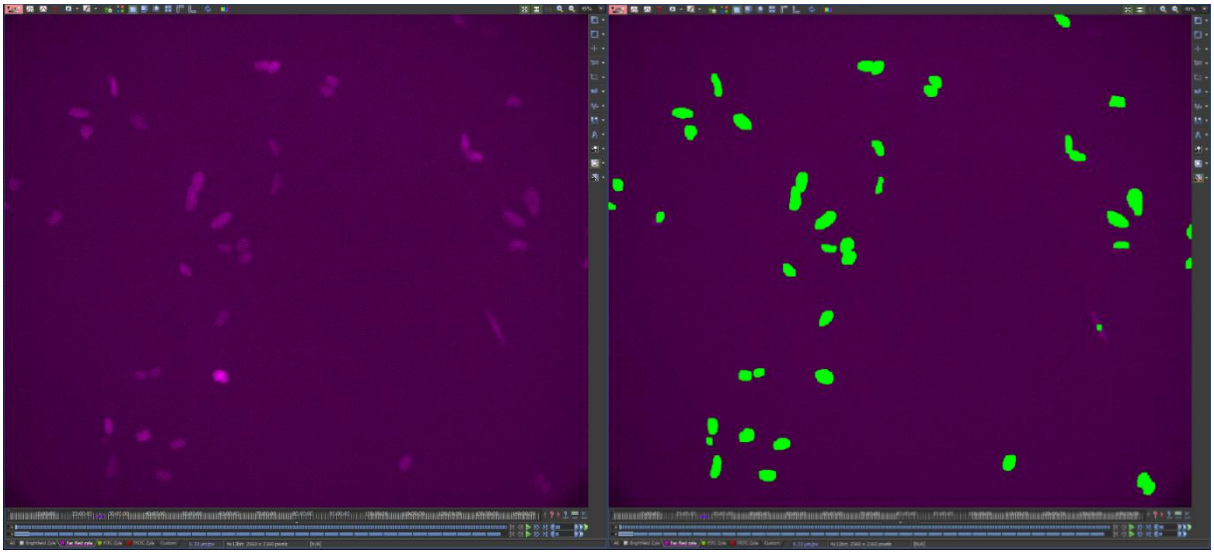

Figure 91: Cell nuclei segmentation in NIS Elements AR software

Identifying nuclei by cell segmentation is essential for correct localisation of cells and accurate tracing of them through time. Computer based methods provide a quick and reasonably good level of accuracy but there are still considerable errors where adjacent cells are recognised as one cell or cells are simply not recognised at all. These problems necessitate the labour-intensive manual verification component of analysis as they impact on all further steps.

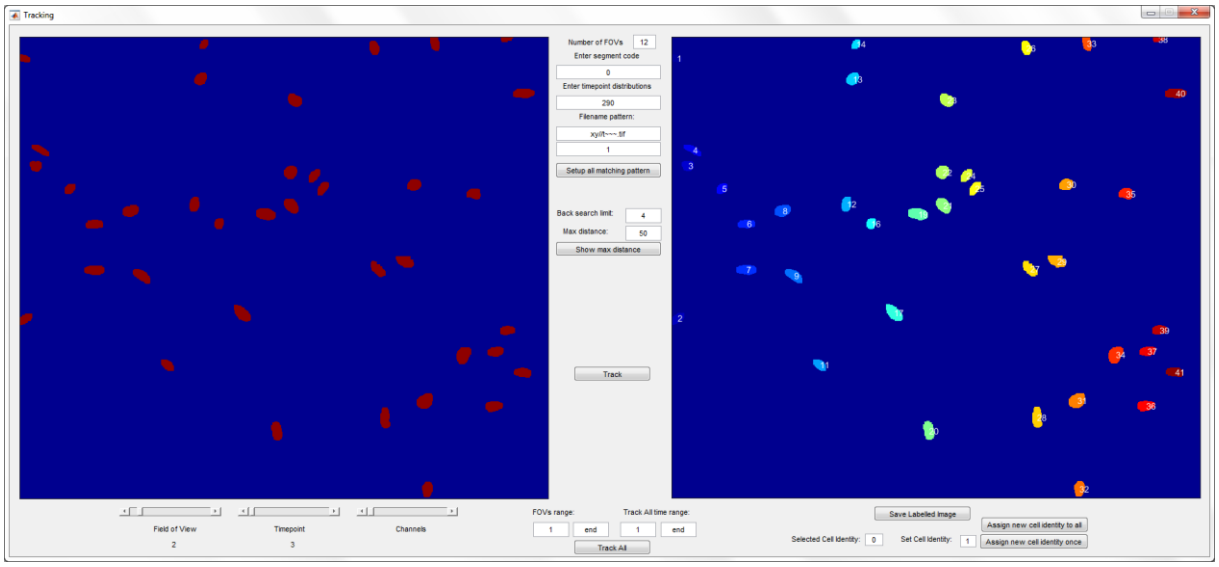

Figure 92: Extracted nuclei masks were tracked through time with custom MATLAB software

Tracking was achieved through matching masks by comparison of centroids across time points, parameters that may be adjusted are the maximum distance a cell can move and still be recognised as the same cell and how many time points may be searched back in time to find a match. This process provides quick and reasonably accurate tracking but cannot compensate for errors in nuclear segmentation and can make errors of its own where many cells are close together.

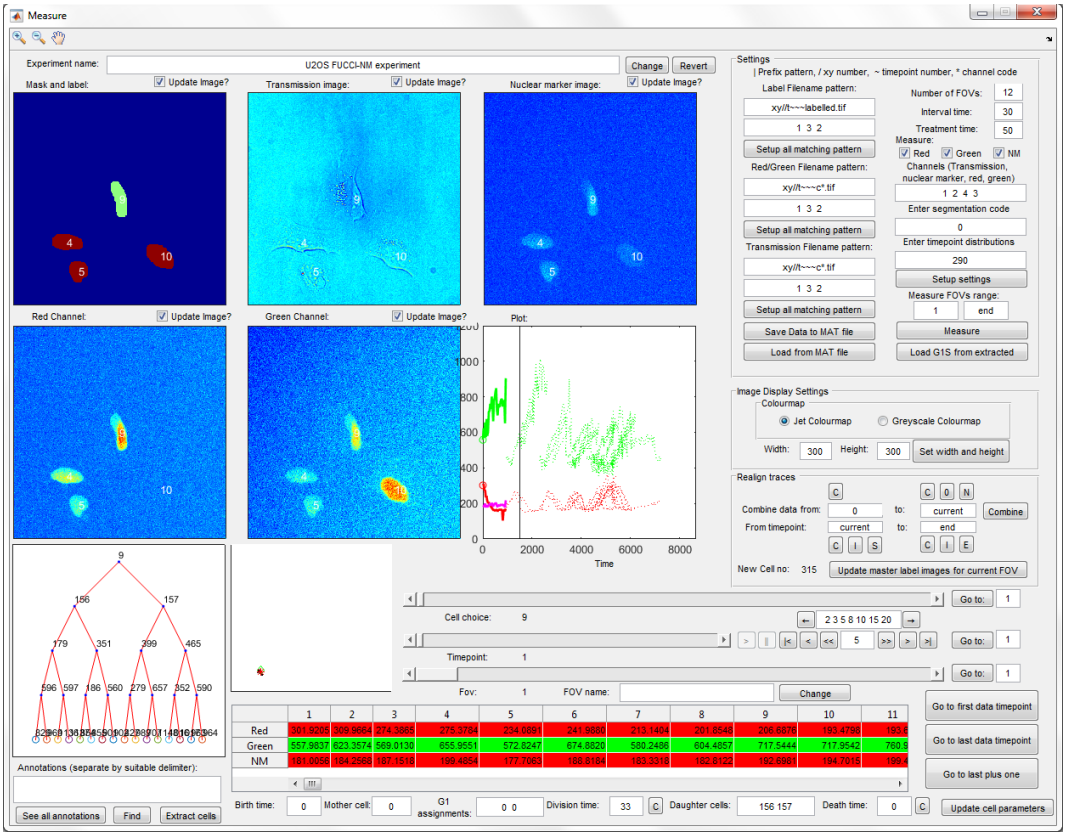

Figure 93: Custom MATLAB software to automatically extract fluorescence measurements and permit manual trace validation and curation

Manual verification of the produced traces is the most labour intensive part of the analysis process. Each cell trace must be checked for errors in cell identification and be curated with the time of death or division as well as with the identity of any daughter cells in order to allow the construction of lineages.

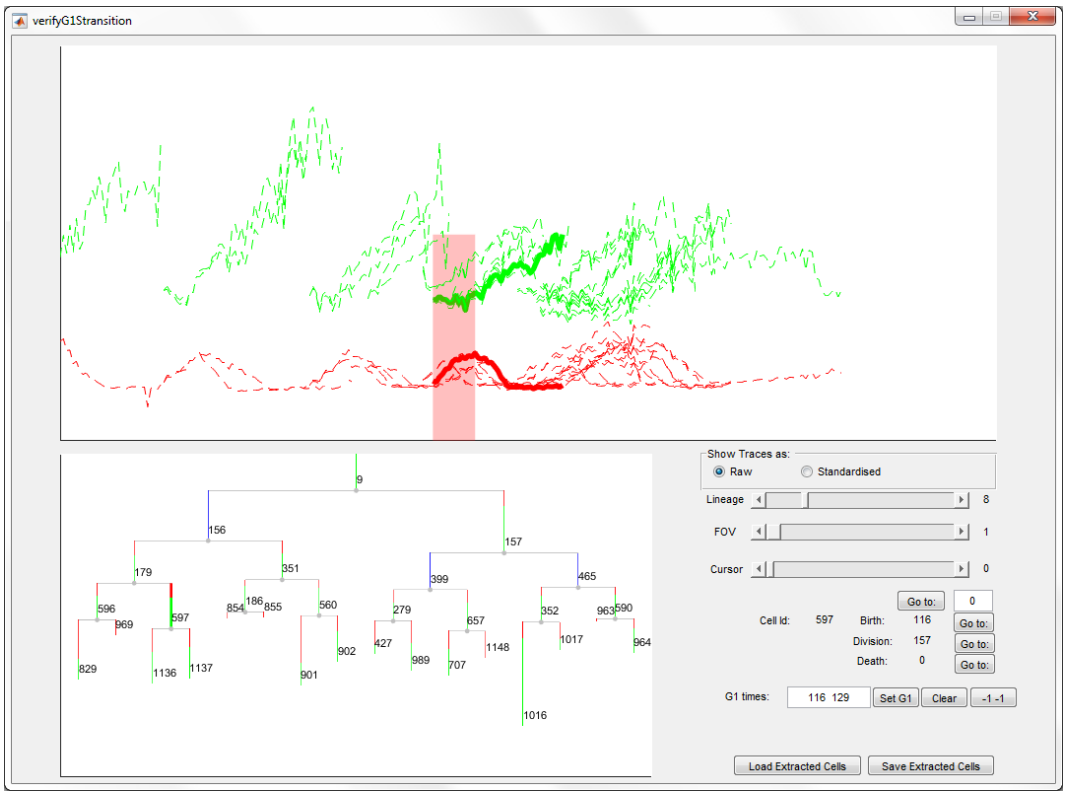

Figure 94: Reviewing FUCCI probe fluorescence is used to determine the G1/S transition

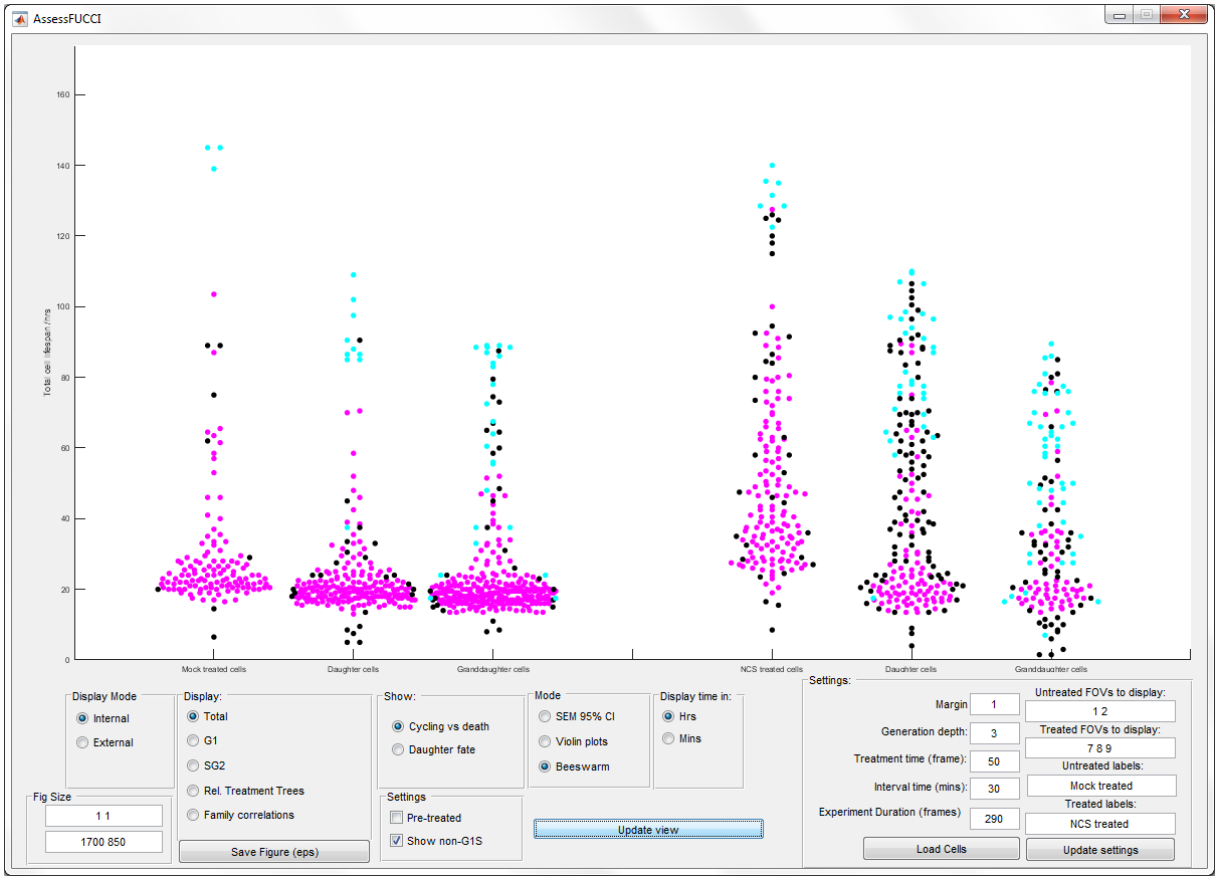

Figure 95: Many of the analyses presented here required custom software to extract and depict the relevant information